Modeling and Design for Future Wireless Cellular Networks: Coverage, Rate, and Security

He Wang

B.E. (Beijing Jiaotong University, Beijing)
M.E. (Beijing Univ. of Posts and Telecomm., Beijing)

July 2013

A Thesis Submitted for the Degree of Doctor of Philosophy
of The Australian National University

Australian
National
University

Research School of Engineering
College of Engineering and Computer Science
The Australian National University

Declaration

The contents of this thesis are the results of original research and have not been submitted for a higher degree to any other university or institution.

Much of the work in this thesis has been published or has been submitted for publication as journal papers or conference proceedings.

The research work presented in this thesis has been performed jointly with Dr. Mark C. Reed (UNSW Canberra and The Australian National University), Dr. Xiangyun Zhou (The Australian National University), and Dr. Ming Zhao (Australian Communication and Media Authority). The substantial majority of this work was my own.

He Wang
Research School of Engineering,
College of Engineering and Computer Science,
The Australian National University,
Canberra, ACT 0200,
Australia.

Acknowledgements

This thesis and the work it embodies would not have been possible without the continual support of a number of individuals and organizations. I would like to take this opportunity to express my gratitude to everyone who has contributed to the production of this thesis.

I want to gratefully acknowledge and express my sincere thanks to my supervisors and friends, Dr. Mark C. Reed, Dr. Xiangyun (Sean) Zhou, and Dr. Leif Hanlen, for their invaluable support, guidance, and encouragement throughout my PhD studies. They are always willing to give very generously their time for my research - their doors were always open. Their wisdom, academic insight, sharp focus, and on-going belief were constant sources of motivation for me to achieve the outcome included in this thesis. I am truly privileged to have had them as mentors.

I would like to thank Prof. John M. Cioffi from Stanford University and Prof. Jeffrey G. Andrews from the University of Texas at Austin for kindly welcoming me to visit their research groups. The discussions with John and Jeffrey stimulated many interesting ideas in my research area of wireless networks.

I must give my thanks to Dr. Ming Zhao (Australian Communications and Media Authority), Dr. Zhenning Shi (National ICT Australia), and Dr. Bathiya Senanayake (The Australian National University) for their collaboration on some of the work produced during my PhD study. The discussions with Dr. Parastoo Sadeghi (The Australian National University), Dr. David Smith (National ICT Australia), and Dr. Wayes Tushar (The Australian National University) also inspired me.

Thanks must go to The Australian National University and National ICT Australia (NICTA) for providing the PhD scholarship, along with a wealth of other support. Special thanks to Mark for his help in arranging my scholarship. I would also like to thank Australian Research Council Communications

Research Network (ACoRN) Travel Grant, ANU Vice-Chancellor Travel Grant, and NICTA Networks Research Group for supporting my conference attendances and university visits.

It is my great pleasure to carry out my post-graduate study and research in Canberra Research Laboratory (CRL) at NICTA and Applied Signal Processing (ASP) group at Research School of Engineering, The Australian National University. I would like to thank everyone for making them friendly and desirable environments for research and study. Special thanks should be given to Ms. Elspeth Davies, the department administrator for all her assistance.

I thank my parents for everything they have provided for me in terms of a good education, spiritual guidance, and financial support. Without their love and encouragement, it is impossible for me to achieve every little success in both professional career and personal life. Last but not least, I would like to give my special thanks to my wife Bei Wang (Janet) for her enduring support, encouragement, and understanding.

Abstract

Accompanied by the wide penetration of smartphones and other personal mobile devices in recent years, the foremost demand for cellular communications has been transformed from offering subscribers a way to communicate through low data rate voice call connections initially, into providing connectivity with good coverage, high data rate, as well as strong security for sensitive data transmission.

To satisfy the demands for improved coverage and data rate, the cellular network is undergoing a significant transition from conventional macrocell-only deployment to heterogeneous network (HetNet), in which a multitude of radio access technologies can be co-deployed intelligently and flexibly. However, the small cells newly introduced in HetNet, such as picocells and femtocells, have complicated the network topology and the interference environment, thus presenting new challenges in network modeling and design.

In recent studies, performance analyses were carried out accurately and tractably with the help of Poisson point process (PPP)-based base station (BS) model. This PPP-based model is extended in this work with the impact of directional antennas taken into account. The significance of this extension is emphasized by the wide usage of directional antennas in sectorized macrocell cells. Moreover, studies showed that little coverage improvement can be achieved if small cells are randomly deployed in a uniform-distributed way. This fact inspires us to explore the effect of the non-uniform BS deployment. We propose a non-uniform femtocell deployment scheme, in which femtocell BSs are not utilized if they are located close to any macrocell BSs. Based upon our analytical framework, this scheme can provide remarkable improvements on both coverage and data rate, thus stressing the importance of selectively deploying femtocell BSs by considering their relative locations with macrocell BSs.

To alleviate the severe interference problem, the uplink attenuation technique is frequently employed in femtocell receivers to reduce the impact of interference

from unattached terminals such that femtocell communication can take place. In order to analyze and optimize the femtocell system performance with this technique, we propose an analytical framework and demonstrate the performance tradeoff resulted from higher and lower uplink attenuation levels. Furthermore, we provide two improved uplink attenuation algorithms, which adaptively adjust to the information of the scheduled traffic, data rate requirement, and interference condition.

Apart from the cellular coverage and data rate, communication security has been an important issue to be addressed due to the increasing demand for transmitting private and sensitive information over wireless networks. In the last part of the thesis, physical layer security, as a new way to improve wireless secrecy, is studied for cellular networks. By highlighting the unique cellular features offered by the carrier-operated high-speed backhaul, we investigate the probabilistic characterization of the secrecy rate, and identify the performance impacts of cell association and location information exchange between BSs. These results provide necessary network design guidelines for selecting the appropriate cell association method and information exchange range.

List of Publication

Journal Articles

J1. He Wang, Xiangyun Zhou, and Mark C. Reed, "Physical layer security in cellular networks: A stochastic geometry approach", *IEEE Trans. on Wireless Commun.*, vol. 12, no. 6, pp. 2776-2787, Jun. 2013.

J2. He Wang, Xiangyun Zhou, and Mark C. Reed, "Coverage and Throughput Analysis with a Non-uniform Femtocell Deployment", submitted to *IEEE Transactions on Wireless Communications*.

Conference Papers

C1. He Wang, Ming Zhao, and Mark C. Reed, "Outage analysis for WCDMA femtocell with uplink attenuation", in *Proc. IEEE 1st Int'l Workshop on Femtocell Networks (GLOBECOM'10 Wkshps)*, Miami, USA, Dec. 2010, pp. 664-668.

C2. He Wang, Ming Zhao, and Mark C. Reed, "Optimal adaptive uplink attenuation algorithms for WCDMA femtocell", in *Proc. IEEE Global Commun. Conf. (GLOBECOM'11)*, Houston, USA, Dec. 2011, pp. 1-5.

C3. He Wang and Mark C. Reed, "A novel tractable framework to analyse heterogeneous cellular networks", in *Proc. 6th IEEE Int'l Workshop on Heterogeneous, Multi-Hop, Wireless, and Mobile Networks (GLOBECOM'11 Wkshps)*, Houston, USA, Dec. 2011, pp. 287-292.

C4. He Wang and Mark C. Reed, "Tractable model for heterogeneous cellular networks with directional antennas", in *Proc. 2012 Australian Commun.*

Theory Workshop (AusCTW'12), Wellington, New Zealand, Jan./Feb. 2012, pp. 61-65.

C5. He Wang, Xiangyun Zhou, and Mark C. Reed, "On the physical layer security in large scale cellular networks"', in *Proc. 2013 IEEE Wireless Commun. and Networking Conf. (WCNC'13)*, Shanghai, China, Apr. 2013, pp. 2503-2508.

C6. He Wang, Xiangyun Zhou, and Mark C. Reed, "Analytical evaluation of coverage-oriented femtocell network deployment", in *Proc. IEEE Int'l Conf. on Commun. (ICC'13)*, Budapest, Hungary, June 2013, pp. 4567-4572.

The following publications are also the results from my Ph.D. study but not included in this thesis:

C7. Zhenning Shi, Ming Zhao, Mark C. Reed, and He Wang, "Uplink interference scenarios in two-tier networks", in *Proc. 44th Annual Asilomar Conf. on Signals, Systems, and Computers (Asilomar'10)*, Pacific Grove, USA, Nov. 2010, pp. 1-5.

C8. Zhenning Shi, He Wang, Ming Zhao, and Mark C. Reed, "An uplink analytical model for two-tiered 3G femtocell networks", in *Proc. 8th Int'l Symp. on Modeling and Optimization in Mobile, Ad Hoc, and Wireless Networks (WiOpt'10)*, Avignon, France, May. 2010, pp. 367-372.

C9. Zhenning Shi, Ming Zhao, Mark C. Reed, and He Wang, "On the uplink coverage and capacity of UMTS femtocells in enterprise environment", in *Proc. 2nd Int'l Workshop on Femtocells (CWiND'10)*, Luton, UK, Jun. 2010, pp. 1-3.

C10. Zhenning Shi, Ming Zhao, He Wang, and Mark C. Reed, "On the uplink capacity and coverage of relay-assisted UMTS cellular network with multiuser detection", in *Proc. 2012 IEEE Wireless Commun. and Networking Conf. (WCNC'12)*, Paris, France, Apr. 2012, pp. 2979-2983.

Acronyms

3GPP	Third Generation Partner Project
ABSF	almost blank subframe
ADC	analog-to-digital convertor
AULA	adaptive uplink attenuation algorithm
BS	base station
CCDF	complementary cumulative distribution function
CDF	cumulative distribution function
CDMA	code-division multiple access
CoMP	coordinated multipoint
CPICH	common pilot channel
CSG	closed subscriber group
DAS	distributed antenna system
DSL	digital subscriber line
eICIC	enhanced inter-cell interference coordination
FAP	femtocell access point
FER	frame error rate
HNB	home NodeB
HetNet	heterogeneous network
HSPA	High Speed Packet Access
IEEE	Institute of Electrical and Electronics Engineers
ITU	International Telecommunication Union
LLN	law of large numbers
LTE	Long Term Evolution
MAC	medium access control
OFDM	orthogonal frequency-division multiplexing
PDF	probability density function
PGFL	probability generating functional

PMF	probability mass function
PPP	Poisson point process
QoS	quality of service
RAT	radio access technology
RRH	remote radio head
SINR	signal-to-interference-and-noise ratio
SNR	signal-to-noise ratio
SON	self-organizing network
WCDMA	Wideband CDMA
WiMAX	Worldwide Interoperability for Microwave Access
WLAN	wireless local area network

Notation

$\approx$	approximately equal to
$\triangleq$	defined as equal to ($a \triangleq b : a$ is defined as b)
$*$	convolution operator
$\arg\max_x f(x)$	value of x that maximizes the function $f(x)$
$\arg\min_x f(x)$	value of x that minimizes the function $f(x)$
$\|x\|$	absolute value (amplitude) of x
$\angle x$	argument of x
x_{dB}	value of x expressed in decibel unit
$\log_x(y)$	the log, base x, of y
γ	Euler-Mascheroni constant
$\mathbb{R}$	field of all real numbers
α	path loss exponent
L_0	path loss constant at the reference distance $r_0 = 1$m
b, q	constants to approximate the distribution of Voronoi cell area
$\mathbf{1}(A)$	indicator function, equal to 1 if Event A is true and 0 otherwise
$\Gamma(x)$	Gamma function
$E_1(x)$	exponential integral
$\mathcal{L}_X(x)$	Laplace transform of random variable X
$Q(x)$	Gaussian Q-function
$f_X(x)$	probability density function of random variable X
$F_X(x)$	cumulative distribution function of random variable X
$\bar{F}_X(x)$	complementary cumulative distribution function of random variable X
$\mathbb{P}[\mathbf{A}]$	probability of event $\mathbf{A}$
$\mathbb{E}[\cdot]$	expectation operator
$\mathbb{E}_X[\cdot]$	expectation operator over random variable X
$\mathbb{E}[\cdot \mid \cdot]$	conditional expectation operator

$X \sim p_X$	random variable X with distribution p_X
$X \sim \exp(\mu)$	exponential distributed random variable X with mean value μ
$\mathcal{N}(\mu, \sigma^2)$	normal distribution with mean μ and variance σ^2
$\{x : \mathcal{C}\}$	set containing all x that satisfy condition $\mathcal{C}$
$\mathcal{B}(p, r)$	closed ball centered at p and of radius r
$A(\mathcal{X})$	area measure of the region $\mathcal{X}$
$\Lambda(\mathcal{X})$	a point process's intensity measure for the region $\mathcal{X}$
$C_0(\lambda)$	area measure of a randomly chosen Voronoi cell formed by a homogeneous PPP with the density λ
$P_{rx}(x, y)$	received power at the receiver at the location of x, from the transmitter at the location of y

Contents

List of Figures

List of Tables

Chapter 1

Introduction

During the past decades, we have witnessed the commercial success of mobile cellular communications in both developed and emerging markets. By providing reliable and inexpensive mobile voice services to a majority of the world's population, the mobile cellular communications industry has become an indispensable part of our daily life. In recent years, the proliferation of media-hungry smartphones and plethora of other Internet-connected mobile devices having powerful multimedia capabilities made the industry enter the mobile broadband era.

As the cellular technologies evolve, there are many metrics that should be optimized during the network design process. Among all these metrics, coverage, data rate, and security are highly concerned by the cellular service providers, thus becoming the central topics to be discussed in this thesis.

1.1 Heterogeneous Networks: The Solution for Coverage and Rate

Providing satisfactory and ubiquitous cellular coverage has become a prerequisite for the success of a cellular communications networks. Although it can be an intimidating task to satisfy not only the outdoor mobile subscribers but also the indoor ones, reliable in-building coverage is widely regarded as a criterion to differentiate the service quality, especially considering the fact that most of voice and data services are initiated from indoor environments [1].

On the other hand, the increasing demand for mobile broadband data services presents new challenges for cellular service operators and the whole industry. As global mobile-broadband penetration is still substantially lower than the tradi-

tional cellular subscriptions reported by International Telecommunication Union (ITU) [2], a huge reserve of potential users are expected to embrace the mobile data services in the near future. Furthermore, the recent tremendous development of cloud-based applications is pushing the mobile data traffic requirement even higher [3]. Predicted by the industry report [4] updated by Cisco Systems this year, the global mobile data traffic will experience a 13-fold increase from 2012 to 2017. Similar growth is forecast in another independent report completed by Ericsson [5].

Nevertheless, the wireless link efficiency is approaching its fundamental limits. Over the last decade, new cellular standards including Third Generation Partnership Project (3GPP)-based High Speed Packet Access (HSPA) [6] and Long Term Evolution (LTE) [7, 8], and Institute of Electrical and Electronics Engineers (IEEE) 802.16-based Worldwide Interoperability for Microwave Access (WiMAX) [9] have been newly developed and deployed worldwide. These new technologies allow operators to efficiently exploit wider spectrums with higher data rates and improved quality of user experience. Nevertheless, radio link performance is fast approaching the theoretical limitation and from a pure link-budget viewpoint, a relatively high signal-to-noise ratio (SNR) is required to achieve the high data rates [10, 11], which is unavailable in most cases. On the other hand, spectrum available to operators has been, is, and will continue to be limited and expensive [12]. Considering this fact, extending the transmission bandwidth incrementally or even aggregating multiple component spectrums [13] are both unsustainable to meet this mobile data traffic explosion [14]. As the traffic volumes are likely to increase faster than the rise in spectral efficiency as well as the amount of spectrum being made available, the capacity and data rates offered by the existing network with enhanced radio access will no longer be sufficient [15]. There is a need for a new approach to improve the data rates and the approach of choice is by further reducing the cell size and thus enhancing spatial reuse of spectrum. Over the begone decades, it has been shown that it is the most effective manner to increase the area spectral efficiency, and provides a scalable solution to the forecasted mobile broadband demand in the future.

1.1.1 Homogeneous Macrocell-Only Networks

Conventionally, cellular networks are homogeneously deployed by using a macrocell-oriented network planning and optimization process. This homogeneous cellular

system comprises a collection of user terminals and a network of high-power tower-mounted base stations (also called macrocell BSs) in a planned layout. In this planned layout, all the BSs have similar characteristics, such as similar transmit power levels, antenna configurations (numbers, heights, and antenna sectorization), receiver noise levels, and similar backhaul connectivity to the core network. Additionally, all BSs provide unrestricted access to all the mobile subscribers in the network with comparable quality of service (QoS), and every BS serves a similar number of user terminals. Through the macrocell-oriented planning and optimization, the locations of the BSs are carefully chosen, and the settings of BS parameters are further optimized to achieve the desirable performances, that is, the maximized cellular coverage and minimized interference between BSs [16].

To cope with the growth in traffic demand mentioned earlier, the system spectral efficiency can be further enhanced by the densification of the traditional macrocells, which can include the technique of cell splitting and sectorization [17]. In dense urban areas, the inter-site distance between two neighboring macrocell BSs can be down to 100-200 m, thus enhancing the spectral efficiency significantly [18]. Furthermore, increasing the density of BSs has proved to be the only scalable method to provide the necessary capacity [15, 19].

1.1.2 Heterogeneous Networks

Continuing on the trend of reducing the cell size to cope with the data throughput requirement, more BSs are required to achieving higher frequency reuse. However, implementing more macrocell BSs sometimes involves the high capital and operating expense, and a lack of available sites in a practical deployment [11, 20]. Moreover, additional data traffic capacity is required in some particular scenarios, such as indoor/outdoor hot spot locations, and therefore the traffic demand is non-uniform over the whole deployment area [21]. All these factors combine to conclude that a more flexible deployment model is desired for operators to improve broadband user experience in a cost-effective manner [17].

Currently, the flexible deployment model involving a more advanced network topology is adopted. In this topology, a range of radio access technologies (RATs) coexist, and macrocells are further complemented by a multitude of small cells that bring the network closer to the users and improve spectral efficiency per unit area [22, 23]. These small cells can consist of various classes of low power BSs including picocell BSs, femtocell BSs [24], relays [25, 26], and remote radio heads

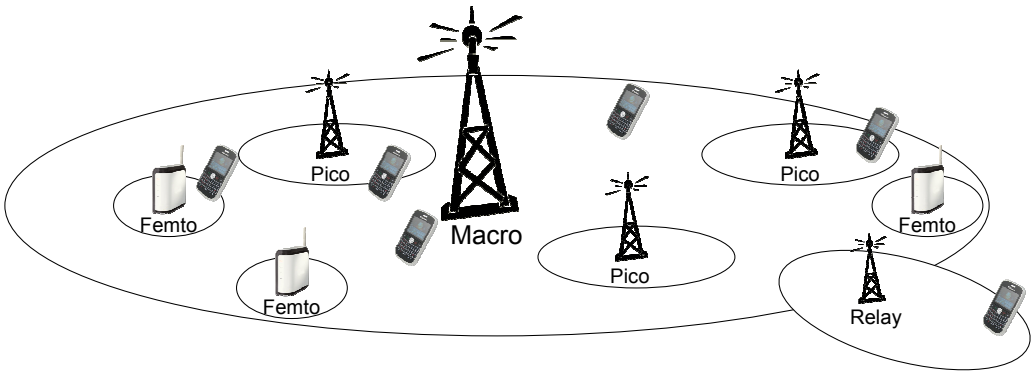

Figure 1.1: Illustration of a cellular network consisting of macrocell, picocell, femtocell BSs, and relay nodes. This evolved network topology is referred to as the heterogeneous network.

(RRHs) in distributed antenna systems (DASs) [1, 27]. As shown in Fig. 1.1, these techniques can be more scalable and economical to cater to the huge traffic demand forecasted and enable infrastructure resources to be located close to places with high coverage and data demands. Generally speaking, there are two major options to realize the heterogeneous cellular deployment: small cells co-channel deployed operators' licensed spectrum and wireless local area network (WLAN) access points in unlicensed spectrum [28]. In this thesis, the focus is primarily on the co-channel option.

Accordingly, the networks become significantly more heterogeneous in terms of transmit powers (and thus coverage ranges), antenna configurations, supported frequency bands, transmission bandwidths, access control policies, communication protocols, and backhaul connectivity. Taking transmit powers for instance, the macrocell BSs at high power level (around 46 dBm) are underlaid with other tiers, which are formed by picocell BSs, femtocell BSs, and relays transmitting at substantially lower power levels and contributing to completely diverse cellular coverage. In our discussion, the term *"tier"* is used to describe the network comprising a single class of BSs. Currently, this more complex evolved network topology with diverse radio technologies and overlapping geographical coverage, also referred to as heterogeneous networks (HetNets), has attracted significant attention from both industrial and academic communities [14, 29–33].

It should be noted that implementing smaller cells to complement macrocells in traffic-intensive hot spots with the aim of improved frequency reuse efficiency is not a brand new idea. In the era of voice services, deploying microcells under-

Table 1.1: Major characteristics of different BS in HetNet [1, 37].

Type	Tx power	Coverage	Capacity	Backhaul
Macrocell BS	46 dBm	Few km	< 1000 users	Dedicated wired
Picocell BS	23-30 dBm	< 300 m	$10 - 50$ users	Dedicated wired
Femtocell BS	10-23 dBm	< 30 m	< 5 users	Wired Internet access
Relay	23-30 dBm	< 300 m	$10 - 50$ users	Wireless
RRH	46 dBm	Few km	< 1000 users	Optical fiber

neath macrocells were investigated analytically in [34]. Some of the most critical problems in HetNets were identified by Lagrange in his pioneering study [35], and the networks with multiple access techniques proved superior to macrocell-only networks in terms of system cost [36].

Different from the careful network planning for macrocell-only networks, the placement of small cell BSs may be more or less ad hoc, and even the operator-deployed picocell is only based upon a rudimental knowledge of coverage issues and data traffic distribution (e.g. hot spots) in the network. Because of their lower transmit power levels and smaller physical sizes, picocell, femtocell, and relay BSs can offer flexible site acquisitions [11]. Thanks to the advanced interference management and self-organizing network (SON) techniques, the overall throughput provided by the HetNets can be increased as the number of deployed small cells grows [33].

The major characteristics of different BSs are summarized in Table 1.1 and detailed descriptions are provided as follow.

Picocell

Picocell BS is a low power, operator-deployed wireless access point using the same backhaul and access features compliant with classical macrocells [37]. It has small physical dimensions, in which an antenna radiating a transmit power ranging from 23 to 30 dBm is usually integrated. It should be noted that omni-directional antenna is typically installed, different from the directional antenna used for macrocell BSs. By covering a radio range of 300 m and serving a few tens of mobile users, picocell can be deployed to fill the macrocell coverage hole, or provide extra data service in the wireless hot spot areas. Furthermore, through the capacity data-offloading effect, more frequency/time resources of the macrocell networks

can be released, which is beneficial to macrocell terminals as well.

Femtocell

Being an important part of HetNet, femtocell access point (FAP), otherwise called femtocell BS or home NodeBs (HNBs) in the 3GPP standard, is usually defined as a low-power device operating in the licensed spectrum [38, 39]. Backhauled onto the operator's network via the wired Internet connection, such as digital subscriber line (DSL), cable broadband access, or fiber, femtocells are designed to provide voice and high data-rate sustained services for indoor environments, where a majority of user traffic comes from. As a result of off-loading indoor traffic from the macrocells to femtocells and employing smaller cell sizes, femtocells bring a multitude of benefits, including more efficient spatial reuse of spectrum, enhanced coverage and capacity for indoor applications, reduced capital costs and operational costs, better user experiences, and lower churn of subscribers [24, 40]. Aiming to cover a range less 30 m, the femtocell BS is operated with a transmit power less than 23 dBm.

Relay

With the similar transmit power and coverage range as picocell, relay is generally defined as operator-deployed access point that decodes the data sent from the donor BS or from the user terminal, re-encodes and forwards to the destination. By boosting the signal strength and improving the cellular coverage for the existing networks, e.g., in cell edge areas, relays play an indispensable role in the future HetNet. As Relay is able to be installed where wired backhaul is unavailable, it is able to provide extra flexibility for cellular deployment [25, 26].

RRH

Usually connecting conventional macrocell BSs with optical fibers, RRHs are the compact-size and high-power remote radio units mounted in the bad cellular coverage areas [1, 37]. As the radio circuitry is installed near the antenna, RRHs minimize the losses of power in the antenna cable. RRHs are in charge of radio interface, but still rely on central macrocell BSs for control and baseband signal processing. They also enhance the flexibility in the network deployment process.

In HetNet deployment, cellular networks are brought close to the end users to offer better coverage and data rate. Unlike the macrocell BSs, which frequently involve the high expenditure and long installation cycle, the small cells in HetNet can be intelligently utilized, depending on the coverage and rate demands.

For instance, multiple HSPA-based femtocell BSs can be deployed in an enterprise deployment scenario, which significantly contributes to an improved indoor coverage, as illustrated in Fig. 1.2. Through a system-level simulation, we demonstrate the heat maps and probability density functions (PDFs) of the core metric for cellular coverage performance, that is, E_c/I_o of the best pilot channel[1] from all candidate BSs, where E_c/I_o is defined as the ratio between the bit energy of the pilot channel and the density of total interference power [41]. The simulation is conducted under the conditions where no femtocell BS and 4 femtocell BSs with 20dBm transmit power are deployed for the particular indoor environment.

On the other hand, offloading mobile users from heavily loaded macrocells (where most of their resources are occupied for users' traffic demand) to other lightly loaded small cell infrastructures can be beneficial to the network performance. As demonstrated in the Fig. 1.3, different numbers of HSPA-based picocells are simulated to be co-channel deployed with a traditional macrocell network. We demonstrate the cumulative distribution functions (CDFs) of individual user's data rate (averaging over macrocell- and picocell-connected users) for different conditions. It indicates that all the users, both served by macrocell and picocell BSs, benefit from the data-offloading from macrocells to picocells. Specifically, 70% of the users with 10 picocells deployed per macrocell, the data rate increases from less than 500 kbps to more than 3 Mbps, an increase of 6 times.

1.1.3 Technical Challenges of HetNet Deployment

In a typical HetNet topology, enhanced small cells should be able to be flexibly deployed with or without macrocell coverage, in outdoor and indoor environments, by using both ideal and non-ideal backhaul connections [42]. Consequently, the cellular network topology will be fundamentally changed and some long-standing modeling, design, and optimization principles well known in the macrocell-only age will need to be adjusted extensively. This in turn introduces new technical challenges [20]. In this section, the most important aspects on the cellular

[1]Common pilot channel (CPICH) in 3GPP-based HSPA system

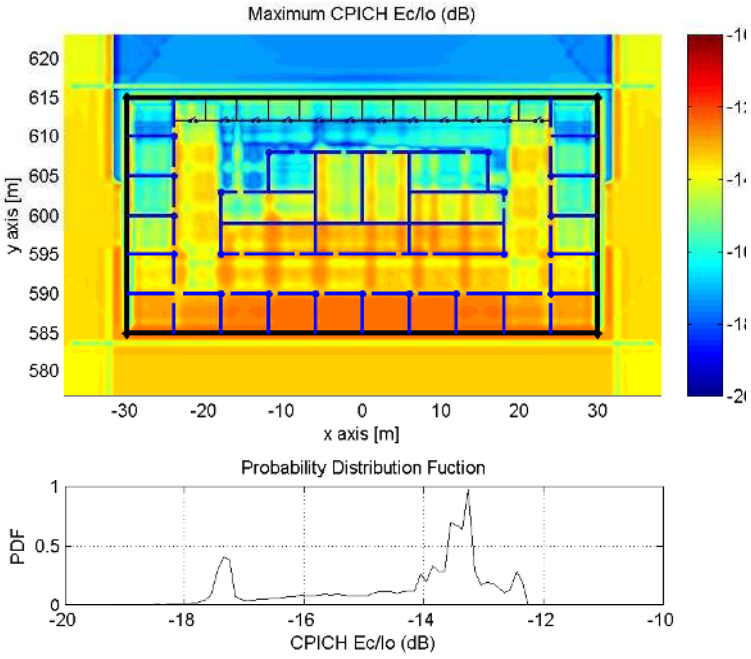

(a) Without Femtocell BS deployed indoor

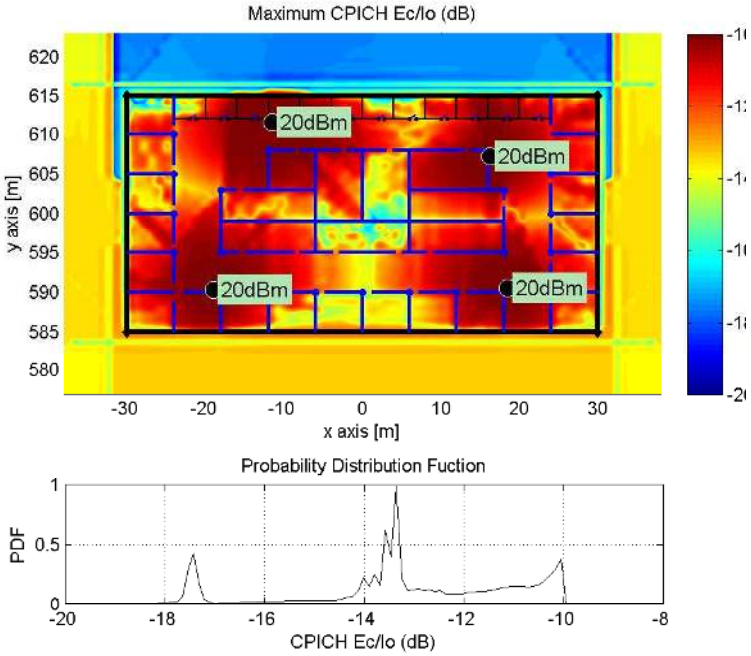

(b) With 4 Femtocell BS deployed indoor

Figure 1.2: Illustration of cellular coverage for an enterprise scenario, without or with 4 HSPA-based femtocell BSs deployed indoor. The heat maps and PDFs of maximum pilot channel (CPICH) E_c/I_o are demonstrated.

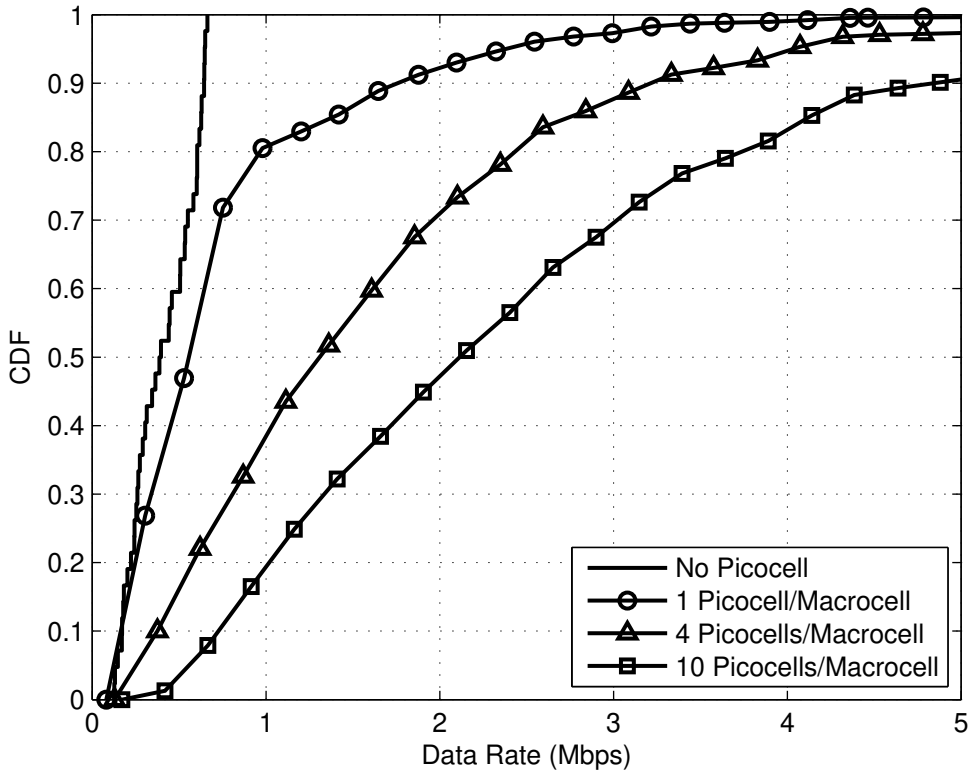

Figure 1.3: Illustration of the improvement on single user data rate by offloading users to picocells. The CDF curves are demonstrated for different scenarios, where 1, 4, and 10 HSPA-based picocells are deployed in the region originally covered by one macrocell.

network theory and implementation will be presented.

The Impact of Cell Load

In traditional macrocell-only network, macrocell BSs generally cover relatively large regions and support a large number of users. Thanks to the law of large numbers (LLN), a strong correlation between downlink received signal-to-interference-plus-noise (SINR) and achieved data rate at each user can be observed [20]. Because of the presence of this correlation, the received SINR distribution can be representative enough to characterize the achievable single user data throughput [43].

However, in the heterogeneous deployment, the cell load plays an increasing role in determining the data rate obtainable for each user terminal. Covering fairly limited areas, small cells are frequently lightly-loaded (i.e., associated with a small

number of users), and the correlation between received SINR and achievable data rate becomes weak as LLN is not applicable any more: The data traffic throughput performance will significantly vary from lightly-loaded cells to heavily-loaded cells [20, 44, 45]. The impact of cell load should be taken into consideration when the analysis of HetNets is conducted [46].

Cell Association Policy

In a homogeneous macrocell-only network, mobile users are typically assumed to connect to the BSs with the strongest signal strength, that is, the BS providing maximum long-term downlink received power, whereas the unwanted signals received from other BSs are treated as interference usually to be minimized accordingly. However, to decide the cell association policy in a HetNet deployment, it is necessary to take into account the newly introduced factors, such as uplink-downlink imbalance, cell load disparity, and the femtocell user association settings such as closed subscriber group (CSG) mode.

As mentioned in the previous section, the coverage areas of macrocells and small cells can be quite different owing to the large transmit power disparities. However, similar conclusions cannot be extended to the uplink scenario, where the strength of the received signal mostly depends on the terminal transmit power, which is the same for all classes of BSs. If the cell association policy is optimized for uplink only, that is, to enable users access the BSs providing the best uplink transmissions, the cell boundaries will be determined by the uplink path losses to each BS, which is extremely different from the downlink scenario [47]. This uplink-downlink imbalance creates difficulties in choosing an optimal cell association policy for both uplink and downlink at the same time, unlike the macrocell-only network scenario where uplink and downlink boundaries are closely matched [11]. Routing the uplink and downlink traffics into different BSs may be a possible solution, but it also generates more system design problems difficult to solve in the near future [20].

Another imbalance to be taken into account is the disparity of cell loads between macrocells and small cells [48]. The large coverage of macrocell BSs may limit the picocells' offloading effect, in which macrocell BSs are resource constrained while the picocell BSs are lightly loaded. Considering the cell loads in HetNet, the optimal cell association model does not necessarily require mobile users to access the strongest BSs, but aims to balance the loads between macro-

cells and small cells [44].

To deal with the above-mentioned imbalances of uplink-downlink and cell loads, an approach to incorporate a positive cell association bias for picocells, namely *cell range expansion*, has been widely studied [49–51]. By associating the mobile users with a picocell BS, although the downlink received power from the closest macrocell BS is higher, the cell range expansion expands the picocell coverage to mitigate the uplink-downlink imbalance [11]. Furthermore, by increasing the accessibility of picocell BSs to offload more users toward them, the cell range expansion enables a more equitable distribution of radio resources among all the users [44].

Unlike picocells, femtocell BSs may selectively serve users, namely operating in CSG mode in 3GPP terminology, in which cell access is not permissible to all users. In other words, only those users included in the femtocell's access control list, namely femtocell subscribers, are allowed to access the femtocell resources [30,52]. Such femtocells in CSG mode are commonly referred to as *closed femtocells*. As the nonsubscribers are not guaranteed to connect with the nearest BS, they probably experience and also generate significantly increased intercell interference which is generally undesired [53–55]. The closed femtocell can be regarded as an extreme opposite case of cell range expansion for the nonsubscribers, in which the femtocell coverage is shrunk to zero. Though generating a number of near-far interference issues and being not optimized for nonsubscribers [52, 53, 56, 57], CSG mode is still frequently preferred by the customers because of their demand for dedicated and secure femtocell environments [58,59].

Interference Management

Recent studies have already proven that increasing the density of co-channel BSs (even with different transmit power levels) will not deteriorate the received SINR distribution for a randomly chosen user terminal [60–62], given the condition that all the BSs are randomly placed and the user can access the strongest BS in the downlink. The main cause of this phenomenon is that the increased interference level from denser neighboring BSs is counterbalanced by the better serving signal from the closer serving BS [20,61].

However, in practical scenarios, there are the cell range expanded picocells (with positively biased cell association) and closed femtocells (with negatively biased cell association for nonsubscribers) as mentioned in the previous section.

Both techniques force some mobile users not to access the BSs with the strongest downlink signals and the best received SINR, which in turn prevents them from establishing and maintaining reliable communications with their serving cells and poses further difficulties on interference management:

- ***Cell Range Expanded Picocell***: In the uplink, intercell interference can be significantly mitigated as the cell boundaries are pushed away from picocells. In the downlink, more interference from the macrocell BS can be received by the picocell users located in the expanded regions, which leads to degraded downlink signal quality [49, 63].

- ***Closed Femtocell***: In the uplink, the power control scheme implemented in nonsubscriber terminal increases the transmit power level to compensate for the path losses to its far serving macrocell, jamming the uplink of the nearby closed femtocell(s). In the downlink, the closed femtocell BSs generate dead zones (otherwise known as coverage holes) for nonsubscribers that are effectively jammed by signals from close-by femtocell BSs [64, 65]. Considering the unplanned nature of femtocell deployment, the interference conditions can be severe in some particular locations.

If extra spectrum is available, multiple-carrier deployment will substantially simplify interference management in both the above-mentioned scenarios [66–69]. For instance, by operating macrocells and the cell range expanded picocells on dedicated frequency carriers, we can guarantee the transmit power levels, and biasing characteristics are the same for all the BSs on each of the component carriers, which makes each frequency layer homogeneous [30]. Similarly, in a heterogeneous deployment, if orthogonal spectrum bands are assigned to macrocells and closed femtocells, a nonsubscriber can avoid coverage holes by simply staying at the macrocell-dedicated carrier [59]. Although multiple-carrier deployment effectively mitigates the potential interference problem, this method is inefficient in terms of spectrum reuse [54] and sometimes infeasible because of the lack of multiple frequency bands for HetNet deployment [17]. Although far more complicated from the technical perspective, operators are more interested in the efficient co-channel HetNet deployment, in which the following interference management techniques can be further considered:

- ***eICIC in Picocell***: As mentioned, picocell users in the cell-expanded regions will suffer severe interference from nearby macrocell BSs. To address

this challenge, time-domain enhanced inter-cell interference coordination (eICIC) technique was proposed [37, 70]. In the eICIC scheme adopted in LTE release 10, the dominant interfering macrocell BS blanks specific subframes so that an interference-free communication tunnel can be established between the mobile user in the cell-expanded region and the serving picocell. The blanked subframes are referred to as *almost blank subframes* (ABSFs) in 3GPP terminology, indicating that some basic physical channels, for example, pilot, synchronization, and broadcast channels, may still be transmitted, so as to support backward compatibility with legacy LTE release 8 terminals [71, 72]. The eICIC scheme based on ABSF is proved to be effective in mitigating downlink intercell interference for range expanded picocells [37], and there were extensive studies to propose and evaluate new scheduling algorithms in optimizing eICIC's resource allocation [63, 73–75].

- ***Uplink Attenuation in CDMA Femtocell***: For the code division multiple access (CDMA)-based femtocell BSs co-channel operated with existing macrocell network, significant uplink interference from the nearby uncontrolled nonsubscribers can be experienced. As mentioned earlier, this uplink interference problem can be much severer for closed femtocells, especially when we consider the fact that the minimum coupling loss between terminals and femtocell BSs can be as low as 30-40 dB [65, 76]. Furthermore, the out-of-band radiation from femtocell BSs operating in adjacent bands also contributes to the uplink interference particularly in dense deployments [24]. The technique, uplink attenuation, can be utilized to mitigate the interference of this case [65, 77]. Specifically, in the presence of high out-of-cell interference, attenuation is applied at the femtocell uplink receiver to bring the level of out-of-cell interference down to be comparable to the thermal noise level [77], which is performed by an analog attenuator prior to analog-to-digital convertor (ADC). The aim for this uplink attenuation is to ensure that the noise rise of the resultant signals remains below a system-defined threshold such that the femtocell signal acquisition unit can function normally.

- ***Downlink Transmit Power Self-Calibration in Femtocell***: When the downlink transmit power for a femtocell BS is determined, the impact of femtocells on existing macrocell networks and the need to maintain good femtocell coverage should be balanced. As the femtocell coverage is

highly related to its relative location with neighboring macrocell BSs, a self-calibration algorithm with minimal network intervention can be employed to adapt femtocell transmit downlink powers depending upon received macrocell signal levels [65]. By adaptively adjusting the transmit power level, the femtocell can minimize the interference onto nonsubscribers while maintaining satisfactory coverage for femtocell subscribers [78, 79].

Mobility Management

In cellular networks, one of the most important aspects in mobility management is handover, which involves the effort to maintain QoS in connected mode when transferring a user terminal's active connection from its serving cell to a target cell [80, 81]. In conventional macrocell-only network, the same set of handover-related parameters, such as handover hysteresis and time to trigger [82], is usually configured throughout the network. However, because of the heterogeneous characteristics for different kinds of access techniques and particular cell association requirements, cell-specific handover parameters should be optimized individually [83–85]. For example, when high-mobility terminals pass through the small cell coverage areas, unnecessary handovers (otherwise known as called ping-pongs) are performed if the handovers are easy to be triggered. Provided, on the other hand, the users intrude deep into small cell regions before handover occurs and thus experience handover failures when the serving signals from macrocell BSs are degraded quickly, this is also not a good outcome. To balance the tradeoff between ping-pongs and handover failures, mobility-based solutions are needed and were proposed [86].

1.2 Security Enhancement in Future Cellular Networks

Reducing macrocell cell size and introducing HetNet are associated with the aim of improved cellular coverage and rate; however, there are still other aspects to be taken care of, one of them being security. Because of the broadcast nature of the wireless medium, cellular systems are vulnerable and susceptible to attacks, which always make the security be a crucial issue in the research. Specifically, the cellular network designers always have to face the challenges presented by

an unauthorized receiver located within the transmission range and capable of eavesdropping the unicast transmissions toward legitimate users, and this factor will not change in the near future.

Traditionally, most security techniques in modern cellular standards, such as Wideband CDMA (WCDMA) and LTE, involve means of encryption algorithms in the upper layers of the protocol stacks, e.g., medium access control (MAC) and other layers above physical layer [87,88]. Based on a hard mathematical problem, these cryptographic techniques provide computational-based security. It ignores the message transmission phase and only aims to prevent the malicious users to extract the secret information from the received bit sequence. Typically, the security is guaranteed if the malicious users do not have sufficient computational capacity to solve some mathematical problem. For such techniques, although the expenditure of interception may be very high, providing robust encryption algorithms is becoming ever more challenging, due to the continuing development of computing devices.

1.2.1 Physical Layer Security

As the data security is so critically significant, it is desirable to seek for additional protection that can complement cryptography. One promising concept is achieving information-theoretic security in the physical layer of wireless networks, that is, *physical layer security*, which protects the message transmission phase by exploiting the physical properties of the wireless channel, such as noise, interference, and fading.

The foundation of physical layer security is laid by Wyner. In his pioneering study, the wiretap channel model for point-to-point communication was proposed [89], which was extended to broadcast channels with confidential messages by Csiszár and Körner [90]. Based on these initial results, a positive secrecy capacity, defined as the maximum transmission rate at which the eavesdropper is unable to obtain any information, can be achieved if the intended receiver enjoys a better channel than the potential eavesdropper. Compared with classical computational security, the main advantage of physical layer security is perfect secrecy achievable, but with no computational restrictions required to be placed on the eavesdroppers.

In this thesis, we consider physical layer security as a new security enhancement for future cellular networks. Different from other large-scale networks (such

as ad hoc networks), there are unique characteristics owned by cellular networks. For instance, cellular networks own the carrier-operated high-speed backhaul networks connecting individual BSs and the core-network infrastructures, which provide us potential means of BS cooperation, such as associating mobile users to the optimal BS with secrecy considerations and exchanging information to guarantee better secure links. Considering the fact that the cellular service area is divided into cells, each BS is able to know the circumstances within its own cell (e.g., the location as well as the identity of each user, that is, whether the user is a potential eavesdropper or not). The identity and location information of mobile users in the other cells can be obtained by information exchange between BSs via the backhaul networks.

1.3 Modeling of Cellular Networks

From both industrial and academic viewpoints, one of the most important topics is to model cellular networks in an appropriate way, thus evaluating related network metrics, such as cellular coverage, achievable rate, and secrecy performance. As the cellular network is undergoing the transformation from macrocell-only to heterogeneous deployment, the increased topology complexity proposes new challenges in network modeling [20, 91].

1.3.1 Grid Model and System-Level Simulation

For macrocell-only networks where BSs are usually set apart evenly, placing the BSs on a two-dimensional grid (e.g., a square lattice or a more widely used hexagonal lattice according to the idealized cellular structure) with mobile users either randomly or deterministically located is commonly accepted for network modeling [8]. Although analytical results can be obtained for particular user-locations in the simplified grid model considering only limited number of interferers [18], analytical expressions of the received SINR and other useful performance metrics are unavailable for more general cases, such as a randomly located typical mobile user. System-level simulations based on this grid model have been extensively employed in both research and industry evaluations [8, 92].

However, the drawbacks of the grid-model-based simulation are also serious. In addition to the immense effort in building a simulator and the inefficient Monte Carlo simulations involved, this method is disadvantaged by the difficulty to val-

idate other organizations' scenarios and interpret the results. More importantly, because of its intractability, it is impossible to efficiently identify the key design parameters and their corresponding impacts on system performance through the grid-model-based simulations [43]. It should be noted that the grid model only represents a highly idealized scenario with regularly placed cells, different from real deployments, where the cell areas noticeably vary because of the practical considerations, such as the availability of certain site locations, parameters specifically tuned for each BS, and so on.

1.3.2 Wyner Model

The Wyner model is another widely accepted model to capture the cellular interactions among multiple BSs [93]. As a more tractable model compared with the above-mentioned grid model, the Wyner model typically simplifies the interference environment to one dimension, in which equal channel gains from limited number of neighboring interfering BSs are assumed [93–95]. This oversimplified model is accurate when the roughly constant interference exists due to a large number of simultaneous interferers over the space, thus making this model ideal for the scenario of a loaded CDMA uplink [96]. Nevertheless, for future cellular networks (e.g., LTE and WiMAX) with orthogonal multiple access such as the orthogonal frequency-division multiplexing (OFDM) systems, the Wyner model's assumptions become particularly inaccurate because the performance highly depends on the user locations [97]. To investigate the network-wise performance metrics for OFDM-based future cellular networks, we need a network model that can precisely characterize the performance impact of users' relative locations.

1.3.3 Stochastic Geometry Model

Currently, stochastic geometry [98] is proved to be a helpful mathematic tool in analyzing large-scale wireless networks [99]. By assuming wireless communication nodes scattered according to certain spatial random distribution, the network model based upon stochastic geometry allows us to study the probabilistic network behaviors and corresponding performance metrics [100–102].

Among the different kinds of spatial distributions, Poisson point process (PPP) is ideal to model the set of communication nodes contained in large-scale wireless networks [103]. Mathematically, a two-dimensional homogeneous PPP can

be defined by the requirement that the random variables (defined as the counts of the number of points inside each of a number of non-overlapping finite subregions of $\mathbb{R}^2$) should each have a Poisson distribution and should be independent of each other [98]. Different from the regular grid-based model, scattering wireless nodes according to spatial PPP introduces total randomness for the node deployment, and only the node density variable is required to characterize this stochastic process. Counter-intuitively, the randomness introduced by the PPP-based model helps it to be more tractable in performance analysis, because it has closed-form results on interference and SINR distributions for certain signal attenuation laws [103, 104]. By accepting the PPP-based topology for random wireless networks, important results on connectivity, coverage, and throughput have been successfully derived [105–111].

The PPP-based model for cellular networks have been in use for more than 10 years [112,113]. In both the pioneering studies, the locations of macrocell BSs were considered as realizations of a stochastic point process, but the important key metrics related to practical engineering were still untouched. Brown *et al.* also adopted the PPP-based model and incorporated practical cellular factors (e.g., frequency reuse, shadowing fading) into their analysis [114, 115]. However, these studies did not compare the performance results obtained from this PPP-based model with practical cellular networks. Without necessary validation, it is difficult to persuade other researchers to accept and adopt this new model in their own studies.

Fortunately, Andrews *et al.* completed a validation for the PPP-based model in their recent studies [43,116]. It has been shown that compared with the practical network deployment, modeling the cellular network with BS locations drawn from a homogeneous PPP is as accurate as the traditional grid models. Although this validation was based upon the comparison with one practical cellular deployment, there is still a belief that macrocell deployment by operators becomes increasingly irregular and random network model becomes more suitable [117]. When the networks are densified, ideal macrocell locations are no longer available under the constraints of terrain, high concentrated buildings, and so on. In a newly finished study, Błaszczyszyn *et al.* provided another important justification for the PPP-based model: For any homogeneous BS distribution (including the one formed by grid models), as long as the log-normal shadowing variance is sufficiently high, any statistical measure based on the signal propagation is identi-

cal to an equivalent PPP-based model [118]. Furthermore, the PPP-based model was proved to be effective in evaluating particular cellular techniques, such as fractional frequency reuse [119, 120] and multi-cell cooperation [121, 122]. Different from the downlink scenarios mentioned earlier, the uplink can also be studied by the PPP-based network model, even considering the more complex intercell interference conditions with power control algorithms [123].

Stepping into the era of HetNets, the complexity of system-level simulations substantially grows with the increased number of BSs. For instance, several picocell BSs and dozens of femtocell BSs can be installed under a single macrocell BS coverage umbrella, which presents new challenges for traditional simulations based upon Monte Carlo experiments. Furthermore, the newly introduced small cells are prone to be irregularly spaced or even randomly scattered, which requires the network modeling to be robust to spatial randomness [124, 125]. To understand the impact of many important network parameters (e.g., cell association biasing) and to explore the depth insights on the diverse radio characteristics in HetNets, new tractable spatial modeling methodology is increasingly required. Considering flexible cell association, the received downlink SINR has been characterized by using the multi-tier version PPP-based models [57,60,61,126]. Because of the random deployment of femtocell BSs, the PPP-based model can also help to understand the co-channel-deployed femtocell network performance [69, 127, 128].

Moreover, this alteration of the impact of the cell load on throughput performance also requires us to focus more on "user perceived throughput distribution" in a HetNet (which considers data offloading to small cells and resource sharing between intracell users), rather than the general SINR received at the user terminal [20]. By studying the probabilistic characterization of the number of intracell users in different tiers [129], the resource sharing was well investigated to show the benefits brought by the small cell traffic offloading [46, 130].

1.4 Thesis Outline and Contributions

We outline of the rest chapters and emphasize the contributions of each chapter as follows:

Chapter 2 - Tractable Model for Heterogeneous Networks with Directional Antennas

In Chapter 2, an introductory description to the stochastic-geometry-based HetNet model is provided, and this model is also used as the basic methodology in the following Chapter 3 and Chapter 5.

Furthermore, as directional antennas are widely used to sectorize the macrocell cells in practical cellular systems, it is of importance to model and investigate the impact of directional antennas. The main contributions of this chapter are summarized as follows:

1. We extend the original HetNet model to the one which takes the impact of directional antennas into consideration. Furthermore, the coverage performance obtained from this extended model is still tractable even considering a complex directional antenna gain function.

2. Based upon the analysis in this chapter, we demonstrate the impact of directional antenna patterns on the coverage performance, which helps us to identify the performance gap between a practical directional antenna model and an ideal one.

The results in this chapter have been presented in the following publications which are listed again for ease of reference:

C3. He Wang and Mark C. Reed, "A novel tractable framework to analyse heterogeneous cellular networks", in *Proc. 6th IEEE Int'l Workshop on Heterogeneous, Multi-Hop, Wireless and Mobile Networks (GLOBECOM'11 Wkshps)*, Houston, USA, Dec. 2011, pp. 287-292.

C4. He Wang and Mark C. Reed, "Tractable model for heterogeneous cellular networks with directional antennas", in *Proc. 2012 Australian Commun. Theory Workshop (AusCTW'12)*, Wellington, New Zealand, Jan./Feb. 2012, pp. 61-65.

Chapter 3 - Analytical Evaluation on a Non-uniform Femtocell Deployment

Chapter 3 considers a two-tier cellular deployment scenario. For the heterogeneous networks containing the small cell tier, randomly deployed small cells do

not give any remarkable improvement in coverage probability [60–62]. The main cause of this phenomenon is the increased network interference from having more small cell BSs in the areas with satisfactory macrocell coverage, when the small cell BSs are uniformly deployed at random. This fact inspires us to raise one interesting question, that is,

Q. Whether or not we can improve both coverage and throughput performances by not using the small cell BSs (e.g., femtocell BSs) at undesirable locations, in other words, utilizing them non-uniformly?

To answer this question, Chapter 3 proposes and evaluates an intuitive way to non-uniformly deploy femtocell, based upon which the significance of selectively deploying the femtocell BSs is explored.

The proposed non-uniform femtocell deployment scheme is not complicated to realize: By defining the *inner region* as the union of locations within a prescribed distance from any macrocell BSs, and the *outer region* as the union of locations outside the inner region, the non-uniform femtocell deployment scheme simply avoids using femtocell BSs within the inner region. There are two ways to implement this non-uniform deployment scheme in practical, i.e., *femtocell deactivation* and *smart femtocell deployment*. In femtocell deactivation, the femtocell BSs located within the inner region are deactivated, which helps to reduce unnecessary operating expense from the decreased femtocell BS energy consumption. To implement smart femtocell deployment, femtocell BSs are deployed in the outer region only. The main contributions of this chapter are summarized as follows:

1. We propose the above mentioned non-uniform femtocell deployment scheme. In this scheme, femtocell BSs are not utilized in the region within a certain distance away from any macrocell BSs. Through two ways of implementations, namely, femtocell deactivation and smart femtocell deployment, we can guarantee that most of the active femtocell BSs are located in the relatively poor macrocell coverage areas.

2. By employing the PPP-based BS model in the analysis, we provide the probabilistic characterization of the downlink coverage and single user throughput at a randomly located mobile user in this new scheme. To our knowledge, it is the first study to derive analytical results on a non-uniform femtocell deployment.

3. For femtocell deactivation, we demonstrate that the same cellular coverage performance as the uniform femtocell deployment can be maintained if the size of the inner region is appropriately chosen. Our numerical result demonstrates that more than 50% of femtocell BSs can be turned off to save the femtocell BS energy consumption and thus operating expense, without compromising on the coverage performance.

4. For smart femtocell deployment, we show that both the coverage and single user throughput can be significantly improved over the uniform femtocell deployment. This finding demonstrates the performance improvements achievable by implementing a simple non-uniform femtocell deployment, which highlights the significance of selectively deploying the femtocell BSs, taking their relative locations with macrocell BSs into account.

The results in Chapter 3 have been presented in the following publications which are listed again for ease of reference:

J2. He Wang, Xiangyun Zhou, and Mark C. Reed, "Coverage and Throughput Analysis with a Non-uniform Femtocell Deployment", submitted to *IEEE Transactions on Wireless Communications*.

C6. He Wang, Xiangyun Zhou, and Mark C. Reed, "Analytical evaluation of coverage-oriented femtocell network deployment", in *Proc. IEEE Int'l Conf. on Commun. (ICC'13)*, Budapest, Hungary, June 2013, pp. 4567-4572.

Chapter 4 - Analysis on Femtocell Uplink Attenuation Algorithms

By implementing uplink attenuation in CDMA-based femtocell receivers, the intercell interference caused by nearby uncontrolled users can be mitigated significantly and the noise rise of the resultant signals staying below a system-defined threshold such that the femtocell signal acquisition unit can function normally.

As a result of the uplink attenuation operation to desensitize the receiver, users connected to the femtocell BSs increase their transmit power to overcome the attenuation, thus generating higher uplink interference to nearby BSs [131, 132] and causing an increase in the power consumption of attached femtocell users. Additionally, because the maximum power of femtocell users may be restricted to avoid the impact on macrocells [40], the increased transmit power level due to

uplink attenuation might increase the chance of outage events at the edge of the femtocell, if certain SINR levels at the receiver need to be maintained.

In order to balance the interference mitigation effect and increased femtocell user transmit power, Chapter 4 focuses on analyzing the impact of uplink attenuation algorithms on the system performance. Specifically, the main contributions of this chapter are summarized as follows:

1. We analyze femtocell's uplink environment where the uplink attenuation technique is implemented, and derive an analytical result of the outage probability under certain fixed level of uplink attenuation.

2. We demonstrate the tradeoff between higher level uplink attenuation resulting in a higher probability to reach the maximum power cap and lower level attenuation with less interference mitigation. Based on this tradeoff given by the analytical result, the fixed optimal uplink attenuation factor which minimizes the outage probability is determined, which is beneficial to practical system design.

3. In this chapter, we propose two adaptive uplink attenuation algorithms, both of which aim to minimize the outage probability by adaptively adjusting the uplink attenuation factor based upon the information of the scheduled traffic, SINR requirements for each femtocell user, and the current interference power at femtocell receiver. Simulation Results show that both adaptive schemes are able to achieve better performance improvement over the traditional algorithm.

The results in this chapter have been presented in the following publications which are listed again for ease of reference:

C1. He Wang, Ming Zhao, and Mark C. Reed, "Outage analysis for WCDMA femtocell with uplink attenuation", in *Proc. IEEE 1st Int'l Workshop on Femtocell Networks (GLOBECOM'10 Wkshps)*, Miami, USA, Dec. 2010, pp. 664-668.

C2. He Wang, Ming Zhao, and Mark C. Reed, "Optimal adaptive uplink attenuation algorithms for WCDMA femtocell", in *Proc. IEEE Global Commun. Conf. (GLOBECOM'11)*, Houston, USA, Dec. 2011, pp. 1-5.

Chapter 5 - Physical Layer Security in Large-Scale Cellular Networks

In Chapter 5, we focus on investigating the secrecy performance in large-scale cellular networks. As mentioned in Section 1.2, achieving information-theoretic security by protecting the physical layer of wireless networks is an promising way to guarantee secrecy communications for future cellular networks; however, most of the previous studies on security communications in large-scale networks were concentrated on ad hoc networks.

Chapter 5 provides the analytical results to quantify the secrecy rate performance. Specifically, the following secure communication links are under investigation: Confidential messages are prepared to be conveyed to a mobile user, while certain other mobile users should not have the access to the messages and hence are treated as potential eavesdroppers. The serving BS should ensure the messages delivered to the intended user successfully while keeping perfect secrecy against all potential eavesdroppers.

Several attention-grabbing questions about achieving information-theoretic security in large-scale cellular networks can be raised as follows:

Q1. If BS information exchange via the backhaul networks is ideal, i.e., the serving BS fully acquires potential eavesdroppers' location information, what is the secrecy rate achievable at a randomly located mobile user?

Q2. Comparing with connecting to nearest BS, how much performance improvement can be obtained by optimally choosing the serving BS?

Q3. How will the performance be degraded if the information exchange between BSs no longer exists?

Q4. To achieve a certain level of secrecy performance, how many nearby BSs should participate in the information exchange between BSs?

Aiming to answer the above questions, we provide analysis on the probability distribution of the secrecy rate and hence the average secrecy rate achievable for a randomly located mobile user in a large-scale cellular network, in which different assumptions are made on the cell association and location information exchange between BSs. The major contributions of this chapter are summarized as follows:

1. Through the analysis by using the PPP-based stochastic geometry model for BS distribution, we quantify the secrecy rate performance in large-scale

cellular networks, taking into account the unique characteristics owned by cellular networks.

2. In this chapter, we identify and analyze a unique feature of secure transmissions, i.e., the optimal BS is often not the nearest BS. Our results show that only marginal gain can be obtained by optimally choosing the serving BS rather than associating to the nearest one. In other words, keeping the nearest BS to be used for secure transmission still achieves near-optimal secrecy performance, which is a very useful message to the network designers.

3. Our analysis sheds light into the impact of the availability of eavesdroppers' location information on the achievable secrecy rate. In particular, the secrecy performances for the scenarios with no location information exchange and limited exchange with neighboring cells are derived, which demonstrate the critical role of this kind of BS cooperation. This result provides network designers with practical guidelines in deciding on the necessary information exchange range, i.e., how many nearby BSs should participate in the information exchange for achieving a certain level of secrecy performance.

The results in this chapter have been presented in the following publications which are listed again for ease of reference:

J1. He Wang, Xiangyun Zhou, and Mark C. Reed, "Physical layer security in cellular networks: A stochastic geometry approach", *IEEE Trans. on Wireless Commun.*, vol. 12, no. 6, pp. 2776-2787, Jun. 2013.

C5. He Wang, Xiangyun Zhou, and Mark C. Reed, "On the physical layer security in large scale cellular networks"', in *Proc. 2013 IEEE Wireless Commun. and Networking Conf. (WCNC'13)*, Shanghai, China, Apr. 2013, pp. 2503-2508.

Chapter 2

Tractable Model for Heterogeneous Networks with Directional Antennas

2.1 Introduction

A proper model for cellular networks is frequently the first step in an evaluation task, aiming to achieve performance metrics like cellular coverage, achievable rate, and secrecy performance. Since directional antennas are widely used to sectorize the original macrocell cells in practical cellular systems, it is interesting to investigate the impact by employing antennas other than omni-directional ones, which is commonly regarded as the default antenna patterns for stochastic-geometry-based BS model.

Recently, utilizing stochastic geometry to develop a new large-scale cellular network model has attracted much attention in the research community [43, 57, 60, 61, 116, 117, 119, 125–130]. Compared with traditional methods, such as the grid model and the Wyner model, this newly proposed approach utilizes a certain distributed point process to model the locations of BSs. Accordingly, mathematical results on stochastic geometry can be used to study the average behavior over different spatial realizations of this random network model. Recent studies have shown that the network models with BS locations drawn from a PPP can be as accurate as the traditional grid models, compared with an actual cellular network deployment for both single-tier and multiple-tier scenarios [43, 61]. By providing a more tractable analytical method, the PPP-based model gives the

pessimistic lower bound on the coverage performance and other related metrics. Furthermore, the geometry characteristics of user-planned or unplanned BS locations in HetNets can be well captured by this stochastic geometry model, which makes the PPP-based model even more suitable for HetNets.

The remainder of the chapter is organized as follows. Firstly, the PPP-based HetNet model is introduced in Section 2.2, in which the corresponding analytical result on the coverage performance is also provided. It should be noted that the tractable framework in Section 2.2 has been presented already by Jo *et al.* [60]. Nevertheless, the content in this section provides the necessary introduction of the PPP-based HetNet model not only for the remaining parts of this chapter, but also for the following Chapter 3 and Chapter 5 in which this methodology is adopted.

Considering the directional antenna patterns used in practical cellular deployment, we extend the original tractable model for downlink HetNet (in which all tiers employ omni-directional antennas) to the one with directional antennas in Section 2.3. Based on our analysis in Section 2.4, the expression for coverage probability is still easy to calculate even considering a complex directional antenna gain function. By investigating the numerical results obtained from the extended model, the impact of implementing directional antennas is demonstrated in Section 2.5, which leads us to the conclusion in Section 2.6.

2.2 The PPP-based HetNet Model and Coverage Performance

A K-tier HetNet consisting of macrocell, picocell and/or femtocell BSs is assumed in this analysis, where spatial deployment densities and transmit powers may be different across tiers. BSs in the i-th tier are spatially distributed as a homogeneous PPP Φ_i with density λ_i in the whole Euclidean plane, which have the same transmit power value $P_{\mathrm{TX},i}$.

In this chapter, we consider an independent collection of mobile users, located according to some independent homogeneous point process. Without any loss of generality, we assume that the randomly chosen mobile user under analysis is at the origin, which is otherwise called the *typical user* in our following study.

The standard power loss propagation model is used with path loss exponent $\alpha > 2$ and path loss constant L_0 at the reference distance $r_0 = 1$ m. (L_0 is

regarded as a constant in this analysis since shadowing effect is excluded here.) To include the random channel effects such as fading and shadowing, we assume that the typical mobile user experiences independent Rayleigh fading from the serving and interfering BSs. The noise power is additive and constant with value σ^2, but no specific distribution is assumed in general.

2.2.1 Cell Association Model

In our analysis, we assume that all BSs are open access and the mobile users are connected to the BS providing maximum long-term received power, which can be regarded as a widely used special case [43] of the general cell association model [60]. Different from the cell association model employed in [61], we define the long-term received power from an i-th tier BS located at x as $P_{\mathrm{TX},i}L_0\|x\|^{-\alpha}$. Consequently, the resultant cell association model can average out the fluctuation caused by Rayleigh fading and eliminate unnecessary handovers when the mobile users are located not far from cell boundaries. Here, κ and φ are respectively the selected tier number and the BS location, i.e.,

$$[\kappa, \varphi] = \arg \max_{i\in\mathbb{K}, x\in\Phi_i} \left[P_{\mathrm{TX},i}L_0\|x\|^{-\alpha}\right], \tag{2.1}$$

in which $\mathbb{K} \triangleq \{1, 2, \cdots, K\}$. For simplicity, we use P_i to replace the product of $P_{\mathrm{TX},i}$ and L_0 in this chapter, i.e., $P_i = P_{\mathrm{TX},i}L_0$ for $i \in \mathbb{K}$.

The cell association regions for a three-tier HetNet with this cell association model can be demonstrated in Fig. 2.1, where the cell boundaries for macrocells, picocells and femtocells are marked by different colors.

Remark. Different from associating to the BS providing the maximum instantaneous SIR or SINR in [57, 61, 133], we employ the above cell association model to simulate practical mobility management. In cellular networks, such as WCDMA and LTE [134], the mobile terminals perform cell access or cell reselection based on their received pilot channel power levels, and the measurement is performed over enough resource blocks in LTE (or time intervals in WCDMA) to averaged out the frequency-selective fading and fast fading, thus primarily taking large-scale propagation effects (such as path loss and shadowing effects) into account. Therefore, associating mobile users to the BS with maximum instantaneous SIR or SINR (even it is due to a peak value of a fast fluctuation) is not always a reasonable assumption compared with the model used here.

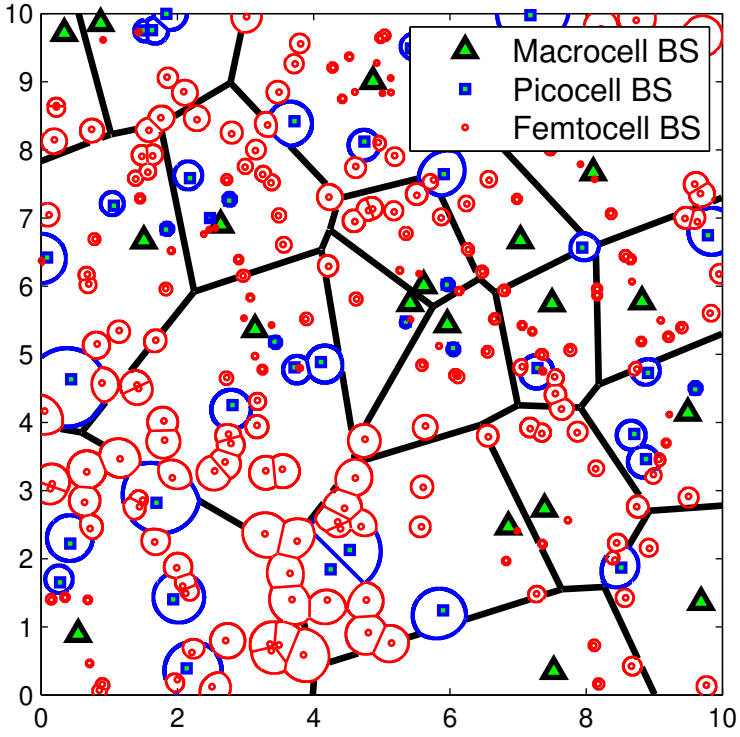

Figure 2.1: Cell association regions in a three-tier cellular network (macrocell, picocell and femtocell tiers), with density ratio $\lambda_3 = 4\lambda_2 = 20\lambda_1$. Transmit power levels have the relationship of $P_{1,tx}/P_{2,tx} = 11$dB and $P_{1,tx}/P_{3,tx} = 26$dB.

2.2.2 Tractable Framework on Coverage Probability

Based upon the above-mentioned cell association model, all the interfering BSs must have smaller values of long-term received power levels. Accordingly, the received downlink SINR expression is

$$\text{SINR} = \frac{P_\kappa h \|\varphi\|^{-\alpha}}{I + \sigma^2}, \tag{2.2}$$

in which h denotes the channel fading gain from the serving BS, and I is the cumulative interference from all BSs except the κ-th tier BS located at φ (the serving BS for the typical user), i.e.,

$$I = \sum_{i \in \mathbb{K}} I_i = \sum_{i \in \mathbb{K}} \sum_{x \in \Phi_i \setminus \{\varphi\}} P_i h_x \|x\|^{-\alpha}, \tag{2.3}$$

where h_x is the value for the interfering BS at the location of x, and I_i is defined as the interference component from the i-th tier. Based upon the above-mentioned Rayleigh fading assumption, all these channel fading gains, h and $\{h_x : x \in \Phi_i\}$, follow the exponential distribution with the unitary mean value. In this study, no intracell interference is included since the orthogonal multiple access within a cell is assumed.

The coverage probability at the typical user is defined as

$$p_c(T) = \mathbb{P}[\text{SINR} > T], \tag{2.4}$$

that is, the probability of a target SINR T (or SINR threshold) achievable at the typical user. This coverage probability is also exactly the complementary cumulative distribution function (CCDF) of the received SINR. Similar to the methodology in [60], we present the general procedure to obtain the analytical result on the coverage performance as follows.

Firstly, we define the maximum value of the long-term received powers from all BSs as $P_{LT,\max}$, i.e.,

$$P_{LT,\max} \triangleq P_\kappa \|\varphi\|^{-\alpha}. \tag{2.5}$$

Hence, for the typical user in a K-tier HetNet with the above-mentioned cell association model, the coverage probability can be derived as

$$\begin{aligned} p_c(T) &= \mathbb{P}\Big[\frac{P_\kappa h \|\varphi\|^{-\alpha}}{I+\sigma^2} > T\Big] \\ &\overset{(a)}{=} \int_0^\infty \mathbb{P}\Big[\frac{P_\kappa h \|\varphi\|^{-\alpha}}{I+\sigma^2} > T \mid P_{LT,\max} = t\Big] f_{P_{LT,\max}}(t)\mathrm{d}t \\ &\overset{(b)}{=} \int_0^\infty \mathbb{P}\Big[h > \frac{T(I+\sigma^2)}{t} \mid P_{LT,\max} = t\Big] f_{P_{LT,\max}}(t)\mathrm{d}t \\ &\overset{(c)}{=} \int_0^\infty \exp(-\frac{T\sigma^2}{t}) \mathcal{L}_I(\frac{T}{t} \mid P_{LT,\max} = t) f_{P_{LT,\max}}(t)\mathrm{d}t, \end{aligned} \tag{2.6}$$

in which

- step (a) converts the original probability into the integral of the conditional probability;
- step (b) is based on the definition of $P_{LT,\max}$;
- step (c) follows the Rayleigh fading assumption, i.e., $h \sim \exp(1)$, and $\mathcal{L}_I(\cdot \mid P_{LT,\max})$ is the Laplace transform of the cumulative interference I when

the maximum long-term received power from all BSs is $P_{LT,\max}$, i.e., $\mathcal{L}_I(s \mid P_{LT,\max}) = \mathbb{E}_I\big[e^{-sI} \mid P_{LT,\max}\big]$.

It should be noted that $\exp(-T\sigma^2/t)$ and $\mathcal{L}_I(\frac{T}{t} \mid P_{LT,\max} = t)$ respectively represent the impact of the noise and the interference.

Based upon the above definition, the CDF of the random variable $P_{LT,\max}$ can be derived as

$$\begin{aligned} F_{P_{LT,\max}}(t) = \mathbb{P}\Big[P_\kappa \|\varphi\|^{-\alpha} \leqslant t\Big] &\overset{(a)}{=} \prod_{i\in\mathbb{K}} \mathbb{E}_{\Phi_i}\Big[\prod_{x\in\Phi_i} \mathbf{1}\big(P_i\|x\|^{-\alpha} \leqslant t\big)\Big] \\ &\overset{(b)}{=} \prod_{i\in\mathbb{K}} \exp\Big(-\pi\lambda_i\big(\frac{P_i}{t}\big)^{2/\alpha}\Big) \\ &= \exp\Big(-\pi\sum_{i\in\mathbb{K}} \lambda_i P_i^{2/\alpha} t^{-2/\alpha}\Big), \end{aligned} \tag{2.7}$$

where $\mathbf{1}(\cdot)$ is the indicator function, which is equal to 1 if the input event is true and 0 otherwise. It should be noted that step (a) is obtained due to the independence between different tiers, and step (b) follows the PPP's void probability, that is, the probability that the region $\mathcal{X}$ contains no point drawn from the homogeneous PPP with the density value of λ is $\exp\big(-\lambda A(\mathcal{X})\big)$, in which $A(\mathcal{X})$ is the area measure of the region $\mathcal{X}$ [98]. Consequently, the PDF can be found as

$$\begin{aligned} f_{P_{LT,\max}}(t) &= \frac{\mathrm{d}F_{P_{LT,\max}}(t)}{\mathrm{d}t} \\ &= \frac{2\pi}{\alpha}\big(\sum_{i\in\mathbb{K}} \lambda_i P_i^{2/\alpha}\big)\cdot(t^{-\frac{2}{\alpha}-1})\exp\Big[-\pi\big(\sum_{i\in\mathbb{K}} \lambda_i P_i^{2/\alpha}\big)\cdot t^{-\frac{2}{\alpha}}\Big]. \end{aligned} \tag{2.8}$$

On the other hand, the Laplace transform $\mathcal{L}_I(\frac{T}{t} \mid P_{LT,\max} = t)$ in (2.6) is

$$\begin{aligned} &\mathcal{L}_I(\frac{T}{t}|P_{LT,\max} = t) \\ &= \mathbb{E}_I\big[\exp(-\frac{T}{t}\cdot I) \mid P_{LT,\max} = t\big] \\ &\overset{(a)}{=} \prod_{i\in\mathbb{K}} \mathbb{E}_{\Phi_i}\big[\exp(-\frac{T}{t}\cdot\sum_{x\in\Phi_i\setminus\{\varphi\}} P_i h_x \|x\|^{-\alpha}) \mid P_{LT,\max} = t\big] \\ &\overset{(b)}{=} \prod_{i\in\mathbb{K}} \mathbb{E}_{\Phi_i}\Big[\prod_{x\in\Phi_i\setminus\{\varphi\}} \mathbb{E}_{h_x}\Big[\exp\big(-\frac{T}{t}P_i h_x\|x\|^{-\alpha}\big)\Big] \mid P_{LT,\max} = t\Big] \\ &\overset{(c)}{=} \prod_{i\in\mathbb{K}} \mathbb{E}_{\Phi_i}\Big[\prod_{x\in\Phi_i\setminus\{\varphi\}} \frac{1}{1+\frac{T}{t}P_i\|x\|^{-\alpha}} \mid P_{LT,\max} = t\Big], \end{aligned} \tag{2.9}$$

in which

- step (a) follows the definition of the cumulative interference I in (2.3) and the independence between different tiers;

- step (b) is based on the independence among $\{h_x : x \in \Phi_i\}$ and their further independence from the PPPs $\{\Phi_i : i \in \mathbb{K}\}$;

- step (c) is derived according to the Rayleigh fading assumption for all the interferers, i.e., $h_x \sim \exp(1)$. Specifically, the inner expectation expression can be derived as

$$\begin{aligned}\mathbb{E}_{h_x}\big[\exp(-\frac{T}{t}P_i h_x \|x\|^{-\alpha})\big] &= \int_0^\infty \exp(-\frac{T}{t}P_i\|x\|^{-\alpha}g) f_{h_x}(g)\mathrm{d}g \\ &= \int_0^\infty \exp(-\frac{T}{t}P_i\|x\|^{-\alpha}g)\exp(-g)\mathrm{d}g \\ &= \frac{1}{1+\frac{T}{t}P_i\|x\|^{-\alpha}}. \end{aligned} \tag{2.10}$$

Based upon the result for PPP's probability generating functional (PGFL) [98], $\mathcal{L}_I(\frac{T}{t}|P_{LT,\max}=t)$ can be further derived as

$$\begin{aligned}\mathcal{L}_I(\frac{T}{t}|P_{LT,\max}=t) &= \prod_{i\in\mathbb{K}} \mathbb{E}_{\Phi_i}\Big[\prod_{x\in\Phi_i\setminus\{\varphi\}} \frac{1}{1+\frac{T}{t}P_i\|x\|^{-\alpha}} \mid P_{LT,\max}=t\Big] \\ &\overset{(a)}{=} \prod_{i\in\mathbb{K}} \exp\Big(-2\pi\lambda_i \int_{\left(\frac{P_i}{t}\right)^{\frac{1}{\alpha}}}^\infty \Big(1-\frac{1}{1+\frac{T}{t}P_i v^{-\alpha}}\Big) v\mathrm{d}v\Big) \\ &= \prod_{i\in\mathbb{K}} \exp\Big(-2\pi\lambda_i \int_{\left(\frac{P_i}{t}\right)^{\frac{1}{\alpha}}}^\infty \Big(\frac{1}{1+\frac{v^\alpha}{TP_i/t}}\Big) v\mathrm{d}v\Big) \\ &\overset{(b)}{=} \prod_{i\in\mathbb{K}} \exp\Big(-2\pi\lambda_i \int_{T^{-2/\alpha}}^\infty \frac{1}{1+u^{\alpha/2}}\cdot\frac{1}{2}\cdot\Big(\frac{TP_i}{t}\Big)^{2/\alpha}\mathrm{d}u\Big) \\ &\overset{(c)}{=} \prod_{i\in\mathbb{K}} \exp\Big(-\pi\lambda_i\Big(\frac{P_i}{t}\Big)^{2/\alpha}\rho(T,\alpha)\Big), \end{aligned} \tag{2.11}$$

in which

- step (a) is derived because of the result for PPP's probability generating functional (PGFL) [98]. Specifically, for a measurable function $f(x) : \mathbb{R}^2 \to [0,\infty)$, the PGFL of a PPP Φ (which exists in the region $\mathcal{X} \subset \mathbb{R}^2$) is defined

and derived as below,

$$\mathcal{G}[f] \triangleq \mathbb{E}\prod_{x\in\Phi} f(x) = \exp\Big(-\int_{x\in\mathcal{X}} \big(1-f(x)\big)\Lambda(\mathrm{d}x)\Big), \tag{2.12}$$

where $\Lambda(\mathrm{d}x)$ is the intensity measure of PPP Φ;

- The integration limit in step (a) is from $(P_i/t)^{1/\alpha}$ to ∞, because all interfering BSs' long-term received powers should be positive and not greater than $P_{LT,\max} = t$, i.e., $P_i v^{-\alpha} \leqslant t$, thus giving $v \in [(P_i/t)^{1/\alpha}, \infty)$. It should be noted that the resultant interfering BSs in each tier constitute PPPs over the entire plane except the circular regions around the origin;

- step (b) is obtained by changing the variable to $u = \frac{v^2}{(TP_i/t)^{2/\alpha}}$;

- step (c) follows the definition of the function $\rho(T,\alpha)$, i.e.,

$$\rho(T,\alpha) \triangleq T^{2/\alpha}\int_{T^{-2/\alpha}}^{\infty} \frac{1}{1+u^{\alpha/2}}\mathrm{d}u. \tag{2.13}$$

After obtaining $f_{P_{LT,\max}}(t)$ in (2.8) and $\mathcal{L}_I(\frac{T}{t} \mid P_{LT,\max} = t)$ in (2.11), we can substitute them into (2.6) to reach the result for the coverage probability, that is,

$$p_c(T) = \frac{2\pi}{\alpha}\sum_{i\in\mathbb{K}} \lambda_i P_i^{2/\alpha}\int_0^{\infty} \exp(-\frac{T\sigma^2}{t}) \exp\Big(-\pi\sum_{i\in\mathbb{K}}\lambda_i P_i^{2/\alpha}\big[1+\rho(T,\alpha)\big]t^{-2/\alpha}\Big)t^{-\frac{2}{\alpha}-1}\mathrm{d}t. \tag{2.14}$$

For the scenario with frequency reuse factor $N_i > 1$, $i \in \mathbb{K}$, where BSs randomly occupy one of N_i frequency points for the i-th tier, the result in (2.14) can be easily extended as

$$p_c(T) = \frac{2\pi}{\alpha}\sum_{i\in\mathbb{K}} \lambda_i P_i^{2/\alpha}\int_0^{\infty} \exp(-\frac{T\sigma^2}{t}) \exp\Big(-\pi\sum_{i\in\mathbb{K}}\lambda_i P_i^{2/\alpha}\big[1+\frac{\rho(T,\alpha)}{N_i}\big]t^{-2/\alpha}\Big)t^{-\frac{2}{\alpha}-1}\mathrm{d}t. \tag{2.15}$$

2.3 Extended Model with Directional Antennas

Different from the omni-directional antenna model used in the previous section, directional antennas and sectorization, the techniques commonly used in macro-cell BS deployment, are considered in the following sections, which make the analysis more comparable to practical scenarios.

Firstly, we extend the original analysis framework for the HetNet with different antenna patterns across tiers. Specifically, the properties of the i-th tier can be presented by the tuple $\{\lambda_i, P_i, G_i(\cdot), N_i\}$, in which $G_i(\cdot)$ is the antenna gain pattern function for this tier. Considering frequency reuse utilized practically, we assume that N_i sectors at the directional antenna BSs are operated at N_i different frequency points (where N_i frequencies are randomly allocated to N_i sectors), which can guarantee that the frequency reuse factor is equal to N_i [43].

Here, we assume that the directions of N_i directional antennas are aligned uniformly, i.e., the central angles of N_i sectors are circularly uniformly-distributed over the range $[0, 2\pi)$. In other words, each sector within a BS is separated from the neighboring ones by $2\pi/N_i$. Therefore, if one sector's central angle is provided, the directions of other sectors in this BS can be determined.

For a certain frequency point $f \in \{1, 2, ..., N_i\}$, the directional antenna at location of x has a sector angle $\theta_f(x)$ (defined as the angle between the central direction of the antenna and the positive real axis). Its antenna gain in direction of the mobile user at origin is $G_i\big(\tau_f(x)\big)$, in which $\tau_f(x)$ is provided by

$$\tau_f(x) \triangleq \big(\angle x - \theta_f(x)\big) \mod 2\pi, \tag{2.16}$$

where $\angle x$ is the argument of x and the resultant angle $(\angle x - \theta_f(x))$ is shifted to the range of $[0, 2\pi)$.

In this analysis, we assume that $\theta_1(x)$ is uniformly random-distributed over $[0, 2\pi)$, and accordingly the central angles for other sectors can be determined, i.e., $\theta_f(x), f \in \{2, ..., N_i\}$ are selected respectively from the elements of $\big\{\theta : \theta = (\theta_1(x) - 2\pi(j-1)/N_i) \mod 2\pi, j \in \{2, \cdots, N_i\}\big\}$. Given the assumption that $\theta_1(x)$ is uniformly random-distributed over $[0, 2\pi)$, $\tau_1(x)$ can also be regarded as a uniformly distributed random variable over $[0, 2\pi)$.

Depending on the pattern of sector antenna, $G_{i,\max}$ is defined as the i-th tier maximum directional antenna gain from all the N_i sectors located at x toward

the typical user, which can be viewed as a function of $\tau_1(x)$, i.e.,

$$\begin{aligned} G_{i,\max}\big(\tau_1(x)\big) &\triangleq \max_{j\in\{1,2,\cdots,N_i\}} G_i\big(\tau_j(x)\big) \\ &= \max_{j\in\{1,2,\cdots,N_i\}} G_i\bigg(\Big(\tau_1(x) - \frac{2\pi(j-1)}{N_i}\Big) \mod 2\pi\bigg), \end{aligned} \tag{2.17}$$

It should be noted that which frequency point is selected to serve the typical user is independent of the maximum directional antenna gain $G_{i,\max}\big(\tau_1(x)\big)$, and $\{G_{i,\max}\big(\tau_j(x)\big)\}$ for $j \in \{1, 2, \cdots, N_i\}$ have the same value.

2.3.1 Cell Association Model

Different from the model in Section 2.2, we define the long-term received power from an i-th tier BS at x as $P_i G_{i,\max}\big(\tau_1(x)\big)\|x\|^{-\alpha}$ in the extended model to take the impact of directional antennas into account. By associating with the sector providing the maximum long-term received power, we can obtain the selected tier number and the BS location (also denoted by κ and φ, respectively), i.e.,

$$[\kappa, \varphi] = \arg \max_{i\in\mathbb{K}, x\in\Phi_i} \big[P_i G_{i,\max}\big(\tau_1(x)\big)\|x\|^{-\alpha}\big]. \tag{2.18}$$

Without any loss of generality, we assume that the frequency point f_s is utilized by the serving sector. Here, we define the random variable $P_{LT,\max}$ as the maximum long-term received power from all BSs (including all available sectors), i.e.,

$$P_{LT,\max} \triangleq P_\kappa G_{\kappa,\max}\big(\tau_1(\varphi)\big)\|\varphi\|^{-\alpha}. \tag{2.19}$$

2.4 Analysis on the Impact of Directional Antennas

In this section, we analyze the extended model with directional antennas taken into account. By using the tool of the stochastic geometry cellular network model, the main results are the probabilistic characterizations of the downlink coverage, which is based upon the statistical property of the maximum long-term received power from all BSs' all sectors obtained in 2.4.1.

2.4.1 Maximum Long-Term Received Power

Firstly, we focus on the statistical property of the random variable $P_{LT,\max}$, i.e., the maximum long-term received power from all BSs' all sectors. Here, $G_{i,\max}$ is used to denote the random variable of the i-th tier maximum directional antenna gain toward the typical user, for a randomly chosen BS in the whole plane.

Lemma 2.1. *The CDF of random variable $P_{LT,\max}$, i.e., the maximum long-term received power from all BSs (including all available sectors), can be provided by*

$$F_{P_{LT,\max}}(t) = \prod_{i\in\mathbb{K}} \Big[\exp\Big(-2\pi\lambda_i \int_0^{\infty} \big(1 - F_{G_{i,\max}}(\frac{r^{\alpha}t}{P_i})\big) r \mathrm{d}r \Big) \Big], \tag{2.20}$$

in which the function $F_{G_{i,\max}}(\cdot)$ is the CDF of the i-th tier maximum directional antenna gain $G_{i,\max}$, where $G_{i,\max}$ is regarded as a random variable.

Proof. See Appendix A.1. □

Based on the CDF of $P_{LT,\max}$ given above, we can get the probability density function (PDF) $f_{P_{LT,\max}}(t)$ solved by numerical derivative of $F_{P_{LT,\max}}(t)$, that is,

$$f_{P_{LT,\max}}(t) = \mathrm{d}F_{P_{LT,\max}}(t)/\mathrm{d}t. \tag{2.21}$$

2.4.2 Coverage Probability

Based upon the above-mentioned cell association model, the received downlink SINR expression is provided accordingly by

$$\mathrm{SINR} = \frac{P_{\kappa} G_{\kappa,\max}\big(\tau_1(\varphi)\big) h \|\varphi\|^{-\alpha}}{I + \sigma^2}, \tag{2.22}$$

in which I is the cumulative interference from all sectors utilizing the frequency point f_s, except the κ-th tier sector located at φ (the serving sector for the typical user), i.e.,

$$I = \sum_{i\in\mathbb{K}} I_i = \sum_{i\in\mathbb{K}} \sum_{x\in\Phi_i\setminus\{\varphi\}} P_i G_i\big(\tau_{f_s}(x)\big) h_x \|x\|^{-\alpha}, \tag{2.23}$$

where I_i is still defined as the interference component from the i-th tier. Next we focus on the coverage probability $p_c(T)$ by presenting the following theorem.

Theorem 2.2. *For a typical user in a K-tier heterogeneous cellular network with directional antennas implemented (with parameters tuple $\{\lambda_i, P_i, G_i(\cdot), N_i\}$ for the*

i-th tier), the coverage probability can be provided by

$$p_c(T) = \int_0^\infty \exp(-\frac{T\sigma^2}{t}) \exp\Big(- \frac{1}{2t^{2/\alpha}} \sum_{i\in\mathbb{K}} \lambda_i P_i^{2/\alpha} M_i(T,\alpha)\Big) f_{P_{LT,\max}}(t)\mathrm{d}t, \quad (2.24)$$

in which $M_i(T,\alpha)$ can be regarded as the property of the i-th tier and defined as

$$M_i(T,\alpha) = \int_0^{2\pi} \big(G_{i,\max}(\theta)\big)^{\frac{2}{\alpha}} \rho\Big(\frac{TG_i(\theta)}{G_{i,\max}(\theta)}, \alpha\Big)\mathrm{d}\theta. \quad (2.25)$$

Proof. See Appendix A.2. □

Remark. Considering *omni-directional antennas and single frequency band* employed in all tiers as a special case, we have $G_{i,\max}(\tau) = G_i(\tau) = 1$ for $\tau \in [0, 2\pi)$ and $i \in \mathbb{K}$. Consequently we can easily have the CDF of G_i and $G_{i,\max}$, that is,

$$F_{G_{i,\max}}(x) = F_{G_i}(x) = \mathbf{1}\big(x \in [1,\infty)\big), \quad \text{for } i \in \mathbb{K}. \quad (2.26)$$

By substituting the CDF of $G_{i,\max}$ into Lemma 2.1, the CDF of random variable $P_{LT,\max}$ can be expressed as

$$\begin{aligned} F_{P_{LT,\max}}(t) &= \prod_{i\in\mathbb{K}} \Big[\exp\Big(- 2\pi\lambda_i \int_0^\infty \big(1 - F_{G_{i,\max}}(\frac{r^\alpha t}{P_i})\big) r\mathrm{d}r\Big)\Big] \\ &= \prod_{i\in\mathbb{K}} \Big[\exp\Big(- 2\pi\lambda_i \int_0^{(\frac{P_i}{t})^{\frac{1}{\alpha}}} r\mathrm{d}r\Big)\Big] \\ &= \exp\Big(- \pi \sum_{i\in\mathbb{K}} \lambda_i P_i^{2/\alpha} t^{-2/\alpha}\Big), \end{aligned} \quad (2.27)$$

which is identical to the one provided in (2.7). As anticipated, by substituting $G_{i,\max}(\tau) = G_i(\tau) = 1$ for $\tau \in [0, 2\pi)$ and (2.27) into (2.24), we have the same format of coverage probability expression as (2.14).

Remark. Next, we consider the special case of *omni-directional antennas* in all tiers with frequency reuse factor N_i for i-th tier (BSs randomly choose one of N_i frequency points, in order to guarantee that the frequency reuse factor is equal to N_i), we have $G_{i,\max}(\tau) = 1$ for $\tau \in [0, 2\pi)$, and $G_i(\tau) = 1$ for $\tau \in [0, 2\pi)$ if the BS under consideration uses the frequency point f_s. Consequently, the CDF of

G_i and $G_{i,\max}$ can be respectively derived as

$$F_{G_i}(x) = \frac{N_i - 1}{N_i}\mathbf{1}\big(x \in [0, \infty)\big) + \frac{1}{N_i}\mathbf{1}\big(x \in [1, \infty)\big), \quad \text{for } i \in \mathbb{K}, \tag{2.28}$$

and

$$F_{G_{i,\max}}(x) = \mathbf{1}\big(x \in [1, \infty)\big), \quad \text{for } i \in \mathbb{K}. \tag{2.29}$$

Identical to (2.27), the CDF of random variable $P_{LT,\max}$ can be derived, and subsequently $M_i(T, \alpha)$, the property of the i-th tier, becomes

$$\begin{aligned} M_i(T, \alpha) &= \int_0^{2\pi} \big(G_{i,\max}(\theta)\big)^{\frac{2}{\alpha}} \rho\Big(\frac{TG_i(\theta)}{G_{i,\max}(\theta)}, \alpha\Big) \mathrm{d}\theta \\ &\overset{(a)}{=} 2\pi \cdot \rho(T, \alpha) \cdot \frac{1}{N_i} + 2\pi \cdot \rho(0, \alpha) \cdot \frac{N_i - 1}{N_i} \\ &= \frac{2\pi}{N_i}\rho(T, \alpha). \end{aligned} \tag{2.30}$$

As expected, by substituting the expression of $F_{P_{LT,\max}}(t)$ and (2.30) into (2.24), the final coverage probability can be derived the same as the result in (2.15).

2.5 Numerical Results

In this section, we present the numerical results on the coverage performance for a two-tier HetNet, where the macrocell tier (marked as the first tier) is underlaid with picocell or femtocell tier (marked as the second tier). Specifically, the macrocell BSs at high power level, i.e., $P_{\mathrm{TX},1} = 46$ dBm, are co-deployed with lower power level femtocell BSs with $P_{\mathrm{TX},2} = 20$ dBm or picocell BSs with $P_{\mathrm{TX},2} = 30$ dBm. The macrocell tier density is per square km in all numerical results. The path loss constant and exponent are respectively assumed to be $L_0 = -34$ dB and $\alpha = 4$. The thermal noise power is $\sigma^2 = -104$ dBm. Monte Carlo simulations are also conducted to compare with our analysis for the purpose of model validation.

Considering practical examples of HetNets with directional antennas implemented, we assume directional antennas are only used in the macrocell tier, where the number of sectors in a sectorized BS is $N_1 = 3$. In our analysis, there are two ways to model the directional antennas, namely, directional antenna model-1

(abbreviated as DA-1) and directional antenna model-2 (abbreviated as DA-2), the antenna gain functions $G_1(\cdot)$ of which are provided in the Table 2.1. The variables with dB in their subscripts denote the corresponding variables in decibel unit.

Table 2.1: Directional antenna models for the macrocell tier

	Antenna Gain Function $G_1(\tau)$ (or $G_{1,dB}(\tau)$ in decibel unit)
DA-1	$G_{1,dB}(\tau) = G_{m,dB} - \min\left[12(\frac{\tau-\pi}{\beta})^2, G_{s,dB}\right]$, for $\tau \in [0, 2\pi)$, in which $\beta = 80\pi/180$, $G_{s,dB} = 20$ dB, and $G_{m,dB} = 6.19$ dB.
DA-2	$G_1(\tau) = \begin{cases} 3 & \text{if } \tau \in [0, \frac{2\pi}{3}) \\ 0 & \text{otherwise.} \end{cases}$

It should be noted that the antenna pattern of DA-1 is widely used in system-level simulations [40, 135], and DA-2 is a simplified ideal directional antenna model. In both models, the antenna gains are normalized for $\tau \in [0, 2\pi)$ to make a fair comparison. The antenna gain of DA-1 is expressed in decibel unit, whereas the counterpart for DA-2 is in linear unit. As mentioned earlier, the three sectors of the macrocell BS occupy three different frequency points, and the resultant antenna patterns of DA-1 and DA-2 are respectively shown in Fig. 2.2(a) and Fig. 2.2(b).

Other than the macrocell tier, picocell and femtocell BSs always use the omni-directional antennas with frequency reuse factor $N_2 = 3$. For the frequency point f_s, we have $G_2(\tau) = 1$ for $\tau \in [0, 2\pi)$ if the omni-directional antennas BS choose to use this frequency point.

Because $\theta_1(x)$ is assumed to be randomly distributed over $[0, 2\pi)$ and $x \in \mathbb{R}^2$, $\tau_1(x)$ can be regarded as a uniformly distributed random variable over the range of $[0, 2\pi)$. Therefore, for DA-1, the CDF of $G_{1,dB}$ (the value of random variable $G_i(\tau)$ in decibels) can be provided by

$$F_{G_{1,dB}}(x) = \begin{cases} 0 & \text{if } x < G_{m,dB} - G_{s,dB} \\ 1 - \frac{\beta}{\pi}\sqrt{\frac{G_{m,dB}-x}{12}} & \text{if } G_{m,dB} - G_{s,dB} \leqslant x < G_{m,dB} \\ 1 & \text{if } x \geqslant G_{m,dB}. \end{cases} \tag{2.31}$$

As β is set to be 80 degrees in this model, which guarantees the main lob is

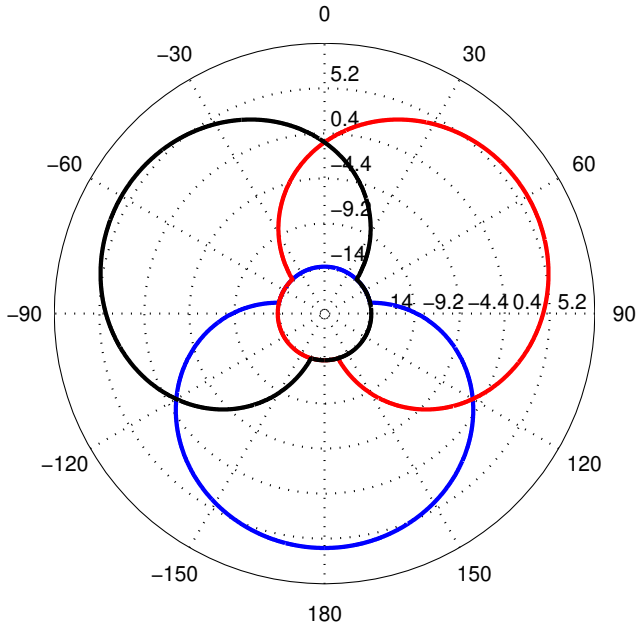

(a) Directional Antenna Pattern 1 (DA-1)

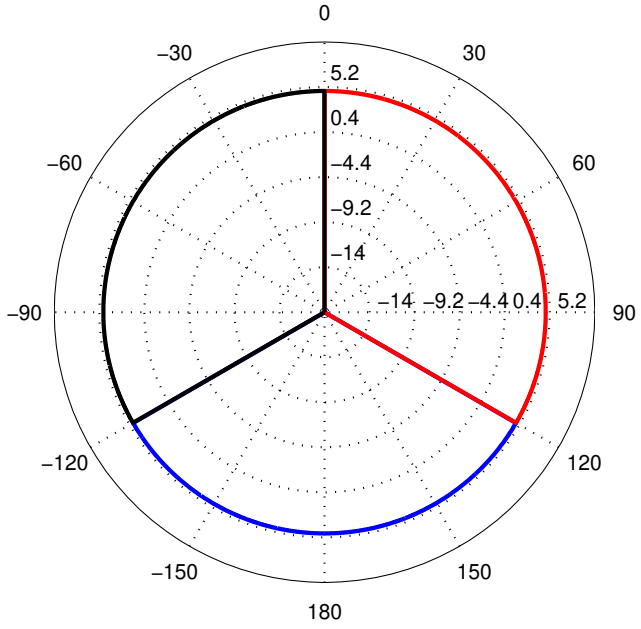

(b) Directional Antenna Pattern 1 (DA-2)

Figure 2.2: Illustration of Directional antenna patterns for DA-1 and DA-2, in which different colors represent the gain patterns in decibel unit for different sectors.

overlapped with the lobs from the two other co-site sectors, the CDF of $G_{1,\max,dB}$ can be expressed as

$$F_{G_{1,\max,dB}}(x) = \begin{cases} 0 & \text{if } x < G_{m,dB} - 12\left(\frac{\pi/3}{\beta}\right)^2 \\ 1 - \frac{3\beta}{\pi}\sqrt{\frac{G_{m,dB}-x}{12}} & \text{if } G_{m,dB} - 12\left(\frac{\pi/3}{\beta}\right)^2 \leqslant x < G_{m,dB} \\ 1 & \text{if } x \geqslant G_{m,dB}. \end{cases} \quad (2.32)$$

On the other hand, for DA-2, the CDF of G_1 can be provided as below, since $\tau_f(x)$ is uniformly distributed over the range of $[0, 2\pi)$, that is,

$$F_{G_1}(x) = \begin{cases} 0 & \text{if } x < 0 \\ \frac{2}{3} & \text{if } 0 \leqslant x < 3 \\ 1 & \text{if } x \geqslant 3, \end{cases} \quad (2.33)$$

and the CDF of $G_{1,\max}$ can be expressed as

$$F_{G_{2,\max}}(x) = \begin{cases} 0 & \text{if } x < 3 \\ 1 & \text{if } x \geqslant 3. \end{cases} \quad (2.34)$$

Consequently, by substituting the above CDF functions into Lemma 2.1 and Theorem 2.2, we can obtain the coverage probabilities achieved at the typical mobile user under different conditions, which are demonstrated in the Fig. 2.3 and Fig. 2.4. In Fig. 2.3, we consider the scenarios in which femtocell BSs (always with omni-directional antennas) are overlaid with macrocell BSs with frequency reuse factors of both tiers equal to 1 and 3. The black points and curve represent the baseline, i.e., frequency reuse factor $N_1 = N_2 = 1$ and omni-directional antennas are implemented for both tiers. By adopting frequency reuse with $N_1 = N_2 = 3$ for both tiers, we assume that the macrocell BSs utilize the above-mentioned DA-1 and DA-2. Similarly, picocell BSs, rather than femtocell BSs, are co-deployed in Fig. 2.4.

By comparing with the simulation results for both DA-1 and DA-2, it can be shown that the coverage probability (or equivalently, the distribution of received SINR) can be well captured by the analytical results obtained from Theorem 2.2. Furthermore, through Fig. 2.3 and Fig. 2.4, we can illustrate the impact of directional antennas installed in the macrocell tier on the coverage probability at the typical user. It can be shown that frequency reuse factor $N_1 = N_2 = 3$ for

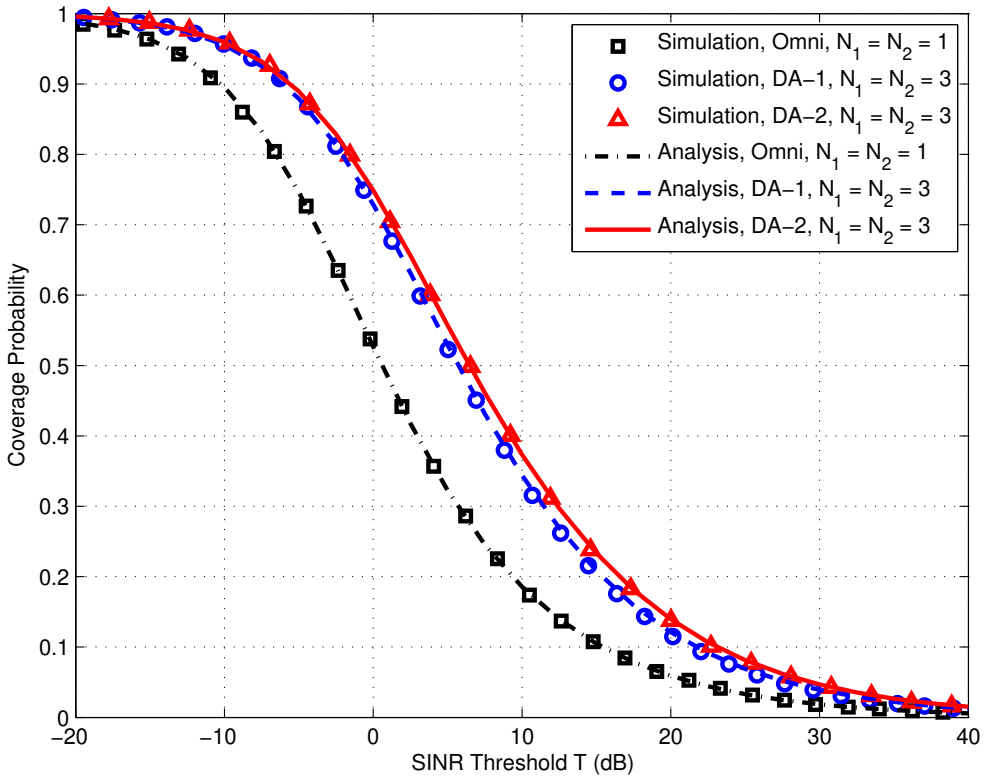

Figure 2.3: Probability of coverage for a two-tier HetNet with frequency reuse factors of both tiers equal to 1 and 3. For frequency reuse scenario with $N_1 = N_2 = 3$, macrocell BSs are equipped with DA-1 or DA-2 directional antennas; for the scenario frequency reuse factor $N_1 = N_2 = 1$, macrocell BSs are equipped with omni-directional antennas. For both scenarios, femtocell BSs with omni-directional antennas ($P_{\mathrm{TX},2} = 20$ dBm) are co-deployed with the density of $\lambda_2 = 10$.

both DA-1 and DA-2 guarantees a performance improvement over the case with frequency reuse factor $N_1 = N_2 = 1$, but the achievable improvements are different between DA-1 and DA-2. This difference can be regarded as the impact of antenna gain pattern on the coverage performance. Specifically, the antenna pattern DA-1, which is more comparable to the practical implementation, wastes signal energy in the regions covered by the other two co-site sectors; on the other hand, DA-2 can be regarded as an ideal directional antenna pattern, but it is not physically achievable. Taking the femtocell co-deployed scenario in Fig. 2.3 as an instance, compared with the baseline with frequency reuse factor $N_1 = N_2 = 1$, the probability coverage is improved from 0.19 to 0.34 if DA-1 implemented and

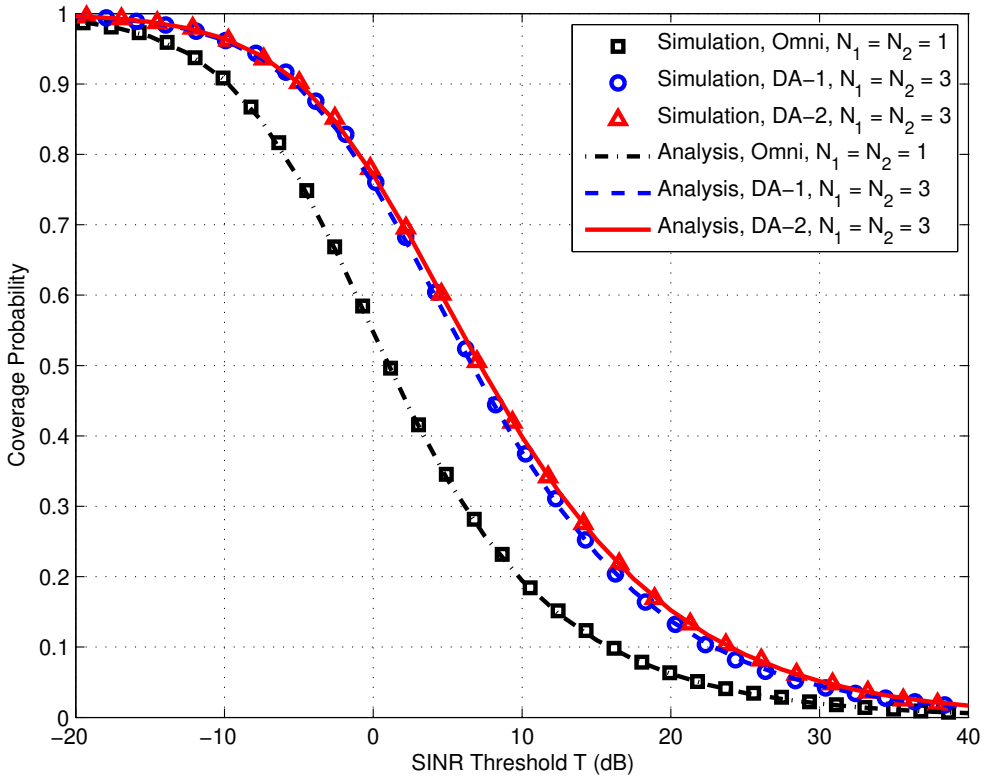

Figure 2.4: Probability of coverage for a two-tier HetNet with frequency reuse factors of both tiers equal to 1 and 3. For frequency reuse scenario with $N_1 = N_2 = 3$, macrocell BSs are equipped with DA-1 or DA-2 directional antennas; for the scenario frequency reuse factor $N_1 = N_2 = 1$, macrocell BSs are equipped with omni-directional antennas. For both scenarios, picocell BSs with omni-directional antennas ($P_{\mathrm{TX},2} = 30$ dBm) are co-deployed with the density of $\lambda_2 = 10$.

to 0.37 for DA-2 when the SINR threshold T is set to be 10 dB. Similar trends can be observed from the picocell counterpart in Fig. 2.4, and the performance gap between DA-1 and DA-2 is slightly smaller. Obviously, in order to obtain a model more comparable to practical implementation, the impact of directional antenna pattern should be taken into consideration for both femtocell and picocell scenarios.

2.6 Summary of Contributions

In this chapter, we have provided an introduction to the PPP-based stochastic geometry model for HetNets, with the explanation of the cell association model

and the tractable framework for the coverage performance in detail. This model is also used as the basic methodology in the following Chapter 3 and Chapter 5.

Furthermore, as directional antennas are widely used to sectorize the macrocell cells in practical cellular systems, we have extended the original model to take the impact of directional antennas into account. The numerical results provided in this chapter validated the analytical expressions of the coverage probability achieved at a randomly chosen mobile user. Based upon this analysis, we observed the impact of directional antenna patterns on the coverage performance, which helped us to identify the performance gap between a practical directional antenna model and an ideal one.

Chapter 3

Analytical Evaluation of a Non-uniform Femtocell Deployment

3.1 Introduction

The concept of femtocell, an important part of HetNets, is widely regarded as an effective way to provide better cellular coverage, and also to increase data rate by alleviating mobile data traffics from public macrocells [38, 39].

Having femtocells co-deployed, the cellular coverage performance of a HetNet strongly depends on the femtocell BSs' locations. With a constant preconfigurable transmit power, which is a mode commonly implemented in current solutions [48, 136], the femtocell coverage range is significantly reduced when it is close to a macrocell BS site [60], resulting in poor off-loading of users to the femtocell. More interestingly, when the femtocell BSs are uniformly deployed at random, increasing the density of femtocell BSs does not give any remarkable improvement in the coverage probability even when femtocells are open access [60, 61]. The main cause of this phenomenon is the increased network interference from having more femtocell BSs in satisfactory macrocell areas. One interesting question can be raised from the above discussion:

Q. Whether or not we can improve both coverage and throughput performances by not using the femtocell BSs at undesirable locations, in other words, utilizing femtocell BSs non-uniformly?

In this chapter, we aim to answer this question by proposing an intuitive and interesting non-uniform femtocell deployment scheme. Based upon the PPP-based BS model as described in Chapter 2, we analyze the impact of the proposed scheme on both the downlink coverage and throughput performance. Through the analysis in this chapter, we highlight the significance of selectively deploying the femtocell BSs, taking their relative locations with macrocell BSs into account. It should be noted that we focus on the open-access femtocells in this chapter, which are operated by the cellular service providers and offer femtocell access to all the users in the networks [38, 52].

In Section 3.2, we give a detailed description of the proposed non-uniform femtocell deployment scheme along with two implementation methods, namely, femtocell deactivation and smart femtocell deployment. Through this scheme, most of the active femtocell BSs are guaranteed to be located in the relatively poor macrocell coverage areas.

After providing the corresponding analysis results for uniform femtocell deployment in Section 3.3, the probabilistic characterization of the downlink coverage and the achievable single user throughput of the proposed non-uniform femtocell deployment scheme is investigated in Section 3.4. The benefits provided by the non-uniform femtocell deployment are demonstrated through the numerical results in Section 3.5, which help us to reach the insights in Section 3.6.

3.2 Non-uniform Femtocell Deployment

In our analysis, the union of locations within a prescribed distance from any macrocell BSs is defined as the *inner region*, whereas the union of locations outside the inner region is defined as the *outer region*. Here, we consider an intuitive and interesting idea: We simply avoid using femtocell BSs within the inner region. Considering the practical constraints, there are two ways to implement this non-uniform deployment scheme:

1. ***Femtocell Deactivation***: If the femtocell BSs are deployed uniformly in the network, as illustrated in Fig. 3.1(a), the ones located within the inner region are deactivated, marked as red-filled squares therein. The overall *de facto* femtocell BS density is decreased compared with the uniform deployment. This method can be achieved easily in practice: A listening modem receiving downlink signals can be implemented to estimate its distance from

the serving BS [65], and subsequently determine the femtocell BS's on/off status. One direct benefit from the deactivation is the reduced operating expense from the decreased femtocell BS energy consumption.

2. ***Smart Femtocell Deployment***: In this method, we deploy the femtocell BSs in the outer region only. Compared with the above-mentioned "femtocell deactivation", this smart deployment moves the inner region femtocell BSs to the outer region, as illustrated in Fig. 3.1(b), where the blue-filled squares represent the newly added active BSs in the outer region.

It should be noticed that Haenggi introduced a non-uniform small cell deployment model that also incorporates dependencies between different tiers of cellular network [125]. The superposed tiers in Haenggi's model are deployed on the edges and at the vertices of the Voronoi cells formed by the macrocell BSs, that is, the poorest macrocell coverage locations. In contrast, our scheme regards the previously defined outer region as the poor macrocell coverage area, in which open-access femtocell BSs are utilized. Additionally, our study provides not only the new model, but also the analysis on both coverage and throughput performance.

3.3 System Model

3.3.1 Two-Tier Cellular Network Model

Like the analysis conducted in Chapter 2, we consider a downlink HetNet employing an orthogonal multiple access technique and consisting of two tiers, the macrocell and femtocell tiers (otherwise called the first and second tiers), which are spatially distributed as two-dimensional processes Φ_1 and Φ_2, with different transmit powers $P_{\mathrm{TX},1}$ and $P_{\mathrm{TX},2}$. The same transmit power holds across each tier. The macrocell-tier process Φ_1 is modeled as a homogeneous PPP with density λ_1. Furthermore, the collection of mobile users, located according to an independent homogeneous PPP Φ_{MS} of density λ_{MS}, is assumed in this chapter. We consider the process $\Phi_{MS} \cup \{0\}$ obtained by adding a user at the origin of the coordinate system, which is the typical user under consideration. This is allowed by Slivnyak's Theorem [98], which states that the properties observed by a typical point of the PPP Φ_{MS}, are identical to those observed by the origin in the process $\Phi_{MS} \cup \{0\}$.

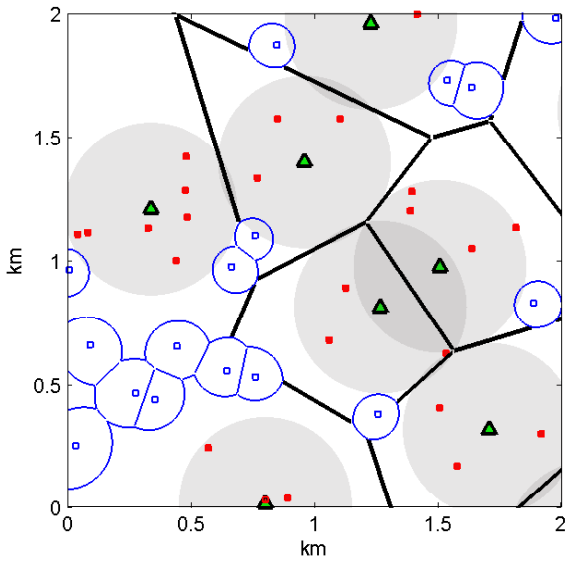

(a) Femtocell Deactivation

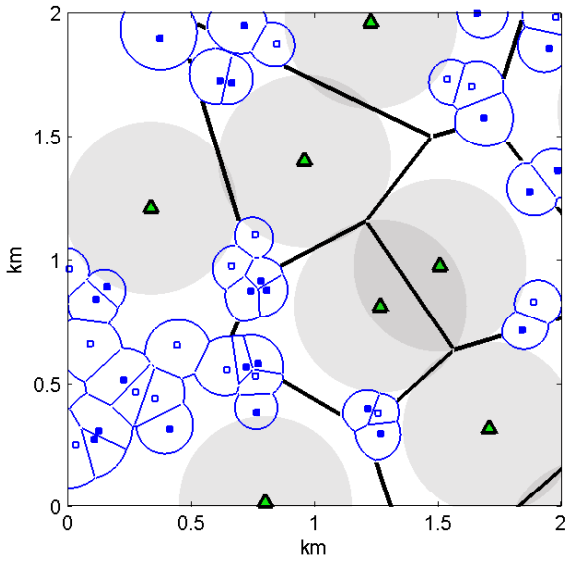

(b) Smart Femtocell Deployment

Figure 3.1: Illustration of cell association regions for a two-tier network with femtocell deactivation and smart femtocell deployment implemented, based on the cell association model provided in 2.2.1. Macrocell BSs (triangles) and femtocell BSs (squares) are randomly scattered. In the inner region (shadow areas), the deactivated femtocell BSs are marked as red-filled squares in Fig. 3.1(a), which are reinstalled at the new locations in the outer region for the smart femtocell deployment, and marked as blue-filled squares in Fig. 3.1(b). The remaining femtocell BSs are always active, and marked as blue non-filled squares.

Here, we use the standard power loss propagation model with path loss exponent $\alpha > 2$ and path loss constant L_0 at the reference distance $r_0 = 1$ m, just similar to the one used in the previous chapter. We also assume that the typical mobile user experiences Rayleigh fading from the serving and interfering BSs. The impact of fading on the signal power follows the exponential distribution with the unitary mean value. The noise power is assumed to be additive and constant with value σ^2.

3.3.2 Cell Association and Resource Allocation Model

As described earlier, all BSs are assumed to be open access. Moreover, just like Chapter 2, we still assume that mobile users are connected to the BS providing maximum long-term received power. Specifically, the selected tier index κ can be given as

$$\kappa = \arg \max_{i \in \{1,2\}} \left[P_{\mathrm{TX},i} L_0 (R_i)^{-\alpha} \right], \tag{3.1}$$

in which R_i is the minimum distance from the i-th tier BSs to the typical mobile user at the origin, that is,

$$R_i = \min_{x \in \Phi_i} \|x\|. \tag{3.2}$$

For simplicity, we also use P_i to replace the product of $P_{\mathrm{TX},i}$ and L_0, i.e., $P_i = P_{\mathrm{TX},i} L_0, i \in \{1, 2\}$, as we did in Chapter 2.

We assume that all the BSs employ a saturated resource allocation model [46, 137], in which full buffer traffic model holds for every user; in other words, a BS always has data to transmit if there are mobile users camped on it. The available resources at each BS are assumed to be allocated evenly among all its associated mobile users to simulate the Round-Robin scheduling with the most fairness.

3.3.3 Received SINR for Data Channels

Different from the received SINR model used in Chapter 2, in this chapter, we focus on cellular data channels. Therefore, we assume that no interference is generated from a BS if it has no user associated, because the frequency-time blocks are usually left blank when they are not allocated for data transmissions in practical scenarios [6]. We use $\{\Phi_i' : i \in \{1, 2\}\}$ to denote the process constructed by the remaining i-th tier BSs (i.e., the loaded BSs in the i-th tier) excluding the

ones not associated with users (i.e., unloaded BSs).

By employing the cell association model described in Subsection 3.3.2 to choose the serving cell, the downlink received SINR at the typical user can be expressed as

$$\mathrm{SINR} = \frac{P_\kappa h (R_\kappa)^{-\alpha}}{I + \sigma^2}, \tag{3.3}$$

where $I = \sum_{i\in\{1,2\}} I_i = \sum_{i\in\{1,2\}} \sum_{x\in\Phi_i'\setminus\{x_o\}} P_i h_x \|x\|^{-\alpha}$ is the cumulative interference from all the loaded BSs (except the BS at x_o from the κ-th tier serving for the mobile user at o), and I_i is defined as the interference component from the i-th tier. Here, h is employed to denote the channel fading gain from the serving BS, and h_x is the value for the interfering BS at the location of x. Based upon the Rayleigh fading assumption, all these channel fading gains, h and $\{h_x : x \in \Phi_i' \setminus \{x_o\}\}$ follow the exponential distribution with the unitary mean value. In our study, no intracell interference is incorporated as we assume that the orthogonal multiple access is employed among intracell users.

3.3.4 Analysis on Uniform Femtocell Deployment

Before proposing the non-uniform femtocell deployment scheme, we firstly focus on the uniform femtocell deployment, where all the femtocell BSs in Φ_2 remain active and are located as a homogeneous PPP with density λ_2. Following the analysis in [46, 60], the results for this uniform femtocell deployment are briefly presented here for the purpose of comparison.

Mobile User Resource Sharing

Firstly, the per-tier association probabilities for the uniform femtocell deployment, that is, the probabilities for the typical user to associate with the macrocell and femtocell tiers, denoted by $\mathcal{Q}_{1,u}$ and $\mathcal{Q}_{2,u}$, were derived in [60]:

$$\mathcal{Q}_{1,u} = \frac{\lambda_1}{\lambda_1 + \lambda_2 \left(\frac{P_2}{P_1}\right)^{2/\alpha}} \quad \text{and} \quad \mathcal{Q}_{2,u} = \frac{\lambda_2}{\lambda_1 \left(\frac{P_1}{P_2}\right)^{2/\alpha} + \lambda_2}. \tag{3.4}$$

As proved in [46], the area of the i-th tier cells, defined as $\mathcal{C}_{i,u}$, can be well approximated by the Voronoi cell area formed by a homogeneous PPP with the density value $\lambda_i/\mathcal{Q}_{i,u}$, i.e., $\mathcal{C}_{i,u} \approx \mathcal{C}_0(\lambda_i/\mathcal{Q}_{i,u})$, in which $C_0(y)$ is the area of a typical Voronoi cell of a homogeneous PPP with density y. We define the equivalent

density $\lambda_{i,eq,u}$ to denote the value $\lambda_i/\mathcal{Q}_{i,u}$, that is,

$$\lambda_{1,eq,u} = \lambda_1 + \lambda_2\big(\frac{P_2}{P_1}\big)^{2/\alpha} \quad \text{and} \quad \lambda_{2,eq,u} = \lambda_1\big(\frac{P_1}{P_2}\big)^{2/\alpha} + \lambda_2. \tag{3.5}$$

For the distribution of Voronoi cell area formed by a homogeneous PPP, there is no known closed form expression for its distribution [138]; however, some precise estimates can be conducted [139, 140]. By following the result in [140], the approximated PDF of the i-th tier cell area $\mathcal{C}_{i,u}$ can be expressed by using gamma function

$$f_{\mathcal{C}_{i,u}}(x) \approx (b\lambda_{i,eq,u})^q x^{q-1} \exp(-b\lambda_{i,eq,u}x)/\Gamma(q), \tag{3.6}$$

where $q = 3.61$, $b = 3.61$, and $\Gamma(x) = \int_0^\infty t^{x-1}e^{-t}\mathrm{d}t$ is the standard gamma function.

Based on this approximation, the probability mass function (PMF) of the number of users in a randomly chosen i-th tier cell can be derived as

$$\begin{aligned}\mathbb{P}[N_{i,c,u} = n] &= \int_0^\infty \mathbb{P}[N_{i,c,u} = n \mid \mathcal{C}_{i,u} = x] f_{\mathcal{C}_{i,u}}(x)\mathrm{d}x \\ &\approx \frac{b^q}{n!} \cdot \frac{\Gamma(n+q)}{\Gamma(q)} \cdot \frac{(\lambda_{MS})^n(\lambda_{i,eq,u})^q}{(\lambda_{MS} + b\lambda_{i,eq,u})^{n+q}}, \\ &\qquad \text{for } n \in \{0,1,2,...\} \text{ and } i \in \{1,2\}.\end{aligned} \tag{3.7}$$

On the other hand, given the condition that the typical user is enclosed in the cell, the PDF of the i-th tier cell area $\mathcal{C}_{i,u}$ was derived in [46, 129], that is,

$$f_{\mathcal{C}_{i,u}|o\in\mathcal{C}_{i,u}}(x) = \frac{x f_{\mathcal{C}_{i,u}}(x)}{\mathbb{E}[\mathcal{C}_{i,u}]}, \tag{3.8}$$

which helps to obtain the distribution of the number of in-cell users sharing the resource with the typical user

$$\begin{aligned}\mathbb{P}[N_{i,u} = n] \approx \frac{b^q}{n!} \cdot \frac{\Gamma(n+q+1)}{\Gamma(q)} \Big(\frac{\lambda_{MS}}{\lambda_{i,eq,u}}\Big)^n \Big(b + \frac{\lambda_{MS}}{\lambda_{i,eq,u}}\Big)^{-(n+q+1)}, \\ \text{for } n \in \{0,1,2,...\} \text{ and } i \in \{1,2\}.\end{aligned} \tag{3.9}$$

As the cell coverage regions are mutually disjointed and PPP Φ_{MS} has the property of complete independence [98], the numbers of users in different cells

are independent. For a randomly chosen i-th tier cell, its probability to be an unloaded cell is $\mathbb{P}[N_{i,c,u} = 0]$. Hence, the process Φ'_i, (i.e., the i-th tier loaded BSs excluding the BSs without users associated,) can be approximated by a homogeneous PPP with the density $\lambda'_{i,u} = \lambda_i \cdot (1 - \mathbb{P}[N_{i,c,u} = 0])$.

Coverage Probability

We use $\mathrm{SINR}_{i,u}$ to denote the received SINR at the typical user served by the i-th tier for this uniform deployment. Then the coverage probability at the typical user is $p_c(T) = \mathbb{P}[\mathrm{SINR}_{i,u} > T]$ for the i-th tier, i.e., the probability of a target SINR T (or SINR threshold) achievable at the typical user. This coverage probability is also exactly the CCDF of the received SINR.

If the typical user is served by the i-th tier, its coverage probability can be expressed as

$$\begin{aligned} p_{c,i,u}(T) &= \mathbb{P}[\mathrm{SINR}_{i,u} > T] \\ &= 2\pi\lambda_{i,eq,u} \int_{x>0} x \exp(-\frac{Tx^{\alpha}\sigma^2}{P_i}) \\ &\quad \cdot \exp\Big[-\pi x^2 \Big[\lambda_{i,eq,u} + \rho(T,\alpha)\lambda'_{i,eq,u}\Big]\Big] \mathrm{d}x, \quad \text{for } i \in \{1,2\}, \end{aligned} \tag{3.10}$$

where the function $\rho(T,\alpha)$ is defined in Section 2.2.2 already, i.e., $\rho(T,\alpha) \triangleq T^{2/\alpha} \int_{T^{-2/\alpha}}^{\infty} \frac{1}{1+u^{\alpha/2}} \mathrm{d}u$, and the variables $\{\lambda'_{i,eq,u} : i \in \{1,2\}\}$ can be defined as

$$\lambda'_{1,eq,u} = \lambda'_{1,u} + \lambda'_{2,u}\big(\frac{P_2}{P_1}\big)^{2/\alpha} \quad \text{and} \quad \lambda'_{2,eq,u} = \lambda'_{1,u}\big(\frac{P_1}{P_2}\big)^{2/\alpha} + \lambda'_{2,u}. \tag{3.11}$$

Single User Throughput

Similar to the resource allocation model used in [46], the throughput achievable at the typical user served by the i-th tier, denoted by $\mathcal{R}_{i,u}$, can be derived as

$$\begin{aligned} \mathbb{P}[\mathcal{R}_{i,u} > \rho] &= \mathbb{P}\Big[\frac{W}{N_{i,u}+1}\log_2(1+\mathrm{SINR}_{i,u}) > \rho\Big] \\ &= \mathbb{P}\big[\mathrm{SINR}_{i,u} > 2^{(N_{i,u}+1)\rho/W} - 1\big] \\ &\approx \mathbb{E}_{N_{i,u}}\big[p_{c,i,u}\big(2^{(N_{i,u}+1)\rho/W} - 1\big)\big] \\ &= \sum_{n=0}^{\infty} \mathbb{P}[N_{i,u} = n] \cdot p_{c,i,u}\big(2^{(n+1)\rho/W} - 1\big), \quad \text{for } i \in \{1,2\}, \end{aligned} \tag{3.12}$$

where the BS's bandwidth W is evenly allocated among all its associated users, namely, the typical user and the other $N_{i,u}$ in-cell users, as stated in the resource allocation model mentioned earlier. It should be noted that the approximation is achieved by assuming the independence between the distribution of $\mathrm{SINR}_{i,u}$ and $N_{i,u}$ and this assumption was proved to be accurate [46].

3.4 Analysis on Non-uniform Femtocell Deployment

In this section, we analyze the proposed non-uniform femtocell deployment scheme, which aims to maintain all the active femtocell BSs deployed in the areas with unsatisfactory macrocell coverage. Based upon our analysis using the tool of the stochastic geometry cellular network model, the main results are the probabilistic characterizations of the downlink coverage and the achievable single user throughput presented in Subsections 3.4.4 and 3.4.5, respectively. The first three subsections (i.e., Subsections 3.4.1, 3.4.2, and 3.4.3) formally define the inner and outer regions and present important intermediate results.

As described in Section 3.1, there are two ways to implement the proposed non-uniform femtocell deployment scheme, femtocell deactivation and smart femtocell deployment. In femtocell deactivation, the femtocell BSs within the inner region are deactivated, whereas femtocell BSs are deployed in the outer region only in smart femtocell deployment. From the analysis viewpoint, the smart femtocell deployment scheme can be viewed as femtocell deactivation with an increased femtocell-tier density in the outer region. Therefore, we focus only on femtocell deactivation here and the performance analysis of smart femtocell deployment can be readily obtained by increasing the value of femtocell density.

3.4.1 Inner and Outer Regions

By implementing the femtocell deactivation scheme, all the femtocell BSs in the inner region stay inactive and other femtocell BSs in the outer region remain active. Specifically, the inner region A_{inner} are defined as the union of locations where the distance from the nearest macrocell BS site is no larger than D, and the outer region A_{outer} are defined as the union of locations where the distances

from any macrocell BSs are larger than D, that is,

$$A_{inner} = \bigcup_{x \in \Phi_1} B(x, D) \quad \text{and} \quad A_{outer} = \mathbb{R}^2 \setminus A_{inner}, \tag{3.13}$$

where D is the radius of inner region in this chapter. By following PPP's void probability [98], the typical user's probabilities to be located in the inner region A_{inner} and the outer region A_{outer} are

$$\mathbb{P}[o \in A_{inner}] = 1 - \exp(-\pi\lambda_1 D^2) \quad \text{and} \quad \mathbb{P}[o \in A_{outer}] = \exp(-\pi\lambda_1 D^2). \tag{3.14}$$

Therefore, if the two tiers are originally distributed according to the homogeneous PPPs with the densities λ_1 and λ_2, the resultant active femtocell-tier density after the proposed deployment scheme will be a function of the location, that is,

$$\lambda_2(x) = \begin{cases} 0 & \text{for } x \in A_{inner} \\ \lambda_2 & \text{for } x \in A_{outer}, \end{cases} \tag{3.15}$$

which makes the femtocell-tier process Φ_2 become a *Poisson hole process* [141], and the average density for the active femtocell BSs over the whole plane become $\mathbb{E}[\lambda_2(x)] = \lambda_2 \cdot \mathbb{P}[o \in A_{outer}]$.

3.4.2 The Distribution of the Distance from Serving BS

First we define X_1 and X_2 as the distance between the typical user and its serving BS, given the condition that the user is served by the first and second tier respectively, and focus on the statistic characteristics of X_1 and X_2. It should be noted that X_1 and X_2 are random variables, because of the randomness introduced by the location of BSs. In this section, we will derive the PDFs of X_1 and X_2 for the typical user in A_{inner} and A_{outer}, respectively.

Similar to the notation in previous section, R_1 and R_2 are used to denote the typical user's distance from the nearest BS in the first and second tier respectively. It should be noted that R_i does not request the serving BS is served by the i-tier, which is different from X_i. The relationship between X_i and R_i is $\mathbb{P}[X_i \leqslant x] = \mathbb{P}[R_i \leqslant x \mid \kappa = i]$.

Lemma 3.1. *The PDF of X_1, conditioned on that the typical user is in the inner*

region, can be approximated as

$$f_{X_1|o\in A_{inner}}(x) \approx \frac{2\pi\lambda_1 x}{[1-\exp(-\pi\lambda_1 D^2)]}\exp(-\pi\lambda_1 x^2), \quad \textit{for } x \leqslant D. \tag{3.16}$$

Proof. As the event of $X_1 \leqslant x$ is the event of $R_1 \leqslant x$ based on the condition that the user is associated with macrocell, the CDF of X_1 for the inner region typical user can be expressed as

$$\begin{aligned} F_{X_1|o\in A_{inner}}(x) &= \mathbb{P}[X_1 \leqslant x \mid o \in A_{inner}] \\ &= \mathbb{P}[R_1 \leqslant x \mid \kappa = 1, o \in A_{inner}] \\ &\overset{(a)}{\approx} \mathbb{P}[R_1 \leqslant x \mid R_1 \leqslant D] \\ &= \frac{1-\exp(-\pi\lambda_1 x^2)}{1-\exp(-\pi\lambda_1 D^2)}, \quad \text{for } x \leqslant D, \end{aligned} \tag{3.17}$$

where the approximation in step (a) is conducted by assuming that the inner region typical user always gets service from the macrocell tier. This assumption is reasonable from the practical implementation viewpoint: The transmit powers of macrocell BSs should be much larger than femtocell BSs, that is, $P_1 \gg P_2$, which makes the fact that the inner region typical user is served by a femtocell BS with a small probability.

Subsequently, the PDF of X_1 in (3.16) can be found by differentiating the CDF, i.e.,

$$f_{X_1|o\in A_{inner}}(x) = \frac{\mathrm{d}F_{X_1|o\in A_{inner}}(x)}{\mathrm{d}x}, \tag{3.18}$$

which completes the proof. □

It should be noted that the inner region users are assumed to be served by macrocell BSs only, which makes it unnecessary to derive the PDF of X_2 for inner region typical user, that is, $f_{X_2|o\in A_{inner}}(x)$.

Lemma 3.2. *The PDF of X_1, conditioned on that the typical user is in the outer region, can be approximated as*

$$f_{X_1|o\in A_{outer}}(x) \approx \frac{2\pi[\lambda_1 + \lambda_2\big(\frac{P_2}{P_1}\big)^{2/\alpha}] \cdot x \exp\big(-\pi[\lambda_1 + \lambda_2\big(\frac{P_2}{P_1}\big)^{2/\alpha}]x^2\big)}{\exp\big(-\pi[\lambda_1 + \lambda_2\big(\frac{P_2}{P_1}\big)^{2/\alpha}]D^2\big)}, \quad \textit{for } x > D. \tag{3.19}$$

Proof. See Appendix B.1. □

Lemma 3.3. *The PDF of X_2, conditioned on that the typical user is in the outer region, can be approximated as*

$$f_{X_2|o\in A_{outer}}(x) \approx \begin{cases} M \cdot 2\pi\lambda_2 x \exp(-\pi\lambda_2 x^2) & \text{for } x \leqslant \left(\frac{P_2}{P_1}\right)^{1/\alpha} D \\ M \cdot \left[\frac{2\pi x\lambda_2}{\exp(-\pi\lambda_1 D^2)} \cdot \exp\left(-\pi[\lambda_1\left(\frac{P_1}{P_2}\right)^{2/\alpha} + \lambda_2]x^2\right)\right] & \text{for } x > \left(\frac{P_2}{P_1}\right)^{1/\alpha} D, \end{cases} \tag{3.20}$$

where the constant M is

$$M = \frac{\exp(-\pi\lambda_1 D^2)}{\exp(-\pi\lambda_1 D^2) - \lambda_1 \exp\left(-\pi[\lambda_1 + \lambda_2(\frac{P_2}{P_1})^{2/\alpha}]D^2\right)/(\lambda_1 + \lambda_2(\frac{P_2}{P_1})^{2/\alpha})}. \tag{3.21}$$

Proof. See Appendix B.2. □

3.4.3 The Density of Loaded BSs

As stated in Section 3.3, we assume that the interference signal at the data channel is only generated from the loaded BSs (i.e., the BSs having at least one user associated). We use the process Φ'_i to denote the i-th tier loaded BSs for the non-uniform femtocell deployment scheme, excluding the unloaded BSs without users associated. It should be noted that Φ'_1 is the process over the entire plane, whereas Φ'_2 exists in the outer region only. We are interested in the density of Φ'_i over its deployment region, i.e., λ'_i, which will be used to estimate the interference process later on.

Before obtaining this result, we focus on the cell association probabilities firstly, that is, the probability of the typical user served by the macrocell or femtocell tier.

Lemma 3.4. *The probability of the typical user served by the macrocell tier, $\mathcal{Q}_1 = \mathbb{P}[\kappa = 1]$, can be approximated by*

$$\mathcal{Q}_1 \approx 1 - \exp(-\pi\lambda_1 D^2) + \frac{\lambda_1}{\lambda_1 + \lambda_2\left(\frac{P_2}{P_1}\right)^{2/\alpha}} \cdot \exp\Big(-\pi[\lambda_1 + \lambda_2\left(\frac{P_2}{P_1}\right)^{\frac{2}{\alpha}}]D^2\Big). \tag{3.22}$$

Proof. From its definition, $\mathcal{Q}_1 = \mathbb{P}[\kappa = 1]$ can be expanded as

$$\begin{aligned} \mathcal{Q}_1 &= \mathbb{P}[\kappa = 1, o \in A_{inner}] + \mathbb{P}[\kappa = 1, o \in A_{outer}] \\ &\approx \mathbb{P}[o \in A_{inner}] + \mathbb{P}[\kappa = 1, o \in A_{outer}], \end{aligned} \tag{3.23}$$

in which the approximation is based upon the fact that the inner region typical user is associated with the femtocell tier with a small probability. The latter part of (3.23), that is, the probability of accessing the macrocell tier and locating in A_{outer}, is provided by

$$\begin{aligned} &\mathbb{P}[\kappa = 1, o \in A_{outer}] \\ &= \mathbb{P}[\kappa = 1 \mid o \in A_{outer}] \cdot \mathbb{P}[o \in A_{outer}] \\ &= \int_D^\infty \mathbb{P}[\kappa = 1 \mid R_1 = x, o \in A_{outer}] \cdot f_{R_1|o\in A_{outer}}(x)\mathrm{d}x \cdot \mathbb{P}[o \in A_{outer}] \\ &= \int_D^\infty \mathbb{P}[R_2 > \big(\frac{P_2}{P_1}\big)^{1/\alpha} x \mid o \in A_{outer}] f_{R_1|R_1>D}(x)\mathrm{d}x \cdot \mathbb{P}[o \in A_{outer}] \\ &\overset{(a)}{\approx} \int_D^\infty \exp(-\pi\lambda_2\big(\frac{P_2}{P_1}\big)^{2/\alpha} x^2) \cdot \frac{2\pi\lambda_1 r \exp(-\pi\lambda_1 r^2)}{\exp(-\pi\lambda_1 D^2)}\mathrm{d}x \cdot \exp(-\pi\lambda_1 D^2) \\ &= \frac{\lambda_1}{\lambda_1 + \lambda_2\big(\frac{P_2}{P_1}\big)^{2/\alpha}} \cdot \exp\Big(- \pi[\lambda_1 + \lambda_2\big(\frac{P_2}{P_1}\big)^{\frac{2}{\alpha}}]D^2\Big), \end{aligned} \tag{3.24}$$

where we approximate the density of femtocell BSs in the vicinity of the outer region typical user as λ_2 in step (a). By substituting (3.24) and the expression of $\mathbb{P}[o \in A_{inner}]$ in (3.14) into (3.23), we reach the result in (3.22), which completes the proof. □

For cell association to the femtocell tier, we only consider the case in which the typical user is in the outer region. This is because the active femtocell BSs are all located in the outer region, and there is a very minimal chance for a inner region user to get associated with a femtocell BS.

Lemma 3.5. *The probabilities of the outer region typical user associated with the macrocell tier and the femtocell tier, namely,* $\mathcal{Q}_{1,outer} = \mathbb{P}[\kappa = 1 \mid o \in A_{outer}]$ *and* $\mathcal{Q}_{2,outer} = \mathbb{P}[\kappa = 2 \mid o \in A_{outer}]$*, can be estimated by*

$$\mathcal{Q}_{1,outer} \approx \frac{\lambda_1}{\lambda_1 + \lambda_2\big(\frac{P_2}{P_1}\big)^{2/\alpha}} \cdot \exp\Big(- \pi\lambda_2\big(\frac{P_2}{P_1}\big)^{\frac{2}{\alpha}} D^2\Big), \tag{3.25}$$

and

$$\mathcal{Q}_{2,outer} \approx 1 - \frac{\lambda_1}{\lambda_1 + \lambda_2 \left(\frac{P_2}{P_1}\right)^{2/\alpha}} \cdot \exp\Big(- \pi \lambda_2 \big(\frac{P_2}{P_1}\big)^{\frac{2}{\alpha}} D^2 \Big). \tag{3.26}$$

Proof. This result $\mathcal{Q}_{2,outer} = \mathbb{P}[\kappa = 2 \mid o \in A_{outer}]$ can be obtained by $\mathcal{Q}_{2,outer} = 1 - \mathbb{P}[\kappa = 1, o \in A_{outer}]/\mathbb{P}[o \in A_{outer}]$, in which $\mathbb{P}[\kappa = 1, o \in A_{outer}]$ and $\mathbb{P}[o \in A_{outer}]$ are provided in (3.24) and (3.14). Thus, $\mathcal{Q}_{1,outer}$ can be easily obtained because of $\mathcal{Q}_{1,outer} = 1 - \mathcal{Q}_{2,outer}$. □

Lemma 3.6. *The density of Φ_i' over the corresponding macrocell- and femtocell-tier deployment regions can be respectively approximated by*

$$\lambda_1' \approx \lambda_1 \bigg[1 - \Big(\frac{\lambda_1 b}{\lambda_{MS} \mathcal{Q}_1 + b\lambda_1} \Big)^q \bigg], \tag{3.27}$$

and

$$\lambda_2' \approx \lambda_2 \bigg[1 - \Big(\frac{\lambda_2 b}{\lambda_{MS} \mathcal{Q}_{2,outer} + b\lambda_2} \Big)^q \bigg]. \tag{3.28}$$

Proof. See Appendix B.3 □

It should be noticed that λ_1' is the density of Φ_1' over the whole plane, and λ_2' is the density of Φ_2' in the outer region only. This difference comes from the non-uniform femtocell deployment scheme. For simplicity, we use the homogenous PPP with density λ_1' over the entire plane and the PPP with density λ_2' on the outer region, respectively, to analyze the interference signal.

3.4.4 Coverage Probability

Now we present the result on the coverage probability $p_c(T)$, that is, the probability that the instantaneous SINR at the typical user's data channel is above a target SINR threshold T. The coverage probability is equivalent to the CCDF of SINR. The coverage probabilities given the typical user is located in the inner region and the outer region, are presented in Theorem 3.7 and Theorem 3.8, respectively.

Theorem 3.7. *The coverage probability for the typical user in the inner region*

A_{inner} is approximated by

$$p_{c,A_{inner}}(T) \approx \frac{2\pi\lambda_1}{[1-\exp(-\pi\lambda_1 D^2)]} \int_0^D \exp\big(-\frac{T\sigma^2 x^\alpha}{P_1}\big) \exp\Big(-\pi\big[\lambda_1+\lambda_1'\rho(T,\alpha)\big]x^2\Big) \exp\Big(-\pi\lambda_2' D^2 \rho\big(\frac{P_2 T x^\alpha}{P_1 D^\alpha},\alpha\big)\Big) x\mathrm{d}x. \quad (3.29)$$

Proof. See Appendix B.4. □

Theorem 3.8. *The coverage probability for the typical user in the outer region A_{outer} is provided by*

$$p_{c,A_{outer}}(T) = \sum_{i\in\{1,2\}} p_{c,i,A_{outer}}(T)\cdot\mathbb{P}[\kappa=i \mid o\in A_{outer}], \quad (3.30)$$

where

$$p_{c,1,A_{outer}}(T) \approx \frac{2\pi[\lambda_1+\lambda_2\big(\frac{P_2}{P_1}\big)^{2/\alpha}]}{\exp\big(-\pi[\lambda_1+\lambda_2\big(\frac{P_2}{P_1}\big)^{2/\alpha}]D^2\big)} \int_D^\infty \exp\big(-\frac{T\sigma^2 x^\alpha}{P_1}\big) \cdot \exp\Big(-\pi\big[\big(\lambda_1+\lambda_2\big(\frac{P_2}{P_1}\big)^{2/\alpha}\big)+\rho(T,\alpha)\big(\lambda_1'+\lambda_2'\big(\frac{P_2}{P_1}\big)^{2/\alpha}\big)\big]x^2\Big)x\mathrm{d}x, \quad (3.31)$$

and

$$p_{c,2,A_{outer}}(T) = 2\pi\lambda_2 M\cdot\int_0^{(\frac{P_2}{P_1})^{\frac{1}{\alpha}}D} x\exp\big(-\frac{T\sigma^2x^\alpha}{P_2}\big) \cdot\exp\Big(-\pi\lambda_1' D^2\rho\big(\frac{P_1 T x^\alpha}{P_2 D^\alpha},\alpha\big)\Big)\exp\Big(-\pi\big(\lambda_2+\lambda_2'\rho(T,\alpha)\big)x^2\Big)\mathrm{d}x + \frac{2\pi\lambda_2 M}{\exp(-\pi\lambda_1 D^2)}\int_{(\frac{P_2}{P_1})^{\frac{1}{\alpha}}D}^\infty x\exp\big(-\frac{T\sigma^2x^\alpha}{P_2}\big) \cdot\exp\Big(-\pi\big[\big(\lambda_1\big(\frac{P_1}{P_2}\big)^{2/\alpha}+\lambda_2\big)+\rho(T,\alpha)\big(\lambda_1'\big(\frac{P_1}{P_2}\big)^{2/\alpha}+\lambda_2'\big)\big]x^2\Big)\mathrm{d}x. \quad (3.32)$$

Proof. See Appendix B.5. □

The following Corollary 3.9 provides the coverage probability for a randomly chosen typical user, which can be obtained easily by expanding the coverage probability into inner and outer regions.

Corollary 3.9. *For a typical user, the coverage probability is*

$$p_c(T) = p_{c,A_{inner}}(T)\cdot\mathbb{P}[o\in A_{inner}] + p_{c,A_{outer}}(T)\cdot\mathbb{P}[o\in A_{outer}], \quad (3.33)$$

where $\mathbb{P}[o \in A_{inner}]$ *and* $\mathbb{P}[o \in A_{outer}]$ *are given in (3.14).*

3.4.5 Single User Throughput

In this section, we derive another and the most important analytical result of this chapter, the probabilistic characteristics of the achievable single user throughput (denoted by $\mathcal{R}$) for the proposed non-uniform femtocell deployment. Similar to the coverage probability analysis in Subsection 3.4.4, we will first focus on the throughput in the inner and outer regions separately.

Theorem 3.10. *The CCDF of the throughput achieved at the typical user in the inner region* A_{inner} *is provided by*

$$\mathbb{P}[\mathcal{R} > \rho \mid o \in A_{inner}] \approx \sum_{n=0}^{\infty} \mathbb{P}[N_1 = n] \cdot p_{c,A_{inner}}\big(2^{(n+1)\rho/W} - 1\big), \tag{3.34}$$

where N_1 *is the number of in-cell users sharing the resource with the macrocell typical user, and its PMF is approximated as*

$$\mathbb{P}[N_1 = n] \approx \frac{b^q}{n!} \cdot \frac{\Gamma(n+q+1)}{\Gamma(q)} \cdot \Big(\frac{\lambda_{MS}}{\lambda_1/\mathcal{Q}_1}\Big)^n \Big(b + \frac{\lambda_{MS}}{\lambda_1/\mathcal{Q}_1}\Big)^{-(n+q+1)}, \quad \text{for } n \in \{0,1,2,...\}, \tag{3.35}$$

in which $\mathcal{Q}_1$ *is given in Lemma 3.4.*

Proof. See Appendix B.6. □

Theorem 3.11. *The CCDF of the throughput achieved at the typical user in the outer region* A_{outer} *is provided by*

$$\mathbb{P}[\mathcal{R} > \rho \mid o \in A_{outer}] \approx \sum_{i \in \{1,2\}} \sum_{n=0}^{\infty} \mathbb{P}[N_i = n] \cdot p_{c,i,A_{outer}}\big(2^{(n+1)\rho/W} - 1\big) \cdot \mathcal{Q}_{i,outer}, \tag{3.36}$$

where the values of $\mathcal{Q}_{1,outer}$ *and* $\mathcal{Q}_{2,outer}$ *are provided in Lemma 3.5,* $\mathbb{P}[N_1 = n]$ *is given in (3.35), and* $\mathbb{P}[N_2 = n]$ *is the distribution of the number of in-cell user*

sharing the resource with the femtocell typical user, that is,

$$\mathbb{P}[N_2 = n] \approx \frac{b^q}{n!} \cdot \frac{\Gamma(n+q+1)}{\Gamma(q)} \cdot \Big(\frac{\lambda_{MS}}{\lambda_2/\mathcal{Q}_{2,outer}}\Big)^n \Big(b + \frac{\lambda_{MS}}{\lambda_2/\mathcal{Q}_{2,outer}}\Big)^{-(n+q+1)}, \quad \text{for } n \in \{0,1,2,...\}. \quad (3.37)$$

Proof. See Appendix B.7. □

The following Corollary 3.12 provides the distribution of the throughput achieved for a typical user, which can be obtained easily by expanding the distribution expression into inner and outer regions.

Corollary 3.12. *Considering resource sharing, the CCDF of the throughput achieved at the typical user can be expressed as*

$$\mathbb{P}[\mathcal{R} > \rho] = \mathbb{P}[\mathcal{R} > \rho \mid o \in A_{inner}] \cdot \mathbb{P}[o \in A_{inner}] + \mathbb{P}[\mathcal{R} > \rho \mid o \in A_{outer}] \cdot \mathbb{P}[o \in A_{outer}], \quad (3.38)$$

where $\mathbb{P}[o \in A_{inner}]$ *and* $\mathbb{P}[o \in A_{outer}]$ *are given in (3.14).*

3.5 Numerical Results

In this section, we present numerical results on the coverage and single user throughput for the proposed non-uniform femtocell deployment scheme. Here, we assume the transmit powers of macrocell and femtocell BSs as $P_{\mathrm{TX},1} = 46$ dBm and $P_{\mathrm{TX},2} = 20$ dBm, respectively. The macrocell-tier density is $\lambda_1 = 1$ per square km, and the mobile user density is $\lambda_{MS} = 10$ per square km in all numerical results. The path loss constant and exponent are assumed to be $L_0 = -34$ dB and $\alpha = 4$. The thermal noise power is $\sigma^2 = -104$ dBm. Monte Carlo simulations are also conducted to compare with our analysis for the purpose of model validation. The single user throughput demonstrated in our results are the rates achievable over the BS's bandwidth of 1 Hz, that is, $W = 1$ Hz.

In our numerical results for femtocell deactivation, λ_2 denotes the femtocell BS deployment density before the deactivating operation. To conduct a fair comparison with uniform deployment, the femtocell BS density of the smart femtocell deployment scheme in the outer region is set to be $\lambda_2/\mathbb{P}[o \in A_{outer}]$, which guarantees the average density over the whole plane becomes λ_2, identical to the uniform

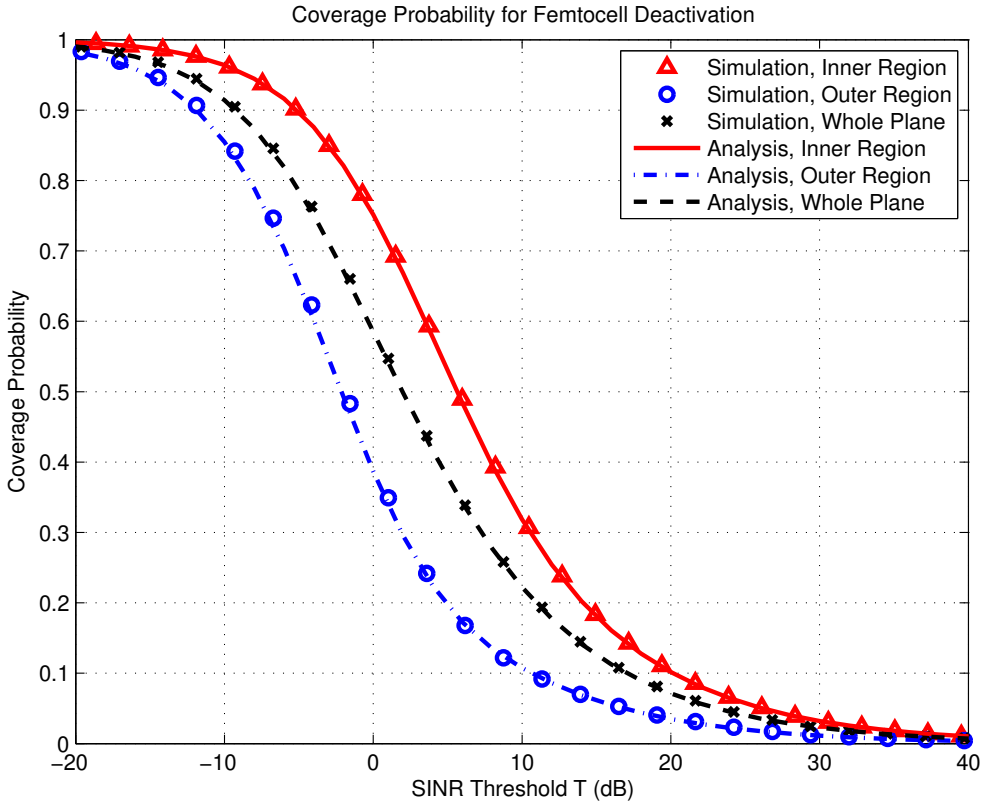

Figure 3.2: Coverage probability (or equivalently, the CCDF of received SINR) for femtocell deactivation, $D = 500$ m and $\lambda_2/\lambda_1 = 10$.

femtocell deployment.

3.5.1 Coverage Performance

Fig. 3.2 demonstrates the results of coverage probability (or equivalently, the CCDF of received SINR) with femtocell deactivation, given the condition of $D = 500$ m, $\lambda_2/\lambda_1 = 10$. Firstly, the analytical results, that is, the approximations derived for inner and outer regions in this chapter, are reasonably accurate. Through combining the results of outer and inner regions by using (3.33), the coverage probability curve for randomly chosen users is also illustrated therein.

In Fig. 3.3, the coverage probability curves for different schemes are compared, by which we can conclude that the analysis on femtocell deactivation and smart femtocell deployment precisely matches the simulation result. Furthermore, we can observe two phenomena, that is, femtocell deactivation will not hurt the coverage performance, and the non-uniform smart femtocell deployment scheme

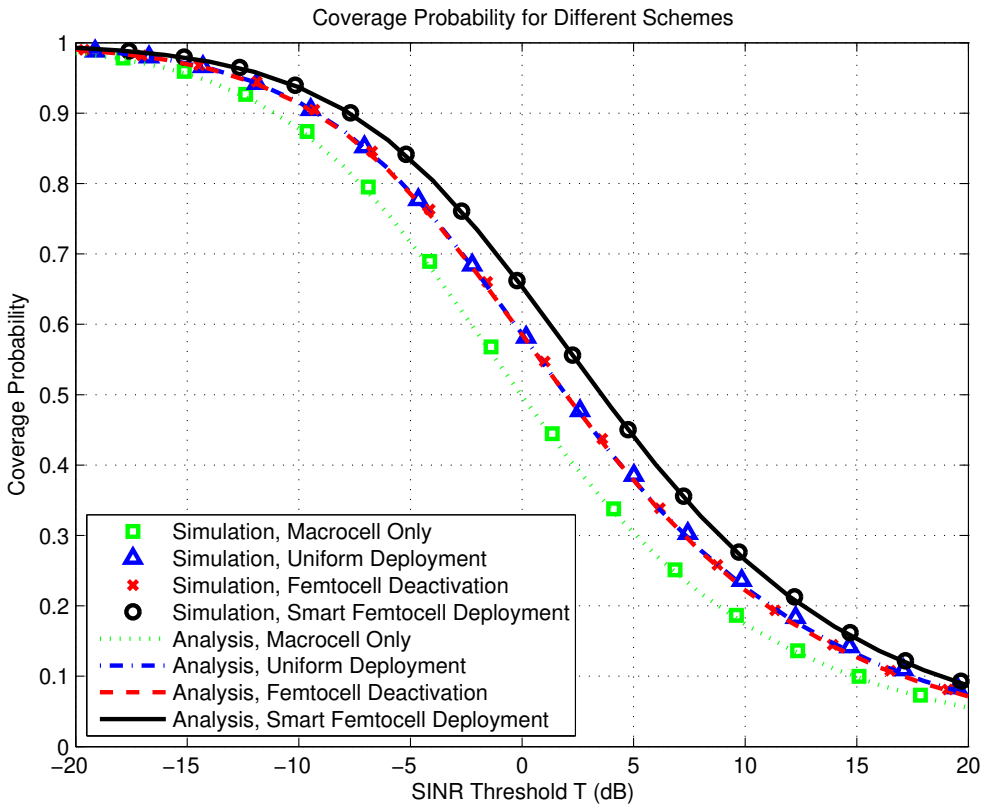

Figure 3.3: Coverage probability (or equivalently, the CCDF of received SINR) for different schemes, $D = 500$ m and $\lambda_2/\lambda_1 = 10$.

outperforms both macrocell only and two-tier uniform deployments.

Furthermore, by presenting the achievable coverage probability versus the inner region radius D in Fig. 3.4 and Fig. 3.5, we can see the importance of properly dividing inner and outer regions on the coverage performance. For an appropriated chosen D value, the scheme of femtocell deactivation can achieve nearly the same coverage performance as two-tier uniform femtocell deployment, even with a significantly lower *de facto* femtocell density. For instance, femtocell deactivation with $D = 500$ m, which means that 54.4% of femtocell BSs are deactivated, is as good as uniform deployment on coverage probability for SINR threshold $T = -5$ dB. This result is surprising as more than half of the femtocell BS energy consumption and the corresponding operating expense can be saved with the same level of coverage performance.

By compensating the femtocell density in the outer region, significant coverage improvement can be obtained for smart femtocell deployment. To take the

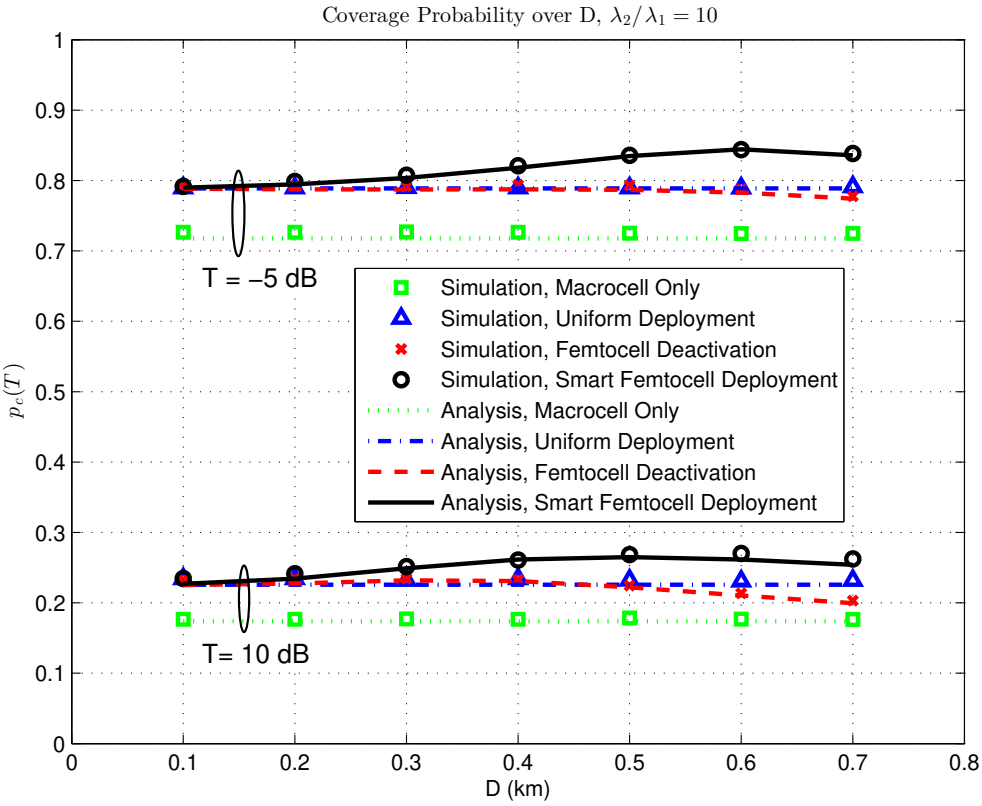

Figure 3.4: Coverage probability (or equivalently, the CCDF of received SINR) for different schemes, with the tier density ratio $\lambda_2/\lambda_1 = 10$. The SINR thresholds are set to be $T = -5$ dB and $T = 10$ dB.

case of $\lambda_2/\lambda_1 = 10$ and $T = -5$ dB as an example, the achievable coverage probability is around 85% at $D = 600$ m for smart femtocell deployment, compared with 79% for uniform two-tier deployment, and 73% for the case with macrocell tier deployed only. Similar enhancements can be observed with a different SINR threshold (i.e., $T = 10$ dB) or a different femtocell density (i.e., $\lambda_2/\lambda_1 = 5$). It should be noted that the slight mismatches between simulation and analytical results in Fig. 3.4 and Fig. 3.5 come from the approximation used in the analysis, but the performance trend can be well captured by the analytical results. More importantly, both schemes of femtocell deactivation and smart femtocell deployment do not incur any further network resources: we just turn off the femtocell BSs located in the inner region in femtocell deactivation scheme, or deploy femtocell BSs in the outer region only for smart femtocell deployment scheme.

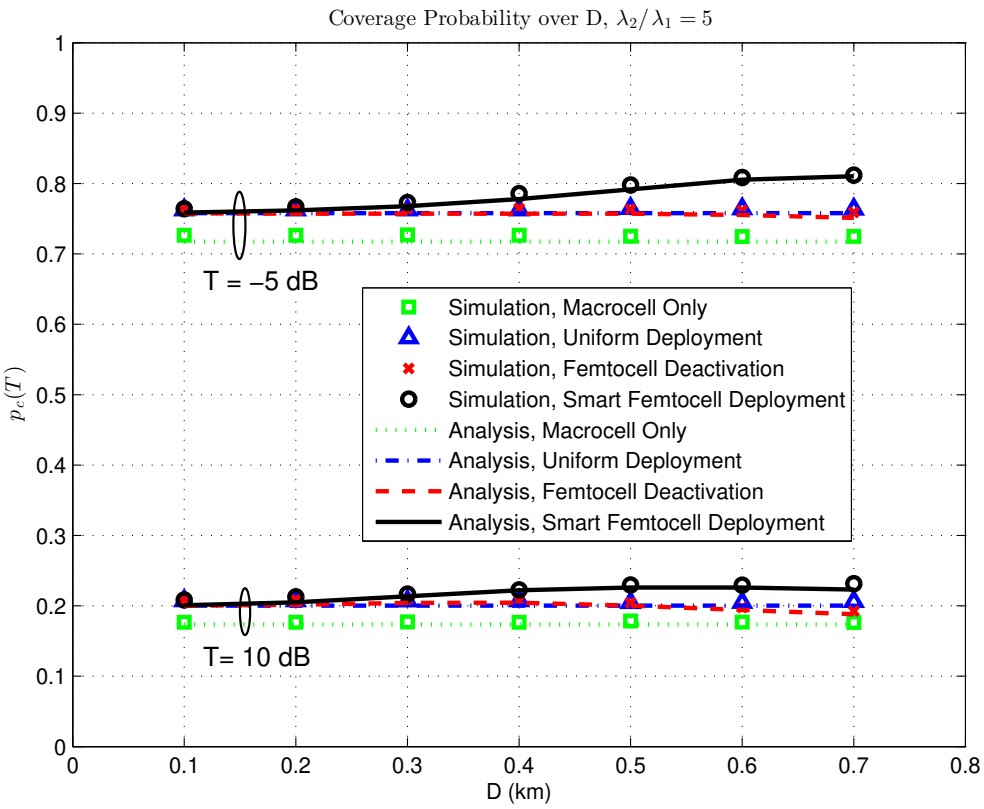

Figure 3.5: Coverage probability (or equivalently, the CCDF of received SINR) for different schemes, with the tier density ratio $\lambda_2/\lambda_1 = 5$. The SINR thresholds are set to be $T = -5$ dB and $T = 10$ dB.

3.5.2 Throughput Performance

To validate the analytical single user throughput performances for the proposed schemes, the CCDF curves for the inner and outer regions obtained from Theorem 3.10 and Theorem 3.11 are compared with the simulation counterparts in Fig. 3.6. It can be shown that the throughput distributions are well captured by the analytical results. By combining the inner and outer region results in Corollary 3.12, we compare the single user throughput performances for different deployment schemes in Fig. 3.7. The analytical results for both femtocell deactivation and smart femtocell deployment are reasonably accurate. For femtocell deactivation, basically it only reduces high-rate users' performance at the same time not hurting low-rate users, compared with the uniform case. As low-rate users are usually much more of a concern to the cellular service providers [142], this scheme has the desirable property of being able to significantly reduce the

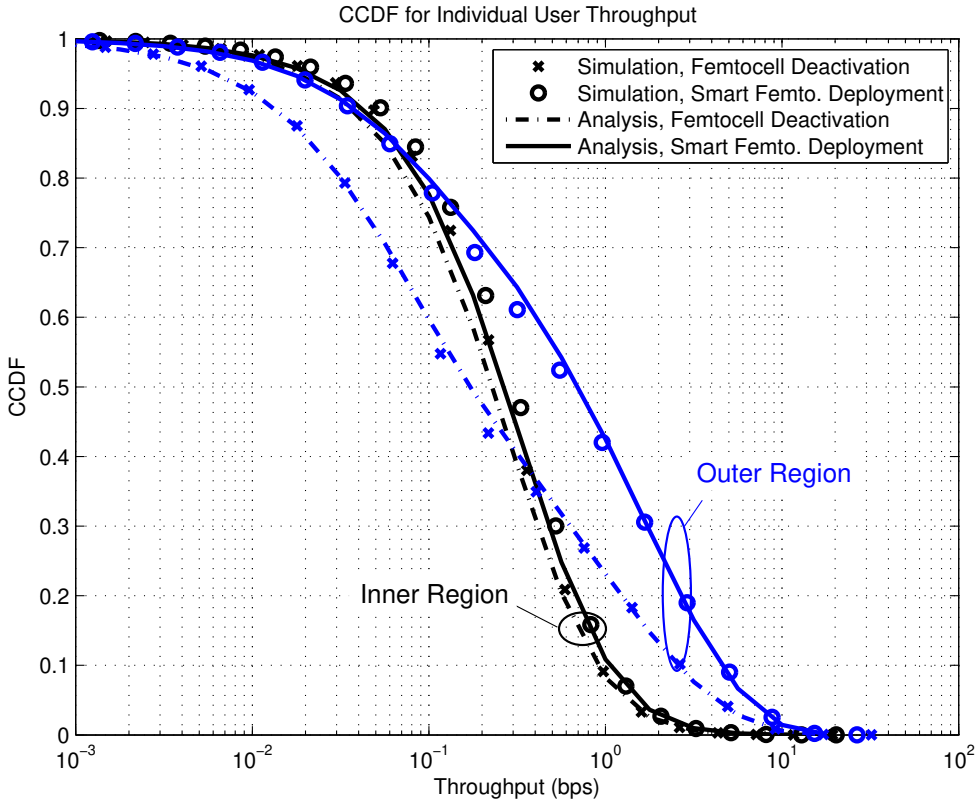

Figure 3.6: Single user throughput distribution (CCDF curves) for inner and outer regions, $D = 500$ m and $\lambda_2/\lambda_1 = 10$.

resource while taking care of the low-rate users. For smart femtocell deployment, it increases all users' performance, especially the low-rate ones. Take the worst 10% users for instance, the highest achievable rate among these users is increased from 0.025 bps in the uniform case to 0.043 bps in the smart deployment case, which is a 72% improvement.

From the single user throughput performances versus the inner region radius D demonstrated in Fig. 3.8 and Fig. 3.9, we can see the impact of the inner region radius D on the single user throughput performance. For femtocell deactivation, optimally choosing D can significantly reduce the resource at the same time not hurting the low-rate users' performance: for example, D can get up to 400 m in both figures for $\rho = 0.02$ bps. For smart femtocell deployment: optimally choosing D results in noticeable improvement for both low-rate and high-rate users. Our analytical results provide tools to design the value of D to maximize the benefits to a target group of users of the operator's choice. To take $\lambda_2/\lambda_1 = 10$

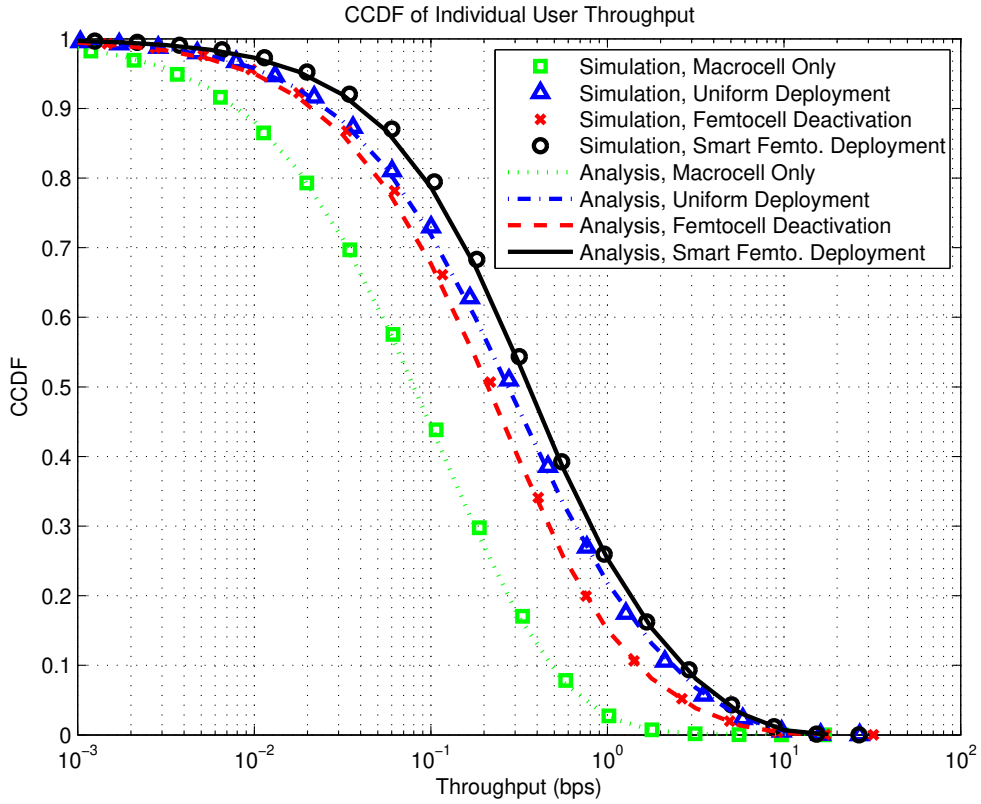

Figure 3.7: Single user throughput distribution (CCDF curves) for different schemes, $D = 500$ m and $\lambda_2/\lambda_1 = 10$.

as an example, $D = 400$ m and $D = 500$ m can achieve near-optimal values of $\mathbb{P}[\mathcal{R} > \rho]$ for high- and low-rate thresholds, respectively.

3.6 Summary of Contributions

In this chapter, we have studied the downlink coverage and throughput performance of the cellular networks with the newly proposed non-uniform femtocell deployment scheme. There are two ways to implement this scheme, i.e., femtocell deactivation and smart femtocell deployment. Using the tools from stochastic geometry, we provided the probabilistic characterization of the downlink coverage and single user throughput at a randomly located mobile user in this new scheme. To our knowledge, it is the first study to derive analytical results on a non-uniform femtocell deployment.

The numerical results validated the analytical expressions and approxima-

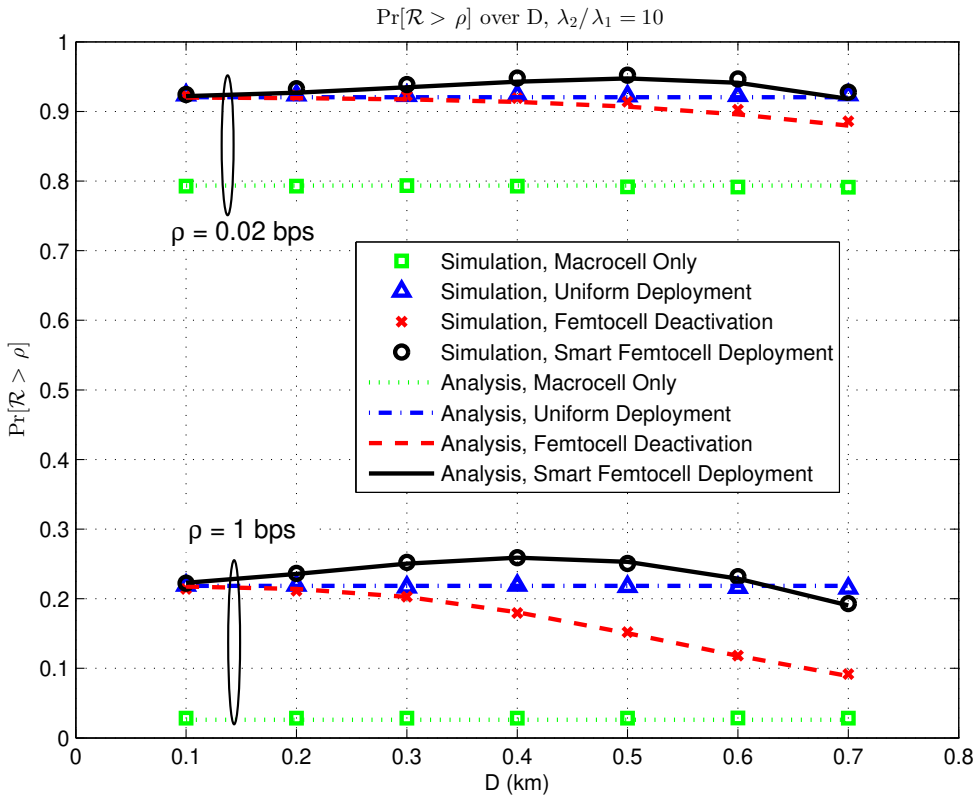

Figure 3.8: $\mathbb{P}[\mathcal{R} > \rho]$ over D for different schemes, with the tier density ratio $\lambda_2/\lambda_1 = 10$. The rate thresholds are set to be $\rho = 0.02$ bps and $\rho = 1$ bps.

tions, and provided the following important message: By carefully choosing the parameters for the proposed femtocell deactivation scheme, more than 50% of femtocell BSs can be turned off to save the femtocell BS energy consumption and the operating expense, but achieve the same coverage performance as deploying femtocell uniformly. By compensating the femtocell density in the poor macrocell coverage regions, the smart femtocell deployment, compared with uniform femtocell deployment, can obtain noticeable improvement on the coverage and the data throughput with no extra cost of network resource incurred.

This interesting finding demonstrates the performance improvements achievable by implementing a simple non-uniform femtocell deployment, and emphasizes the importance of selectively deploying the femtocell BSs by taking their relative locations with macrocell BSs into account.

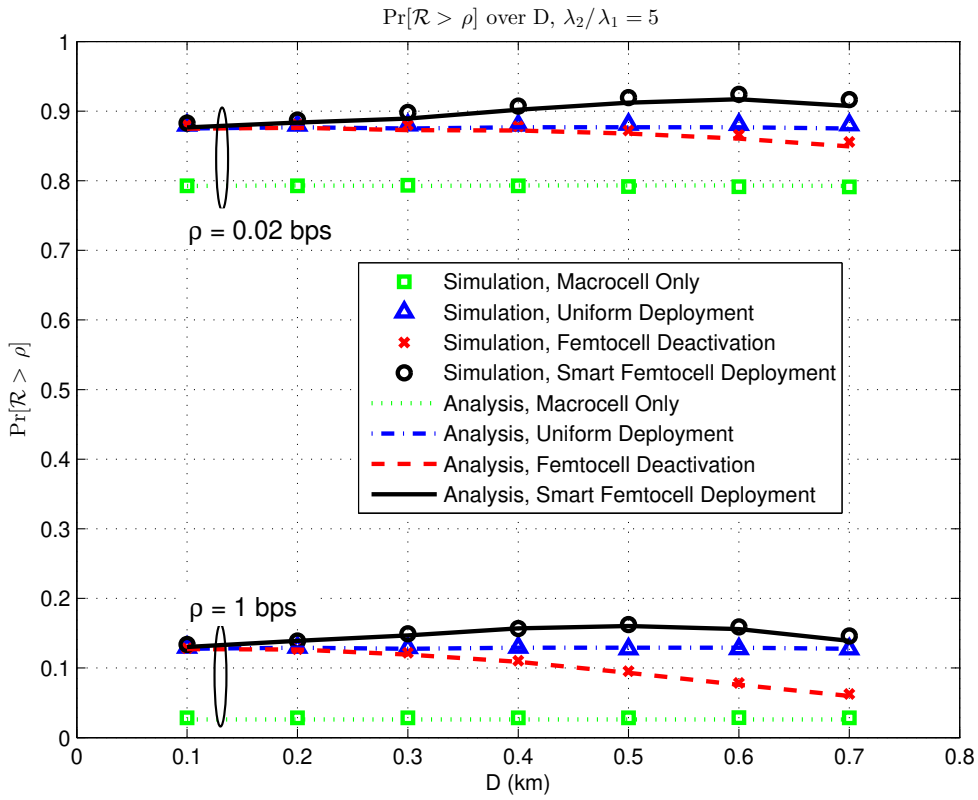

Figure 3.9: $\mathbb{P}[\mathcal{R} > \rho]$ over D for different schemes, with the tier density ratio $\lambda_2/\lambda_1 = 5$. The rate thresholds are set to be $\rho = 0.02$ bps and $\rho = 1$ bps.

Chapter 4

Analysis on Femtocell Uplink Attenuation Algorithms

4.1 Introduction

It is well known that the uplink interference experienced at the receivers of femtocell BSs is one of the most significant problems for CDMA-based femtocells, especially when they are co-channel deployed with existing macrocell network and operated in CSG mode. Because of the CSG mode employed, the nearby nonsubscribers (including macrocell users and femtocell users served by other femtocell BSs) are unable to be controlled by the femtocell BSs. The power control scheme implemented in nonsubscriber terminal increases the transmit power level to compensate for the path losses to its serving macrocell far away, jamming the uplink of the nearby femtocells. Considering the fact that the minimum coupling loss between user terminal's transmitter and femtocell BS's receiver can be as low as 30-40 dB in practical implementation, the signals emitted from the close-by nonsubscribers may cause disastrous interference problems at the CSG femtocell BSs [65,76]. Furthermore, the out-of-band radiation also contributes to the uplink interference, even when femtocells are operating in adjacent bands particularly in dense deployments [24].

Proper interference mitigation techniques, such as uplink attenuation, can be employed to tackle this significant interference case [65]. Specifically, in the presence of high out-of-cell interference, attenuation (or a large noise figure value equivalently) is applied at the femtocell uplink receiver's frontend to bring the level of out-of-cell interference down to be comparable to the thermal noise level

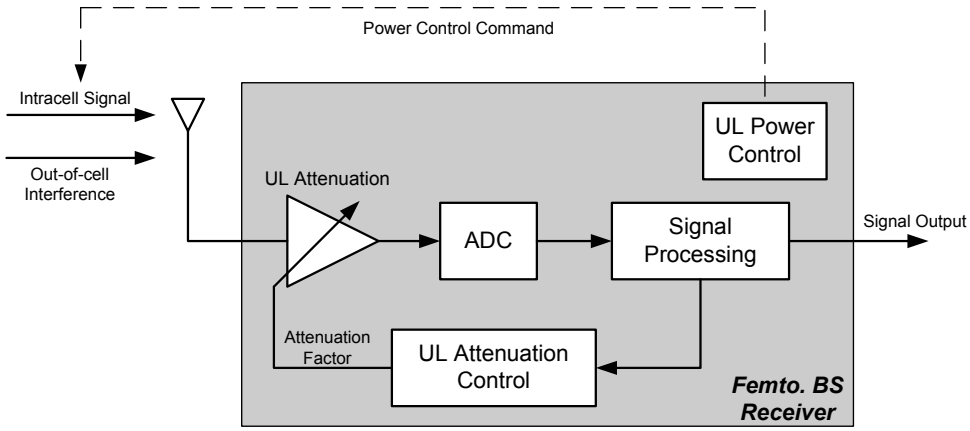

Figure 4.1: The diagram of uplink attenuation for femtocell BS receiver.

[77], which is performed by an analog attenuator prior to the ADC, as shown in Fig. 4.1. The aim for this uplink attenuation is to ensure the noise rise of the resultant signals staying below a system-defined threshold such that the femtocell signal acquisition unit can function normally. As a result of the uplink attenuation operation to desensitize the receiver, users connected to the femtocell BSs increase their transmit power levels to overcome the attenuation, thus generating higher uplink interference to nearby BSs [131, 132] and causing an increase in the power consumption for attached femtocell users. Additionally, because the maximum power of femtocell users may be restricted to avoid the impact on macrocells [40], the increased transmit power level due to uplink attenuation might increase the chance of outage events at the edge of the femtocell, since certain SINR levels at the receiver need to be maintained for preset qualities of service.

Based upon the above discussion, we analyze the femtocell uplink environment where the uplink attenuation technique is implemented, and demonstrate the tradeoff between higher level uplink attenuation resulting in a higher probability to reach the maximum power cap and lower level attenuation with less interference mitigation. This tradeoff can provide us useful information in practical system design and inspire us to propose new adaptive uplink attenuation algorithms: Conventional adaptive uplink attenuation algorithm tries to maintain the out-of-cell interference contribution to femtocell noise rise at a constant value; however, this is not an optimal approach in terms of minimizing system's outage probability. In this chapter, we aim to propose new adaptive uplink attenuation

algorithms taking the above tradeoff into account.

This chapter is organized as follows. In Section 4.2, the system model used in this chapter and the uplink attenuation are introduced. Section 4.3 derives the analytical results on the outage probability with fixed uplink attenuation, based on which the above mentioned tradeoff can be demonstrated quantitatively. In Section 4.4, two novel adaptive algorithms are proposed, both of which aim to minimize the outage probability by adaptively adjusting the uplink attenuation factor based on the information available at the femtocell receiver. Section 4.5 provides numerical results and Section 4.6 concludes the chapter.

4.2 System Model

We consider the uplink scenario with a CDMA-based femtocell BS, where some uplink out-of-cell interference sources, such as mobile users not served by this femtocell BS, exist nearby. The variable M is used to indicate the number of active femtocell users, which simultaneously request the data services from the femtocell BS. In this chapter, we utilize X to denote any power, SINR or other ratio variables in linear unit, and X_{dB} to denote the corresponding variables in decibel unit, i.e., $X = 10^{X_{dB}/10}$.

At the receiver of the target femtocell BS, the SINR for the j-th femtocell user (otherwise called E_b/I_o specifically, defined as the ratio between the bit energy of desired signal and the density of interference and noise power), denoted by γ_j, can be presented in terms of the received powers of different femtocell users as

$$\gamma_j = \frac{\frac{P_{\mathrm{RX},j}}{R}}{\sum\limits_{i:i\neq j} \frac{P_{\mathrm{RX},j}}{W} + \frac{I}{W} + N_0}, \quad \text{for } j = 1, 2, ..., M, \tag{4.1}$$

where I is the interference power (introduced by the unattached users and other uncontrolled sources) received at the femtocell BS, R denotes the information bit rate required by femtocell users, W denotes the system bandwidth, N_0 is background noise power spectral density, and $P_{\mathrm{RX},j}$ is the power level received at the femtocell receiver from the j-th user.

4.2.1 Uplink Power Control and Noise Rise

The SINR requirements, denoted as $\{\gamma_j^* : j = 1, 2, ..., M\}$, for the various femtocell users vary with time due to the changes in multipath fading environment and imperfections in power control algorithm. In particular, the required SINR for the j-th femtocell user can be provided by

$$\gamma_j^* = \gamma_j^{\text{target}} \delta_j^{\gamma}, \quad \text{for } j = 1, 2, ..., M, \tag{4.2}$$

in which γ_j^{target} presents the target SINR which is a function of the target frame error rate (FER) and the multipath conditions, and δ_j^{γ} denotes the error in the power control algorithm. It should be noted that γ_j^* is the SINR being demanded by the power control algorithm at that particular time point.

Field trials have shown that the SINR requirements $\{\gamma_j^* : j = 1, 2, ..., M\}$ are well modeled by log-normal random variables [143]. Moreover, we can assume that the fading processes which cause the SINR requirement fluctuations are independent for different femtocell users [144, 145]. Based on the analysis mentioned earlier, we model the SINR requirements $\{\gamma_j^* : j = 1, 2, ..., M\}$ at any given time by independent and identically distributed log-normal random variables, i.e., $\gamma_{j,dB}^* = 10 \log_{10} \gamma_j^* \sim \mathcal{N}(m_{\gamma_{dB}}, \sigma_{\gamma_{dB}}^2)$, for $j = 1, 2, ..., M$. In order to meet the SINR requirement, the required received power levels $\{P_{\text{RX},j}^* : j = 1, 2, ..., M\}$ must satisfy the power control equations as below,

$$\gamma_j^* = \frac{\frac{P_{\text{RX},j}^*}{R}}{\sum\limits_{i:i\neq j} \frac{P_{\text{RX},i}^*}{W} + \frac{I}{W} + N_0}, \quad \text{for } j = 1, 2, ..., M. \tag{4.3}$$

In previous studies, it has been proved that the power control is feasible, namely, the series of equations (4.3) have positive solutions for $P_{\text{RX},j}^*$ (i.e., $P_{\text{RX},j}^* \in (0, \infty)$) for $j = 1, 2, ..., M$, if and only if the following condition can be fulfilled [145, 146]:

$$\sum_{i=1}^{M} \left(\frac{\gamma_i^*}{\frac{W}{R} + \gamma_i^*} \right) < 1. \tag{4.4}$$

For simplicity, we define the left side of (4.4) as ω, i.e., $\omega \triangleq \sum_{i=1}^{M} \left(\frac{\gamma_i^*}{W/R + \gamma_i^*} \right)$. It should be noted that the randomness of ω is introduced by the random variable set $\{\gamma_i^* : j = 1, 2, ..., M\}$. Provided the condition in (4.4) can be satisfied, the

required received power for the j-th user can be derived as

$$P^*_{\mathrm{RX},j} = \frac{1}{1-\omega} \cdot \frac{\gamma^*_j}{\frac{W}{R}+\gamma^*_j} \cdot (N_0 W + I)\,, \quad \text{for } j = 1, 2, ..., M. \tag{4.5}$$

After the process of uplink power control, the transmit power of each user terminal is adjusted to make sure all the received power targets $\{P^*_{\mathrm{RX},j} : j = 1, 2, ..., M\}$ can be maintained.

The term *noise rise* or *rise-over-thermal (RoT)* is used as a measure of the increase in interference due to the transmission activity in the cell [6], and can be expressed as

$$RoT = \underbrace{\frac{I}{N_0 W}}_{Unattached\ Users} + \underbrace{\frac{\sum_{i=1}^{M} P^*_{\mathrm{RX},i}}{N_0 W}}_{Femtocell\ Users}, \tag{4.6}$$

where the first term denotes the noise rise caused by unattached users, and the second term represents the noise rise caused by femtocell users. For example, 0 dB noise rise indicates an unloaded system and 3 dB noise rise implies a power spectral density due to uplink transmission equal to the noise spectral density.

The noise rise has an impact on the cell coverage and uplink cell load. For instance, an extremely large noise rise will result in an unstable status for the CDMA-based BS, and also the loss of coverage for some user terminals, which may not have sufficient transmission power to reach the required SINR at the BS [147]. Therefore, the uplink scheduler must keep the noise rise within acceptable limits, defined as the threshold value RoT^* in our analysis.

4.2.2 Uplink Attenuation

For a practical femtocell deployment, significant uplink interference such as a penetrating signal from unattached user terminals in the proximity may exist because of restricted cell association policy (e.g., CSG mode) and unplanned locations [65]. The uplink interference can cause a substantial noise rise level at the femtocell BS, from which poor performance can arise. To resolve this problem, uplink attenuation algorithm was proposed [77], in which the uplink signal is attenuated when the femtocell receiver is being jammed by strong interference. Through desensitizing the interference by attenuating the signal at the femtocell receiver (which can be regarded as introducing a higher noise figure), the interference becomes more comparable to thermal noise. Hence, the noise rise level

can be maintained below the target value, which guarantees a stable operating point for the femtocell receiver.

Specifically, the uplink attenuation is implemented only when the noise rise level is higher than the threshold value RoT^*, i.e.,

$$RoT = \frac{I + \sum_{i=1}^{M} P^*_{\mathrm{RX},i}}{N_0 W} > RoT^*. \tag{4.7}$$

If uplink attenuation is applied, power control equations in (4.3) become

$$\gamma^*_j = \frac{\eta \frac{P^*_{\mathrm{RX},j}}{R}}{\eta\big(\sum\limits_{i:i\neq j} \frac{P^*_{\mathrm{RX},i}}{W}\big) + \eta\frac{I}{W} + N_0}, \quad \text{for } j = 1, 2, ..., M, \tag{4.8}$$

where $\eta \in (0, 1]$ is defined as the *attenuation factor* in this chapter. The RoT level after employing uplink attenuation (denoted by RoT_{atten}) should be no more than the threshold value RoT^*, i.e.,

$$RoT_{\mathrm{atten}} = \frac{\eta I + \eta \sum_{i=1}^{M} P^*_{\mathrm{RX},i}}{N_0 W} \leqslant RoT^*. \tag{4.9}$$

Impact of Uplink Attenuation on RoT

Through algebraic manipulation, the required received power levels $\{P^*_{\mathrm{RX},j} : j = 1, 2, ..., M\}$ under certain level of uplink attenuation can be derived from (4.8) and (4.9):

$$P^*_{\mathrm{RX},j}(\eta) = \frac{1}{\eta} \cdot \frac{(N_0 W)\big(1 + RoT_{\mathrm{atten}}\big)\gamma^*_j}{\frac{W}{R} + \gamma^*_j}, \quad \text{for } j = 1, 2, ..., M. \tag{4.10}$$

By substituting (4.10) into (4.9), we can eliminate all the variables $\{P^*_{\mathrm{RX},j} : j = 1, 2, ..., M\}$ in the expression and derive the relationship between RoT_{atten} and ω, i.e.,

$$RoT_{\mathrm{atten}} = \underbrace{\eta \frac{I}{N_0 W}}_{Unattached\ Users} + \underbrace{\big(1 + RoT_{\mathrm{atten}}\big)\ \omega}_{Femtocell\ Users}, \tag{4.11}$$

in which the former part denotes the noise rise introduced by the interference generated by unattached users and latter part presents the value from femtocell-controlled users.

For the extreme case in which the interference power from the nearby un-

attached users becomes zero (i.e., $I = 0$), the RoT_{atten} becomes

$$RoT_{\text{atten}} = \frac{\omega}{1-\omega}, \quad \text{if } I = 0, \tag{4.12}$$

which is not related with the uplink attenuation factor η at all.

Uplink Attenuation Threshold

In order to guarantee that the noise rise level after attenuation should be no larger than the threshold value RoT^*, there is a requirement for the uplink attenuation to be satisfied (i.e., the maximum attenuation factor value able to fulfill the required noise rise level), which can be obtained by the following Lemma.

Lemma 4.1. *Assuming $I > 0$, the required uplink attenuation factor should be no larger than the following threshold η^*, i.e., $\eta \leqslant \eta^*$, and the value of η^* can be obtained by*

$$\eta^* \triangleq \frac{N_0 W RoT^*}{I}\left[1 - \left(1 + \frac{1}{RoT^*}\right)\omega\right]. \tag{4.13}$$

Proof. Based upon the equation (4.11) and $I > 0$, there is a relationship between uplink attenuation factor η and the resultant noise rise RoT_{atten}, i.e.,

$$\eta = \frac{N_0 W RoT_{\text{atten}}}{I}\left[1 - \left(1 + \frac{1}{RoT_{\text{atten}}}\right)\omega\right], \tag{4.14}$$

from which we can observe that the uplink attenuation factor η is monotonically increased with RoT_{atten}. To satisfy the requirement $RoT_{\text{atten}} \leqslant RoT^*$, we should have

$$\begin{aligned} \eta &= \frac{N_0 W RoT_{\text{atten}}}{I}\left[1 - \left(1 + \frac{1}{RoT_{\text{atten}}}\right)\omega\right] \\ &\leqslant \frac{N_0 W RoT^*}{I}\left[1 - \left(1 + \frac{1}{RoT^*}\right)\omega\right], \end{aligned} \tag{4.15}$$

in which the right part of the inequality can be regarded as the uplink attenuation factor threshold in (4.13), which completes the proof. □

From (4.15), it can be concluded that in order to maintain the value of RoT_{atten} to be no larger than RoT^*, the value of η should be no larger than the threshold η^*. It should be noted that threshold η^* can also be regarded as the random variable,

where the randomness is introduced by the random variable ω, otherwise by the variables $\{\gamma_j^* : j = 1, 2, ..., M\}$.

4.3 Analysis on Fixed Uplink Attenuation Performance

In this section, we focus on the instantaneous outage event for a single femtocell user if the technique of uplink attenuation is applied. Specifically, there are two possible ways to cause an outage event:

- Event $\mathbf{A}_{out}$: the power control or uplink attenuation cannot have a feasible solution, which means that the SINR requirements $\{\gamma_j^* : j = 1, 2, ..., M\}$ and the target noise rise RoT^* cannot be satisfied jointly.

- Event $\mathbf{B}_{out}$: the maximum transmit power at a certain femtocell user terminal is exceeded. It should be noted that this maximum power requirement can be caused by the physical implementation or additional limitation to control uplink interference to macrocell BSs [40].

Obviously, both the Events $\mathbf{A}_{out}$ and $\mathbf{B}_{out}$ highly depend on the uplink attenuation factor η, and it is of importance to determine the outage probability trend over the range of η.

The probability of outage for a certain value of uplink attenuation factor η can be given by

$$p_{out}(\eta) = \mathbb{P}[\mathbf{A}_{out}] + \big(1 - \mathbb{P}[\mathbf{A}_{out}]\big)\mathbb{P}[\mathbf{B}_{out} \mid \mathbf{A}_{out}^c], \tag{4.16}$$

where $\mathbf{A}_{out}^c$ is the complement of the event $\mathbf{A}_{out}$, i.e., $\mathbf{A}_{out}^c$ is the event that the power control and uplink attenuation equations have a feasible solution.

4.3.1 Power Control and Uplink Attenuation Feasibility

Firstly, we focus on the probability of event $\mathbf{A}_{out}$, in which the power control and uplink attenuation are unable to have a feasible solution at the same time.

Based on Lemma 4.1, in order to guarantee the target noise rise thresholds $\{\gamma_j^* : j = 1, 2, ..., M\}$, an uplink attenuation factor value η should satisfy $\eta \leqslant \eta^*$,

which is equivalent to the requirement for ω, i.e.,

$$\omega \leqslant \frac{RoT^*}{1+RoT^*}\Big(1-\frac{I\eta}{N_0 W RoT^*}\Big). \tag{4.17}$$

Remark. If the equation (4.17) can be satisfied, ω can easily satisfy $\omega < 1$, because $RoT^* > 0$. Since $\omega < 1$ can guarantee that the equations in (4.8) have a feasible solution, (4.17) become the condition for both feasible power control and uplink attenuation.

Theorem 4.2. *The probability of the event* $\mathbf{A}_{out}$ *is provided by*

$$\mathbb{P}[\mathbf{A}_{out}] = 1 - F_\omega\bigg(\frac{RoT^*}{1+RoT^*}\Big(1-\frac{I\eta}{N_0 W RoT^*}\Big)\bigg), \tag{4.18}$$

in which $F_\omega(\cdot)$ *is the CDF of the random variable* ω*.*

Proof. From Lemma 4.1, the probability of the event $\mathbf{A}_{out}$ can be derived as

$$\begin{aligned}\mathbb{P}[\mathbf{A}_{out}] &= \mathbb{P}\left(\eta > \eta^*\right) = F_{\eta^*}(\eta)\\ &= \mathbb{P}\bigg(\omega > \frac{RoT^*}{1+RoT^*}\Big(1-\frac{I\eta}{N_0 W RoT^*}\Big)\bigg)\\ &= 1 - F_\omega\bigg(\frac{RoT^*}{1+RoT^*}\Big(1-\frac{I\eta}{N_0 W RoT^*}\Big)\bigg),\end{aligned} \tag{4.19}$$

where $F_{\eta^*}(\cdot)$ is the CDF of η^*. □

Since ω is defined as $\omega \triangleq \sum_{i=1}^{M}\big(\frac{\gamma_i^*}{W/R+\gamma_i^*}\big)$, defining $\alpha_i \triangleq (W/R\gamma_i^*)$ for $j = 1, 2, ..., M$ can give us

$$\omega = \sum_{i=1}^{M}\frac{1}{1+\alpha_i}, \tag{4.20}$$

which make us turn to find the distribution of α_i for $j = 1, 2, ..., M$. Following the analysis in [145], modeling $\{\gamma_i^* : j = 1, 2, ..., M\}$ as log-normal random variables, i.e., $\gamma_{i,dB}^* = 10\log_{10}\gamma_i^* \sim \mathcal{N}(m_{\gamma_{dB}}, \sigma_{\gamma_{dB}}^2)$, for $j = 1, 2, ..., M$, can help us to reach the PDF of $1/(1+\alpha_i)$ as follows,

$$f_{\frac{1}{1+\alpha_i}}(x) = \frac{10}{\ln 10}\frac{1}{\sqrt{2\pi\sigma_{\gamma_{dB}}^2}}\frac{1}{x(1-x)}\cdot\exp\bigg[-\frac{\big(10\log_{10}\big(\frac{R}{W}\frac{1-x}{x}\big)+m_{\gamma_{dB}}\big)^2}{2\sigma_{\gamma_{dB}}^2}\bigg],$$
$$\text{for } 0<x<1 \quad \text{and} \quad i = 1, 2, ..., M. \tag{4.21}$$

Due to the assumption that all the random variables in the set $\{\gamma_i^* : j = 1, 2, ..., M\}$ are independent of each other, the PDFs of $1/(1+\alpha_i)$ have the same distribution for different users, and the PDF of $\omega = \sum_{i=1}^{M}(\frac{1}{1+\alpha_i})$ can be achieved by repeated numerical convolution of $f_{\frac{1}{1+\alpha_i}}(x)$, i.e.,

$$f_\omega(x) = \underbrace{f_{\frac{1}{1+\alpha}}(x) * \cdots * f_{\frac{1}{1+\alpha}}(x)}_{M}, \tag{4.22}$$

through which the CDF of ω can be obtained by numerical integral

$$\begin{aligned} F_\omega(x) &= \int_0^x f_\omega(x)\mathrm{d}x \\ &= \int_0^x \underbrace{f_{\frac{1}{1+\alpha}}(x) * \cdots * f_{\frac{1}{1+\alpha}}(x)}_{M}\,\mathrm{d}x. \end{aligned} \tag{4.23}$$

Hence, by substituting (4.23) into (4.18), the probability for event $\mathbf{A}_{out}$ can be reached.

4.3.2 Probability to Reach Transmit Power Cap

We now discuss the probability of event $\mathbf{B}_{out}$, in which the required transmit power in a certain femtocell user exceeds the transmit power cap denoted by $P_{\mathrm{TX},max}$. Without any loss of generality, we focus on the j-th femtocell user in the femtocell under study. Assuming perfect power control employed to compensate the path loss and shadowing fading in the uplink channel, the required transmit power of the j-th femtocell user after applying uplink attenuation is provided by,

$$P_{\mathrm{TX},j}(\eta) = \frac{P^*_{\mathrm{RX},j}(\eta)}{L_0(r)^{-\alpha} \cdot Z_j}, \quad \text{for } j = 1, 2, ..., M, \tag{4.24}$$

in which $L_0(r)^{-\alpha}$ is the path loss value, the variable Z_j presents shadowing fading for the j-th femtocell user, and the required received power level $P^*_{\mathrm{RX},j}$ can be regarded as a function of η, written as $P^*_{\mathrm{RX},j}(\eta)$. For the path loss model used here, α and L_0 are respectively the path loss exponent and constant, and r represents the distance between the femtocell user and femtocell BS. The counterpart of the shadowing fading in decibel unit is denoted by $Z_{j,dB}$, which is modeled as a zero-mean normal random variable with variance $\sigma^2_{Z_{dB}}$ for the indoor environments [148].

As discussed before, the probability of event $\mathbf{B}_{out}$ for the j-th femtocell user is the probability that the required transmit power exceeds the physical limitation, i.e., the maximum power value $P_{\mathrm{TX},max}$. Therefore, $\mathbb{P}[\mathbf{B}_{out} \mid \mathbf{A}_{out}^{c}]$ in (4.16) can be given by

$$\mathbb{P}[\mathbf{B}_{out} \mid \mathbf{A}_{out}^{c}] = \mathbb{P}\Big(\frac{P_{\mathrm{RX},j}^{*}(\eta)}{L_0(r)^{-\alpha} \cdot Z_j} > P_{\mathrm{TX},max} \mid \mathbf{A}_{out}^{c}\Big). \tag{4.25}$$

Given a certain attenuation factor η, the required received power of the j-th user, i.e., $P_{\mathrm{RX},j}^{*}(\eta)$ in the above equation, can be viewed as a random variable depending on $\{\gamma_j^{*} : j = 1, 2, ..., M\}$, therefore we turn to analyze the statistical property of $P_{\mathrm{RX},j}^{*}(\eta)$ and finally derive the outage probability.

It should be noted that it is difficult to reach the statistical property of $P_{\mathrm{RX},j}^{*}(\eta)$ based on the condition of $\mathbf{A}_{out}^{c}$, since this condition has changed the distribution of the SINR requirements $\{\gamma_j^{*} : j = 1, 2, ..., M\}$. However, considering the fact that the communication system should work only when $\mathbb{P}[\mathbf{A}_{out}]$ is relatively small, the influence of the condition $\mathbf{A}_{out}^{c}$ is limited, which guarantees the following approximation possible,

$$\mathbb{P}[\mathbf{B}_{out} \mid \mathbf{A}_{out}^{c}] \approx \mathbb{P}[\mathbf{B}_{out}]. \tag{4.26}$$

The numerical results in the Section 4.5 show that it is a reasonable accurate approximation.

Similar to the discussion in [145], we can fairly assume $P_{\mathrm{RX},j}^{*}(\eta)$ to be log-normally distributed, thus making $P_{\mathrm{RX},j,dB}^{*}(\eta)$ have a normal distribution. Here we use $m_{P_{dB}}(\eta)$ and $\sigma_{P_{dB}}^{2}(\eta)$ to represent the mean and variance of $P_{\mathrm{RX},j,dB}^{*}(\eta)$, respectively. Based upon this assumption, the probability of the event $\mathbf{B}_{out}$ can be provided in the following Theorem.

Theorem 4.3. *The probability of the event* $\mathbf{B}_{out}$ *is*

$$\mathbb{P}[\mathbf{B}_{out}] = Q\Bigg(\frac{P_{\mathrm{TX},max,dB} + L_{0,dB} - \alpha \cdot 10\log_{10}(r) - m_{P_{dB}}(\eta)}{\sqrt{\sigma_{P_{dB}}^{2}(\eta) + \sigma_{Z_{dB}}^{2}}}\Bigg), \tag{4.27}$$

where $Q(\cdot)$ *is Gaussian Q-function, that is, the complementary CDF of a zero-mean, unit-variance normal random variable.*

Proof. The correlation between required received signal power $P_{\mathrm{RX},j,dB}^{*}(\eta)$ and shadowing fading variable $Z_{j,dB}$ is close to zero, which comes from the fact that the

fluctuations in $P^*_{\mathrm{RX},j,dB}(\eta)$ are mainly due to multipath fading and imperfections in power control, whereas the fluctuations in Z_j come from shadowing fading. Therefore, the probability of the event $\mathbf{B}_{out}$ can be expressed as

$$\begin{aligned}\mathbb{P}[\mathbf{B}_{out}] &= \mathbb{P}\Big(\frac{P^*_{\mathrm{RX},j}(\eta)}{L_0(r)^{-\alpha}\cdot Z_j} > P_{\mathrm{TX},max}\Big)\\ &= \mathbb{P}(P^*_{\mathrm{RX},j,dB}(\eta) - L_{0,dB} + \alpha\cdot 10\log_{10}(r) - Z_{j,dB} > P_{\mathrm{TX},max,dB})\\ &= Q\bigg(\frac{P_{\mathrm{TX},max,dB} + L_{0,dB} - \alpha\cdot 10\log_{10}(r) - m_{P_{dB}}(\eta)}{\sqrt{\sigma^2_{P_{dB}}(\eta) + \sigma^2_{Z_{dB}}}}\bigg), \qquad (4.28)\end{aligned}$$

which completes the proof. □

Next, we focus on finding the mean and variance of $P^*_{\mathrm{RX},j,dB}(\eta)$, that is, $m_{P_{dB}}(\eta)$ and $\sigma^2_{P_{dB}}(\eta)$. Since $P^*_{\mathrm{RX},j,dB}(\eta)$ is normally distributed, $m_{P_{dB}}(\eta)$ and $\sigma^2_{P_{dB}}(\eta)$ can be expressed in terms of the first and second moment of $P^*_{\mathrm{RX},j}(\eta)$ (denoted by $m_P(\eta)$ and $\delta_P(\eta)$, respectively) as

$$m_{P_{dB}}(\eta) = 20\log_{10} m_P(\eta) - 5\log_{10}\delta_P(\eta), \qquad (4.29)$$

and

$$\sigma^2_{P_{dB}}(\eta) = \frac{1}{\varphi}\big[10\log_{10}\delta_P(\eta) - 20\log_{10} m_P(\eta)\big]. \qquad (4.30)$$

Furthermore, based on the results from [145], $P^*_{\mathrm{RX},j}(\eta)$ can be regarded as approximately independent with each other. Conditioned on this assumption, we can obtain $m_P(\eta)$ and $\delta_P(\eta)$ in terms of the first and second moment of the random variable γ^*_j, denoted by m_γ and δ_γ, that is,

$$m_P(\eta) = \frac{m_\gamma(I + \frac{N_0W}{\eta})}{\frac{W}{R} - (M-1)m_\gamma}, \qquad (4.31)$$

and

$$\begin{aligned}\delta_P(\eta) = \frac{\delta_\gamma}{\big(\frac{W}{R}\big)^2 - (M-1)\delta_\gamma}\bigg\{&\Big[(M-1)m_P(\eta) + I\Big]^2\\ &+ \frac{2N_0W}{\eta}\Big[(M-1)m_P(\eta) + I\Big] + \frac{N_0^2W^2}{\eta^2} - (M-1)m_P(\eta)^2\bigg\}. \qquad (4.32)\end{aligned}$$

Table 4.1: Relationship between $\min_{\eta}\{\mathbb{P}[\mathbf{A}_{out}]\}$ and Event $\mathbf{C}_{out}$. The parameter values for this example are $W = 5$ MHz, $RoT^{*}_{dB} = 12$ dB, $m_{\gamma_{dB}} = 7$ dB and $\sigma_{\gamma_{dB}} = 2.5$ dB.

Rate	$M = 2$		$M = 3$	
	$\min \mathbb{P}[\mathbf{A}_{out}]$	$\mathbf{C}_{out}$	$\min \mathbb{P}[\mathbf{A}_{out}]$	$\mathbf{C}_{out}$
15 kbps	0.0%	No	0.0%	No
30 kbps	0.0%	No	0.0%	No
60 kbps	0.0%	No	0.0%	No
120 kbps	0.0%	No	0.0%	No
240 kbps	0.0%	No	3.6%	No
360 kbps	1.3%	No	28.0%	No
Rate	$M = 4$		$M = 5$	
	$\min \mathbb{P}[\mathbf{A}_{out}]$	$\mathbf{C}_{out}$	$\min \mathbb{P}[\mathbf{A}_{out}]$	$\mathbf{C}_{out}$
15 kbps	0.0%	No	0.0%	No
30 kbps	0.0%	No	0.0%	No
60 kbps	0.0%	No	0.0%	No
120 kbps	0.0%	No	1.4%	No
240 kbps	26.7%	No	67.2%	Yes
360 kbps	77.8%	Yes	97.6%	Yes

It should be noted that (4.31) and (4.32) exist only if

$$\frac{W}{R} > (M-1)m_{\gamma}, \tag{4.33}$$

and

$$\left(\frac{W}{R}\right)^{2} > (M-1)\delta_{\gamma}. \tag{4.34}$$

We define that the event $\mathbf{C}_{out}$ happens when either of the conditions (4.33) and ((4.34)) cannot be satisfied. From the simulation results shown in Table 4.1, event $\mathbf{C}_{out}$ would not happen when the minimum value of $\mathbb{P}[\mathbf{A}_{out}]$ satisfies $\min_{\eta}\{\mathbb{P}[\mathbf{A}_{out}]\} < 30\%$, which is a fairly reasonable assumption for normally working femtocell receivers. Thus, we make the assumption that $\min_{\eta}\{\mathbb{P}[\mathbf{A}_{out}]\} < 30\%$ can always be satisfied in our following discussion, which means conditions of (4.33) and (4.34) can be consequentially fulfilled.

Because of the assumption given in section 4.2, i.e., $\gamma^{*}_{j,dB} = 10\log_{10}\gamma^{*}_{j} \sim$

$\mathcal{N}(m_{\gamma_{dB}}, \sigma^2_{\gamma_{dB}})$, the first and second moment of γ_j^* can be derived based on $m_{\gamma_{dB}}$ and $\sigma_{\gamma_{dB}}$, i.e.,

$$m_\gamma = \exp\left(\frac{(\varphi\sigma_{\gamma_{dB}})^2}{2}\right)\exp\left(\varphi m_{\gamma_{dB}}\right), \tag{4.35}$$

and

$$\delta_\gamma = \exp\left(2(\varphi\sigma_{\gamma_{dB}})^2\right)\exp\left(2\varphi m_{\gamma_{dB}}\right), \tag{4.36}$$

where $\varphi = \ln(10)/10$.

Through the above analysis, the result of $\mathbb{P}[\mathbf{B}_{out}]$ can be reached, which can approximate $\mathbb{P}[\mathbf{B}_{out} \mid \mathbf{A}^c_{out}]$ and be combined with $\mathbb{P}[\mathbf{A}_{out}]$ obtained in Section 4.3.1 to estimate the overall outage probability $p_{out}(\eta)$ through (4.16).

4.4 Adaptive Uplink Attenuation Algorithms

Conventionally, the adaptive uplink attenuation algorithm tries to maintain the out-of-cell interference contribution to the femtocell noise rise at a constant value $RoT_{out,dB}$, (e.g., 3 dB,) which is corresponding to the equation to compute the "adaptive attenuation factor" as shown below,

$$\eta_{\text{adaptive}} = \frac{N_0 W RoT_{out}}{I}. \tag{4.37}$$

In the logarithm domain, the above equation can be rewritten as,

$$\eta_{\text{adaptive},dB} = RoT_{out,dB} - \left(\frac{I}{N_0 W}\right)_{dB}. \tag{4.38}$$

The adaptive algorithm shown above considers the influence of uplink interference signal strength, and can be used to effectively mitigate the interference from nearby unattached user terminals. However, the higher level uplink attenuation results in a higher probability to reach the maximum power cap, and lower level attenuation results in less interference mitigation as shown in previous section. This tradeoff has not been taken into consideration in the conventional algorithm.

As mentioned, the uplink attenuation scheme should apply the necessary level of attenuation (small enough η value to ensure that the noise rise of the resultant signals stays below a system-defined threshold). However, as the maximum power of femtocell user terminals may be further restricted to avoid the impact on macrocells [40], the increased transmit power due to uplink attenuation may

easily create a larger outage probability at the edge of the femtocell, if certain SINR values at the femtocell receiver for satisfactory performances should be sustained. To optimize the outage probability by balancing both effects, optimal adaptive uplink attenuation algorithms are proposed in this chapter.

4.4.1 Adaptive Uplink Attenuation Algorithm I (AULA-I)

A smaller η value leads to increased transmit power requirements of femtocell user terminals, which result in a higher probability to exceed the transmit power cap and increase the interference to other co-channel deployed cellular services. Therefore, the attenuation factor that can just restrain the femtocell noise rise below the threshold value RoT^* is the necessary value to minimize the required transmit power, which has been shown in (4.15) and helps us to obtain the adaptive uplink attenuation factor in this algorithm,

$$\eta_{\text{adaptive}} = \frac{N_0 W RoT^*}{I}\left[1 - \left(1 + \frac{1}{RoT^*}\right)\omega\right] = \frac{N_0 W RoT'_{out}}{I}, \tag{4.39}$$

where RoT'_{out} is the adaptive noise rise value allocated to the contribution of out-of-cell interference, i.e.,

$$RoT'_{out} = \frac{RoT^*}{\left[1 - \left(1 + \frac{1}{RoT^*}\right)\omega\right]^{-1}}. \tag{4.40}$$

This algorithm to determine the uplink attenuation factor η is named as *adaptive uplink attenuation algorithm I (AULA-I)* in this chapter.

Due to the physical meaning of uplink attenuation, the uplink attenuation factor should satisfy $\eta \in (0, 1]$, which implies $\eta_{\text{adaptive}} > 0$. If we want to achieve a feasible solution for adaptive uplink attenuation, the following condition should be satisfied:

$$\omega < \frac{RoT^*}{1 + RoT^*}. \tag{4.41}$$

If this condition can be fulfilled, equation (4.8) will have a feasible solution, because ω can easily satisfy $\omega < 1$ (since $RoT^* > 0$).

It is worth mentioning that the term on the denominator of equation (4.40) denotes the RoT margin allocated for femtocell-connected users, denoted as

RoT_{margin} here, i.e.,

$$RoT_{\text{margin}} = \left[1 - \left(1 + \frac{1}{RoT^*}\right)\omega\right]^{-1}. \quad (4.42)$$

Hence, the attenuation factor obtained in this algorithm can be expressed in log-scale form accordingly,

$$\eta_{\text{adaptive},dB} = RoT^*_{dB} - RoT_{\text{margin},dB} - \left(\frac{I}{N_0 W}\right)_{dB}. \quad (4.43)$$

It should be noted that, compared with the conventional adaptive uplink attenuation algorithm given by equation (4.37), this optimal AULA-I scheme utilizes data rate R and the SINR requirement information $\{\gamma_j^* : j = 1, 2, ..., M\}$ to adapt the noise rise allowances for the interference from femtocell-connected user terminals and the out-of-cell interference.

Complexity. From a practical point of view, this adaptive algorithm uses little extra computation in (4.42) and (4.43) to achieve the attenuation factor in each power control cycle and the added complexity can be negligible.

4.4.2 Adaptive Uplink Attenuation Algorithm II (AULA-II)

The SINR requirements, denoted as $\{\gamma_j^* : j = 1, 2, ..., M\}$, for the various femtocell user terminals in the femtocell vary with time due to changes in channel environment and imperfections in the power control algorithm. Field trials reported in [143] have shown that the SINR requirements $\{\gamma_j^* : j = 1, 2, ..., M\}$ are well modeled by log-normal random variables. Moreover, we can assume that the fading processes which cause the fluctuations in SINR requirements for the different femtocell users are independent.

Based on above modeling of $\{\gamma_j^* : j = 1, 2, ..., M\}$, we can reach the optimal value of η by minimizing the outage probability equation given in Section 4.3, as follows,

$$\eta_{\text{adaptive}} = \arg\min_{\eta} \left\{p_{out}(\eta)\right\}. \quad (4.44)$$

This method to obtain the uplink attenuation factor is named as *adaptive uplink attenuation algorithm II (AULA-II)* in our analysis. It should be noted that

AULA-II utilizes the statistical property of SINR requirements and do not have to deal with the instantaneous SINR values for each femtocell user, compared with AULA-I. Although both algorithms are designed to minimize the probability of outage event, the latter one is only based on the statistical property of the SINR requirement whereas the former one utilizes the instantaneous value of required data rate for femtocell users. The statistical property of SINR requirement can be obtained from femtocell BS's observation.

Complexity. We need little extra computation to implement AULA-II since the analytical result for $p_{out}(\eta)$ can be utilized and the optimal value of η is calculated whenever the number of femtocell users or data rates are changed.

Remark. Both AULA-I and AULA-II are algorithms implemented at the femtocell receivers, without incurring any modification to the air interface protocol. The SINR and data rate requirement parameters are controlled by femtocell BS and the interference power level can be estimated by subtracting the in-cell users' contribution from the total received signal power. Hence, no extra wireless channel resources or user terminal supports are needed to employ this scheme.

4.5 Numerical Results

In this section, we illustrate the outage analysis by comparing analytical outage probability curves resulting from numerical evaluation with straightforward simulation results. Furthermore, the simulation results of newly developed optimal adaptive uplink attenuation are also provided. The system parameter values used here are summarized in Table 4.2.

4.5.1 Fixed Uplink Attenuation Performance

In Fig. 4.2 and Fig. 4.3, the curves of $\mathbb{P}[\mathbf{A}_{out}]$ and $\mathbb{P}[\mathbf{B}_{out} \mid \mathbf{A}_{out}^c]$ over the range of η are respectively provided, where the interference power received at the femtocell receiver is -75 dBm. As expected, $\mathbb{P}[\mathbf{A}_{out}]$ and $\mathbb{P}[\mathbf{B}_{out} \mid \mathbf{A}_{out}^c]$ are monotone non-decreasing and monotone non-increasing functions of η, respectively.

Firstly, it can be illustrated from Fig. 4.2 that the analytical results in Theorem 4.2 are reasonably accurate compared with simulation results. On the other hand, the mismatch between the analytical and simulated $\mathbb{P}[\mathbf{B}_{out} \mid \mathbf{A}_{out}^c]$ in Fig. 4.3 increases when η is taken to be a larger value. This effect is caused

Table 4.2: System parameter values for numerical results

Parameter values	Description
$W = 5$ MHz	operating bandwidth
$N_0 = -167$ dBm/Hz	background noise power spectral density
$M = 2$ or 3	the number of femtocell-connected users
$r = 20$ m	distance between femtocell BS and its user
$P_{\mathrm{TX},max,dB} = 10$ dBm	maximum user terminal transmit power
$\eta_{\min} = 0.001$	minimum uplink attenuation factor
$I_{dB} = -85 \sim -65$ dBm	interference power received at the femtocell
$RoT^*_{dB} = 12$ dB	noise rise level threshold
$L_{0,dB} = -38.5$ dB	path loss constant
$\alpha = 2$	path loss exponent
$\sigma_{Z_{dB}} = 8$ dB	shadowing fading standard deviation
$m_{\gamma_{dB}} = 7$ dB	mean value for SINR in decibels
$\sigma_{\gamma_{dB}} = 2.5$ dB	standard deviation for SINR in decibels

by the less accurate approximation of $\mathbb{P}[\mathbf{B}_{out} \mid \mathbf{A}^c_{out}] \approx \mathbb{P}[\mathbf{B}_{out}]$ in our analysis. However, this discrepancy has limited influence on the overall outage probability results $p_{out}(\eta)$ provided in Fig. 4.4, generated by substituting the results of $\mathbb{P}[\mathbf{A}_{out}]$ and $\mathbb{P}[\mathbf{B}_{out} \mid \mathbf{A}^c_{out}]$ into the equation (4.16). This is because $\mathbf{A}_{out}$ is the dominant factor for the part of lower attenuation level in $p_{out}(\eta)$ curve (higher value of η), thus mitigating the effect of mismatch coming from the less accurate approximation mentioned earlier.

Experienced a lower interference level of $I = -85$ dBm, Fig. 4.5 is able to demonstrate the tradeoff similar to the counterpart in Fig. 4.4. The close match between the analysis and simulation plots presented both in Fig. 4.4 and Fig. 4.5 illustrates the accuracy of our analytical results derived in this chapter.

Moreover, the results in Fig. 4.4 and Fig. 4.5 demonstrate the performance tradeoff between high and low level of uplink attenuation. Specifically, a higher uplink attenuation (i.e., a smaller value of η) results in a higher probability to reach the maximum power cap, which causes Event $\mathbf{B}_{out}$ to happen; on the other hand, a lower level attenuation (i.e., a larger value of η) provides less interference mitigation, which can result in a exceeded noise rise level. Obviously, based upon this phenomenon, the system designer can select an optimal uplink attenuation

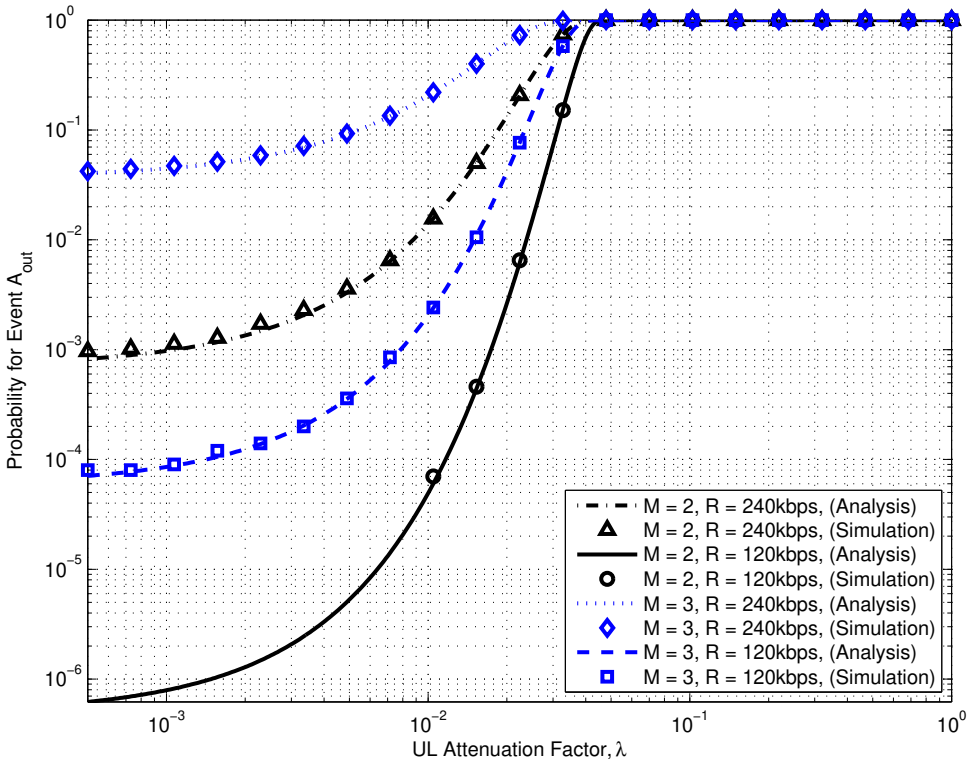

Figure 4.2: The probability of Event $\mathbf{A}_{out}$ versus the uplink attenuation factor η, where the fixed level of uplink attenuation is applied and the interference level at the femtocell receiver is $I_{dB} = -75$ dBm.

factor which balances the performance tradeoff and minimizes the outage probability under certain circumstance. For instance, observed from Fig. 4.4 where $I = -75$ dBm, the optimal η should be chosen around 0.01 for two femtocell-connected users with the data rate of 120 kbps, which guarantees the outage probability less than 6×10^{-4}, whereas the optimal value is 0.04 for the counterpart in Fig. 4.5, where $I = -85$ dBm.

4.5.2 Adaptive Uplink Attenuation Performance

Fig. 4.6 shows the empirical CDF for the uplink attenuation factor $\eta_{\text{adaptive},dB}$ obtained from AULA-I, with received interference power level at -75 dBm. Compared with the constant uplink attenuation factor from the conventional AULA (i.e., $\eta_{\text{adaptive},dB} = -22.01$ dB for all these four cases if $RoT_{out} = 3$ dB is assumed), it can be observed that the resultant $\eta_{\text{adaptive},dB}$ adjusts according to different

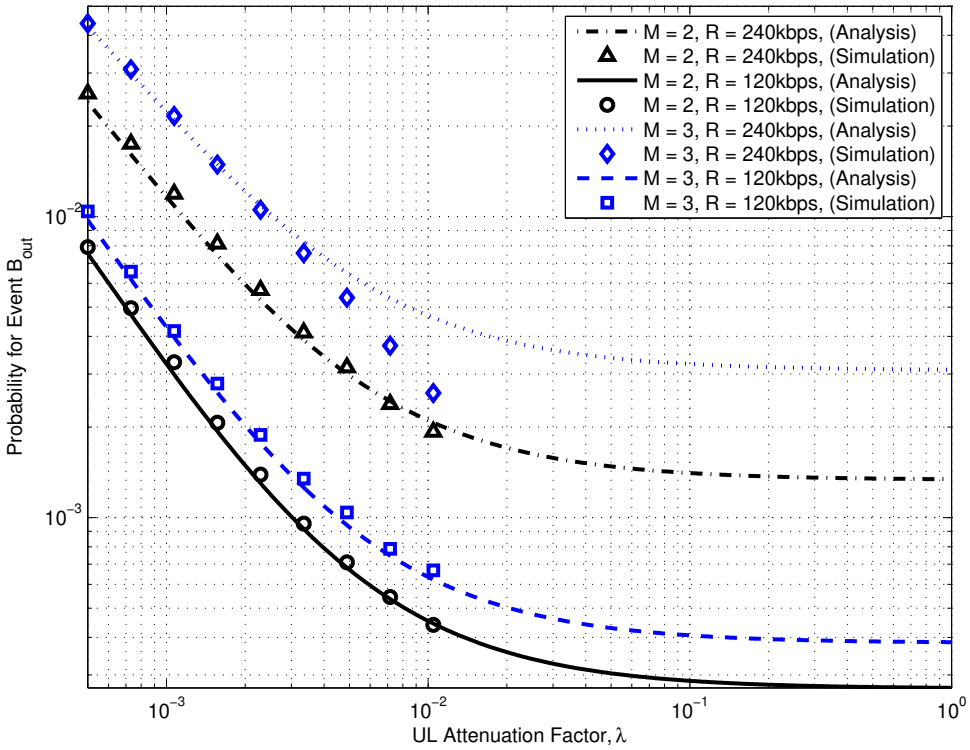

Figure 4.3: The probability of Event $\mathbf{B}_{out}$ under the condition that Event $\mathbf{A}_{out}$ do not happen, i.e., $\mathbb{P}[\mathbf{B}_{out} \mid \mathbf{A}_{out}^{c}]$, versus the uplink attenuation factor η, where the fixed level of uplink attenuation is applied and the interference level at the femtocell receiver is $I_{dB} = -75$ dBm.

number of femtocell users and data rates applied. Specifically, under the condition of $R = 240$ kbps, 50% of η_{adaptive} is less than -17.5 dB for $M = 3$, while the median value of $\eta_{\text{adaptive},dB}$ is around -15.5 dB for $M = 2$. For $R = 120$ kbps, the median values of $\eta_{\text{adaptive},dB}$ are -15.0 dB and -14.2 dB for $M = 3$ and $M = 2$, respectively. AULA-I is more likely to have a larger value of $\eta_{\text{adaptive},dB}$ (less attenuation level) for all these four cases, compared with the conventional AULA, thus making the possibility of event $\mathbf{B}_{out}$ smaller and saving more transmit power for each femtocell terminals (which can be concluded from (4.10)). It should also be noted that the variation of the resultant $\eta_{\text{adaptive},dB}$ here is coming from the fact that AULA-I adapts to the different SINR requirements, which are modeled as random variables to simulate the practical environment.

Fig. 4.7 and Fig. 4.8 show the outage probability at the locations r away from femtocell BS for different levels of out-of-cell interference power. The num-

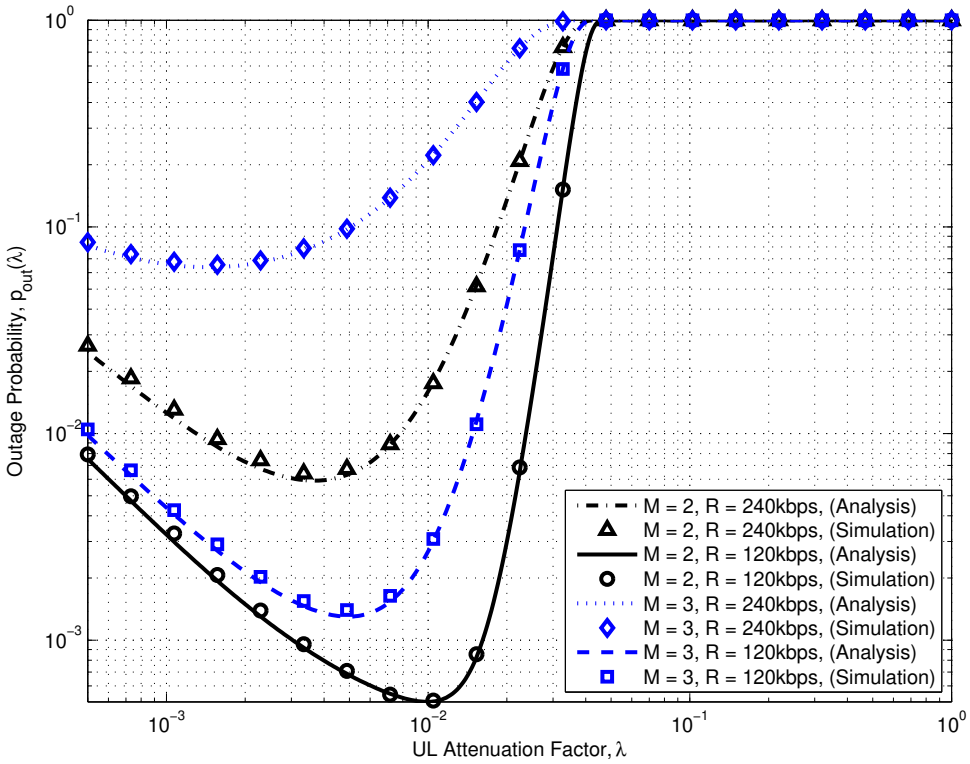

Figure 4.4: The overall outage probability versus the uplink attenuation factor η, where the fixed level of uplink attenuation is applied and the interference level at the femtocell receiver is $I_{dB} = -75$ dBm.

ber of femtocell users in the femtocell is assumed to be 2 in Fig. 4.7 and 3 in Fig. 4.8. It can be observed from both figures that AULA-II outperforms the conventional algorithm and AULA-I achieves best performance for both candidate data rates. Specifically, in Fig. 4.7, to guarantee 6×10^{-3} outage probability for $R = 240$ kbps, AULA-I can tolerate 6 dB more interference power compared with the conventional algorithm. Though limited improvement achieved compared with AULA-I, AULA-II can still tolerate 2.5 dB more interference power compared with the conventional AULA. For the case of $R = 120$ kbps, AULA-I can achieve 1 dB enhancement of interference tolerance capacity.

Furthermore, it should be noted that the outage probabilities for the conventional AULA have higher error floors, which can be observed from the system performance with the decreased the interference power level. The error floors are demonstrated clearly for $R = 240$ kbps in both Fig. 4.7 and Fig. 4.8. This fact

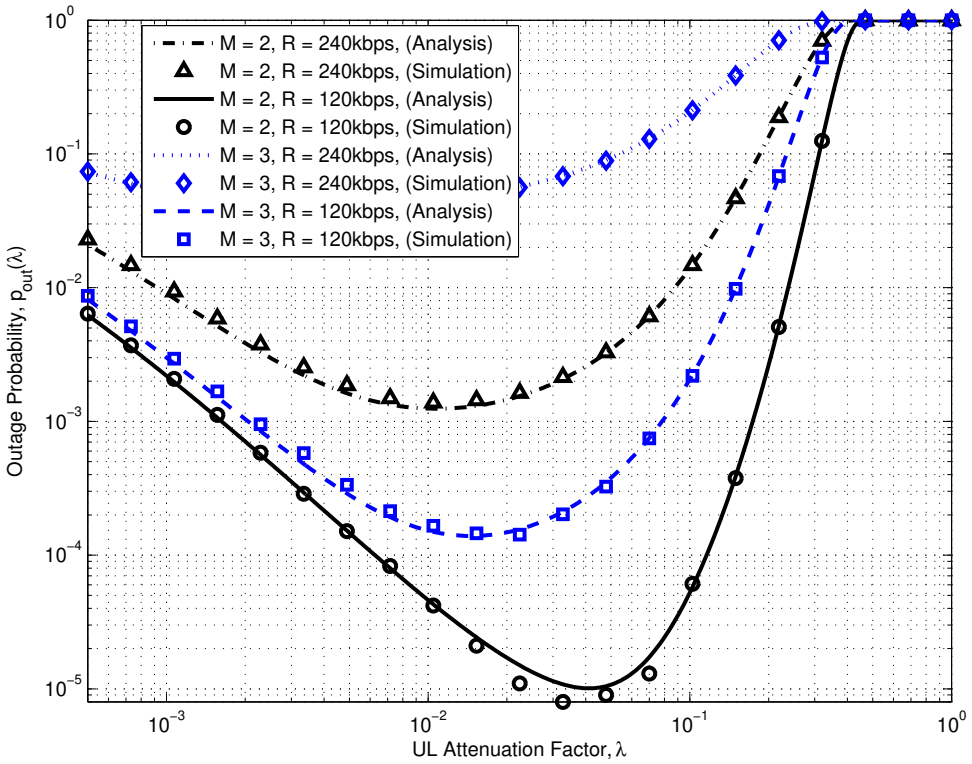

Figure 4.5: The overall outage probability versus the uplink attenuation factor η, where the fixed level of uplink attenuation is applied and the interference level at the femtocell receiver is $I_{dB} = -85$ dBm.

can be explained by the fact that the conventional AULA (employing equation (4.38)) does not change the attenuation factor effectively when the interference is relatively low, which makes it loss the ability to adjust the attenuation factor according to the instantaneous RoT. On the other hand, the proposed algorithms have lower error floors and lower outage probability.

4.6 Summary of Contributions

In this chapter, we investigated an important technique implemented in CDMA-based femtocell receivers, namely, uplink attenuation algorithms. By employing this technique at the femtocell uplink receiver, high out-of-cell interference can be brought down to ensure that the noise rise of the resultant signals remains below a system-defined threshold such that the femtocell signal acquisition unit

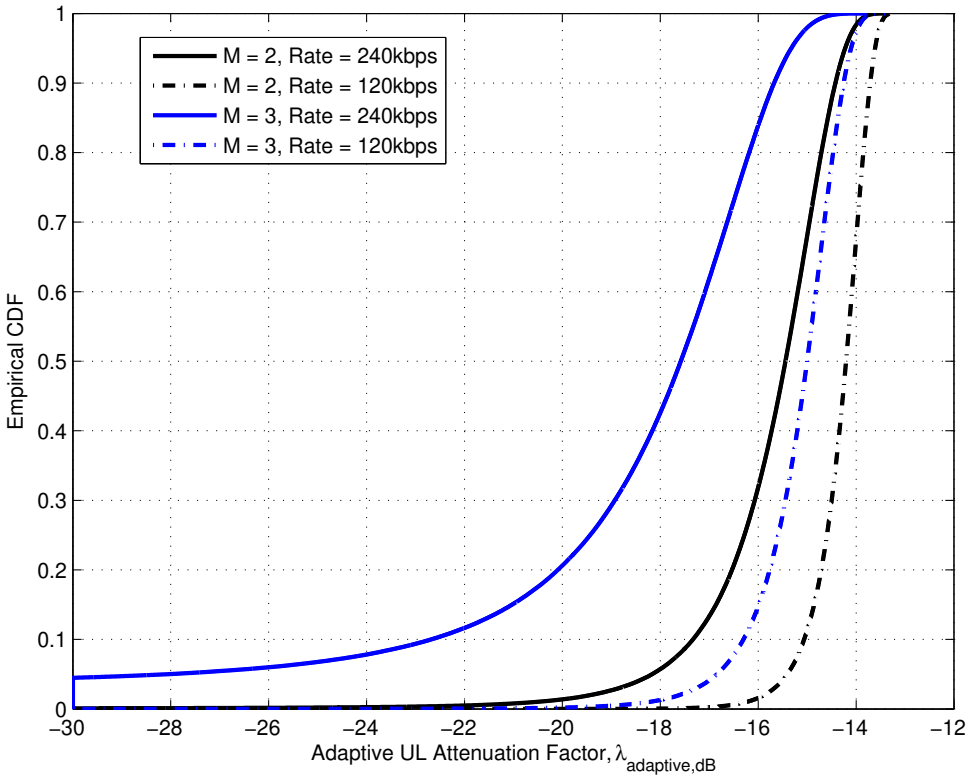

Figure 4.6: Simulation result for the empirical CDF of the adaptive uplink attenuation factor $\eta_{\text{adaptive},dB}$ in AULA-I, where the interference level at the femtocell receiver is $I_{dB} = -75$ dBm.

can function normally. By proposing an analytical framework to evaluate the coverage/outage probability taking the uplink attenuation into account, following contributions were made in our study:

1. Through analyzing the femtocell uplink environment, an analytical result of the coverage/outage probability under certain fixed level of uplink attenuation was derived.

2. We demonstrated the tradeoff between higher level uplink attenuation resulting in a higher probability to reach the maximum power cap and lower level attenuation with less interference mitigation alternatively. Based on this tradeoff, the fixed optimal uplink attenuation factor which minimizes the outage probability can be determined, which is beneficial to practical system design.

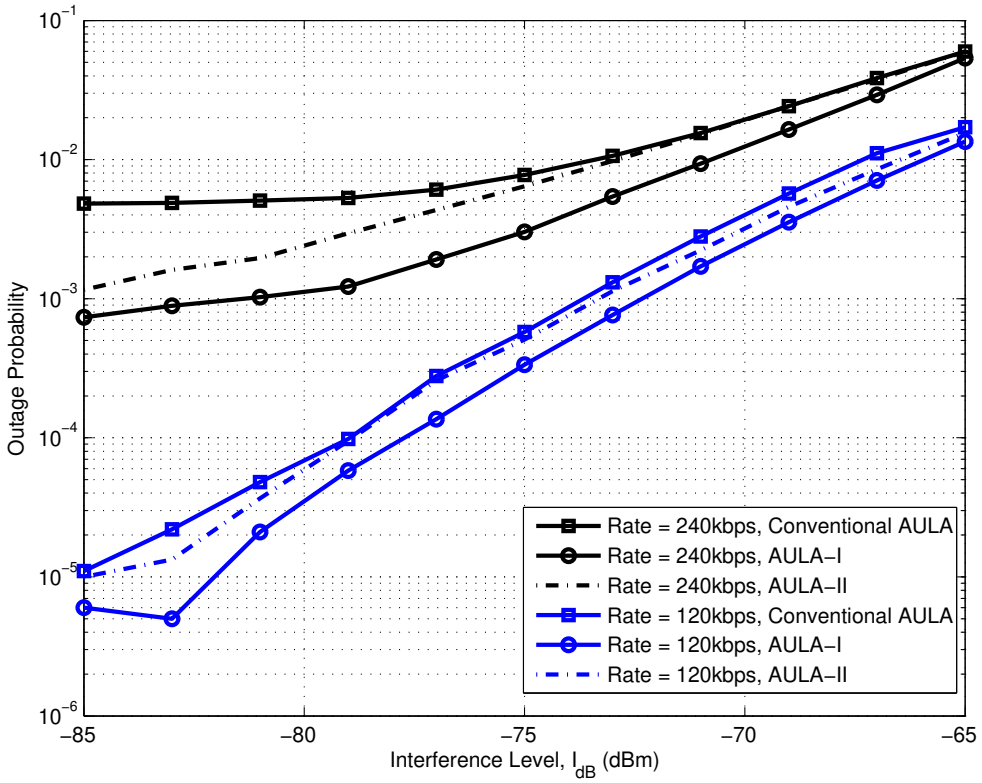

Figure 4.7: Simulation result for the outage probability versus the interference level at the femtocell receiver I_{dB}, where the number of active femtocell users is $M = 2$.

3. In this chapter, we proposed two adaptive uplink attenuation algorithms, both of which aim to minimize the outage probability by adaptively adjusting the uplink attenuation factor based upon the information of the scheduled traffic, SINR requirements for each femtocell-connected user, and the current interference power at femtocell receiver. Simulation Results show that both adaptive schemes are able to achieve better performance improvement over the traditional algorithm.

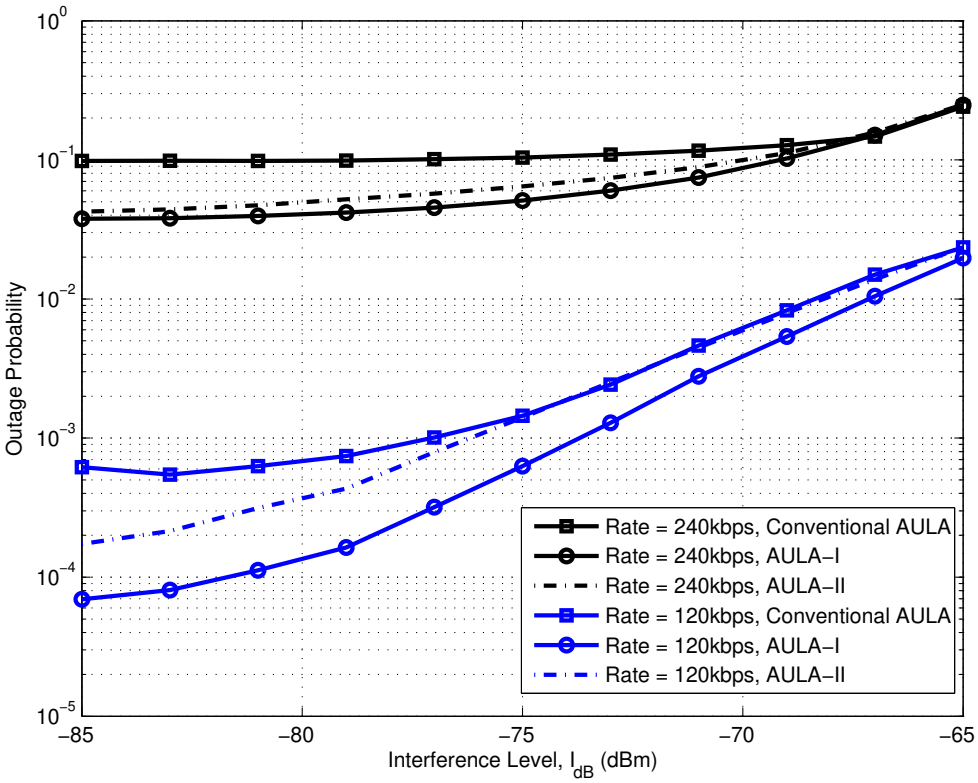

Figure 4.8: Simulation result for the outage probability versus the interference level at the femtocell receiver I_{dB}, where the number of active femtocell users is $M = 3$.

Chapter 5

Physical Layer Security in Large-Scale Cellular Networks

5.1 Introduction

Different from the objective of HetNet, which is generally associated with improved coverage and increased data rate for the cellular customers, another important metric that should be focused on is security. The concept of achieving information-theoretic security by protecting the physical layer of wireless networks has attracted attention widely in the research community recently [149–159]. Different from traditional cryptographic methods employed in the upper layers of the protocol stacks [87,88], information-theoretic security is achieved by exploiting the difference between channels of legitimate users and that of eavesdroppers, which requires the intended receivers enjoys a better channel than the potential eavesdropper [89,90].

Achieving security in large-scale networks attracted extensive attention in recent years. Unlike point-to-point scenarios, the communication between nodes in large-scale networks strongly depends on the location distribution and the interactions between nodes. Based on the assumption that legitimate nodes and eavesdroppers are distributed randomly in space, the studies on secure communications for large-scale wireless networks have been conducted recently, from the information-theoretic viewpoint. Secrecy communication graphs describing secure connectivity over a large-scale network with eavesdroppers present were investigated in [149–153]. Focusing on the transmission capacity of secure communications, the throughput cost of achieving a certain level of security in an

interference-limited network was analyzed in [158, 159].

It should be noted that most of the studies on security communications in large-scale networks were concentrated on ad hoc networks. For cellular networks, there are still dozens of particular characteristics to be considered. Therefore, unlike most existing studies on analyzing large-scale networks, this chapter focuses on the secrecy performance in large-scale cellular networks, rather than ad hoc networks. Specifically, cellular networks' unique characteristics different from ad hoc networks are taken into account in our analysis: the carrier-operated high-speed backhaul networks connecting individual BSs and the core-network infrastructures, which provide us potential means of BS cooperation, such as associating mobile users to the optimal BS with secrecy considerations and exchanging information to guarantee better secure links.

The following scenario of secure communication in cellular networks is considered in this chapter: confidential messages are prepared to be conveyed to a mobile user, while certain other mobile users should not have the access to the messages and hence are treated as potential eavesdroppers. The serving BS should ensure the messages delivered to the intended user successfully while keeping perfect secrecy against all potential eavesdroppers. Considering the fact that the cellular service area is divided into cells, each BS knows the location as well as the identity of each user (i.e., whether the user is a potential eavesdropper or not) in its own cell. The identity and location information of mobile users in the other cells can be obtained by information exchange between BSs via the backhaul networks.

Several attention-grabbing questions can be raised from the above discussion:

Q1. If BS information exchange via the backhaul networks is ideal, i.e., the serving BS fully acquires potential eavesdroppers' location information, what is the secrecy rate achievable at a randomly located mobile user?

Q2. Comparing with connecting to nearest BS, how much performance improvement can be obtained by optimally choosing the serving BS?

Q3. How will the performance be degraded if the information exchange between BSs no longer exists?

Q4. To achieve a certain level of secrecy performance, how many nearby BSs should participate in the information exchange between BSs?

As described in Chapter 2, modeling BSs to be randomly placed points in a plane and utilizing stochastic geometry [98, 100] to analyze cellular networks was proved to be an analytical tool with improved tractability and reasonable precision [43,118]. Therefore, in this chapter, we adopt the PPP-based stochastic geometry model for BS distribution, i.e., modeling BSs to be homogeneous PPP in a plane, to investigate the secrecy performance in large-scale cellular networks.

It should be noted that a similar study to evaluate secrecy performance of large-scale cellular networks was conducted in [160]; however, it mainly focused on the scaling behavior of the eavesdropper's density to allow full coverage over the entire network, without taking the achievable secrecy rate into account. In contrast, we provide analytical results on the statistics of the secrecy rate at a typical mobile user under different cell association models and eavesdroppers' location information exchanging assumptions mentioned earlier.

In Section 5.2, we present the system model and general assumptions to achieve physical layer security in the large-scale cellular network. Section 5.3 shows the main result of this chapter, in which we obtain simple analytical results for achievable secrecy rates under different assumptions on the cell association and location information exchange between BSs as follows:

- *Scenario-I*: the serving BS fully acquires potential eavesdroppers' location information; the nearest BS from the intended user is chosen as the serving BS.

- *Scenario-II*: the serving BS fully acquires potential eavesdroppers' location information; the BS providing best secrecy performance at the intended user is chosen as the serving BS.

- *Scenario-III*: the serving BS partially acquires potential eavesdroppers' location information; the nearest BS from the intended user is selected as the serving BS.

Specifically, in these three scenarios, the probabilistic characteristics of the achievable secrecy rates $\hat{R}_s$ and the average secrecy rates achievable $\mathbb{E}[\hat{R}_s]$ are provided. Section 5.4 respectively provides numerical results on the achievable secrecy rate for all scenarios. Through investigating the numerical results, the impacts of optimal cell association and exchanging information are provided to answer the above-mentioned questions. Finally, the concluding remarks are given in Section 5.5.

5.2 System Model

We consider the downlink scenario of a cellular network utilizing an orthogonal multiple access technique and composed of a single class of BSs, macro BS for instance. We focus on the performance achieved by a randomly chosen typical mobile user. Similar to Chapter 2 and Chapter 3, we still conduct the analysis based on the PPP-based BS model, in which BSs are assumed to be spatially distributed as a two-dimensional homogeneous PPP Φ_{BS} of density λ_{BS}. Different from the studies in previous two chapters, all BSs here have the same transmit power value P_{BS}, because of the single-tier assumption.

An independent collection of mobile users, located according to an independent homogeneous PPP Φ_{MS} of density λ_{MS}, is assumed. We consider the process $\Phi_{MS} \cup \{0\}$ obtained by adding a user at the origin of the coordinate system. By Slivnyak's Theorem [98], this user can be taken as the typical user, since adding a user is identical to conditioning on a user at that location.

5.2.1 Signal Propagation Model

The standard power loss propagation model is used with path loss exponent $\alpha > 2$. Hence, the received power at the receiver x_i from the transmitter x_j is written as

$$P_{rx}(x_i, x_j) = P_{BS}\|x_i - x_j\|^{-\alpha}. \tag{5.1}$$

The noise power is assumed to be additive and constant with value σ^2 for all users, but no specific distribution is assumed.

In this chapter, we assume that there is no in-band interference at downlink receivers. This assumption is achievable by a carefully planned frequency reuse pattern, where the interfering BSs are far away to have the serving BS occupying some resource blocks exclusively in a relatively large region, and the interference can be incorporated in the constant noise power.

5.2.2 Achievable Secrecy Rate

We consider a scenario where confidential messages are prepared to be delivered to the typical user, while certain individuals among other mobile users, treated as potential malicious eavesdroppers by the network, should be kept from accessing them. We model a fraction of the other mobile users randomly chosen from

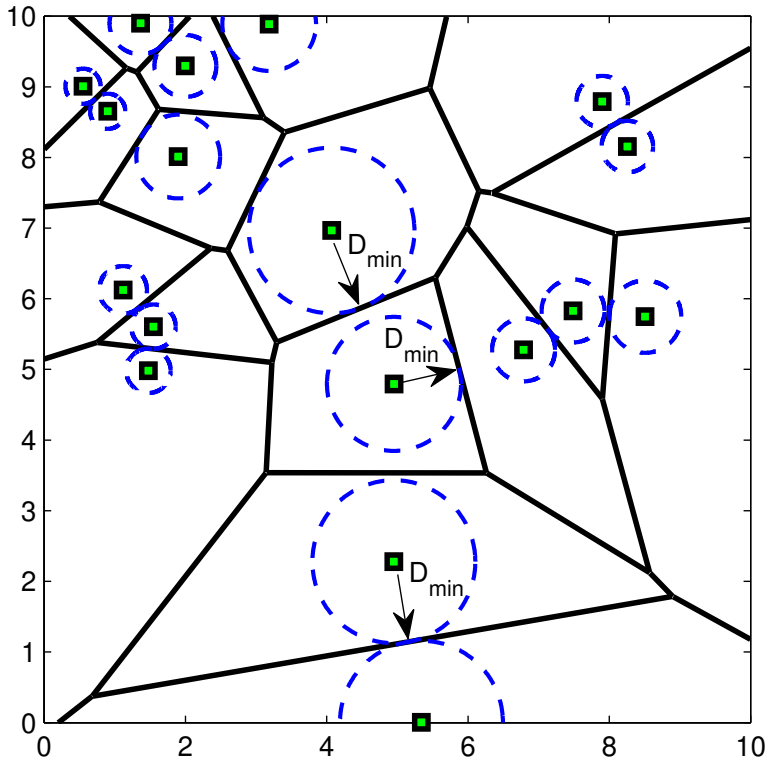

Figure 5.1: Illustration of PPP-distributed BSs' cell boundaries. Each user is associated with the nearest BS, and BSs (represented by green squares) are distributed according to PPP. $D_{\min}$ is defined as BS's minimum distance to its cell boundaries.

Φ_{MS} (the process constructed by all other users except the typical user) as the eavesdroppers, i.e., a thinned PPP with the density of λ_e, denoted by Φ_e.

Here we assume that each BS knows both the location and the identity (i.e., whether the user is a potential eavesdropper or not) of each mobile user in its own cell, and the cell of each BS is the Voronoi cell containing the BS, where the Voronoi tessellation is formed by PPP Φ_{BS} [98], as shown in Fig. 5.1. The identity and location information of mobile users in the other Voronoi cells can be obtained by the information exchange between BSs via backhaul networks.

Firstly, if we suppose the ideal case where the serving BS located at x knows the locations of all eavesdroppers in the plane, which requires that the location and identity information of all users is shared completely through the backhaul network, the maximum secrecy rate achievable at the typical mobile user is given

by [150, 161], as

$$R_s = \max\left\{ \log_2\left(1+\frac{P_{rx}(0,x)}{\sigma^2}\right) - \log_2\left(1+\frac{P_{rx}(e^*(x),x)}{\sigma^2}\right), 0\right\}, \tag{5.2}$$

where

$$\begin{aligned} e^*(x) &= \arg\max_{e\in\Phi_e} P_{rx}(e,x) \\ &= \arg\min_{e\in\Phi_e} \|e-x\|, \end{aligned} \tag{5.3}$$

i.e., $e^*(x)$ is the location of the most detrimental eavesdropper, which is the nearest one from the serving BS in this case.

Next, assuming limited information exchange between BSs, there are regions in which the eavesdroppers' location information is unknown to the serving BS, which is denoted by $\Theta \subset \mathbb{R}^2$. When this happens, the serving BS assumes the worst case, i.e., eavesdroppers can lie at any points in Θ. Hence, the achievable secrecy rate is still given by (5.2), but $e^*(x)$ should be

$$e^*(x) = \arg\max_{e\in\Phi_e\cup\Theta} P_{rx}(e,x), \tag{5.4}$$

where the detrimental eavesdropper is chosen from the union of the eavesdropper set Φ_e and the unknown region Θ.

It should be noticed that the randomness introduced by Φ_{BS} and Φ_e makes the achievable secrecy rate R_s at the typical user a random variable. Furthermore, the distribution of R_s is mixed, i.e., R_s has a continuous distribution on $(0,\infty)$ and a discrete component at 0. For $R_s \in (0,\infty)$, the CCDF of R_s is given as

$$\bar{F}_{R_s}(R_0) = \mathbb{P}\left(\log_2\left(1+\frac{P_{rx}(0,x)}{\sigma^2}\right) - \log_2\left(1+\frac{P_{rx}(e^*(x),x)}{\sigma^2}\right) > R_0\right), \quad \text{for } R_0 \geqslant 0. \tag{5.5}$$

For the special case of $R_s = 0$, it has the probability $\mathbb{P}(R_s = 0) = 1 - \bar{F}_{R_s}(0)$, which corresponds to the probability that the link to the typical user cannot support any positive secrecy rate.

By assuming that the receivers of both the legitimate user and eavesdroppers operate in the high SNR regime, i.e., $P_{rx}(0,x)/\sigma^2 \gg 1$ and $P_{rx}(e^*(x),x)/\sigma^2 \gg 1$,

we can obtain an approximation of R_s, denoted by $\hat{R}_s$, i.e.,

$$\hat{R}_s = \max\left\{ \log_2\Big(\frac{P_{rx}(0,x)}{\sigma^2}\Big) - \log_2\Big(\frac{P_{rx}(e^*(x),x)}{\sigma^2}\Big), 0 \right\}, \tag{5.6}$$

the CCDF of which is

$$\begin{aligned} \bar{F}_{\hat{R}_s}(R_0) &= \mathbb{P}\Big(\frac{P_{rx}(0,x)}{P_{rx}(e^*(x),x)} > \beta\Big) \\ &= \mathbb{P}\Big(\|e^*(x) - x\| > \beta^{1/\alpha}\|x\|\Big), \quad \text{for } R_0 \geqslant 0, \end{aligned} \tag{5.7}$$

where the threshold β is defined as $\beta \triangleq 2^{R_0}$. In this chapter, we focus on high SNR scenarios and use the above expression to obtain analytical results on the secrecy rate performance. The obtained analytical results give approximations on the secrecy performance at finite SNR values.

Furthermore, from the fact that the achievable secrecy rate R_s should always be non-negative, we can easily reach the conclusion that the high SNR approximation $\bar{F}_{\hat{R}_s}(R_0)$ serves as an upper bound for the CCDF of R_s at finite SNR, i.e.,

$$\begin{aligned} \bar{F}_{R_s}(R_0) &= \mathbb{P}\Big(\frac{\sigma^2 + P_{rx}(0,x)}{\sigma^2 + P_{rx}(e^*(x),x)} > 2^{R_0}\Big) \\ &\leqslant \mathbb{P}\Big(\frac{P_{rx}(0,x)}{P_{rx}(e^*(x),x)} > 2^{R_0}\Big) \\ &= \bar{F}_{\hat{R}_s}(R_0), \qquad \text{for } R_0 \geqslant 0, \end{aligned} \tag{5.8}$$

where the two probability expressions are equal when $R_0 = 0$. Therefore, some of our analytical results on $\bar{F}_{\hat{R}_s}(R_0)$ and $\mathbb{E}[\hat{R}_s]$ under the high SNR assumption, including the exact expressions and upper bounds, give valid upper bounds on the secrecy performances at finite SNR values.

5.3 Secrecy Performance Analysis

In this section, we provide the main results on the probabilistic characteristics of the achievable secrecy rates $\hat{R}_s$ and the average secrecy rates achievable $\mathbb{E}[\hat{R}_s]$ under three major scenarios, where different criterions to choose the serving BS are used and the serving BS can fully or partially acquire the location information of the eavesdroppers, corresponding to the different levels of BS cooperation

introduced. It should be noticed that the BS cooperation considered in this chapter includes only exchanging the identity and location information of the mobile users and selecting the appropriate BS to serve the typical user.

5.3.1 Scenario-I: Full Location Information; Nearest BS to Serve

We firstly assume that the location information of all eavesdroppers can be fully accessed by the serving BS and employ the cell association model by confining mobile users to be served by the nearest BS only. The location and identity information of mobile users in the serving BS's cell can be obtained easily, and other users' information is supplied by other BSs via the backhaul networks. Associating users to the nearest BS is commonly used in related cellular modeling studies [43,114], and equivalently it means that a BS is associated with the users in its Voronoi cell (formed by the PPP Φ_{BS}), thus resulting the Voronoi tessellation for BS coverage areas, as shown in Fig. 5.1.

We define the closed ball centered at p and of radius r as $\mathcal{B}(p,r)$, i.e., $\mathcal{B}(p,r) \triangleq \{m \in \mathbb{R}^2, \|m-p\| \leqslant r\}$, which will be used in our following study.

Theorem 5.1. *Under the conditions of mobile users being served by the nearest BS and the availability of full location information for all eavesdroppers, the CCDF of the achievable secrecy rate obtained at the typical user is given by*

$$\bar{F}_{\hat{R}_s}(R_0) = \frac{1}{1+\frac{\lambda_e}{\lambda_{BS}} \cdot 2^{(2R_0)/\alpha}}, \qquad \textit{for } R_0 \geqslant 0. \tag{5.9}$$

Proof. See Appendix C.1. □

Corollary 5.2. *Under the conditions of mobile users being served by the nearest BS and the availability of full location information for all eavesdroppers, the average secrecy rate achievable at the typical user is provided by*

$$\mathbb{E}[\hat{R}_s] = \frac{\alpha}{2\ln 2} \cdot \ln\Big(\frac{\lambda_{BS}+\lambda_e}{\lambda_e}\Big). \tag{5.10}$$

Proof. Based on the CCDF expression given in Theorem 5.1, the average secrecy rate achievable at the typical user can be obtained by integrating (5.9) from 0 to

∞, i.e.,

$$\begin{aligned}
\mathbb{E}[\hat{R}_s] &= \int_0^{\infty} \frac{1}{1+\frac{\lambda_e}{\lambda_{BS}}\cdot 2^{(2t)/\alpha}}\mathrm{d}t \\
&\overset{(a)}{=} \left[\frac{1}{\ln(2^{2/\alpha})}\cdot \ln\left(\frac{\exp\left[\ln(2^{2/\alpha})t\right]}{1+\frac{\lambda_e}{\lambda_{BS}}\cdot\exp\left[\ln(2^{2/\alpha})t\right]}\right)\right]_0^{\infty} \\
&= \frac{\alpha}{2\ln 2}\ln\left(\frac{1}{\lambda_e/\lambda_{BS}}\right) - \frac{\alpha}{2\ln 2}\ln\left(\frac{1}{1+\lambda_e/\lambda_{BS}}\right) \\
&= \frac{\alpha}{2\ln 2}\cdot\ln\left(\frac{\lambda_{BS}+\lambda_e}{\lambda_e}\right), \qquad (5.11)
\end{aligned}$$

where step (a) follows the indefinite integral result for the form of the integrand herein, which can be found in [162]. □

5.3.2 Scenario-II: Full Location Information; Optimal BS to Serve

Next, we still keep the assumption that the serving BS has all eavesdroppers' location information, which can be achieved by an ideal information exchange between BSs; however, in this scenario, we assume that all BSs can act as candidates to serve the typical user.

This scenario provides us the maximum achievable secrecy rate from the information-theoretic point of view, which tells the network designer the ultimate secrecy performance the cellular network can offer and can be viewed as the optimal BS cooperation scheme considered in this chapter. Obviously, to obtain the optimal secrecy performance, the BS achieving the maximum secrecy rate should be selected. By studying the secrecy performance with the optimal cell association, we are able to quantify the gap between the secrecy performances provided by the optimal BS and the nearest BS.

Based upon these assumptions, the achievable secrecy rate at the typical user becomes

$$\hat{R}_s = \max\left\{\max_{x\in\Phi_{BS}}\left\{\log_2\left(\frac{P_{rx}(0,x)}{\sigma^2}\right) - \log_2\left(\frac{P_{rx}(e^*(x),x)}{\sigma^2}\right)\right\}, 0\right\}, \qquad (5.12)$$

where $e^*(x)$ is given by (5.3).

Theorem 5.3. *Under the conditions of mobile users being served by the optimal BS and the availability of full location information for all eavesdroppers, an upper*

bound for the CCDF of the achievable secrecy rate at the typical user is given by

$$\bar{F}_{\hat{R}_s}(R_0) \leqslant 1 - \exp\Big(- \frac{\lambda_{BS}}{\lambda_e 2^{(2R_0)/\alpha}}\Big), \quad \textit{for } R_0 \geqslant 0, \tag{5.13}$$

and a lower bound is given by

$$\bar{F}_{\hat{R}_s}(R_0) \geqslant \frac{1}{1 + \frac{\lambda_e}{\lambda_{BS}} \cdot 2^{(2R_0)/\alpha}}, \quad \textit{for } R_0 \geqslant 0. \tag{5.14}$$

Proof. See Appendix C.2. □

Theorem 5.4. *Under the conditions of mobile users being served by the optimal BS and the availability of full location information for all eavesdroppers, another upper bound for the CCDF of the achievable secrecy rate at the typical user is given by*

$$\bar{F}_{\hat{R}_s}(R_0) \leqslant 1 - \mathbb{E}_{V_d}\Big[\exp\big(- \frac{4}{(1+2^{R_0/\alpha})^2} \cdot \frac{\lambda_{BS}}{\lambda_e} \cdot V_d\big)\Big], \quad \textit{for } R_0 \geqslant 0, \tag{5.15}$$

where the expectation is taken over the random variable $V_d = C_0(1)$, the area of a typical Voronoi cell of a homogeneous PPP with the unitary density.

Proof. For the set of eavesdropper locations Φ_e, we can define a random set $\mathcal{P}$, the union of all points at which BS can provide the typical user (at the origin) a secrecy rate $\hat{R}_s > R_0$, i.e.,

$$\mathcal{P} \triangleq \Big\{ x \in \mathbb{R}^2 : \|e - x\| > \beta^{1/\alpha}\|x\|, \forall e \in \Phi_e \Big\}, \tag{5.16}$$

which is based upon the assumption that the serving BS knows all eavesdroppers' locations in this scenario. Furthermore, we define $\mathcal{C}$ as the Voronoi cell generated by the process $\Phi_e \cup \{0\}$, the union of the eavesdroppers' locations and the origin. Because of Slivnyak's Theorem, the Voronoi cell around the origin formed by $\Phi_e \cup \{0\}$ has the same property as a randomly chosen Voronoi cell formed by a PPP with density λ_e. It should be noted that $\mathcal{C}$ still contains the origin, but its area is not distributed like the one in (3.8) anymore, since the origin itself belongs to the process $\Phi_e \cup \{0\}$.

The area measures of the random set $\mathcal{P}$ and $\mathcal{C}$ are denoted by $A(\mathcal{P})$ and $A(\mathcal{C})$, respectively. An example of these random sets is illustrated in Fig. 5.2, in which

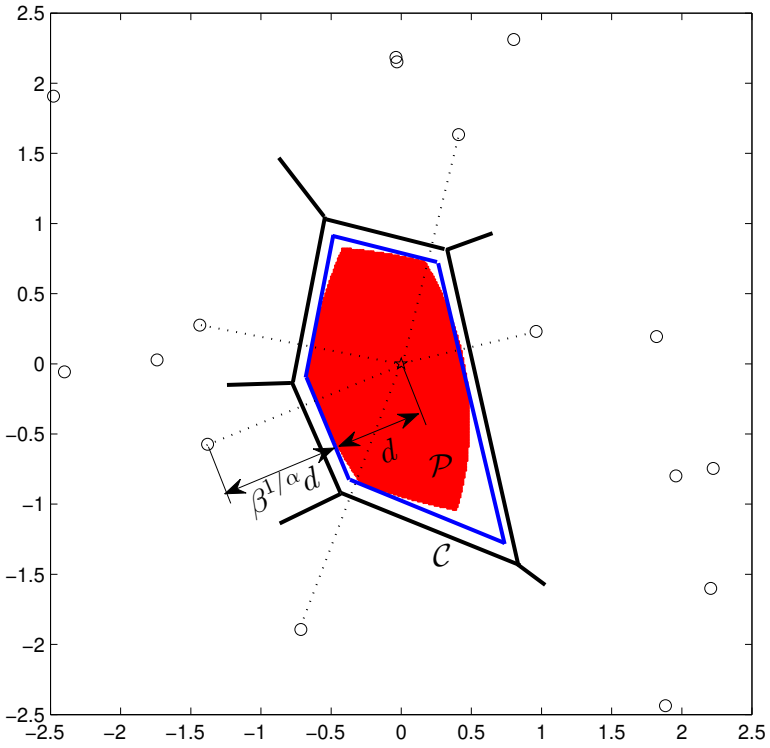

Figure 5.2: Illustration of the relationship between $\mathcal{P}$ (the union of all points at which BS can provide the typical user a secrecy rate $\hat{R}_s > \log_2(\beta)$, where $\beta = 1.25$, represented as the red region) and $\mathcal{C}$ (the Voronoi cell generated by the process $\Phi_e \cup \{0\}$), as defined in the proof of Proposition 5.4. The typical user denoted by a star is located at the origin. A realization of eavesdroppers are scattered and denoted as circles.

we can obtain a straightforward relationship between $A(\mathcal{P})$ and $A(\mathcal{C})$ as

$$A(\mathcal{P}) \leqslant \frac{4}{(1+\beta^{1/\alpha})^2} A(\mathcal{C}), \tag{5.17}$$

if $\beta \geqslant 1$, or equivalently, $R_0 \geqslant 0$.

The value $\left[4/(1+\beta^{1/\alpha})^2\right] A(\mathcal{C})$ is the area measure of the region enclosed by blue lines in Fig. 5.2, which is the exact shape shrunk from $\mathcal{C}$ and has edges tangential to $\mathcal{P}$'s edges. Obviously, for a realization of the BS location Φ_{BS}, the typical user can have a secrecy rate larger than R_0 if and only if there is at least

a BS located in $\mathcal{P}$, which makes the CCDF of the secrecy rate $\hat{R}_s$ become

$$\begin{aligned}
\bar{F}_{\hat{R}_s}(R_0) &= \mathbb{P}\big[\text{No BS exists in } \mathcal{P}\big] \\
&\overset{(a)}{=} 1 - \mathbb{E}_{\mathcal{P}}\Big[\exp\big(-\lambda_{BS} A(\mathcal{P})\big)\Big] \\
&\leqslant 1 - \mathbb{E}_{\mathcal{P}}\Big[\exp\big(-\frac{4\lambda_{BS}}{(1+\beta^{1/\alpha})^2} A(\mathcal{C})\big)\Big] \\
&= 1 - \mathbb{E}_{V_d}\Big[\exp\big(-\frac{4}{(1+\beta^{1/\alpha})^2} \cdot \frac{\lambda_{BS}}{\lambda_e} \cdot V_d\big)\Big], \qquad (5.18)
\end{aligned}$$

where the expectation in step (a) is taken over the random set $\mathcal{P}$. It should be noted that the Voronoi cell $\mathcal{C}$ is formed by the process of $\Phi_e \cup \{0\}$, the union of the eavesdroppers' locations and the origin. Because of Slivnyak's Theorem which states that the properties observed by the node at origin in the process $\Phi_e \cup \{0\}$ is the same as those observed by a typical point of the PPP Φ_e (or equivalently a randomly chosen point of the PPP), the area of the Voronoi cell containing the origin point is distributed as a randomly chosen Voronoi cell, which provides the last step in (5.18). □

Remark. It can be observed that the upper bound obtained in Theorem 5.4 depends on the statistic characteristics of Voronoi cell's area. It provides us an accurate approximation for small positive $\hat{R}_s$ values and complements the upper bound result in Theorem 5.3. Particularly, for the special case of $R_0 = 0$, the region $\mathcal{P}$ turns out to be the Voronoi cell $\mathcal{C}$, thus making the CCDF upper bound become the exact result, i.e.,

$$\bar{F}_{\hat{R}_s}(0) = 1 - \mathbb{E}_{V_d}\Big[\exp\big(-\frac{\lambda_{BS}}{\lambda_e} V_d\big)\Big], \qquad (5.19)$$

and the expression in this extreme case is consistent with the secrecy coverage probability provided in [160]. For high value of R_0, however, the area difference between $A(\mathcal{P})$ and $\big[4/(1+\beta^{1/\alpha})^2\big]\, A(\mathcal{C})$ increases, which makes the approximation in (5.17) become imprecise. This can explain the numerical results we will observe later in Fig. 5.6 and Fig. 5.7, i.e., the discrepancy between the upper bound given by Theorem 5.4 and the simulation result for $R_0 = 5$.

Although there is no known closed form expression of V_d's PDF [138], some accurate estimates of this distribution were produced in [139, 140]. For instance, a simple gamma distribution was used to fit the PDF of V_d derived from Monte

Carlo simulations in [140], i.e.,

$$f_{V_d}(x) \approx \frac{b^q x^{q-1} \exp(-bx)}{\Gamma(q)}, \tag{5.20}$$

which can be regarded as a special case for (3.6), where $q = 3.61$, $b = 3.61$ and $\Gamma(x) = \int_0^\infty t^{x-1}e^{-t}\mathrm{d}t$ is the standard gamma function. By substituting this estimate into (5.15) and simplifying the integral, we can obtain

$$\bar{F}_{\hat{R}_s}(R_0) \approx 1 - \frac{b^q}{\left(b + \frac{4}{(1+2^{R_0/\alpha})^2} \cdot \frac{\lambda_{BS}}{\lambda_e}\right)^q}, \quad \text{for } R_0 \geqslant 0. \tag{5.21}$$

After giving the bounds for $\hat{R}_s$'s CCDF, we focus on the average secrecy rate achievable for a randomly located user.

Corollary 5.5. *Under the conditions of mobile users being served by the optimal BS and the availability of full location information for all eavesdroppers, an upper bound of the average secrecy rate achievable at the typical user is provided by*

$$\mathbb{E}[\hat{R}_s] \leqslant \frac{\alpha}{2\ln 2} \cdot \left[\gamma + \ln\left(\frac{\lambda_{BS}}{\lambda_e}\right) + E_1\left(\frac{\lambda_{BS}}{\lambda_e}\right)\right], \tag{5.22}$$

and a lower bound is provided by

$$\mathbb{E}[\hat{R}_s] \geqslant \frac{\alpha}{2\ln 2} \cdot \ln\left(\frac{\lambda_{BS} + \lambda_e}{\lambda_e}\right), \tag{5.23}$$

where $E_1(x) = \int_x^\infty \exp(-t)\frac{1}{t}\mathrm{d}t$ is the exponential integral and γ is the Euler-Mascheroni constant.

Proof. See Appendix C.3. □

An alternative upper bound of the average secrecy rate achievable can be derived based upon Theorem 5.4, and the corresponding performance is also shown in Section 5.4.

Remark. It should be noted that the optimal BS mentioned here is not necessarily the nearest BS, since it is possible that other BSs can provide higher secrecy rate than the nearest BS. Taking the case illustrated in Fig. 5.3 as an example, the typical user's nearest BS is BS-A, which, however, is hardly capable of providing a secure connection due to its excellent connection to the eavesdropper nearby. Alternatively, choosing BS-B to serve can provide a certain level secrecy rate

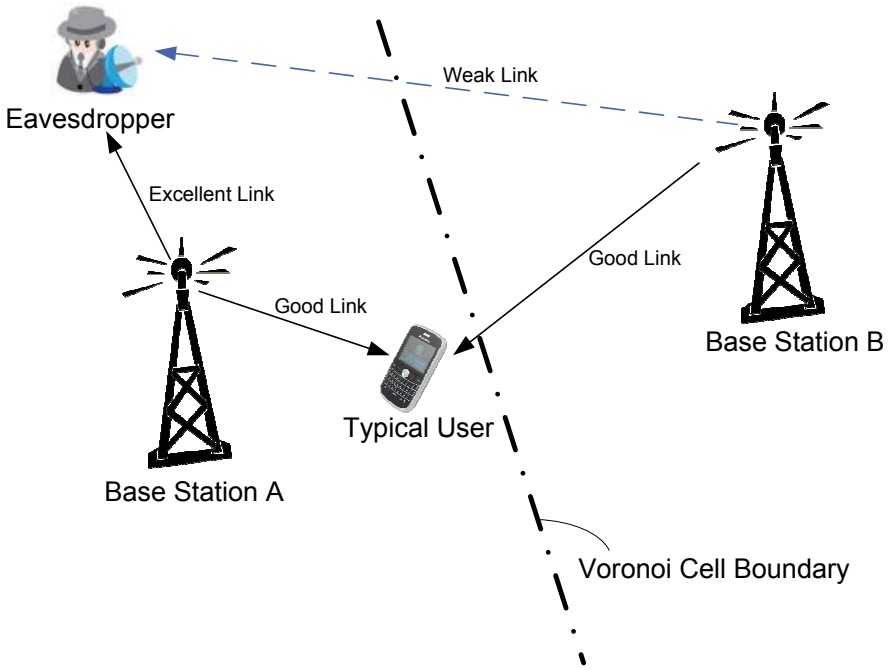

Figure 5.3: An example where the BS providing maximum achievable secrecy rate is not the nearest BS. The typical user's nearest BS is BS-A, which however cannot provide a positive secrecy rate due to its excellent link to the eavesdropper. BS-B, on the other hand, can provide a secrecy connection since there is no eavesdroppers nearby.

if the typical user's channel quality to BS-B is better than the channel to the eavesdropper.

Remark. By comparing the secrecy performance in Scenario-I (the typical user served by the nearest BS) with this scenario (the typical user served by the best BS), we will be able to see the benefit from optimally choosing the serving BS to provide the secure downlink transmission. The numerical illustrations will be provided in Section 5.4.

5.3.3 Scenario-III: Limited Location Information; Nearest BS to Serve

Here, we still assume the same cell association model as Scenario-I, i.e., mobile users are served by the nearest BS, nevertheless only limited users' location and

identity information is known to the serving BS. Considering the backhaul bandwidth cost in practice and the impeding core-network implementation complexity for BS cooperation, the scenarios where the location and identity information is only exchanged with neighboring cells or even no exchange allowed at all are analyzed in this section.

No location and identity information exchange

Firstly, we assume that no location and identity information exchange allowed between BSs, which means that the serving BS only knows the intracell users' location and identity information. As mentioned in section 5.2.2, the unknown region outside the serving cell leads to the worst case assumption that eavesdroppers lie on the serving BS's cell boundaries and limit the achievable secrecy rate.

Before coming to this scenario's secrecy performance, we firstly define the minimum distance from PPP's each point to its own cell boundaries, denoted as $D_{\min}$. In Fig. 5.1, for instant, the $D_{\min}$ of three BSs are illustrated. In the cell tessellation formed by BS PPP with density λ_{BS}, we can simply use the void probability of a PPP to derive

$$\begin{aligned}\mathbb{P}\left(D_{\min} > r\right) &= \mathbb{P}\big[\text{No BS closer than } 2r\big] \\ &= e^{-\pi\lambda_{BS}(2r)^2}.\end{aligned} \tag{5.24}$$

Therefore, the CDF is

$$\begin{aligned}F_{D_{min}}(r) &= \mathbb{P}\left(D_{\min} \leqslant r\right) \\ &= 1 - e^{-\pi\lambda_{BS}(2r)^2},\end{aligned} \tag{5.25}$$

and the PDF can be found as

$$\begin{aligned}f_{D_{\min}}(r) &= \frac{\mathrm{d}F_{D_{min}}(r)}{\mathrm{d}r} \\ &= 8\pi\lambda_{BS} r \exp(-4\pi\lambda_{BS} r^2).\end{aligned} \tag{5.26}$$

Theorem 5.6. *Under the conditions of mobile users being served by the nearest BS and only intracell eavesdroppers' location information available, a lower bound for the CCDF of the achievable secrecy rate obtained at the typical user is given*

by

$$\bar{F}_{\hat{R}_s}(R_0) \geqslant \frac{1}{1+(\frac{\lambda_e}{\lambda_{BS}}+4)\cdot 2^{(2R_0)/\alpha}}, \quad \textit{for } R_0 \geqslant 0. \tag{5.27}$$

Proof. See Appendix C.4. □

Remark. When $\lambda_e \gg \lambda_{BS}$, the impact of cell boundaries on the secrecy rate becomes negligible, since almost surely an eavesdropper exists inside the ball $\mathcal{B}(x_0, D_{min})$ and limits the achievable secrecy rate, thus making (5.27) become (5.9).

Corollary 5.7. *Under the conditions of mobile users being served by the nearest BS and only intracell eavesdroppers' location information available, a lower bound of the average secrecy rate achievable at the typical user is provided by*

$$\mathbb{E}[\hat{R}_s] \geqslant \frac{\alpha}{2\ln 2}\cdot \ln\Big(\frac{5\lambda_{BS}+\lambda_e}{4\lambda_{BS}+\lambda_e}\Big). \tag{5.28}$$

Proof. The lower bound of the average secrecy rate $\mathbb{E}[\hat{R}_s]$ can be derived by integrating (5.27) from 0 to ∞. Since the integrand in this integral has the similar form as (5.9), the same deduction procedure can be performed to obtain this lower bound. □

Remark. Under the condition of mobile users camping on the nearest BS, Scenario-I and this case can be regarded as two extremes: in the former scenario, the location information of all eavesdroppers is shared among BSs, while no location and identity information exchange is allowed in the latter one. By comparing the expressions of (5.10) with (5.28), it is easy to conclude that the latter case's average secrecy rate achievable increases with λ_{BS}/λ_e much slower than the counterpart in Scenario-I. This trend, which will be given numerically in following Section 5.4, demonstrates the impact of the location and identity information exchange between BSs.

Location and identity information exchange limited with neighboring cells only

In order to further characterize how the availability of the location and identity information affects the secrecy performance, we investigate the secrecy rate for

the case where the location information and identity exchange is restricted to the serving BS's neighboring cells only.

Given certain neighboring BSs participating in the information exchange with the serving BS, the region outside the cells covered by these BSs is the unknown region. By considering the worst case scenario that the eavesdroppers can be located anywhere inside the unknown region, the secrecy performance is limited by the minimum distance from the unknown region to the serving BS. As long as the minimum distance is the same, the secrecy performance stays the same regardless of the shape of the unknown region, which means that the consideration of a disk-shape known region does not lose the generality of the result on secrecy rates. Therefore, we apply the following model to represent the known and unknown regions: only the location information of the eavesdroppers with distances less than D_0 from the serving BS is available to it, i.e., the eavesdroppers outside the region $\mathcal{B}(x, D_0)$ are unknown to a BS at x. The value D_0 is called *detection radius* in our analysis.

From a network design perspective, a larger D_0 represents information exchanging feasible with BSs farther away, and in other words, a larger D_0 means that more BSs participate in the information exchange with the serving BS. This scenario provides limited information exchange, which can be regarded as an intermediate case between Scenario-II and Scenario-III(1), and reflects practical considerations, such as the limited bandwidth of the backhaul network and the complexity introduced by extensive information sharing in the practical implementation. By investigating how the achievable secrecy rate changes with D_0, one can obtain insights on the improvement of the secrecy performance as more BSs participate in the information exchange process.

Theorem 5.8. *Under the conditions of mobile users being served by the nearest BS and the detection radius is D_0, the CCDF of the achievable secrecy rate obtained at the typical user is given by*

$$\bar{F}_{\hat{R}_s}(R_0) = \left(1 - \exp\left[-\pi(\lambda_e + \lambda_{BS} 2^{-\frac{2R_0}{\alpha}}){D_0}^2\right]\right) \cdot \frac{1}{1 + \frac{\lambda_e}{\lambda_{BS}} \cdot 2^{(2R_0)/\alpha}}, \quad \text{for } R_0 \geqslant 0. \quad (5.29)$$

Proof. See Appendix C.5. □

Remark. As expected, the general trend can be understood as follows: when

detection radius D_0 decreases, the location information of eavesdroppers surrounding the serving BS reduces, which makes a lower probability to maintain the secrecy rate R_0. As we increase D_0 to infinity, the condition turns to be identical to Scenario-I, thus making (5.29) become (5.9).

Corollary 5.9. *Under the conditions of mobile users being served by the nearest BS and the detection radius is D_0, the average secrecy rate achievable at the typical user is provided by*

$$\mathbb{E}[\hat{R}_s] = \frac{\alpha}{2\ln 2} \cdot \ln\Big(\frac{\lambda_{BS}+\lambda_e}{\lambda_e}\Big) - \frac{\alpha}{2\ln 2} \cdot \Big[E_1\big(\pi\lambda_e D_0^2\big) - E_1\big(\pi(\lambda_e+\lambda_{BS})D_0^2\big)\Big]. \tag{5.30}$$

Proof. See Appendix C.6. □

5.4 Numerical Results

In this section, we present numerical results on the achievable secrecy rate for all three major scenarios, respectively, which are compared with our analysis for the purpose of model validation. Here, we define the value SNR as the received SNR from the serving BS at the distance $r = 1$, i.e., SNR $= P_{BS}/\sigma^2$. All simulation results are conducted with the unitary BS density, i.e., $\lambda_{BS} = 1$.

5.4.1 Numerical Results of Scenario-I

Firstly, for each curve in Fig. 5.4, we show the average secrecy rates achievable at the typical user in Scenario-I, for both path loss exponents of $\alpha = 4$ and $\alpha = 2.5$. As can be seen in this figure, the curves representing the analytical expression (5.10) in Corollary 5.2 match the simulated results for all conditions.

As our analysis in this chapter is conducted under the high SNR assumption, through numerically comparing with simulation results, we find that our analytical results for Scenario-I are very accurate at SNR = 20 dB. Moreover, the results are still sound approximations even at median SNR conditions. Take the case of Scenario-I for instance: The simulation results in Fig. 5.5 show that this approximation is generally accurate even when SNR is as low as 10 dB. Without further explanation, all simulation results in the following Scenario-II and Scneario-III are conducted under SNR = 20 dB.

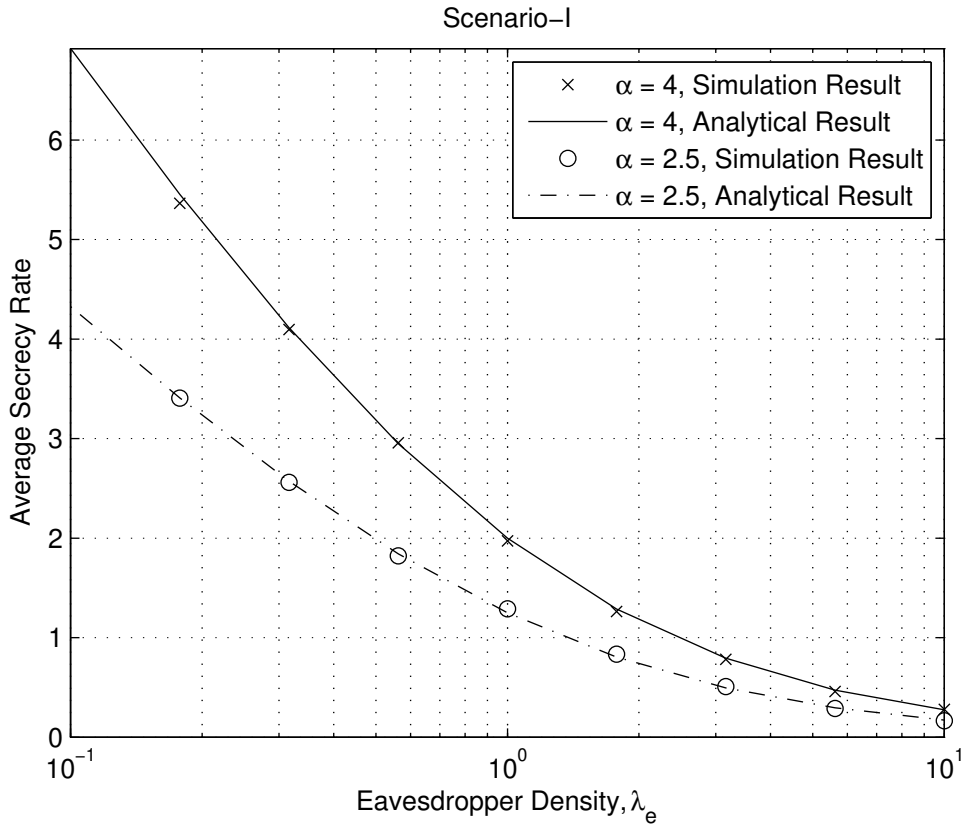

Figure 5.4: The average secrecy rate achievable versus the eavesdropper density λ_e for Scenario-I (full location information; nearest BS to serve). Simulation and analytical results are shown for different path loss exponents α.

5.4.2 Numerical Results of Scenario-II

Fig. 5.6 - Fig. 5.9 demonstrate the results of Scenario-II, the optimal case where all mobile users' location and identity information is completely known and the optimal BS is chosen to maximize the achievable secrecy rate. Fig. 5.6 and Fig. 5.7 show the typical user's secure link coverage probability with the threshold $R_0 = 0$ or $R_0 = 5$ to claim outage. Note that the upper bound in Theorem 5.4 converges to the exact coverage probability in the special case of $R_0 = 0$, which can be observed from the fact that the curves representing the approximation (5.21) based on Theorem 5.4 match the simulated results in Fig. 5.6 and Fig. 5.7. However, this approximation is not precise for large values of R_0, e.g., $R_0 = 5$ and the analytical reason for this inaccuracy is explained in remark after Theorem 5.4. On the other hand, the lower bound and the upper bound in Theorem 5.3 tend to

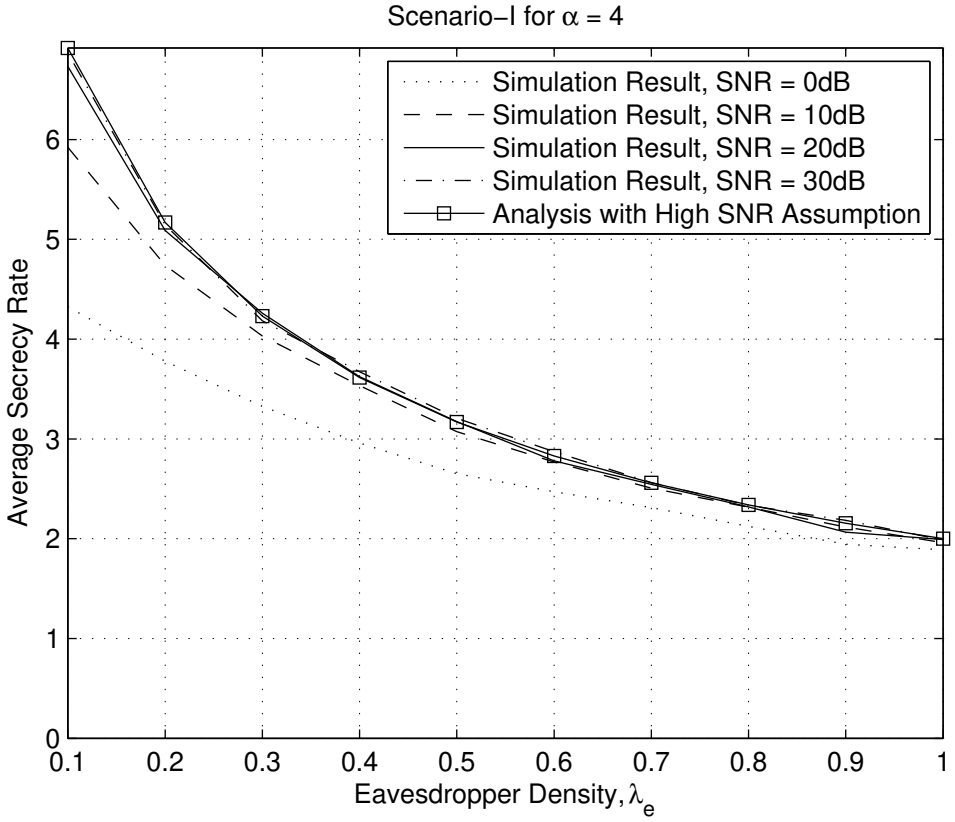

Figure 5.5: The average secrecy rate achievable versus the eavesdropper density λ_e for Scenario-I (full location information; nearest BS to serve). Simulation results are shown for different SNR.

give more accurate approximations of the exact secrecy coverage probability for large values of R_0, which can be regarded as a complementary property to offset the limitation of the upper bound in Theorem 5.4 mentioned earlier. From the results shown in Fig. 5.8 and Fig. 5.9, the upper and lower bounds of the achievable secrecy rates in Corollary 5.5 are also reasonably accurate. Furthermore, the approximations for the average secrecy rates achievable based on Theorem 5.4 are also demonstrated in Fig. 5.8 and Fig. 5.9, and turn out to be inaccurate due to Theorem 5.4's imprecise estimate for large R_0. The achievable secrecy rate given in Scenario-II provides the maximum value over all the scenarios considered in this chapter.

By comparing Fig. 5.4 with Fig. 5.8 and Fig. 5.9, it can be noted that picking the nearest BS to serve can achieve a secrecy rate nearly as much as the optimal

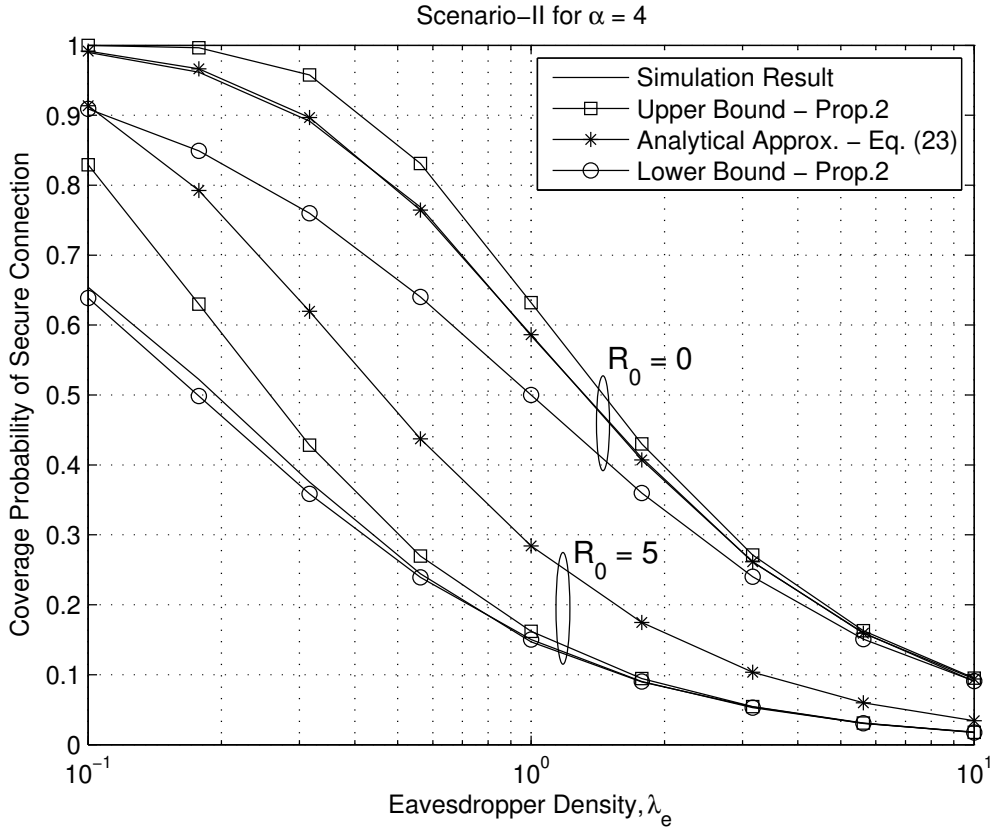

Figure 5.6: The secure coverage probability versus the eavesdropper density λ_e for Scenario-II (full location information; optimal BS to serve). Simulation and analytical results are shown for different thresholds $R_0 = 0$ or 5 to claim outage. (It should be noticed that the approximation provided by Theorem 5.4 becomes the exact coverage probability for the special case of $R_0 = 0$.) Path loss exponent is $\alpha = 4$.

value. For example, the secrecy rate in Scenario-I is approximately 1.9 for $\alpha = 4$ and the eavesdroppers' density $\lambda_e = 1$, compared with around 2.1 for the optimal case in Scenario-II. In other words, there is only marginal benefits from optimally choosing the serving BS instead of simply picking the nearest BS to serve.

5.4.3 Numerical Results of Scenario-III

Fig. 5.10 shows the average secrecy rate achievable for Scenario-III(1), where no location and identity information exchange is allowed and only intracell users' location information is known to the serving BS. Due to the shrinkage of the region where location information is available, the secrecy performance is significantly

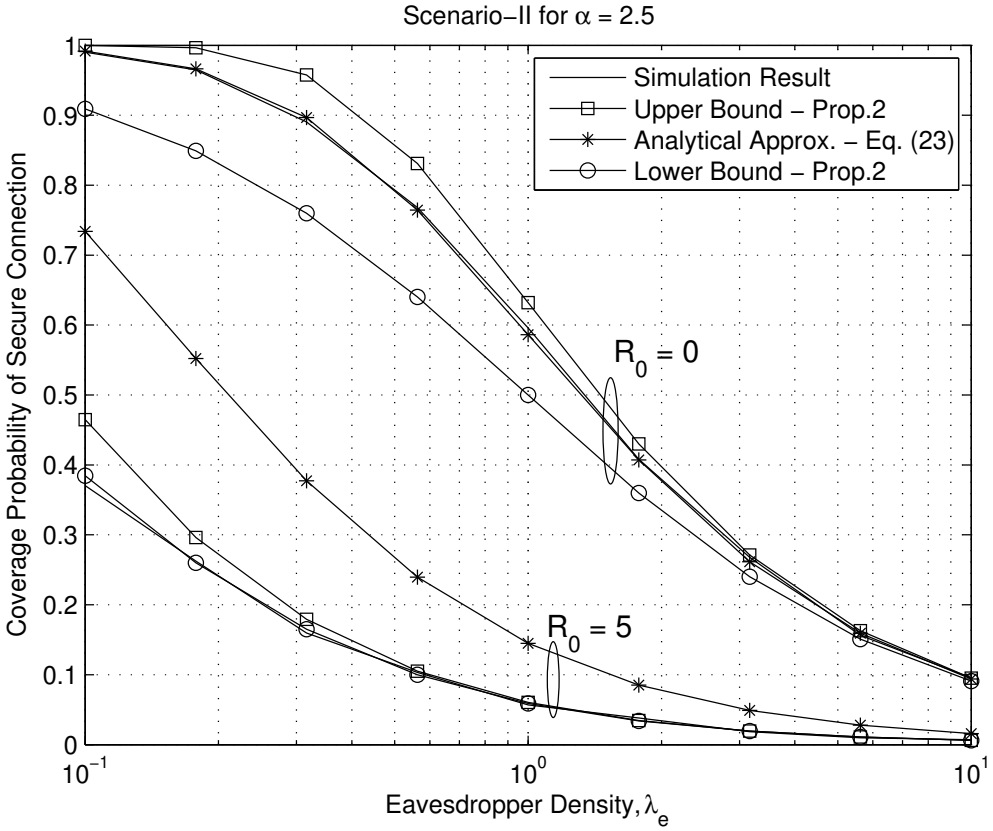

Figure 5.7: The secure coverage probability versus the eavesdropper density λ_e for Scenario-II (full location information; optimal BS to serve). Simulation and analytical results are shown for different thresholds $R_0 = 0$ or 5 to claim outage. (It should be noticed that the approximation provided by Theorem 5.4 becomes the exact coverage probability for the special case of $R_0 = 0$.) Path loss exponent is $\alpha = 2.5$.

degraded compared with the counterpart in Fig. 5.4. For example, the average secrecy rate achievable is around 0.57 for $\alpha = 4$ and $\lambda_e = 1$, whereas the corresponding value can reach around 1.9 for Scenario-I. We also observe a relatively slow drop in the average secrecy rate achievable as λ_e changes from 0.1 toward 1, due to its weak dependence on the density of eavesdroppers in this range of λ_e, which suggests that the lack of location information outside the serving BS's cell becomes the main restrictive factor in determining the secrecy performance. On the other hand, as λ_e increases from 1 to 10, the average secrecy rate achievable accelerates to drop since the eavesdropper density is more influential. It can be shown that the lower bound in (5.28) captures the general trend of the curves

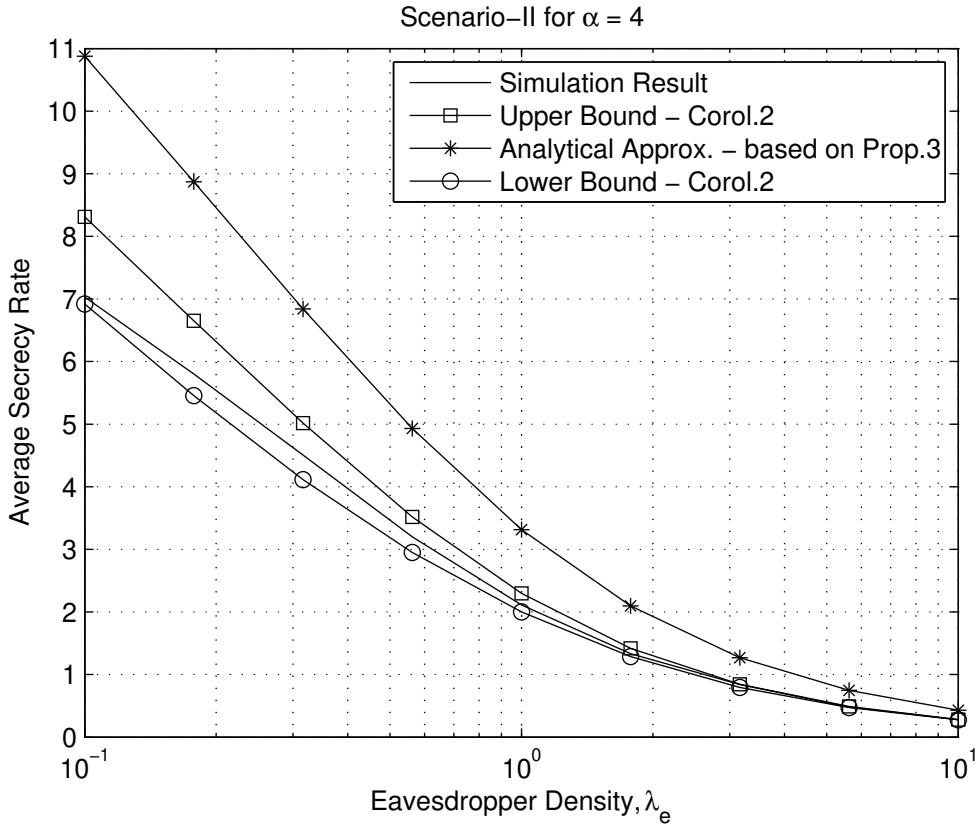

Figure 5.8: The average secrecy rate achievable versus the eavesdropper density λ_e for Scenario-II (full location information; optimal BS to serve). Simulation and analytical results are shown for path loss exponent $\alpha = 4$.

and can be used as a tool to make a precise estimate.

Furthermore, by presenting the average secrecy rate achievable versus the detection radius D_0 in Fig. 5.11 and Fig. 5.12, we can see the importance of eavesdroppers' location information on the secrecy performance. In case of relatively small values of D_0, any increase of the detection radius brings remarkable benefit to the achievable secrecy rate. On the other hand, in case of large D_0, any further increase in the detection radius does not substantially impact the secrecy rate, since the eavesdropper that limits the secrecy performance is usually located not too far away from the serving BS and its distance is likely to be smaller than D_0 when D_0 is sufficiently large. Take the curve with $\alpha = 4$ and $\lambda_e = 0.1$ for instance, the secrecy performance improves significantly as D_0 is increased up to 2, and any further increase from $D_0 = 2$ has a limited effect. This performance trend over the range of detection radius can be utilized to appropriately choose

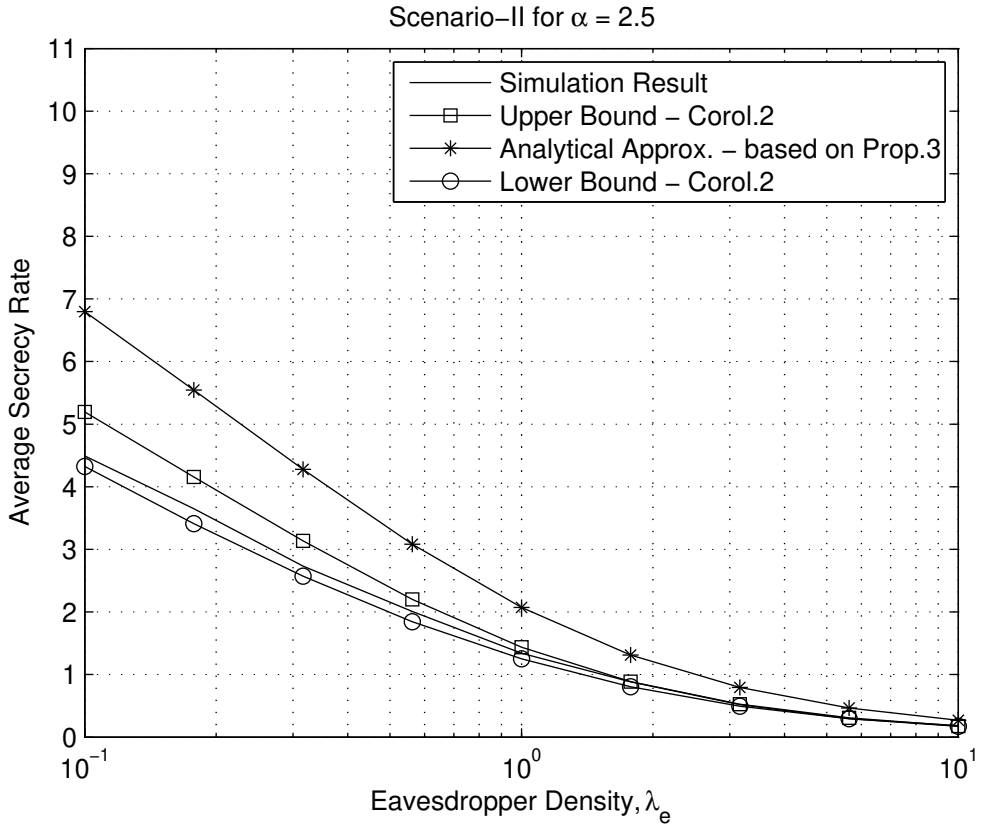

Figure 5.9: The average secrecy rate achievable versus the eavesdropper density λ_e for Scenario-II (full location information; optimal BS to serve). Simulation and analytical results are shown for path loss exponent $\alpha = 2.5$.

the number of neighboring BSs for the information exchange in order to achieve a good secrecy performance whilst taking the implementation cost of such information exchange into consideration. It should be noted that the slight mismatches between simulation and analytical results in Fig. 5.4, Fig. 5.11, and Fig. 5.12 come from the high SNR assumption used in our analysis, and become almost invisible at SNR = 30dB (plots omitted for brevity).

Another fact clearly shown from Fig. 5.8-5.12 is that better performance can be obtained for larger values of path loss exponent α, e.g., the average secrecy rate achievable is higher for $\alpha = 4$ than the counterpart for $\alpha = 2.5$. This is because the resultant larger path loss from larger α indicates worse signal condition to both the eavesdroppers and the typical user, whereas the former effect turns out to be more influential on the secrecy performance.

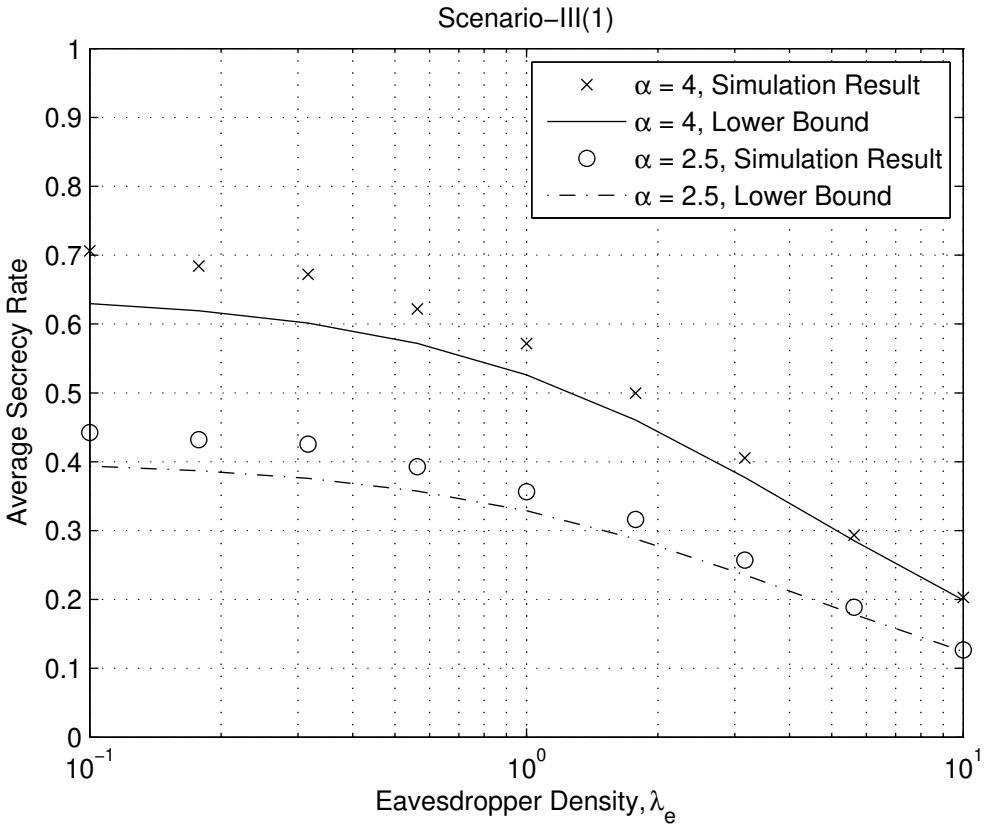

Figure 5.10: The average secrecy rate achievable versus the eavesdropper density λ_e for Scenario-III(1) (no location information exchange; nearest BS to serve). Simulation results and lower bounds are shown for different path loss exponents α.

5.5 Summary of Contributions

In this chapter, we have studied the secrecy performance of cellular networks considering cell association and information exchange between BSs potentially provided by the carrier-operated high-speed backhaul and core-networks. Using the stochastic geometry modeling of cellular networks, analytical results to characterize the secrecy rate have been obtained under different assumptions on the cell association and location information exchange between BSs. The simulation results validated the analytical expressions and approximations. Some specific contributions made in this chapter are as follows.

Addressing Q1 in Section 5.1:

- From the analysis in this chapter, the analytical results have been provided

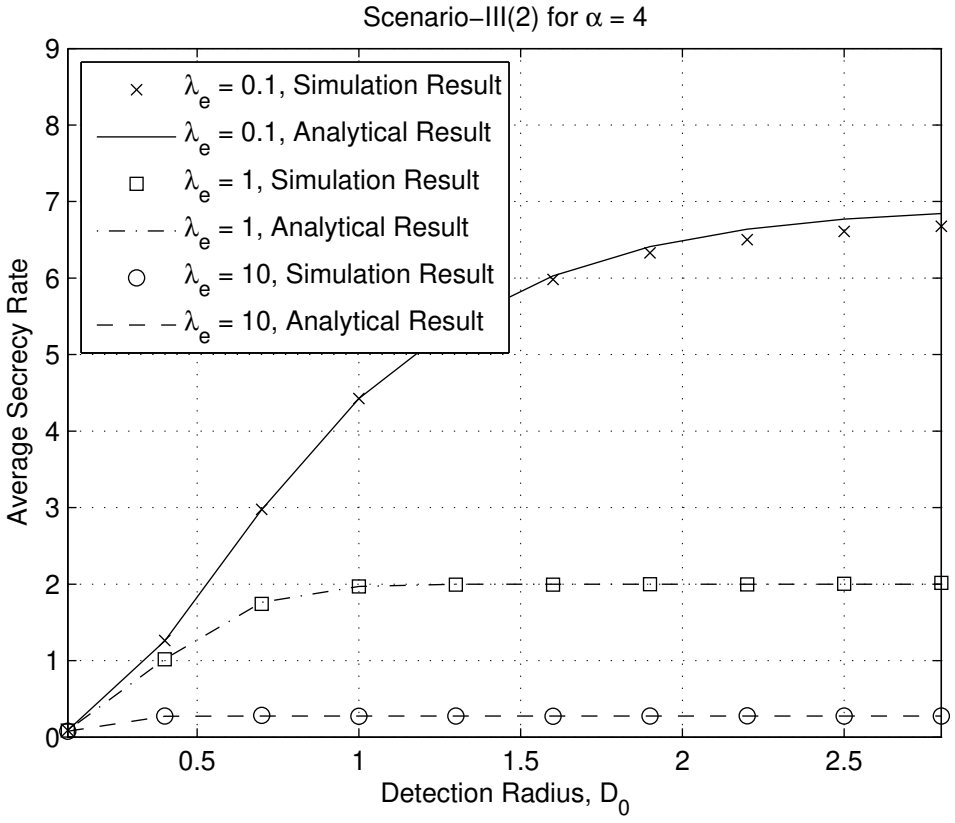

Figure 5.11: The average secrecy rate achievable versus the detection radius D_0 for Scenario-III(2) (location information for users with distances less than D_0; nearest BS to serve). Simulation and analytical results are shown for different eavesdropper densities λ_e and path loss exponent $\alpha = 4$.

for the probabilistic distribution of the secrecy rate, given the condition that BS information exchange via the backhaul networks is ideal.

Addressing Q2 in Section 5.1:

- By comparing the secrecy performance achieved by two cell association models, a unique feature of secure transmissions that the optimal BS is often not the nearest BS has been identified and analyzed in the chapter. Our results showed that only marginal gain can be obtained by optimally choosing the serving BS rather than associating to the nearest one. In other words, keeping the nearest BS to be used for secure transmission still achieves near-optimal secrecy performance, which is a very useful message to the network designers.

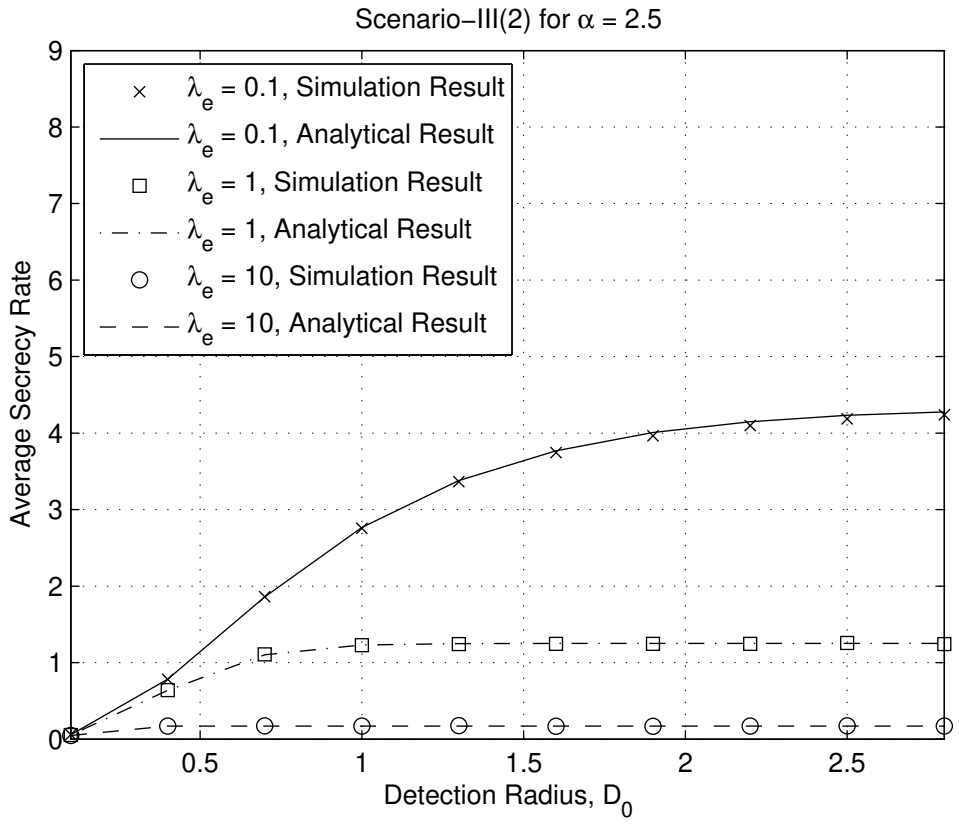

Figure 5.12: The average secrecy rate achievable versus the detection radius D_0 for Scenario-III(2) (location information for users with distances less than D_0; nearest BS to serve). Simulation and analytical results are shown for different eavesdropper densities λ_e and path loss exponent $\alpha = 2.5$.

Addressing Q3 in Section 5.1:

- By studying the performance difference between the two extremes, i.e., location information fully exchanged and no location information exchange, we have reached the conclusion that the location information plays a crucial role in determining the average secrecy rate achievable at the typical user.

Addressing Q4 in Section 5.1:

- In this chapter, we have considered the exchange of eavesdropper's location information between BSs and studied its impact on the secrecy rate performance. Our finding is that it is usually sufficient to allow a small number of neighboring BSs to exchange the location information for achieving close to maximum secrecy rate. Specifically, our analytical result provides network

designers practical guidelines to decide the necessary information exchange range, i.e., how many nearby BSs should participate in the information exchange for achieving a certain level of secrecy performance.

Chapter 6

Conclusions and Future Research Directions

In this chapter we state the general conclusions drawn from this thesis. The summary of contributions can be found at the end of each chapter and are not repeated here. We also outline some future research directions arising from this work.

6.1 Conclusions

In recent years, the acceptance and usage of smartphones and other personal mobile devices have become more widespread, which requires the cellular communications networks to provide high quality connections with good coverage, high data rate, and strong secrecy, rather than only low-data-rate voice-call connections. In the transition to such advanced cellular networks, the research community and the industry are facing new problems in network modeling and design, which become the primary focus of this thesis.

It is well accepted that HetNet, complementing traditional macrocells by a multitude of novel small cells, is a promising technology for future cellular deployment. Small cells, such as picocells and femtocells, can be installed in particular poorly covered regions to effectively improve the cellular coverage condition therein. On the other hand, because of its much more complicated topology, new technical challenges in HetNet modeling and design are presented in front of researchers and engineers.

One of the challenges is how to set up an appropriate analytical framework

to evaluate the metrics of HetNets, such as cellular coverage/outage probability and achievable rate, which are of significance for HetNet deployment. In recent studies, stochastic geometry was used to develop the large-scale cellular network model that was a new approach to conduct tractable and accurate performance analysis. As this stochastic-geometry-based model captures the random characteristics of user-planned or unplanned small cell BS locations, it is particularly suitable for HetNet modeling. In this thesis, an extended model with the impact of directional antennas taken into account has been provided for coverage performance analysis. The significance of this extension is emphasized by the fact that directional antennas are widely used to sectorize the macrocell cells in practical cellular systems.

Recent studies have shown that randomly deploying small cells in a uniform-distributed way cannot give any remarkable improvement in coverage performance. This fact inspired us to focus on the non-uniform approaches to deploy small cells, for instance, not utilizing femtocell BSs in the undesirable regions. In this thesis, we have proposed a non-uniform femtocell deployment scheme along with two implementation approaches for it, i.e., femtocell deactivation and smart femtocell deployment, in which femtocell BSs are not used if they are located within a prescribed distance from any macrocell BSs. Using the stochastic-geometry-based HetNet model, we have provided the probabilistic characterization of the downlink coverage and single user rate at a randomly located mobile user in this new scheme. Based upon our analysis, significant performance improvements brought by this non-uniform femtocell deployment on both coverage and rate have been demonstrated, which emphasized the importance of deploying the femtocell BSs selectively by considering their relative locations with macrocell BSs.

To alleviate the severe noise rise problems experienced at CDMA-based uplink femtocell receivers, attenuation can be applied to bring the intercell interference down to the level comparable to thermal noise, which is a key technique to make femtocell receivers work smoothly and is known by the name uplink attenuation. By proposing an analytical framework to evaluate the coverage/outage probability in a femtocell with this technique, we have demonstrated the tradeoff between higher level uplink attenuation resulting in a higher probability to reach the maximum power cap and lower level attenuation with less interference mitigation. Furthermore, two improved adaptive uplink attenuation algorithms have been

provided in this work, both of which aim to minimize the outage probability by adjusting the uplink attenuation factor adaptively based upon the information of the scheduled traffic, SINR requirements for each femtocell-connected user, and the current interference power at the femtocell receiver.

Other than the improved cellular coverage and rate, how to guarantee the communication security for sensitive data transmissions is another important design issue. As a new way to enhance the security performance, physical layer security has been studied herein for a cellular scenario, in which we highlighted the unique cellular features, such as cell association and information exchange between BSs potentially provided by the carrier-operated high-speed backhaul and core-networks. By using the stochastic-geometry-based BS model, analytical results have been obtained to characterize the secrecy rate under different assumptions on the cell association and location information exchange between BSs. We have derived the probabilistic distribution of the secrecy rate, provided that BS information exchange is ideal and the serving BS is optimally chosen. Using this scenario as a reference, we have identified that only marginal gain would be degraded if the nearest BS not the optimal one is selected to serve subscribers. In other words, keeping the nearest BS for secure transmission still achieves near-optimal secrecy performance, which is a very useful message to the network designers. By studying the performance difference between the two extremes, that is, location information fully exchanged and no location information exchange, we have reached the conclusion that the location information plays a crucial role in determining the average secrecy rate achievable. Based on a further analysis, we have shown that it is frequently sufficient to allow a small number of neighboring BSs to exchange the location information for achieving close to maximum secrecy rate, which can provide network designers practical guidelines to decide the necessary information exchange range, i.e., how many nearby BSs should participate in the information exchange for achieving a certain level of secrecy performance.

6.2 Future Research Directions

In this section, we outline a number of future research directions which arise from the work presented in this thesis.

Stochastic-Geometry-Based Analysis on LTE eICIC: Since eICIC tech-

nique was adopted in LTE release 10 to alleviate the intercell interference introduced by HetNets, extensive studies have been completed to evaluate its performance through grid-model-based system-level simulations. As a result of the inherent intractability for Monte Carlo simulations, it is difficult to compare different results and to directly gain an insight into the performance impact of the core parameters in the eICIC scheme. Conducting the analysis with the help of stochastic-geometry-based HetNet model is a promising way to reach analytical results, based on which eICIC can be further investigated and optimized.

Optimization on the Stochastic-Geometry-Based HetNet Model: In most existing studies on HetNet PPP-based model, different tiers are assumed to be totally independent, which unfortunately does not agree with the practical implementation scenario. Dependence between different tiers' BS distributions has been introduced in our analysis in Chapter 3 and a recent study by Haenggi [125]; however, other parameters' dependence on the BS spatial distribution, such as the impact of BS local density on the transmit power levels, has not been revealed and introduced into the model till now. By investigating practical HetNet deployment data, many aspects of the stochastic-geometry-based model could be further optimized to match a real world HetNet.

Extensions of Physical Layer Security in Large-Scale Cellular Networks: The result in Chapter 5 applied to scenarios where a carefully planned frequency reuse pattern is assumed, and the serving BS can occupy some resource blocks exclusively in a relatively large region, in order to avoid the impact of co-channel interference. After introducing interference, the channel conditions of both legitimate users and eavesdroppers will be degraded, and the impact of the co-channel interference on the secrecy performance of large-scale cellular network is still unknown. Another limitation is that the BS cooperation considered in this chapter is confined to cell association and location information exchange. Coordinated multipoint (CoMP) transmission, as an emerging BS cooperation technique in future cellular network, can be potentially utilized, and its benefit on the secrecy performance is an interesting problem to investigate.

Appendix A

A.1 Proof of Lemma 2.1

As defined in (2.19) of Section 2.3.1, the random variable $P_{LT,\max}$ is the maximum long-term received power from all BSs (including all available sectors). In other words, all the long-term received power levels from interfering sectors should be less than $P_{LT,\max}$. Hence, the CDF of the random variable $P_{LT,\max}$ with the impact of directional antennas taken into consideration can be derived as

$$\begin{aligned} F_{P_{LT,\max}}(t) &= \mathbb{P}[P_{LT,\max} \leqslant t] \\ &= \mathbb{P}\Big[P_\omega G_{\omega,\max}(\varphi)\|\varphi\|^{-\alpha} \leqslant t\Big] \\ &= \prod_{i\in\mathbb{K}} \mathbb{E}_{\Phi_i}\Big[\prod_{x\in\Phi_i} \mathbb{P}\Big[P_i G_{i,\max}(x)\|x\|^{-\alpha} \leqslant t\Big]\Big], \end{aligned} \tag{A.1}$$

where $G_{i,\max}(x)$ can be viewed as a random variable, given x is randomly chosen from the whole plane. As stated in Lemma 2.1, we use $G_{i,\max}$ to denote this random variable. Provided the CDF of the $G_{i,\max}$ is available (which is denoted by $F_{G_{i,\max}}(\cdot)$), we can have

$$\begin{aligned} F_{P_{LT,\max}}(t) &= \prod_{i\in\mathbb{K}} \mathbb{E}_{\Phi_i}\Big[\prod_{x\in\Phi_i} F_{G_{i,\max}}\Big(\frac{\|x\|^\alpha t}{P_i}\Big)\Big] \\ &\overset{(a)}{=} \prod_{i\in\mathbb{K}} \Big[\exp\Big(-\int_{\mathbb{R}^2} \big(1 - F_{G_{i,\max}}(\frac{\|x\|^\alpha t}{P_i})\big)\Lambda_i(\mathrm{d}x)\Big)\Big] \\ &\overset{(b)}{=} \prod_{i\in\mathbb{K}} \Big[\exp\Big(-2\pi\lambda_i \int_0^\infty \big(1 - F_{G_{i,\max}}(\frac{r^\alpha t}{P_i})\big) r\mathrm{d}r\Big)\Big], \end{aligned} \tag{A.2}$$

in which step (a) follows the result of PPP's PGFL provided in (2.12), and $\Lambda_i(\mathrm{d}x)$ represents the intensity measure of PPP Φ_i. Because of the assumption that Φ_i is homogeneous distributed, we can have $\Lambda_i(\mathrm{d}x) = \lambda \mathrm{d}x$, which completes the proof in step (b).

A.2 Proof of Theorem 2.2

The probability of coverage in a K-tier HetNet with directional antennas can be derived as

$$\begin{aligned}
p_c(T) &= \mathbb{P}[\mathrm{SINR} > T] \\
&= \int_{t>0} \mathbb{P}[\mathrm{SINR} > T \mid P_{LT,\max} = t] f_{P_{LT,\max}}(t)\mathrm{d}t \\
&= \int_{t>0} \mathbb{P}\Big[\frac{P_\omega G_{\omega,\max}\big(\tau_1(\varphi)\big) h \|\varphi\|^{-\alpha}}{I+\sigma^2} > T \mid P_{LT,\max} = t\Big] f_{P_{LT,\max}}(t)\mathrm{d}t \\
&\overset{(a)}{=} \int_{t>0} \mathbb{P}\Big[h > T(I+\sigma^2)/t \mid P_{LT,\max} = t\Big] f_{P_{LT,\max}}(t)\mathrm{d}t \\
&\overset{(b)}{=} \int_{t>0} \exp(-\frac{T\sigma^2}{t}) \mathcal{L}_I(\frac{T}{t} \mid P_{LT,\max} = t) f_{P_{LT,\max}}(t)\mathrm{d}t,
\end{aligned} \tag{A.3}$$

where step (a) is derived according to the definition of the random variable $P_{LT,\max}$ in (2.19), and step (b) follows from the Rayleigh fading assumption, i.e., $h \sim \exp(1)$. The expression $\mathcal{L}_I(\cdot \mid P_{LT,\max})$ is the Laplace transform of random variable I, the cumulative interference, provided that the maximum long-term received power from all BSs is $P_{LT,\max}$. Using the definition of the Laplace transform we can obtain

$$\begin{aligned}
&\mathcal{L}_I(s|P_{LT,\max}) = \mathbb{E}_I\big[\exp(-sI) \mid P_{LT,\max}\big] \\
&\overset{(a)}{=} \prod_{i\in\mathbb{K}} \mathbb{E}_{\Phi_i}\Bigg[\prod_{\substack{x\in\Phi_i\setminus\{\varphi\} \\ P_i G_{i,\max}(\tau_1(x))\|x\|^{-\alpha} < P_{LT,\max}}} \mathbb{E}_{h_x,\tau_{f_s}(x)}\Big[\exp\big(-sP_iG_i\big(\tau_{f_s}(x)\big)\cdot h_x\|x\|^{-\alpha}\big)\Big]\Bigg] \\
&\overset{(b)}{=} \prod_{i\in\mathbb{K}} \exp\Big(-\int_0^{2\pi} 2\pi \int_{\left(\frac{P_iG_{i,\max}(\theta)}{P_{LT,\max}}\right)^{\frac{1}{\alpha}}}^{\infty} \big(1-\mathcal{L}_{h_x}(sP_iG_i(\theta)v^{-\alpha})\big) v\mathrm{d}v\lambda_i\frac{\mathrm{d}\theta}{2\pi}\Big) \\
&\overset{(c)}{=} \prod_{i\in\mathbb{K}} \exp\Big(-\lambda_i\int_0^{2\pi} \int_{\left(\frac{P_iG_{i,\max}(\theta)}{P_{LT,\max}}\right)^{\frac{1}{\alpha}}}^{\infty} \big(1-\frac{1}{1+sP_iG_i(\theta)v^{-\alpha}}\big) v\mathrm{d}v\mathrm{d}\theta\Big),
\end{aligned} \tag{A.4}$$

in which step (a) can be derived because the independence among $\{h_x : x \in \Phi_i\}$ and their further independence from the point processes $\{\Phi_i : i \in \mathbb{K}\}$. Because of the independence between h_x and $\tau_{f_s}(x)$, and the fact that $\tau_{f_s}(x)$ can be regarded as a random variable uniformly distributed over $[0, 2\pi)$, the integrand in step (b) can be derived by following the result of the PGFL of a thinned PPP with density $\lambda_i \mathrm{d}\theta/(2\pi)$. The integration limit is from $(P_i G_{i,\max}(\theta)/P_{LT,\max})^{\frac{1}{\alpha}}$ to ∞ in step (b), because all interfering BSs' long-term received powers (including all their sectors) should be positive and not greater than $P_{LT,\max}$, i.e., $P_i G_{i,\max}(\theta) v^{-\alpha} \leqslant P_{LT,\max}$, thus giving $v \in [(P_i G_{i,\max}(\theta)/P_{LT,\max})^{1/\alpha}, \infty)$. Because of the Rayleigh fading assumption, that is, $h_x \sim \exp(1)$, step (c) can be obtained.

By plugging in $s = \frac{T}{t}$ and applying the condition of $P_{LT,\max} = t$, we can have

$$\begin{aligned}
&\mathcal{L}_I(\frac{T}{t} \mid P_{LT,\max} = t) \\
&\quad = \prod_{i\in\mathbb{K}} \exp\Big(- \lambda_i \int_0^{2\pi} \int_{\left(\frac{P_i G_{i,\max}(\theta)}{t}\right)^{\frac{1}{\alpha}}}^{\infty} \big(1 - \frac{1}{1 + \frac{T}{t} P_i G_i(\theta) v^{-\alpha}}\big) v \mathrm{d}v \mathrm{d}\theta \Big) \\
&\quad = \prod_{i\in\mathbb{K}} \exp\Big(- \frac{\lambda_i}{2} \big(\frac{P_i}{t}\big)^{\frac{2}{\alpha}} \int_0^{2\pi} \big(G_{i,\max}(\theta)\big)^{\frac{2}{\alpha}} \rho\Big(\frac{T G_i(\theta)}{G_{i,\max}(\theta)}, \alpha\Big) \mathrm{d}\theta \Big), \qquad \text{(A.5)}
\end{aligned}$$

in which $\rho(T_i, \alpha)$ can be expressed as equation (2.13) and the integral in the last step can be viewed as a property of the i-th tier. By defining this integral as $M_i(T, \alpha)$ in (2.25), we can obtain

$$\begin{aligned}
\mathcal{L}_I(\frac{T}{t} \mid P_{LT,\max} = t) &= \prod_{i\in\mathbb{K}} \exp\Big(- \frac{\lambda_i}{2} \big(\frac{P_i}{t}\big)^{\frac{2}{\alpha}} M_i(T, \alpha) \Big) \\
&= \exp\Big(- \frac{1}{2t^{2/\alpha}} \sum_{i\in\mathbb{K}} \lambda_i P_i^{2/\alpha} M_i(T, \alpha) \Big). \qquad \text{(A.6)}
\end{aligned}$$

Substituting (A.6) and the PDF $f_{P_{LT,\max}}(t)$ (given from numerical derivative of $F_{P_{LT,\max}}(t)$ in (2.20)) into (A.3) completes the proof.

Appendix B

B.1 Proof of Lemma 3.2

Since the event of $X_1 \leqslant x$ is the event of $R_1 \leqslant x$ based on the condition that the user is associated with macrocell, the CDF of X_1 for the outer region typical user is

$$\begin{aligned}
&F_{X_1|o\in A_{outer}}(x)\\
&\quad= \mathbb{P}[X_1 \leqslant x \mid o \in A_{outer}]\\
&\quad= \mathbb{P}[R_1 \leqslant x \mid \omega = 1, o \in A_{outer}]\\
&\quad= \mathbb{P}[R_1 \leqslant x \mid R_1 < \big(\frac{P_1}{P_2}\big)^{1/\alpha} R_2, R_1 > D]\\
&\quad\overset{(a)}{=} \frac{\mathbb{P}[R_1 \leqslant x, R_1 < \big(\frac{P_1}{P_2}\big)^{1/\alpha} R_2 \mid R_1 > D] \cdot \mathbb{P}[R_1 > D]}{\mathbb{P}[R_1 < \big(\frac{P_1}{P_2}\big)^{1/\alpha} R_2, R_1 > D]}, \quad \text{for } x > D, \qquad \text{(B.1)}
\end{aligned}$$

in which step (a) follows Bayes' theorem. The denominator of (B.1) can be derived as

$$\begin{aligned}
&\mathbb{P}[R_1 < \big(\frac{P_1}{P_2}\big)^{1/\alpha} R_2, R_1 > D]\\
&\quad= \int_{D(\frac{P_2}{P_1})^{1/\alpha}}^{\infty} \mathbb{P}[D < R_1 < \big(\frac{P_1}{P_2}\big)^{1/\alpha} r] f_{R_2}(r) \mathrm{d}r\\
&\quad\overset{(b)}{\approx} \int_{D(\frac{P_2}{P_1})^{1/\alpha}}^{\infty} \big[\exp(-\pi\lambda_1 D^2) - \exp(-\pi\lambda_1 \big(\frac{P_1}{P_2}\big)^{2/\alpha} r^2)\big] 2\pi\lambda_2 r \exp(-\pi\lambda_2 r^2) \mathrm{d}r\\
&\quad= \frac{\lambda_1}{\lambda_1 + \lambda_2 \big(\frac{P_2}{P_1}\big)^{2/\alpha}} \cdot \exp\big(-\pi[\lambda_1 + \lambda_2 \big(\frac{P_2}{P_1}\big)^{2/\alpha}] D^2\big), \qquad \text{(B.2)}
\end{aligned}$$

where we approximate the density of femtocell BSs in the vicinity of the outer region typical user as λ_2, and follow the PPP's void probability in step (b). This approximation is accurate as long as the typical user is not located close to the boundary between the inner and outer regions. Based upon the same approximation, the former part of (B.1)'s numerator is derived as

$$\begin{aligned}
&\mathbb{P}[R_1 \leqslant x, R_1 < \big(\frac{P_1}{P_2}\big)^{1/\alpha} R_2 \mid R_1 > D] \\
&\quad = \int_D^x \mathbb{P}[R_2 > \big(\frac{P_2}{P_1}\big)^{1/\alpha} r] f_{R_1|R_1>D}(r)\mathrm{d}r \\
&\quad \approx \int_D^x \exp(-\pi\lambda_2\big(\frac{P_2}{P_1}\big)^{2/\alpha} r^2) \cdot \frac{2\pi\lambda_1 r \exp(-\pi\lambda_1 r^2)}{\exp(-\pi\lambda_1 D^2)}\mathrm{d}r \\
&\quad = \frac{\lambda_1}{\lambda_1 + \lambda_2\big(\frac{P_2}{P_1}\big)^{2/\alpha}} \cdot \frac{1}{\exp(-\pi\lambda_1 D^2)} \cdot \Big[\exp\big(-\pi[\lambda_1 + \lambda_2\big(\frac{P_2}{P_1}\big)^{2/\alpha}]D^2\big) \\
&\qquad\qquad - \exp\big(-\pi[\lambda_1 + \lambda_2\big(\frac{P_2}{P_1}\big)^{2/\alpha}]x^2\big)\Big], \qquad \text{(B.3)}
\end{aligned}$$

in which similar techniques are applied as we derive (B.2).

By substituting (B.2) and (B.3) into (B.1) and differentiating the resultant CDF, we can reach X_1's PDF in (3.19), which completes the proof.

B.2 Proof of Lemma 3.3

Since the event of $X_2 \leqslant x$ is the event of $R_2 \leqslant x$ based on the condition that the user is associated with femtocell, the CDF of X_2 for the outer region typical user can be derived as

$$\begin{aligned}
&F_{X_2|o\in A_{outer}}(x) \\
&\quad = \mathbb{P}[X_2 \leqslant x \mid o \in A_{outer}] \\
&\quad = \mathbb{P}[R_2 \leqslant x \mid \omega = 2, o \in A_{outer}] \\
&\quad \overset{(a)}{=} \mathbb{P}[R_2 \leqslant x \mid R_2 < \big(\frac{P_2}{P_1}\big)^{1/\alpha} R_1, R_1 > D] \\
&\quad \overset{(b)}{=} \frac{\mathbb{P}[R_2 \leqslant x, R_2 < \big(\frac{P_2}{P_1}\big)^{1/\alpha} R_1 \mid R_1 > D] \cdot \mathbb{P}[R_1 > D]}{\mathbb{P}[R_2 < \big(\frac{P_2}{P_1}\big)^{1/\alpha} R_1, R_1 > D]}, \quad \text{for } x > D, \qquad \text{(B.4)}
\end{aligned}$$

where $R_2 < \big(P_2/P_1\big)^{1/\alpha} R_1$ in step (a) is the condition to make the typical user associate with the femtocell tier, and step (b) follows Bayes' theorem. The former

part of (B.4)'s numerator is expressed as

$$\begin{aligned}
&\mathbb{P}[R_2 \leqslant x, R_2 < \big(\frac{P_2}{P_1}\big)^{1/\alpha} R_1 \mid R_1 > D] \\
= &\begin{cases} \mathbb{P}[R_2 \leqslant x] & \text{for } x \leqslant \big(\frac{P_2}{P_1}\big)^{1/\alpha} D \\ \int_D^\infty \mathbb{P}[R_2 \leqslant x, R_2 < \big(\frac{P_2}{P_1}\big)^{1/\alpha} r] f_{R_1|R_1>D}(r)\mathrm{d}r & \text{for } x > \big(\frac{P_2}{P_1}\big)^{1/\alpha} D, \end{cases}
\end{aligned} \tag{B.5}$$

in which the requirement of $R_2 < \big(\frac{P_2}{P_1}\big)^{1/\alpha} R_1$ can be naturally satisfied if $x \leqslant \big(\frac{P_2}{P_1}\big)^{1/\alpha} D$. The integration in the above equation under the condition of $x > (P_2/P_1)^{1/\alpha} D$ can be derived as

$$\begin{aligned}
&\int_D^\infty \mathbb{P}[R_2 \leqslant x, R_2 < \big(\frac{P_2}{P_1}\big)^{1/\alpha} r] f_{R_1|R_1>D}(r)\mathrm{d}r \\
&= \int_{x(\frac{P_1}{P_2})^{1/\alpha}}^\infty \mathbb{P}[R_2 < x] \cdot \frac{2\pi\lambda_1 r \exp(-\pi\lambda_1 r^2)}{\exp(-\pi\lambda_1 D^2)}\mathrm{d}r \\
&\quad + \int_D^{x(\frac{P_1}{P_2})^{1/\alpha}} \mathbb{P}[R_2 < \big(\frac{P_2}{P_1}\big)^{1/\alpha} r] \cdot \frac{2\pi\lambda_1 r \exp(-\pi\lambda_1 r^2)}{\exp(-\pi\lambda_1 D^2)}\mathrm{d}r \\
&\overset{(c)}{\approx} \int_{x(\frac{P_1}{P_2})^{1/\alpha}}^\infty \big[1 - \exp(-\pi\lambda_2 x^2)\big] \cdot \frac{2\pi\lambda_1 r \exp(-\pi\lambda_1 r^2)}{\exp(-\pi\lambda_1 D^2)}\mathrm{d}r \\
&\quad + \int_D^{x(\frac{P_1}{P_2})^{1/\alpha}} \big[1 - \exp(-\pi\lambda_2 \big(\frac{P_2}{P_1}\big)^{2/\alpha} r^2)\big] \cdot \frac{2\pi\lambda_1 r \exp(-\pi\lambda_1 r^2)}{\exp(-\pi\lambda_1 D^2)}\mathrm{d}r \\
&= 1 - \frac{1}{\exp(-\pi\lambda_1 D^2)} \cdot \frac{\lambda_1}{\lambda_1 + \lambda_2 \big(\frac{P_2}{P_1}\big)^{2/\alpha}} \exp\big(-\pi[\lambda_1 + \lambda_2 \big(\frac{P_2}{P_1}\big)^{2/\alpha}] D^2\big) \\
&\quad - \frac{1}{\exp(-\pi\lambda_1 D^2)} \cdot \frac{\lambda_2 \big(\frac{P_2}{P_1}\big)^{2/\alpha}}{\lambda_1 + \lambda_2 \big(\frac{P_2}{P_1}\big)^{2/\alpha}} \exp\big(-\pi[\lambda_1 \big(\frac{P_1}{P_2}\big)^{2/\alpha} + \lambda_2] x^2\big),
\end{aligned} \tag{B.6}$$

in which step (c) is approximated by assuming that the density of femtocell BSs in the vicinity of the outer region typical user is λ_2, similar to the proof in Appendix B.1. The same approximation will help us to derive the denominator

of (B.4), i.e.,

$$\begin{aligned}
&\mathbb{P}[R_2 < \big(\frac{P_2}{P_1}\big)^{1/\alpha} R_1, R_1 > D] \\
&= \int_D^\infty \mathbb{P}[R_2 < \big(\frac{P_2}{P_1}\big)^{1/\alpha} r] \cdot 2\pi\lambda_1 r \exp(-\pi\lambda_1 r^2) \mathrm{d}r \\
&\approx \int_D^\infty \big[1 - \exp(-\pi\lambda_2 \big(\frac{P_2}{P_1}\big)^{2/\alpha} r^2)\big] \cdot 2\pi\lambda_1 r \exp(-\pi\lambda_1 r^2) \mathrm{d}r \\
&= \exp(-\pi\lambda_1 D^2) - \frac{\lambda_1}{\lambda_1 + \lambda_2 \big(\frac{P_2}{P_1}\big)^{2/\alpha}} \cdot \exp\big(-\pi[\lambda_1 + \lambda_2 \big(\frac{P_2}{P_1}\big)^{2/\alpha}] D^2\big). \qquad \text{(B.7)}
\end{aligned}$$

By substituting (B.7), (B.5) and (B.6) into (B.4) and differentiating the resultant CDF, X_2's PDF in (3.20) can be obtained and the proof is completed.

B.3 Proof of Lemma 3.6

Similar to the method used in [46], we use the Voronoi cell area formed by a homogeneous PPP with certain density values to approximate the area of the macrocells and femtocells. The area of the macrocell tier tier cells can be approximated by

$$\mathcal{C}_1 \approx \mathcal{C}_0 \big(\frac{\lambda_1}{\mathcal{Q}_1}\big). \qquad \text{(B.8)}$$

On the other hand, the femtocell-deployed region A_{outer} is the area where femtocell BSs are deployed with the density λ_2. Hence, the area of cells formed by the femtocell tier can be similarly approximated by

$$\mathcal{C}_2 \approx \mathcal{C}_0 \big(\frac{\lambda_2}{\mathcal{Q}_{2,outer}}\big). \qquad \text{(B.9)}$$

Similar to the analysis in Section 3.3, the probabilities of i-th tier cells with no user associated are $\mathbb{P}[N_{i,c} = 0]$, in which $N_{i,c}$ is the number of users in a randomly chosen i-th tier cell,

$$\mathbb{P}[N_{1,c} = n] \approx \frac{b^q}{n!} \cdot \frac{\Gamma(n+q)}{\Gamma(q)} \cdot \frac{(\lambda_{MS})^n (\lambda_1/\mathcal{Q}_1)^q}{(\lambda_{MS} + b\lambda_1/\mathcal{Q}_1)^{n+q}}, \quad \text{for } n \in \{0, 1, 2, ...\}, \qquad \text{(B.10)}$$

and

$$\mathbb{P}[N_{2,c}=n] \approx \frac{b^q}{n!}\cdot\frac{\Gamma(n+q)}{\Gamma(q)}\cdot\frac{(\lambda_{MS})^n(\lambda_2/\mathcal{Q}_{2,outer})^q}{(\lambda_{MS}+b\lambda_2/\mathcal{Q}_{2,outer})^{n+q}}, \quad \text{for } n\in\{0,1,2,...\}. \tag{B.11}$$

Consequently, the average density can be obtained by $\lambda_1' = \lambda_i\cdot(1-\mathbb{P}[N_{i,c}=0])$, which completes the proof.

B.4 Proof of Theorem 3.7

By assuming that the typical user located in the inner region A_{inner} always gets service from macrocell BSs, its coverage probability can be derived as

$$\begin{aligned} p_{c,A_{inner}}(T) &\approx p_{c,1,A_{inner}}(T) \\ &= \mathbb{P}[\mathrm{SINR}_1 > T \mid o\in A_{inner}] \\ &= \int_0^D \mathbb{P}[\mathrm{SINR}_1 > T \mid X_1=x, o\in A_{inner}] f_{X_1|o\in A_{inner}}(x)\mathrm{d}x \\ &\overset{(a)}{=} \int_0^D \exp\big(-\frac{T\sigma^2x^\alpha}{P_1}\big)\prod_{i=1}^{2}\mathcal{L}_{I_i|X_1=x,o\in A_{inner}}\big(\frac{Tx^\alpha}{P_1}\big) f_{X_1|o\in A_{inner}}(x)\mathrm{d}x, \end{aligned} \tag{B.12}$$

where step (a) comes from the Rayleigh fading assumption, and the expression $\mathcal{L}_{I_i|X_1=x,o\in A_{inner}}(\cdot)$ is the Laplace transform of random variable I_i given the condition that the typical user x away from the macrocell serving BS is located in the inner region A_{inner}. Similar to the process to derive the corresponding Laplace transform in Section 2.2.2, we can have

$$\begin{aligned} \prod_{i=1}^{2}\mathcal{L}_{I_i|X_1=x,o\in A_{inner}}\big(\frac{Tx^\alpha}{P_1}\big) \approx \exp\big(-\pi\lambda_1'\rho(T,\alpha)x^2\big) \\ \cdot\exp\big(-\pi\lambda_2' D^2\rho(\frac{P_2Tx^\alpha}{P_1D^\alpha},\alpha)\big). \end{aligned} \tag{B.13}$$

Here we assume the femtocell interference comes from the whole region out of the area $B(o,D)$, which is an optimistic estimation (proved to be accurate by the numerical results).

By substituting the PDF of X_1 conditioned on that the typical user is in the

inner region provided in Lemma (3.1) and the result in (B.13) into (B.12), we can obtain

$$p_{c,A_{inner}}(T) \approx \frac{2\pi\lambda_1}{[1-\exp(-\pi\lambda_1 D^2)]}\int_0^D \exp\big(-\frac{T\sigma^2 x^\alpha}{P_1}\big) \exp\Big(-\pi\big[\lambda_1+\lambda_1'\rho(T,\alpha)\big]x^2\Big)\exp\Big(-\pi\lambda_2' D^2\rho\big(\frac{P_2 T x^\alpha}{P_1 D^\alpha},\alpha\big)\Big)x\mathrm{d}x, \quad \text{(B.14)}$$

which completes the proof.

B.5 Proof of Theorem 3.8

For the outer region typical user served by the macrocell tier, its coverage probability can be expressed as

$$\begin{aligned} p_{c,1,A_{outer}}(T) &= \mathbb{P}[\mathrm{SINR}_1 > T \mid o \in A_{outer}] \\ &= \int_D^\infty \mathbb{P}[\mathrm{SINR}_1 > T \mid X_1 = x, o \in A_{outer}] f_{X_1|o\in A_{outer}}(x)\mathrm{d}x \\ &\overset{(a)}{=} \int_D^\infty \exp\big(-\frac{T\sigma^2 x^\alpha}{P_1}\big)\prod_{i=1}^{2}\mathcal{L}_{I_i|X_1=x,o\in A_{outer}}\big(\frac{Tx^\alpha}{P_1}\big) f_{X_1|o\in A_{outer}}(x)\mathrm{d}x, \end{aligned} \quad \text{(B.15)}$$

where step (a) still follows from the Rayleigh fading assumption, and the expression $\mathcal{L}_{I_i|X_j=x,o\in A_{outer}}(\cdot)$ is the Laplace transform of random variable I_i given the condition that the typical user x away from the macrocell serving BS is located in the outer region A_{outer}. Assuming the interference from femtocell BSs comes from the whole plane, we can approximate this Laplace transform as

$$\mathcal{L}_{I_i|X_1=x,o\in A_{outer}}\big(\frac{Tx^\alpha}{P_1}\big) \approx \exp\big(-\pi x^2\rho(T,\alpha)\mathbb{E}[\lambda_i']\big(\frac{P_i}{P_1}\big)^{2/\alpha}\big). \quad \text{(B.16)}$$

It is a pessimistic assumption since the original femtocell interference from inner area is eliminated due to this non-uniform deployment scheme, and the numerical results in Section 3.5 show that it is still a reasonably accurate approximation.

By substituting the PDF of X_1 conditioned on that the typical user is in the outer region provided in Lemma 3.2, and the result in (B.16) into (B.15), we can

have

$$
\begin{aligned}
&p_{c,1,A_{outer}}(T) \\
&\approx \int_D^{\infty} \exp\big(-\frac{T\sigma^2 x^{\alpha}}{P_1}\big)\exp\big(-\pi x^2\rho(T,\alpha)[\lambda_1' + \lambda_2'\big(\frac{P_2}{P_1}\big)^{2/\alpha}]\big) \\
&\qquad\qquad \cdot \frac{2\pi[\lambda_1 + \lambda_2\big(\frac{P_2}{P_1}\big)^{2/\alpha}]x \cdot \exp\big(-\pi[\lambda_1 + \lambda_2\big(\frac{P_2}{P_1}\big)^{2/\alpha}]x^2\big)}{\exp\big(-\pi[\lambda_1 + \lambda_2\big(\frac{P_2}{P_1}\big)^{2/\alpha}]D^2\big)}\mathrm{d}x \\
&= \frac{2\pi[\lambda_1 + \lambda_2\big(\frac{P_2}{P_1}\big)^{2/\alpha}]}{\exp\big(-\pi[\lambda_1 + \lambda_2\big(\frac{P_2}{P_1}\big)^{2/\alpha}]D^2\big)}\int_D^{\infty}\exp\big(-\frac{T\sigma^2 x^{\alpha}}{P_1}\big) \\
&\qquad\qquad \cdot \exp\Big(-\pi\big[\big(\lambda_1 + \lambda_2\big(\frac{P_2}{P_1}\big)^{2/\alpha}\big) + \rho(T,\alpha)\big(\lambda_1' + \lambda_2'\big(\frac{P_2}{P_1}\big)^{2/\alpha}\big)\big]x^2\Big)x\mathrm{d}x,
\end{aligned}
\tag{B.17}
$$

which completes the proof for the result in (3.31).

If the outer region typical user is served by the femtocell tier, its coverage probability can be given as

$$
\begin{aligned}
p_{c,2,A_{outer}}(T) &= \mathbb{P}[\mathrm{SINR}_2 > T \mid o \in A_{outer}] \\
&= \int_0^{\infty} \mathbb{P}[\mathrm{SINR}_2 > T \mid X_2 = x, o \in A_{outer}] f_{X_2|o\in A_{outer}}(x)\mathrm{d}x \\
&\overset{(a)}{=} \int_0^{\infty} \exp\big(-\frac{T\sigma^2 x^{\alpha}}{P_2}\big)\prod_{i=1}^{2}\mathcal{L}_{I_i|X_2=x,o\in A_{outer}}\big(\frac{Tx^{\alpha}}{P_2}\big) f_{X_2|o\in A_{outer}}(x)\mathrm{d}x,
\end{aligned}
\tag{B.18}
$$

where step (a) follows from the Rayleigh fading assumption. The Laplace transform of random variable I_2 provided that the typical user x away from the femtocell serving BS is located in the outer region A_{outer}, is

$$
\mathcal{L}_{I_2|X_2=x,o\in A_{outer}}\big(\frac{Tx^{\alpha}}{P_2}\big) \approx \exp\big(-\pi\lambda_2'\rho(T,\alpha)x^2\big), \tag{B.19}
$$

and the counterpart for the random variable I_1 can be derived as

$$\begin{aligned}
&\mathcal{L}_{I_1|X_2=x,o\in A_{outer}}\big(\frac{Tx^{\alpha}}{P_2}\big) \\
&= \begin{cases} \exp\Big(-2\pi\lambda_1' \int_D^{\infty} \big(1-\frac{1}{1+x^{\alpha}(\frac{P_1}{P_2})Ty^{-\alpha}}\big) y\mathrm{d}y\Big) & \text{for } x \leqslant \big(\frac{P_2}{P_1}\big)^{1/\alpha} D \\ \exp\Big(-2\pi\lambda_1' \int_{x(\frac{P_1}{P_2})^{\frac{1}{\alpha}}}^{\infty} \big(1-\frac{1}{1+x^{\alpha}(\frac{P_1}{P_2})Ty^{-\alpha}}\big) y\mathrm{d}y\Big) & \text{for } x > \big(\frac{P_2}{P_1}\big)^{1/\alpha} D \end{cases} \\
&= \begin{cases} \exp\Big(-\pi\lambda_1' D^2 \rho(\frac{P_1 T x^{\alpha}}{P_2 D^{\alpha}}, \alpha)\Big) & \text{for } x \leqslant \big(\frac{P_2}{P_1}\big)^{1/\alpha} D \\ \exp\Big(-\pi\lambda_1' (\frac{P_1}{P_2})^{2/\alpha} \rho(T,\alpha) x^2\Big) & \text{for } x > \big(\frac{P_2}{P_1}\big)^{1/\alpha} D. \end{cases}
\end{aligned} \tag{B.20}$$

Subsequently, we can substitute (B.19), (B.20) and the PDF of X_2, conditioned on that the typical user is in the outer region provided in Lemma 3.3, into (B.18). Consequentially, we can obtain the expression of the coverage probability in (3.32).

By combining the results in (3.31) and (3.32), we can reach the coverage performance for a randomly chosen outer region typical user, provided by (3.30). Till here, we complete the proof.

B.6 Proof of Theorem 3.10

The CCDF of the throughput achieved at the inner region typical user, $\mathbb{P}[\mathcal{R} > \rho \mid o \in A_{inner}]$, can be obtained by assuming that all inner region users are served by the macrocell tier, i.e.,

$$\begin{aligned}
&\mathbb{P}[\mathcal{R} > \rho \mid o \in A_{inner}] \\
&\quad \approx \mathbb{P}[\mathcal{R} > \rho \mid \omega = 1, o \in A_{inner}] \\
&\quad = \mathbb{P}\Big[\frac{W}{N_1+1}\log_2(1+\mathrm{SINR}_1) > \rho \mid o \in A_{inner}\Big] \\
&\quad = \mathbb{P}\big[\mathrm{SINR}_1 > 2^{(N_1+1)\rho/W} - 1 \mid o \in A_{inner}\big] \\
&\quad \overset{(a)}{\approx} \mathbb{E}_{N_1}\big[p_{c,A_{inner}}\big(2^{(N_1+1)\rho/W}-1\big)\big] \\
&\quad = \sum_{n=0}^{\infty} \mathbb{P}[N_1 = n] \cdot p_{c,A_{inner}}\big(2^{(n+1)\rho/W}-1\big),
\end{aligned} \tag{B.21}$$

where N_1 is the number of in-cell macrocell MSs sharing the resource with the typical user, and step (a) is approximated by assuming the total independence

between the distribution of SINR_1 and N_1. As indicated in Appendix B.3, the area of the macrocell tier tier cells can be approximated by $\mathcal{C}_1 \approx \mathcal{C}_0\big(\frac{\lambda_1}{\mathcal{Q}_1}\big)$, which helps us to reach the PMF of N_1 in (3.35).

B.7 Proof of Theorem 3.11

The CCDF of the throughput achieved at the outer region typical user, $\mathbb{P}[\mathcal{R} > \rho \mid o \in A_{outer}]$, can be provided by

$$\begin{aligned}
&\mathbb{P}[\mathcal{R} > \rho \mid o \in A_{outer}] \\
&= \sum_{i\in\{1,2\}} \mathbb{P}[\mathcal{R} > \rho \mid \omega = i, o \in A_{outer}] \cdot \mathbb{P}[\omega = i \mid o \in A_{outer}] \\
&= \sum_{i\in\{1,2\}} \mathbb{P}\Big[\frac{W}{N_i+1}\log_2(1+\mathrm{SINR}_i) > \rho \mid o \in A_{outer}\Big] \cdot \mathbb{P}[\omega = i \mid o \in A_{outer}] \\
&\overset{(a)}{\approx} \sum_{i\in\{1,2\}} \mathbb{E}_{N_i}\big[p_{c,i,A_{outer}}\big(2^{(N_i+1)\rho/W}-1\big)\big] \cdot \mathbb{P}[\omega = i \mid o \in A_{outer}] \\
&= \sum_{i\in\{1,2\}} \sum_{n=0}^{\infty} \mathbb{P}[N_i = n] \cdot p_{c,i,A_{outer}}\big(2^{(n+1)\rho/W}-1\big) \cdot \mathbb{P}[\omega = i \mid o \in A_{outer}], \quad \text{(B.22)}
\end{aligned}$$

where N_i is the number of in-cell MSs sharing the resource with the typical user served by the i-th tier, and step (a) is approximated by assuming the total independence between the distribution of SINR_i and N_i. As indicated in Appendix B.3, the area of the femtocell tier tier cells can be approximated by $\mathcal{C}_2 \approx \mathcal{C}_0\big(\frac{\lambda_2}{\mathcal{Q}_{2,outer}}\big)$, which helps us to reach the PMF of N_2 in (3.37).

Appendix C

C.1 Proof of Theorem 5.1

Here we use x_0 to denote the nearest BS from the origin, and we define r_u as the distance from the typical user to the nearest BS, namely, $r_u = \|x_0\|$. The PDF of r_u has been provided in [163], as

$$f_{r_u}(r) = 2\pi\lambda_{BS} r \exp(-\pi\lambda_{BS} r^2). \tag{C.1}$$

Due to the assumption that the serving BS knows all eavesdroppers' locations in this scenario, the most detrimental eavesdropper $e^*(x_0)$ for the BS at x_0 should be the nearest one from x_0, as given in (5.3). Therefore, the CCDF of the achievable secrecy rate $\hat{R}_s$ under this scenario can be derived as

$$\begin{aligned}
\bar{F}_{\hat{R}_s}(R_0) &= \mathbb{P}\Big(\|e^*(x_0) - x_0\| > \beta^{1/\alpha}\|x_0\|\Big) \\
&= \int_0^\infty \mathbb{P}\Big(\|e^*(x_0) - x_0\| > \beta^{1/\alpha} r_u \mid r_u = y\Big) f_{r_u}(y)\mathrm{d}y \\
&= \int_0^\infty \mathbb{P}\big[\text{No Eavesdropper in } \mathcal{B}(x_0, \beta^{1/\alpha} r_u) \mid r_u = y\big] f_{r_u}(y)\mathrm{d}y \\
&\overset{(a)}{=} \int_0^\infty \mathbb{P}\big[\text{No Eavesdropper in } \mathcal{B}(x_0, \beta^{1/\alpha} y)\big] f_{r_u}(y)\mathrm{d}y \\
&\overset{(b)}{=} \int_0^\infty \exp(-\pi\lambda_e \beta^{2/\alpha} y^2) \cdot 2\pi\lambda_{BS} y \exp(-\pi\lambda_{BS} y^2)\mathrm{d}y \\
&= \frac{1}{1 + \frac{\lambda_e}{\lambda_{BS}} \cdot 2^{(2R_0)/\alpha}},
\end{aligned} \tag{C.2}$$

where step (a) is derived based on the independence between Φ_e and Φ_{BS}, and step (b) follows the PPP's void probability and PDF of r_u given in (C.1). Through the deduction above, the CCDF expression of the achievable secrecy rate can be

obtained.

C.2 Proof of Theorem 5.3

For a given BS (not necessarily the nearest BS) located at the position of x, its achievable secrecy rate toward the origin's typical user is larger than R_0 if and only if there is no eavesdroppers located within $\mathcal{B}(x, 2^{(R_0/\alpha)}\|x\|)$. Hence, the achievable secrecy rate's CDF can be derived as

$$\begin{aligned}
F_{\hat{R}_s}(R_0) &= \mathbb{P}(\hat{R}_s \leqslant R_0) \\
&= \mathbb{P}\big[\text{All BSs cannot provide secrecy rate larger than } R_0\big] \\
&= \mathbb{E}_{\Phi_e}\Bigg[\mathbb{E}_{\Phi_{BS}}\Big[\prod_{x\in\phi_{BS}} \mathbf{1}\big(\Phi_e \bigcap \mathcal{B}(x, 2^{\frac{R_0}{\alpha}}\|x\|) \neq 0\big)\Big]\Bigg] \\
&= \mathbb{E}_{\Phi_e}\Bigg[\mathbb{E}_{\Phi_{BS}}\Big[\prod_{x\in\phi_{BS}} \Big[1 - \mathbf{1}\big(\Phi_e \bigcap \mathcal{B}(x, 2^{\frac{R_0}{\alpha}}\|x\|) = 0\big)\Big]\Big]\Bigg] \\
&\overset{(a)}{=} \mathbb{E}_{\Phi_e}\Bigg[\exp\Big[-\lambda_{BS}\int_{\mathbb{R}^2} \mathbf{1}\big(\Phi_e \bigcap \mathcal{B}(x, 2^{\frac{R_0}{\alpha}}\|x\|) = 0\big)\mathrm{d}x\Big]\Bigg] \\
&\geqslant \exp\Bigg[-\lambda_{BS}\int_{\mathbb{R}^2} \mathbb{P}\Big[\Phi_e\big(\mathcal{B}(x, 2^{\frac{R_0}{\alpha}}\|x\|)\big) = 0\Big]\mathrm{d}x\Bigg], \qquad \text{(C.3)}
\end{aligned}$$

where $R_0 \geqslant 0$, step (a) follows from the PGFL of the PPP [98], and Jensen's inequality gives the lower bound for $F_{\hat{R}_s}(R_0)$ in the last step. The part in the integral can be derived by using homogeneous PPP's void probability [98], i.e., $\mathbb{P}\big[\Phi_e\left(\mathcal{B}(x, 2^{(R_0/\alpha)}\|x\|)\right) = 0\big] = \exp(-\pi\lambda_e 2^{(2R_0/\alpha)}\|x\|^2)$, which can be substituted into the integration in (C.3) to obtain the upper bound of the achievable secrecy rate's CCDF in (5.13) easily.

Next, we turn to find the lower bound for the CCDF of the achievable secrecy rate. Here we use $\hat{R}_{s,nearest}$ to denote the achievable secrecy rate where only the nearest BS is accessible, which has been studied in Scenario-I. Since connecting to the nearest BS is always one of the viable options if all BSs are reachable, we can have the usual stochastic order between $\hat{R}_{s,nearest}$ in Scenario-I and $\hat{R}_s$ in the current scenario, i.e., $\mathbb{P}(\hat{R}_{s,nearest} > R_0) \leqslant \mathbb{P}(\hat{R}_s > R_0)$, or equivalently, $\bar{F}_{\hat{R}_s}(R_0) \geqslant \bar{F}_{\hat{R}_{s,nearest}}(R_0)$. Therefore, the conclusion in Theorem 5.1 provides the lower bound in (5.14), which completes the proof.

C.3 Proof of Corollary 5.5

Based on the CCDF bounds given in Theorem 5.3, the upper and lower bound of the average secrecy rate achievable at the typical user can be obtained by integrating (5.13) and (5.14) from 0 to ∞. Specifically, the upper bound can be derived as

$$\begin{aligned}\mathbb{E}[\hat{R}_s] &\leqslant \int_0^{\infty}\Big[1-\exp\Big(-\frac{\lambda_{BS}}{\lambda_e 2^{(2t)/\alpha}}\Big)\Big]\mathrm{d}t \\ &\overset{(a)}{=} \frac{1}{\ln(2^{2/\alpha})}\int_0^{\frac{\lambda_{BS}}{\lambda_e}}\frac{1-\exp(-v)}{v}\mathrm{d}v, \end{aligned} \tag{C.4}$$

where step (a) is derived by employing a change of variables $v=\lambda_{BS}/(\lambda_e 2^{(2t)/\alpha})$. We use the Taylor series expansion of $\exp(-v)$, and the integrand in (C.4) becomes

$$\frac{1-\exp(-v)}{v}=\sum_{k=1}^{\infty}\frac{(-v)^{k-1}}{k!}. \tag{C.5}$$

By integrating both sides of the equation (C.5) and performing simple mathematical operations, we can obtain the relationship

$$\begin{aligned}\int_0^{\frac{\lambda_{BS}}{\lambda_e}}\frac{1-\exp(-v)}{v}\mathrm{d}v &= \int_0^{\frac{\lambda_{BS}}{\lambda_e}}\sum_{k=1}^{\infty}\frac{(-v)^{k-1}}{k!}\mathrm{d}v \\ &= \sum_{k=1}^{\infty}\int_0^{\frac{\lambda_{BS}}{\lambda_e}}\frac{(-v)^{k-1}}{k!}\mathrm{d}v \\ &= -\sum_{k=1}^{\infty}\frac{(-\frac{\lambda_{BS}}{\lambda_e})^{k}}{k\cdot k!}. \end{aligned} \tag{C.6}$$

When $x>0$, the exponential integral $E_1(x)$ can be expanded [164], i.e.,

$$E_1(x)=-\gamma-\ln(x)+\sum_{k=1}^{\infty}\frac{(-1)^{k+1}x^k}{k\cdot k!}. \tag{C.7}$$

Therefore, the above integral can be derived as

$$\int_0^{\frac{\lambda_{BS}}{\lambda_e}}\frac{1-\exp(-v)}{v}\mathrm{d}v = \gamma+\ln\big(\tfrac{\lambda_{BS}}{\lambda_e}\big)+E_1\big(\tfrac{\lambda_{BS}}{\lambda_e}\big). \tag{C.8}$$

Plugging (C.8) into (C.4) gives the upper bound of the average secrecy rate in (5.22).

On the other hand, following the same procedure as the one to prove Corollary 5.2, the lower bound of average secrecy rate can be obtained, which completes the proof.

C.4 Proof of Theorem 5.6

Based on the available intracell eavesdroppers' location information and the assumption that the typical user is served by the nearest BS at x_0, (5.7) becomes

$$\begin{aligned}
&\bar{F}_{\hat{R}_s}(R_0) \\
&= \mathbb{P}\Big(\|e^*(x_0) - x_0\| > \beta^{1/\alpha}\|x_0\|\Big) \\
&\overset{(a)}{=} \mathbb{P}\big[\text{No Eavesdropper in } \mathcal{B}(x_0, \beta^{\frac{1}{\alpha}} r_u); r_u < \beta^{-\frac{1}{\alpha}} D_{\min}\big] \\
&= \int_0^\infty \mathbb{P}\big[\text{No Eavesdropper in } \mathcal{B}(x_0, \beta^{\frac{1}{\alpha}} r_u); D_{\min} > \beta^{\frac{1}{\alpha}} r_u \mid r_u = y\big] f_{r_u}(y)\mathrm{d}y,
\end{aligned} \tag{C.9}$$

where step (a) is based on the fact that eavesdroppers are assumed to be lied in the cell boundaries for the worst case. The probability expression herein can be further derived as

$$\begin{aligned}
&\mathbb{P}\big[\text{No Eavesdropper in } \mathcal{B}(x_0, \beta^{\frac{1}{\alpha}} r_u); D_{\min} > \beta^{\frac{1}{\alpha}} r_u \mid r_u = y\big] \\
&\overset{(b)}{=} \mathbb{P}\big[\text{No Eavesdropper in } \mathcal{B}(x_0, \beta^{\frac{1}{\alpha}} y)\big] \cdot \mathbb{P}\big(D_{\min} > \beta^{\frac{1}{\alpha}} y \mid r_u = y\big) \\
&\geqslant \mathbb{P}\big[\text{No Eavesdropper in } \mathcal{B}(x_0, \beta^{\frac{1}{\alpha}} y)\big] \cdot \mathbb{P}\big(D_{\min} > \beta^{\frac{1}{\alpha}} y\big) \\
&= \exp\big(-\pi\lambda_e(\beta^{\frac{1}{\alpha}} y)^2\big) \int_{\beta^{\frac{1}{\alpha}} y}^\infty f_{D_{\min}}(z)\mathrm{d}z \\
&= \exp\big(-\pi(\lambda_e + 4\lambda_{BS})\beta^{\frac{2}{\alpha}} y^2\big),
\end{aligned} \tag{C.10}$$

where the independence between Φ_e and Φ_{BS} is used to separate the two probability expressions in step (b), and the former part is only dependent on the density of eavesdroppers λ_e and the ball's area $\pi\beta^{2/\alpha}y^2$, but independent of x_0. It should be noticed that the value of r_u has an impact on the distribution of D_{min}, and we need to use $f_{D_{\min}|r_u}(\cdot\,|\,\cdot)$ to derive $\mathbb{P}(D_{\min} > \beta^{\frac{1}{\alpha}} y \mid r_u = y)$ in step (b). Because the tractable result of $f_{D_{\min}|r_u}(\cdot\,|\,\cdot)$ is not available, we ob-

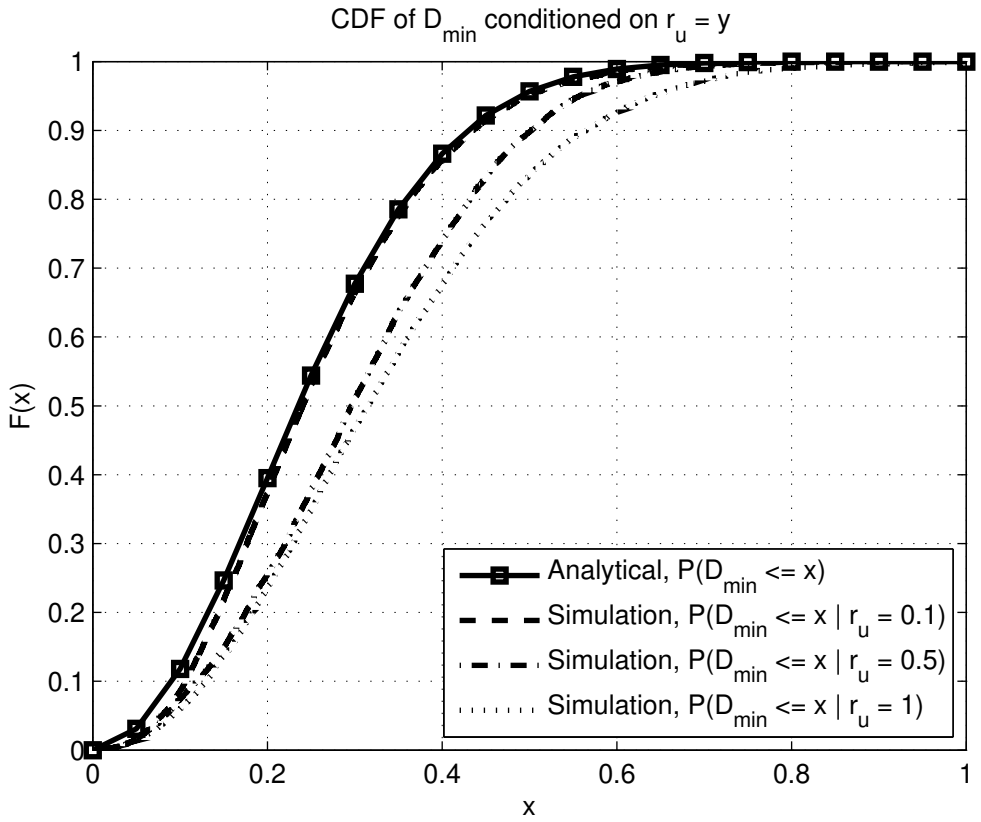

Figure C.1: The relationship between the conditional and unconditional $D_{\min}$.

tain a lower bound (also served as a tractable approximation) expression by ignoring the impact of r_u on the distribution of D_{min}, due to the fact that $\mathbb{P}(D_{\min} > x \mid r_u = y) \geqslant \mathbb{P}(D_{\min} > x)$. The fact is because the condition of a positive r_u leads to a larger $D_{\min}$, which can be demonstrated in the following Fig. C.1.

The lower bound by replacing distribution $f_{D_{min}}(\cdot)$ can provide a good approximation, which will be demonstrated by the numerical comparisons in Section 5.4.

By substituting (C.10) and the PDF of r_u given in (C.1) into (C.9), the lower bound expression (5.27) can be obtained, which completes the proof.

C.5 Proof of Theorem 5.8

Based on the available location information of eavesdroppers with distances less than D_0 and the typical user served by the nearest BS at x_0, (5.7) can be derived

as

$$\begin{aligned}
\bar{F}_{\hat{R}_s}(R_0) &= \mathbb{P}\Big(\|e^*(x_0)-x_0\| > \beta^{1/\alpha}\|x_0\|\Big) \\
&= \mathbb{P}\big[\text{No Eavesdropper in } \mathcal{B}(x_0, \beta^{\frac{1}{\alpha}} r_u); r_u < \beta^{-\frac{1}{\alpha}} D_0\big] \\
&= \int_0^{\beta^{-\frac{1}{\alpha}} D_0} \mathbb{P}\big[\text{No Eavesdropper in } \mathcal{B}(x_0, \beta^{\frac{1}{\alpha}} r_u) \mid r_u = y\big] f_{r_u}(y) \mathrm{d}y \\
&\overset{(a)}{=} \int_0^{\beta^{-\frac{1}{\alpha}} D_0} \mathbb{P}\big[\text{No Eavesdropper in } \mathcal{B}(x_0, \beta^{\frac{1}{\alpha}} y)\big] f_{r_u}(y) \mathrm{d}y \\
&\overset{(b)}{=} \int_0^{2^{-\frac{R_0}{\alpha}} D_0} 2\pi\lambda_{BS} y \cdot \exp(-\pi\lambda_e 2^{\frac{2R_0}{\alpha}} y^2 - \pi\lambda_{BS} y^2) \mathrm{d}y \\
&= \frac{1}{1+\frac{\lambda_e}{\lambda_{BS}} \cdot 2^{(2R_0)/\alpha}} \cdot \Big(1 - \exp\big[-\pi(\lambda_e + \lambda_{BS} 2^{-\frac{2R_0}{\alpha}}) {D_0}^2\big]\Big),
\end{aligned} \tag{C.11}$$

where step (a) follows the independence between Φ_e and Φ_{BS}, and step (b) is derived based on the void probability of PPP and the PDF of r_u. It should be noticed that the probability expression $\mathbb{P}\big[\text{No Eavesdropper in } \mathcal{B}(x_0, \beta^{\frac{1}{\alpha}} y)\big]$ is only dependent on the density of eavesdroppers λ_e and the ball's area $\pi\beta^{2/\alpha} y^2$, but independent of x_0. The integration from 0 to $2^{-\frac{R_0}{\alpha}} D_0$ gives the result which completes the proof.

C.6 Proof of Corollary 5.9

Based on the CCDF expression given in Theorem 5.8, the average secrecy rate achievable at the typical user can be provided by integrating (5.29) from 0 to ∞, i.e.,

$$\begin{aligned}
\mathbb{E}[\hat{R}_s] &= \int_0^{\infty} \frac{1}{1+\frac{\lambda_e}{\lambda_{BS}} \cdot 2^{(2t)/\alpha}} \cdot \Big(1 - \exp\big[-\pi(\lambda_e + \lambda_{BS} 2^{-\frac{2t}{\alpha}}) D_0^2\big]\Big) \mathrm{d}t \\
&= \int_0^{\infty} \frac{1}{1+\frac{\lambda_e}{\lambda_{BS}} \cdot 2^{(2t)/\alpha}} \mathrm{d}t - \int_0^{\infty} \frac{\exp\big[-\pi(\lambda_e + \lambda_{BS} 2^{-\frac{2t}{\alpha}}) D_0^2\big]}{1+\frac{\lambda_e}{\lambda_{BS}} \cdot 2^{(2t)/\alpha}} \mathrm{d}t \\
&\overset{(a)}{=} \frac{\alpha}{2\ln 2} \cdot \ln\Big(\frac{\lambda_{BS}+\lambda_e}{\lambda_e}\Big) - \\
&\qquad \exp(-\pi\lambda_e D_0^2) \int_0^{\infty} \frac{\exp\big[-\pi\lambda_{BS} D_0^2 \cdot 2^{-\frac{2t}{\alpha}}\big]}{1+\frac{\lambda_e}{\lambda_{BS}} \cdot 2^{(2t)/\alpha}} \mathrm{d}t,
\end{aligned} \tag{C.12}$$

where the deduction of the former part in step (a) utilizes the result solved in Corollary 5.2, and subsequently we will focus on the integral in its latter part, i.e.,

$$\begin{aligned}
&\exp(-\pi\lambda_e D_0^2)\int_0^{\infty}\frac{\exp\big[-\pi\lambda_{BS}D_0^2\cdot 2^{-\frac{2t}{\alpha}}\big]}{1+\frac{\lambda_e}{\lambda_{BS}}\cdot 2^{(2t)/\alpha}}\mathrm{d}t\\
&\overset{(b)}{=}\exp(-\pi\lambda_e D_0^2)\int_{\frac{\lambda_e}{\lambda_{BS}}}^{\infty}\frac{\exp(-\pi\lambda_e D_0^2 v^{-1})}{1+v}\cdot\frac{\alpha}{2v\ln 2}\mathrm{d}v\\
&\overset{(c)}{=}\frac{\alpha}{2\ln 2}\int_{\pi\lambda_e D_0^2}^{\pi(\lambda_{BS}+\lambda_e)D_0^2}\frac{1}{s\exp(s)}\mathrm{d}s\\
&=\frac{\alpha}{2\ln 2}\Big[E_1\big(\pi\lambda_e D_0^2\big)-E_1\big(\pi(\lambda_e+\lambda_{BS})D_0^2\big)\Big],
\end{aligned}\tag{C.13}$$

where step (b) and step (c) are obtained by employing changes of variables $v=\frac{\lambda_e}{\lambda_{BS}}\cdot 2^{(2t)/\alpha}$ and $s=\frac{\pi\lambda_e D_0^2}{v}+\pi\lambda_e D_0^2$, respectively, and the last step can be derived by using the definition of the exponential integral. Plugging (C.13) into (C.12) gives the desired result in (5.30), which completes the proof.

Bibliography

[1] J. Zhang and G. d. l. Roche, *Femtocells: Technologies and Deployment*. New York, NY: John Wiley & Sons Ltd., 2010.

[2] "The world in 2013: ICT facts and figures," *International Telecommunication Union (ITU)*, Feb. 2013.

[3] J. Zander and P. Mähönen, "Riding the data tsunami in the cloud: Myths and challenges in future wireless access," *IEEE Commun. Mag.*, vol. 51, no. 3, pp. 145–151, 2013.

[4] "Cisco visual networking index: Global mobile data traffic forecast update, 2012-2017," *Cisco Systems, Inc. White Paper*, Feb. 2013.

[5] "Ericsson mobility report: On the pulse of the networked society," *Ericsson White Paper*, Jun. 2013.

[6] E. Dahlman, S. Parkvall, J. Skold, and P. Beming, *3G Evolution: HSPA and LTE for Mobile Broadband*, 2nd ed. Burlington, MA: Academic Press, 2008.

[7] E. Dahlman, S. Parkvall, and J. Skold, *4G: LTE/LTE-Advanced for Mobile Broadband*. Burlington, MA: Academic Press, 2011.

[8] H. Holma and A. Toskala, *LTE-Advanced: 3GPP Solution for IMT-Advanced*. New York, NY: John Wiley & Sons Ltd., 2012.

[9] J. G. Andrews, A. Ghosh, and R. Muhamed, *Fundamentals of WiMAX: Understanding Broadband Wireless Networking*. Upper Saddle River, NJ: Pearson Education Inc., 2007.

[10] P. Mogensen, W. Na, I. Z. Kovacs, F. Frederiksen, A. Pokhariyal, K. I. Pedersen, T. Kolding, K. Hugl, and M. Kuusela, "LTE capacity compared

to the Shannon bound," in *Proc. IEEE 65th Vehic. Tech. Conf. (VTC'07-Spring)*, Dublin, Ireland, Sep. 2007, pp. 1234–1238.

[11] "LTE Advanced: Heterogeneous networks," *Qualcomm Inc. White Paper*, Jan. 2011.

[12] M. Roetter, "Spectrum for mobile broadband in the Americas: Policy issues for growth and competition," *GSM Association*, Jan. 2011.

[13] Z. Shen, A. Papasakellariou, J. Montojo, D. Gerstenberger, and F. Xu, "Overview of 3GPP LTE-Advanced carrier aggregation for 4G wireless communications," *IEEE Commun. Mag.*, vol. 50, no. 2, pp. 122–130, 2012.

[14] A. Ghosh, N. Mangalvedhe, R. Ratasuk, B. Mondal, M. Cudak, E. Visotsky, T. A. Thomas, J. G. Andrews, P. Xia, H.-S. Jo, H. S. Dhillon, and T. D. Novlan, "Heterogeneous cellular networks: From theory to practice," *IEEE Commun. Mag.*, vol. 50, no. 6, pp. 54–64, 2012.

[15] S. Landström, A. Furuskär, K. Johansson, L. Falconetti, and F. Kronestedt, "Heterogeneous networks - increasing cellular capacity," *Ericsson Review*, no. 1, pp. 1–6, 2011.

[16] L. Song and J. Shen, *Evolved Cellular Network Planning and Optimization for UMTS and LTE*. Boca Raton, FL: CRC Press, 2010.

[17] "Deployment strategies for heterogeneous networks," *Nokia Siemens Networks White Paper*, Jan. 2012.

[18] A. Goldsmith, *Wireless Communications*. New York, NY: Cambridge Univ. Press, 2005.

[19] M.-S. Alouini and A. J. Goldsmith, "Area spectral efficiency of cellular mobile radio systems," *IEEE Trans. Veh. Technol.*, vol. 48, no. 4, pp. 1047–1066, 1999.

[20] J. G. Andrews, "Seven ways that HetNets are a cellular paradigm shift," *IEEE Commun. Mag.*, vol. 51, no. 3, pp. 136–144, 2013.

[21] T. Nakamura, S. Nagata, A. Benjebbour, Y. Kishiyama, H. Tang, X. Shen, N. Yang, and N. Li, "Trends in small cell enhancements in LTE Advanced," *IEEE Commun. Mag.*, vol. 51, no. 2, pp. 98–105, 2013.

[22] S.-P. Yeh, S. Talwar, G. Wu, N. Himayat, and K. Johnsson, "Capacity and coverage enhancement in heterogeneous networks," *IEEE Wireless Commun.*, vol. 18, no. 3, pp. 32–38, 2011.

[23] W. Wang, X. Liu, J. Vicente, and P. Mohapatra, "Integration gain of heterogeneous WiFi/WiMAX networks," *IEEE Trans. Mobile Comput.*, vol. 10, no. 8, pp. 1131–1143, 2011.

[24] J. G. Andrews, H. Claussen, M. Dohler, S. Rangan, and M. C. Reed, "Femtocells: Past, present, and future," *IEEE J. Select. Areas Commun.*, vol. 30, no. 3, pp. 497–508, Apr. 2012.

[25] J. Sydir and R. Taori, "An evolved cellular system architecture incorporating relay stations," *IEEE Commun. Mag.*, vol. 47, no. 6, pp. 115–121, 2009.

[26] K. Loa, C.-C. Wu, S.-T. Sheu, Y. Yuan, M. Chion, D. Huo, and L. Xu, "IMT-Advanced relay standards," *IEEE Commun. Mag.*, vol. 48, no. 8, pp. 40–48, 2010.

[27] J. Zhang and J. G. Andrews, "Distributed antenna systems with randomness," *IEEE Trans. Wireless Commun.*, vol. 7, no. 9, pp. 3636–3646, Sep. 2008.

[28] "A comparison of LTE Advanced HetNets and Wi-Fi," *Qualcomm Inc. White Paper*, Oct. 2011.

[29] A. Ghosh, R. Ratasuk, B. Mondal, N. Mangalvedhe, and T. Thomas, "LTE-Advanced: Next-generation wireless broadband technology," *IEEE Wireless Commun.*, vol. 17, no. 3, pp. 10–22, 2010.

[30] A. Damnjanovic, J. Montojo, Y. Wei, T. Ji, T. Luo, M. Vajapeyam, T. Yoo, O. Song, and D. Malladi, "A survey on 3GPP heterogeneous networks," *IEEE Wireless Commun.*, vol. 18, no. 3, pp. 10–21, 2011.

[31] S. Brueck, "Heterogeneous networks in LTE-Advanced," in *Proc. 8th Int'l Symp. on Wireless Commun. Systems (ISWCS'11)*, Aachen, Germany, Nov. 2011, pp. 171–175.

[32] Y. Murata, M. Hasegawa, H. Murakami, H. Harada, and S. Kato, "The architecture and a business model for the open heterogeneous mobile network," *IEEE Commun. Mag.*, vol. 47, no. 5, pp. 95–101, 2009.

[33] I. Hwang, B. Song, and S. S. Soliman, "A holistic view on hyper-dense heterogeneous and small cell networks," *IEEE Commun. Mag.*, vol. 51, no. 6, pp. 20–21, 2013.

[34] S. S. Rappaport and L.-R. Hu, "Microcellular communication systems with hierarchical macrocell overlays: Traffic performance models and analysis," *Proceedings of the IEEE*, vol. 82, no. 9, pp. 1383–1397, 1994.

[35] X. Lagrange, "Multitier cell design," *IEEE Commun. Mag.*, vol. 35, no. 8, pp. 60–64, 1997.

[36] A. Ganz, C. M. Krishna, D. Tang, and Z. J. Haas, "On optimal design of multitier wireless cellular systems," *IEEE Commun. Mag.*, vol. 35, no. 2, pp. 88–93, 1997.

[37] D. Lopez-Perez, I. Guvenc, G. d. l. Roche, M. Kountouris, T. Q. S. Quek, and J. Zhang, "Enhanced intercell interference coordination challenges in heterogeneous networks," *IEEE Wireless Commun.*, vol. 18, no. 3, pp. 22–30, 2011.

[38] S. R. Saunders, S. Carlaw, A. Giustina, R. R. Bhat, V. S. Rao, and R. Siegberg, *Femtocells: Opportunities and Challenges for Business and Technology*. New York, NY: John Wiley & Sons Ltd., 2009.

[39] V. Chandrasekhar, J. G. Andrews, and A. Gatherer, "Femtocell networks: A survey," *IEEE Commun. Mag.*, vol. 46, no. 9, pp. 59–67, Sep. 2008.

[40] L. T. W. Ho and H. Claussen, "Effects of user-deployed, co-channel femtocells on the call drop probability in a residential scenario," in *Proc. IEEE 18th Int'l Symp. on Personal, Indoor and Mobile Radio Commun. (PIMRC'07)*, Athens, Greece, Sep. 2007, pp. 1–5.

[41] *Requirements for support of radio resource management (FDD)*, 3GPP Tech. Spec. 25.133, Rev. 8.20.0.

[42] *Scenarios and requirements for small cell enhancements for E-UTRA and E-UTRAN*, 3GPP Tech. Report 36.932, Rev. 12.1.0.

[43] J. G. Andrews, F. Baccelli, and R. K. Ganti, "A tractable approach to coverage and rate in cellular networks," *IEEE Trans. Commun.*, vol. 59, no. 11, pp. 3122–3134, Nov. 2011.

[44] Q. Ye, B. Rong, Y. Chen, M. Al-Shalash, C. Caramanis, and J. G. Andrews. User association for load balancing in heterogeneous cellular networks. [Online]. Available: http://arxiv.org/abs/1205.2833

[45] H. S. Dhillon, R. K. Ganti, and J. G. Andrews, "Load-aware modeling and analysis of heterogeneous cellular networks," *IEEE Trans. Wireless Commun.*, vol. 12, no. 4, pp. 1666–1677, 2013.

[46] S. Singh, H. S. Dhillon, and J. G. Andrews. Offloading in heterogeneous networks: Modeling, analysis and design insights. [Online]. Available: http://arxiv.org/abs/1208.1977

[47] K. Azarian, C. Lott, D. Ghosh, and R. A. Attar, "Imbalance issues in heterogeneous DO networks," in *Proc. IEEE 1st Int'l Workshop on Femtocell Networks (GLOBECOM'10 Wkshps)*, Miami, USA, Dec. 2010, pp. 669–673.

[48] J. Weitzen and T. Grosch, "Comparing coverage quality for femtocell and macrocell broadband data services," *IEEE Commun. Mag.*, vol. 48, no. 1, pp. 40–44, Jan. 2010.

[49] R. Madan, J. Borran, A. Sampath, N. Bhushan, A. Khandekar, and T. Ji, "Cell association and interference coordination in heterogeneous LTE-A cellular networks," *IEEE J. Select. Areas Commun.*, vol. 28, no. 9, pp. 1479–1489, 2010.

[50] D. Lopez-Perez, X. Chu, and I. Guvenc, "On the expanded region of picocells in heterogeneous networks," *IEEE J. of Select. Topics in Signal Processing*, vol. 6, no. 3, pp. 281–294, 2012.

[51] K. Kikuchi and H. Otsuka, "Proposal of adaptive control CRE in heterogeneous networks," in *Proc. IEEE 23rd Int'l Symp. on Personal, Indoor and Mobile Radio Commun. (PIMRC'12)*, Sydney, Australia, Sep. 2012, pp. 910–914.

[52] P. Xia, V. Chandrasekhar, and J. G. Andrews, "Open vs. closed access femtocells in the uplink," *IEEE Trans. Wireless Commun.*, vol. 9, no. 12, pp. 3798 –3809, Dec. 2010.

[53] D. Choi, P. Monajemi, S. Kang, and J. Villasenor, "Dealing with loud neighbors: The benefits and tradeoffs of adaptive femtocell access," in *Proc. IEEE Global Commun. Conf. (GLOBECOM'08)*, New Orleans, USA, Dec. 2008, pp. 1–5.

[54] D. Lopez-Perez, A. Valcarce, G. d. l. Roche, and J. Zhang, "OFDMA femtocells: A roadmap on interference avoidance," *IEEE Commun. Mag.*, vol. 47, no. 9, pp. 41–48, Sep. 2009.

[55] G. d. l. Roche, A. Valcarce, D. Lopez-Perez, and J. Zhang, "Access control mechanisms for femtocells," *IEEE Commun. Mag.*, vol. 48, no. 1, pp. 33–39, 2010.

[56] H.-S. Jo, P. Xia, and J. G. Andrews, "Open, closed, and shared access femtocells in the downlink," *EURASIP Journal on Wireless Communications and Networking*, vol. 2012, no. 1, pp. 1–16, 2012.

[57] H. S. Dhillon, R. K. Ganti, and J. G. Andrews, "A tractable framework for coverage and outage in heterogeneous cellular networks," in *Proc. Information Theory and Applications Workshop (ITA'11)*, San Diego, USA, Feb. 2011, pp. 1–6.

[58] A. Golaup, M. Mustapha, and L. B. Patanapongpibul, "Femtocell access control strategy in UMTS and LTE," *IEEE Commun. Mag.*, vol. 47, no. 9, pp. 117–123, Sep. 2009.

[59] P. Lin, J. Zhang, Y. Chen, and Q. Zhang, "Macro-femto heterogeneous network deployment and management: From business models to technical solutions," *IEEE Wireless Commun.*, vol. 18, no. 3, pp. 64–70, 2011.

[60] H.-S. Jo, Y. J. Sang, P. Xia, and J. G. Andrews, "Heterogeneous cellular networks with flexible cell association: A comprehensive downlink SINR analysis," *IEEE Trans. Wireless Commun.*, vol. 11, no. 10, pp. 3484–3495, 2012.

[61] H. S. Dhillon, R. K. Ganti, F. Baccelli, and J. G. Andrews, "Modeling and analysis of K-tier downlink heterogeneous cellular networks," *IEEE J. Select. Areas Commun.*, vol. 30, no. 3, pp. 550–560, Apr. 2012.

[62] H. Wang and M. C. Reed, "Tractable model for heterogeneous cellular networks with directional antennas," in *Proc. 2012 Australian Commun. Theory Workshop (AusCTW'12)*, Wellington, New Zealand, Jan./Feb. 2012, pp. 61–65.

[63] D. Lopez-Perez and X. Chu, "Inter-cell interference coordination for expanded region picocells in heterogeneous networks," in *Proc. 20th Int'l Conf. on Computer Commun. and Networks (ICCCN'11)*, Hawaii, USA, Jul./Aug. 2011, pp. 1–6.

[64] "Interference management in UMTS femtocells," *Femto Forum White Paper*, Dec. 2008.

[65] M. Yavuz, F. Meshkati, S. Nanda, A. Pokhariyal, N. Johnson, B. Raghothaman, and A. Richardson, "Interference management and performance analysis of UMTS/HSPA+ femtocells," *IEEE Commun. Mag.*, vol. 47, no. 9, pp. 102–109, Sep. 2009.

[66] D. Lopez-Perez, A. Valcarce, G. d. l. Roche, E. Liu, and J. Zhang, "Access methods to WiMAX femtocells: A downlink system-level case study," in *Proc. 11th IEEE Singapore Int'l Conf. on Commun. Systems (ICCS'08)*, Guangzhou, China, Nov. 2008, pp. 1657–1662.

[67] L. G. U. Garcia, K. I. Pedersen, and P. E. Mogensen, "Autonomous component carrier selection: Interference management in local area environments for LTE-Advanced," *IEEE Commun. Mag.*, vol. 47, no. 9, pp. 110–116, Sep. 2009.

[68] Y. Bai, J. Zhou, and L. Chen, "Hybrid spectrum sharing for coexistence of macrocell and femtocell," in *Proc. IEEE Int'l Conf. on Commun. Tech. and Applications (ICCTA'09)*, Beijing, China, Oct. 2009, pp. 162–166.

[69] V. Chandrasekhar and J. G. Andrews, "Spectrum allocation in tiered cellular networks," *IEEE Trans. Commun.*, vol. 57, no. 10, pp. 3059–3068, Oct. 2009.

[70] A. Damnjanovic, J. Montojo, J. Cho, H. Ji, J. Yang, and P. Zong, "UE's role in LTE Advanced heterogeneous networks," *IEEE Commun. Mag.*, vol. 50, no. 2, pp. 164–176, 2012.

[71] K. Okino, T. Nakayama, C. Yamazaki, H. Sato, and Y. Kusano, "Pico cell range expansion with interference mitigation toward LTE-Advanced heterogeneous networks," in *Proc. IEEE Int'l Conf. on Commun. (ICC'11)*, Kyoto, Japan, Jun. 2011, pp. 1–5.

[72] M. Shirakabe, A. Morimoto, and N. Miki, "Performance evaluation of inter-cell interference coordination and cell range expansion in heterogeneous networks for LTE-Advanced downlink," in *Proc. 8th Int'l Symp. on Wireless Commun. Systems (ISWCS'11)*, Aachen, Germany, Nov. 2011, pp. 844–848.

[73] S. Deb, P. Monogioudis, J. Miernik, and J. P. Seymour. Algorithms for enhanced inter-cell interference coordination (eICIC) in LTE HetNets. [Online]. Available: http://arxiv.org/abs/1302.3784

[74] J. Wang, X. She, and L. Chen, "Enhanced dynamic inter-cell interference coordination schemes for LTE-Advanced," in *Proc. IEEE 75th Vehic. Tech. Conf. (VTC'12-Spring)*, Yokohama, Japan, May 2012, pp. 1–6.

[75] A. Weber and O. Stanze, "Scheduling strategies for HetNets using eICIC," in *Proc. IEEE Int'l Conf. on Commun. (ICC'12)*, Ottawa, Canada, Jun. 2012, pp. 6787–6791.

[76] "Interference management in UMTS femtocells," *Femto Forum White Paper*, Dec. 2008.

[77] Y. Tokgoz, F. Meshkati, Y. Zhou, M. Yavuz, and S. Nanda, "Uplink interference management for HSPA+ and 1xEVDO femtocells," in *Proc. IEEE Global Commun. Conf. (GLOBECOM'09)*, Honolulu, USA, Dec. 2009, pp. 1–7.

[78] N. Arulselvan, V. Ramachandran, S. Kalyanasundaram, and G. Han, "Distributed power control mechanisms for HSDPA femtocells," in *Proc. IEEE 69th Vehic. Tech. Conf. (VTC'09-Spring)*, Barcelona, Spain, Apr. 2009, pp. 1–5.

[79] V. Chandrasekhar, J. G. Andrews, T. Muharemovic, Z. Shen, and A. Gatherer, "Power control in two-tier femtocell networks," *IEEE Trans. Wireless Commun.*, vol. 8, no. 8, pp. 4316–4328, Aug. 2009.

[80] *Universal Mobile Telecommunications System (UMTS); Handover procedures*, 3GPP Tech. Spec. 23.009, Rev. 11.2.0.

[81] K. Dimou, M. Wang, Y. Yang, M. Kazmi, A. Larmo, J. Pettersson, W. Muller, and Y. Timner, "Handover within 3GPP LTE: Design principles and performance," in *Proc. IEEE 70th Vehic. Tech. Conf. (VTC'09-Fall)*, Anchorage, USA, Sep. 2009, pp. 1–5.

[82] *Evolved Universal Terrestrial Radio Access (E-UTRA); Radio Resource Control (RRC); Protocol specification*, 3GPP Tech. Spec. 36.331, Rev. 8.19.0.

[83] N. Nasser, A. Hasswa, and H. Hassanein, "Handoffs in fourth generation heterogeneous networks," *IEEE Commun. Mag.*, vol. 44, no. 10, pp. 96–103, 2006.

[84] D. Lopez-Perez, I. Guvenc, and X. Chu, "Mobility management challenges in 3GPP heterogeneous networks," *IEEE Commun. Mag.*, vol. 50, no. 12, pp. 70–78, 2012.

[85] K. Kitagawa, T. Komine, T. Yamamoto, and S. Konishi, "Performance evaluation of handover in LTE-Advanced systems with pico cell range expansion," in *Proc. IEEE 23rd Int'l Symp. on Personal, Indoor and Mobile Radio Commun. (PIMRC'12)*, Sydney, Australia, Sep. 2012, pp. 1071–1076.

[86] D. Lopez-Perez, I. Guvenc, and X. Chu, "Mobility enhancements for heterogeneous networks through interference coordination," in *Proc. 2012 IEEE Wireless Commun. and Networking Conference Workshops (WCNCW'12)*, Paris, France, Apr. 2012, pp. 69–74.

[87] *3G security; Security architecture*, 3GPP Tech. Spec. 33.102, Rev. 8.6.0.

[88] C. B. Sankaran, "Network access security in next-generation 3GPP systems: A tutorial," *IEEE Commun. Mag.*, vol. 47, no. 2, pp. 84–91, Feb. 2009.

[89] A. D. Wyner, "The wire-tap channel," *Bell System Technical Journal*, vol. 54, no. 8, pp. 1355–1387, Oct. 1975.

[90] I. Csiszár and J. Körner, "Broadcast channels with confidential messages," *IEEE Trans. Inform. Theory*, vol. 24, no. 3, pp. 339–348, May 1978.

[91] D. S. Deif, H. El-Badawy, and H. El-Hennawy, "Toplogy based modeling and simulation of UMTS-WLAN wireless heterogeneous network," in *Proc. Seventh International Conference On Wireless And Optical Communications Networks (WOCN'10)*, Colombo, Sri Lanka, Sep. 2010, pp. 1–5.

[92] K. S. Gilhousen, I. M. Jacobs, R. Padovani, A. J. Viterbi, L. A. Weaver, and C. E. Wheatley, "On the capacity of a cellular CDMA system," *IEEE Trans. Veh. Technol.*, vol. 40, no. 2, pp. 303–312, May 1991.

[93] A. D. Wyner, "Shannon-theoretic approach to a Gaussian cellular multiple-access channel," *IEEE Trans. Inform. Theory*, vol. 40, no. 6, pp. 1713–1727, Nov. 1994.

[94] S. Shamai and A. D. Wyner, "Information-theoretic considerations for symmetric, cellular, multiple-access fading channels. I & II," *IEEE Trans. Inform. Theory*, vol. 43, no. 6, pp. 1895–1911, 1997.

[95] O. Somekh and S. Shamai, "Shannon-theoretic approach to a Gaussian cellular multiple-access channel with fading," *IEEE Trans. Inform. Theory*, vol. 46, no. 4, pp. 1401–1425, 2000.

[96] A. J. Viterbi, A. M. Viterbi, and E. Zehavi, "Other-cell interference in cellular power-controlled CDMA," *IEEE Trans. Commun.*, vol. 42, no. 234, pp. 1501–1504, 1994.

[97] J. Xu, J. Zhang, and J. G. Andrews, "On the accuracy of the Wyner model in cellular networks," *IEEE Trans. Wireless Commun.*, vol. 10, no. 9, pp. 3098–3109, Sep. 2011.

[98] D. Stoyan, W. S. Kendall, and J. Mecke, *Stochastic Geometry and its Applications*, 2nd ed. New York, NY: John Wiley & Sons Ltd., 1995.

[99] M. Haenggi, J. G. Andrews, F. Baccelli, O. Dousse, and M. Franceschetti, "Stochastic geometry and random graphs for the analysis and design of wireless networks," *IEEE J. Select. Areas Commun.*, vol. 27, no. 7, pp. 1029–1046, Sep. 2009.

[100] F. Baccelli and B. Błaszczyszyn, *Stochastic Geometry and Wireless Networks, Volume I: Theory*. Hanover, MA: Now Publishers Inc., 2009.

[101] S. Srinivasa and M. Haenggi, "Distance distributions in finite uniformly random networks: Theory and applications," *IEEE Trans. Veh. Technol.*, vol. 59, no. 2, pp. 940–949, 2010.

[102] S. Weber and J. G. Andrews, *Transmission Capacity of Wireless Networks*. Hanover, MA: Now Publishers Inc., 2012.

[103] M. Haenggi and R. K. Ganti, *Interference in Large Wireless Networks*. Hanover, MA: Now Publishers Inc., 2009.

[104] A. Busson, "An overview of results on ad hoc network performances using spatial model," in *Proc. IEEE Symp. on Computers and Commun. (ISCC'09)*, Sousse, Tunisia, Jul. 2009, pp. 36–41.

[105] R. K. Ganti and M. Haenggi, "Single-hop connectivity in interference-limited hybrid wireless networks," in *Proc. IEEE Int'l Symp. on Information Theory (ISIT'07)*, Nice, France, Jun. 2007, pp. 366–370.

[106] J. Venkataraman, M. Haenggi, and O. Collins, "Shot noise models for outage and throughput analyses in wireless ad hoc networks," in *Proc. IEEE Military Communications Conference (MILCOM'06)*, Washington, D.C., USA, Oct. 2006, pp. 1–7.

[107] F. Baccelli, B. Błaszczyszyn, and P. Muhlethaler, "An Aloha protocol for multihop mobile wireless networks," *IEEE Trans. Inform. Theory*, vol. 52, no. 2, pp. 421–436, Feb. 2006.

[108] F. Baccelli, B. Błaszczyszyn, and P. Miihlethaler, "Stochastic analysis of spatial and opportunistic Aloha," *IEEE J. Select. Areas Commun.*, vol. 27, no. 7, pp. 1105–1119, Sep. 2009.

[109] X. Yang and A. P. Petropulu, "Co-channel interference modeling and analysis in a Poisson field of interferers in wireless communications," *IEEE Trans. Signal Processing*, vol. 51, no. 1, pp. 64–76, Jan. 2003.

[110] J. G. Andrews, S. Shakkottai, R. Heath, N. Jindal, M. Haenggi, R. Berry, D. Guo, M. Neely, S. Weber, S. Jafar, and A. Yener, "Rethinking informa-

tion theory for mobile ad hoc networks," *IEEE Commun. Mag.*, vol. 46, no. 12, pp. 94–101, 2008.

[111] A. J. Ganesh and G. L. Torrisi, "Large deviations of the interference in a wireless communication model," *IEEE Trans. Inform. Theory*, vol. 54, no. 8, pp. 3505–3517, 2008.

[112] F. Baccelli and S. Zuyev, "Stochastic geometry models of mobile communication networks," in *Frontiers in Queueing: Models and Applications in Science and Engineering*, J. H. Dshalalow, Ed. Boca Raton, FL: CRC Press, 1996, pp. 227–243.

[113] F. Baccelli, M. Klein, M. Lebourges, and S. Zuyev, "Stochastic geometry and architecture of communication networks," *Telecommunication Systems*, vol. 7, no. 1-3, pp. 209–227, 1997.

[114] T. X. Brown, "Cellular performance bounds via shotgun cellular systems," *IEEE J. Select. Areas Commun.*, vol. 18, no. 11, pp. 2443–2455, Nov. 2000.

[115] P. Madhusudhanan, J. G. Restrepo, Y. Liu, and T. X. Brown, "Carrier to interference ratio analysis for the shotgun cellular system," in *Proc. IEEE Global Commun. Conf. (GLOBECOM'09)*, Honolulu, USA, Dec. 2009, pp. 1–6.

[116] R. K. Ganti, F. Baccelli, and J. G. Andrews, "A new way of computing rate in cellular networks," in *Proc. IEEE Int'l Conf. on Commun. (ICC'11)*, Kyoto, Japan, Jun. 2011, pp. 1–5.

[117] C. S. Chen, V. M. Nguyen, and L. Thomas, "On small cell network deployment: A comparative study of random and grid topologies," in *Proc. IEEE 76th Vehic. Tech. Conf. (VTC'12-Fall)*, Québec City, Canada, Sep. 2012, pp. 1–5.

[118] B. Błaszczyszyn, M. K. Karray, and H. P. Keeler. Using poisson processes to model lattice cellular networks. [Online]. Available: http://arxiv.org/abs/1207.7208

[119] T. D. Novlan, R. K. Ganti, A. Ghosh, and J. G. Andrews, "Analytical evaluation of fractional frequency reuse for OFDMA cellular networks," *IEEE Trans. Wireless Commun.*, vol. 10, no. 12, pp. 4294–4305, Dec. 2011.

[120] T. D. Novlan, R. K. Ganti, J. G. Andrews, and A. Ghosh, "A new model for coverage with fractional frequency reuse in OFDMA cellular networks," in *Proc. IEEE Global Commun. Conf. (GLOBECOM'11)*, Houston, USA, Dec. 2011, pp. 1–5.

[121] K. Huang and J. G. Andrews, "A stochastic-geometry approach to coverage in cellular networks with multi-cell cooperation," in *Proc. IEEE Global Commun. Conf. (GLOBECOM'11)*, Houston, USA, Dec. 2011, pp. 1–5.

[122] ——, "Characterizing multi-cell cooperation via the outage-probability exponent," in *Proc. IEEE Int'l Conf. on Commun. (ICC'12)*, Ottawa, Canada, Jun. 2012, pp. 6411–6415.

[123] T. D. Novlan, H. S. Dhillon, and J. G. Andrews. Analytical modeling of uplink cellular networks. [Online]. Available: http://arxiv.org/abs/1203.1304

[124] J. G. Andrews, R. K. Ganti, M. Haenggi, N. Jindal, and S. Weber, "A primer on spatial modeling and analysis in wireless networks," *IEEE Commun. Mag.*, vol. 48, no. 11, pp. 156–163, 2010.

[125] M. Haenggi. A versatile dependent model for heterogeneous cellular networks. [Online]. Available: http://arxiv.org/abs/1305.0947

[126] P. Madhusudhanan, J. G. Restrepo, Y. Liu, T. X. Brown, and K. R. Baker, "Multi-tier network performance analysis using a shotgun cellular system," in *Proc. IEEE Global Commun. Conf. (GLOBECOM'11)*, Houston, USA, Dec. 2011, pp. 1–6.

[127] C. C. Wang, T. Q. S. Quek, and M. Kountouris, "Throughput optimization, spectrum allocation, and access control in two-tier femtocell networks," *IEEE J. Select. Areas Commun.*, vol. 30, no. 3, pp. 561–574, Apr. 2012.

[128] ——, "Stochastic analysis of two-tier networks: Effect of spectrum allocation," in *Proc. IEEE Int'l Conf. on Acoustics, Speech and Signal Processing (ICASSP'11)*, Prague, Czech Republic, May 2011, pp. 2964–2967.

[129] S. M. Yu and S.-L. Kim. Downlink capacity and base station density in cellular networks. [Online]. Available: http://arxiv.org/abs/1109.2992

[130] Y. Zhong and W. Zhang. Multi-channel hybrid access femtocells: A stochastic geometric analysis. [Online]. Available: http://arxiv.org/abs/1108.1257

[131] Z. Shi, M. C. Reed, and M. Zhao, "On uplink interference scenarios in two-tier macro and femto co-existing UMTS networks," *EURASIP Journal on Wireless Communications and Networking*, vol. 2010, no. 1, pp. 1–8, 2010.

[132] Z. Shi, M. Zhao, M. C. Reed, and H. Wang, "Uplink interference scenarios in two-tier networks," in *Proc. 44th Annual Asilomar Conf. on Signals, Systems, and Computers (Asilomar'10)*, Pacific Grove, USA, Nov. 2010, pp. 471–476.

[133] H. S. Dhillon, R. K. Ganti, F. Baccelli, and J. G. Andrews, "Coverage and ergodic rate in K-tier downlink heterogeneous cellular networks," in *Proc. 49th Annual Allerton Conference on Communication, Control, and Computing (Allerton'11)*, Monticello, USA, Sep. 2011, pp. 1–6.

[134] H. Holma and A. Toskala, *LTE for UMTS: OFDMA and SC-FDMA Based Radio Access*. New York, NY: John Wiley & Sons Ltd., 2009.

[135] H. Claussen, "Co-channel operation of macro- and femtocells in a hierarchical cell structure," *Int'l. J. Wireless Inform. Networks*, vol. 15, no. 3-4, pp. 137–147, 2008.

[136] V. Chandrasekhar, M. Kountouris, and J. G. Andrews, "Coverage in multi-antenna two-tier networks," *IEEE Trans. Wireless Commun.*, vol. 8, no. 10, pp. 5314–5327, Oct. 2009.

[137] J. Niu, D. Lee, X. Ren, G. Y. Li, and T. Su, "Scheduling exploiting frequency and multi-user diversity in LTE downlink systems," *IEEE Trans. Wireless Commun.*, vol. 12, no. 4, pp. 1843–1849, 2013.

[138] A. Okabe, B. Boots, and K. Sugihara, *Spatial Tessellations: Concepts and Applications of Voronoi Diagrams*. New York, NY: John Wiley & Sons Ltd., 1992.

[139] A. L. Hinde and R. E. Miles, "Monte Carlo estimates of the distributions of the random polygons of the Voronoi tessellation with respect to a Poisson process," *Journal of Statistical Computation and Simulation*, vol. 10, no. 3-4, pp. 205–223, 1980.

[140] D. Weaire, J. P. Kermode, and J. Wejchert, "On the distribution of cell areas in a Voronoi network," *Philosophical Magazine Part B*, vol. 53, no. 5, pp. L101–L105, 1986.

[141] C.-H. Lee and M. Haenggi, "Interference and outage in Poisson cognitive networks," *IEEE Trans. Wireless Commun.*, vol. 11, no. 4, pp. 1392–1401, 2012.

[142] M. Efthymiou, A. Mackay, A. Dow, and M. Flanagan, "Spatial optimisation: How subscribers can help you optimize your CDMA network," in *Proc. 12th Int'l Telecom. Network Strategy and Planning Symp. (Networks'06)*, New Delhi, India, Nov. 2006, pp. 1–11.

[143] A. M. Viterbi and A. J. Viterbi, "Erlang capacity of a power controlled CDMA system," *IEEE J. Select. Areas Commun.*, vol. 11, no. 6, pp. 892–900, Aug. 1993.

[144] V. V. Veeravalli, A. Sendonaris, and N. Jain, "CDMA coverage, capacity and pole capacity," in *Proc. IEEE 47th Vehic. Tech. Conf. (VTC'97)*, vol. 3, Phoenix, USA, May 1997, pp. 1450–1454.

[145] V. V. Veeravalli and A. Sendonaris, "The coverage-capacity tradeoff in cellular CDMA systems," *IEEE Trans. Veh. Technol.*, vol. 48, no. 5, pp. 1443–1450, Sep. 1999.

[146] S. V. Hanly, "Capacity and power control in spread spectrum macrodiversity radio networks," *IEEE Trans. Commun.*, vol. 44, no. 2, pp. 247–256, 1996.

[147] A. Mader, D. Staehle, and C. Gosswein, "Performance of internet services over the UMTS enhanced uplink," in *Proc. Int'l Conf. on Next Generation Mobile Applications, Services and Technologies (NGMAST'07)*, Cardiff, UK, Sep. 2007, pp. 298–303.

[148] *Propagation data and prediction methods for the planning of indoor radiocommunication systems and radio local area networks in the frequency range 900 MHz to 100 GHz*, ITU Recommendation ITU-R P.1238-7.

[149] M. Haenggi, "The secrecy graph and some of its properties," in *Proc. IEEE Int'l Symp. on Information Theory (ISIT'08)*, Toronto, Canada, Jul. 2008, pp. 539–543.

[150] P. C. Pinto, J. Barros, and M. Z. Win, "Secure communication in stochastic wireless networks - Part I: Connectivity," *IEEE Trans. Inform. Forensics and Security*, vol. 7, no. 1, pp. 125–138, Feb. 2012.

[151] S. Goel, V. Aggarwal, A. Yener, and A. R. Calderbank, "Modeling location uncertainty for eavesdroppers: A secrecy graph approach," in *Proc. IEEE Int'l Symp. on Information Theory (ISIT'10)*, Austin, USA, Jun. 2010, pp. 2627–2631.

[152] P. C. Pinto and M. Z. Win, "Continuum percolation in the intrinsically secure communications graph," in *Proc. 2010 Int'l Symp. on Information Theory and its Applications (ISITA'10)*, Taichung, Taiwan, Oct. 2010, pp. 349–354.

[153] X. Zhou, R. K. Ganti, and J. G. Andrews, "Secure wireless network connectivity with multi-antenna transmission," *IEEE Trans. Wireless Commun.*, vol. 10, no. 2, pp. 425–430, Feb. 2011.

[154] P. C. Pinto, J. Barros, and M. Z. Win, "Secure communication in stochastic wireless networks - Part II: Maximum rate and collusion," *IEEE Trans. Inform. Forensics and Security*, vol. 7, no. 1, pp. 139–147, Feb. 2012.

[155] O. O. Koyluoglu, C. E. Koksal, and H. E. Gamal, "On secrecy capacity scaling in wireless networks," *IEEE Trans. Inform. Theory*, vol. 58, no. 5, pp. 3000–3015, May 2012.

[156] Y. Liang, H. Poor, and L. Ying, "Secrecy throughput of MANETs with malicious nodes," in *Proc. IEEE Int'l Symp. on Information Theory (ISIT'09)*, Seoul, Korea, Jun. 2009, pp. 1189–1193.

[157] C. Capar, D. Goeckel, B. Liu, and D. Towsley, "Secret communication in large wireless networks without eavesdropper location information," in *Proc. 31st Annual IEEE Int'l Conf. on Computer Commun. (IEEE INFOCOM'12)*, Orlando, USA, Mar. 2012, pp. 1152–1160.

[158] X. Zhou, R. K. Ganti, J. G. Andrews, and A. Hjørungnes, "On the throughput cost of physical layer security in decentralized wireless networks," *IEEE Trans. Wireless Commun.*, vol. 10, no. 8, pp. 2764–2775, Aug. 2011.

[159] ——, "Secrecy transmission capacity of decentralized wireless networks," in *Proc. 49th Annual Allerton Conference on Communication, Control, and Computing (Allerton'11)*, Monticello, USA, Sep. 2011, pp. 1726–1732.

[160] A. Sarkar and M. Haenggi, "Secrecy coverage," *Internet Mathematics*, vol. 9, no. 2-3, pp. 199–216, 2013.

[161] M. Bloch, J. Barros, M. R. D. Rodrigues, and S. W. McLaughlin, "Wireless information-theoretic security," *IEEE Trans. Inform. Theory*, vol. 54, no. 6, pp. 2515–2534, Jun. 2008.

[162] A. Jeffrey and H.-H. Dai, *Handbook of Mathematical Formulas and Integrals*, 4th ed. Burlington, MA: Academic Press, 2008.

[163] M. Haenggi, "On distances in uniformly random networks," *IEEE Trans. Inform. Theory*, vol. 51, no. 10, pp. 3584–3586, Oct. 2005.

[164] M. Abramowitz and I. A. Stegun, Eds., *Handbook of Mathematical Functions: with Formulas, Graphs, and Mathematical Tables*, 10th ed. Washington, D.C.: U.S. Govt. Printing Office, 1972.